Advanced electrocorticography and its translation to epilepsy surgery



Eline Schaft

UMC Utrecht Brain Center

Advanced electrocorticography and its translation to epilepsy surgery

Eline V. Schaft

Advanced electrocorticography and its translation to epilepsy surgery
PhD thesis, University of Utrecht
Eline Schaft

ISBN:	978-94-6534-297-9
DOI:	https://doi.org/10.33540/3469
Cover Design:	Sieben Medical Art | siebenmedicalart.nl
Layout:	Eline Schaft
Printing:	ProefschriftMaken | proefschriftmaken.nl

The research in this thesis was financially supported by the European Research Council.

The author gratefully acknowledges the financial support for the publication of this thesis by AD-Tech, Chipsoft, Nederlandse Vereniging van Klinische Neurofysiologie, Neurosoft and UMC Utrecht Brain Center.

© All rights reserved, no part of this publication may be reproduced or transmitted in any form or by any means without the written permission of the writer. The copyright of the articles that have been published, has been transferred to the respective journals.

Advanced electrocorticography and its translation to epilepsy surgery

Geavanceerde elektrocorticografie en de vertaalslag naar epilepsiechirurgie

(met een samenvatting in het Nederlands)

Proefschrift

ter verkrijging van de graad van doctor aan de
Universiteit Utrecht
op gezag van de
rector magnificus, prof. dr. ir. W. Hazeleger,
ingevolge het besluit van het College voor Promoties
in het openbaar te verdedigen op
donderdag 4 juni 2026 des middags te 4.15 uur

door

Eline Vivian Schaft

geboren op 11 augustus 1992
te Leiderdorp

Promotoren:

Prof. dr. G.J.M. Zijlmans
Prof. dr. N.F. Ramsey

Copromotor:

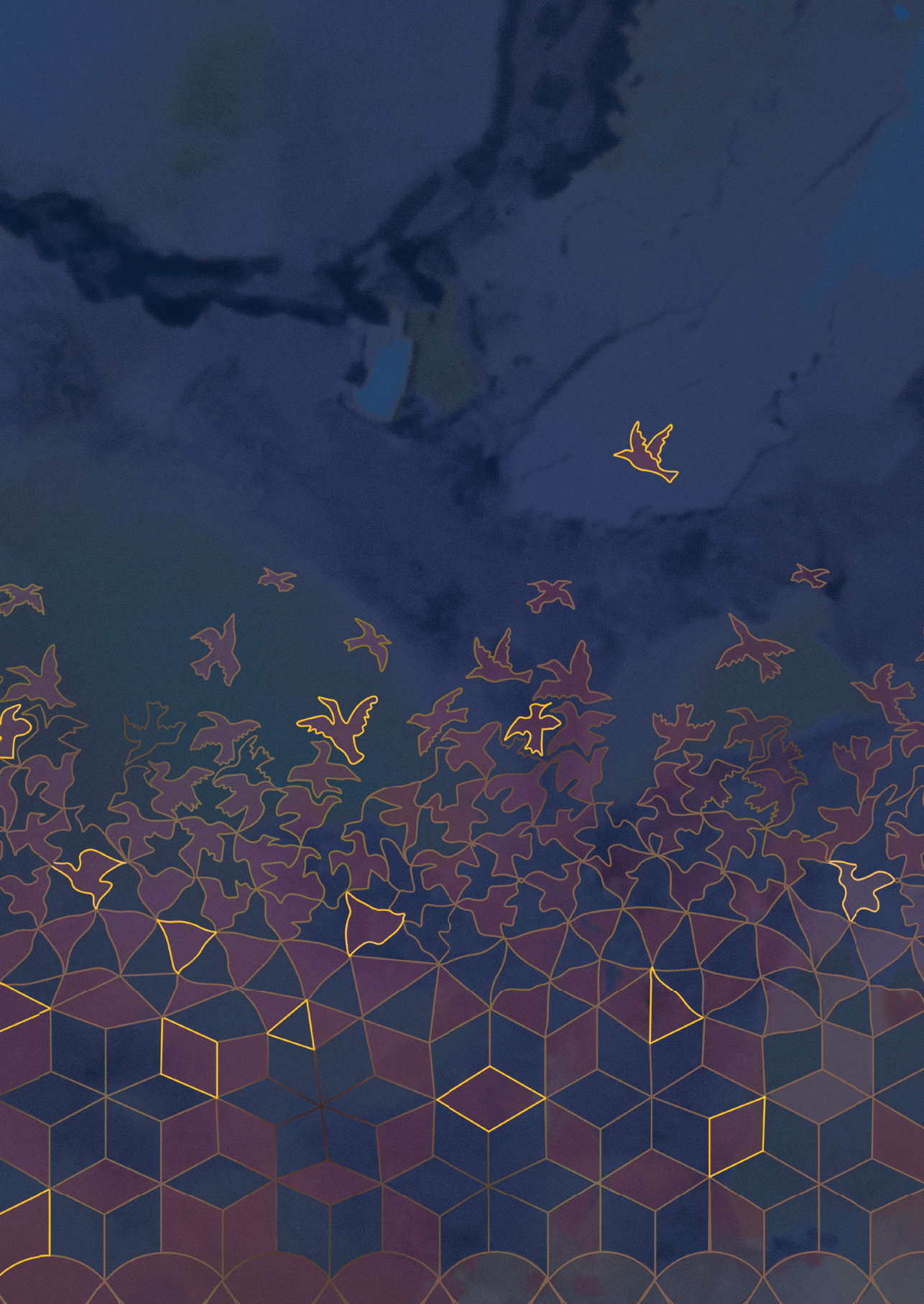
Dr. M.A. van 't Klooster

Beoordelingscommissie:

Prof. dr. K.P.J. Braun
Prof. dr. A. Hillebrand
Prof. dr. D.W.J. Klomp (voorzitter)
Prof. dr. P.A.J.T. Robe
Dr. E. Tolner

Table of contents

Chapter 1	**General Introduction**	7
Part I	**From Spikes to Spectra**	
Chapter 2	Spatial and temporal properties of intraoperatively recorded spikes and high frequency oscillations in focal cortical dysplasia	15
Chapter 3	Spectral entropy variability of intraoperative electrocorticography predicts outcome after epilepsy surgery in patients with focal cortical dysplasia	33
Chapter 4	Explainable artificial intelligence unveils (non-) epileptiform spectral powers in intraoperative electrocorticography	51
Part II	**From Interpretation to Innovation**	
Chapter 5	What is the optimal montage to identify interictal epileptiform discharges and high frequency oscillations in intraoperative electrocorticography?	73
Chapter 6	The spatial relationship between the MRI lesion and intraoperative electrocorticography in focal epilepsy surgery	91
Chapter 7	Implementing intraoperative high-density electrocorticography during epilepsy surgery	109
Chapter 8	**Summary and general discussion**	129
Appendices	References	142
	Nederlandse Samenvatting | Dutch Summary	152
	Dankwoord | Acknowledgements	154
	List of publications	158
	About the author	161



Chapter 1

General introduction



Epilepsy surgery

Epilepsy is a common neurological disorder, affecting 1-2% of the global population.[1] Seizures are manifestations of structural abnormalities, metabolic imbalance or genetic disease in the brain.[2] Focal epilepsy, characterized by seizures originating in specific brain regions, accounts for roughly 60% of all cases.[1] Approximately 30% of these cases are drug-resistant, and seizures persist despite optimal medical therapy. Resective surgery is considered a potential treatment option in these people. The primary goal of surgery is to resect the complete epileptogenic zone without causing motor, speech or visual damage.[3,4] The ultimate aim of epilepsy surgery is to achieve lifelong seizure freedom, which depends largely on the localization accuracy of the epileptogenic zone, a.k.a. the region that needs to be resected to achieve seizure freedom. Currently, the reported seizure freedom after resective surgery ranges between 36 and 76%.[5]

Brain zones involved in epilepsy surgery

Identifying and distinguishing between the various brain zones conceptually linked to the epileptogenic zone is critical for optimizing epilepsy surgery. The epileptogenic zone is a concept: a hypothetical region which cannot be directly observed.[6,7] It is a construct based on (indirect) clinical, electrophysiological, and/or imaging based identified regions that often only partly overlap, with several key zones considered during pre-surgical evaluation.[2,8] (Figure 1A&B)

The structural lesion is an abnormality visible on MRI that is presumed to cause the network disturbance responsible for the epileptic seizures.[9]

- The seizure onset zone is the region where seizures originate, typically identified through long-term invasive EEG: grid implantation or stereo EEG.
- The irritative zone shows interictal epileptiform discharges.
- The symptomatic zone is the region where epileptic activity produces the patient's clinical seizure symptoms and signs.
- Additional information may be gathered from modalities such as MEG, PET, or SPECT, each indicating regions of altered electrophysiological or metabolic activity that might be related to the epileptic network.

All these zones each provide unique insights but are rarely fully congruent.[7] Surgical resection is further constrained by the need to preserve brain regions critical for functions such as movement, speech and vision. The resected tissue in patients who are seizure free after epilepsy surgery is the closest approximation that we have of the true epileptogenic zone. Unfortunately this delineation is currently only possible retrospectively, underscoring the urgent need for novel methodologies to accurately define this zone before and/or during epilepsy surgery.

Intraoperative electrocorticography

In clinical practice, intraoperative electrocorticography (ioECOG) is applied during epilepsy surgery, where it serves as a practical tool to guide the delineation of resection borders. A grid is placed in different positions on the exposed cortex. Recordings are made before resection (pre-resection recordings), during resection (per-resection recordings), and after final resection (post-resection recordings). (Figure 1C) The aim of these recordings is to delineate the borders of the resection based on epileptic activity.[10] Traditionally, this so-called tailoring is based on interictal spikes. Over the past 20 years, high-frequency oscillations (HFOs) have been opted as a new – more specific – biomarker. HFOs are fast oscillations and they are divided into ripples (80-250Hz) and fast ripples (250-500Hz).[11,12]

Post-surgical seizure outcome

The Engel classification is commonly used to evaluate seizure outcome after epilepsy surgery. This classification is widely accepted among clinicians and researchers. The classification consists of four categories[8]:

Engel class I	Free of disabling seizures
IA	Complete seizure free
IB	Only auras, no seizures
IC	Some seizures after surgery, but seizure free for at least 2 years
ID	Seizures occurred only when medication was withdrawn
Engel class II	Only rare disabling seizures.
Engel class III	A reduction in seizure frequency, but still significant number of seizures.
Engel class IV	Little or no change in seizure frequency.

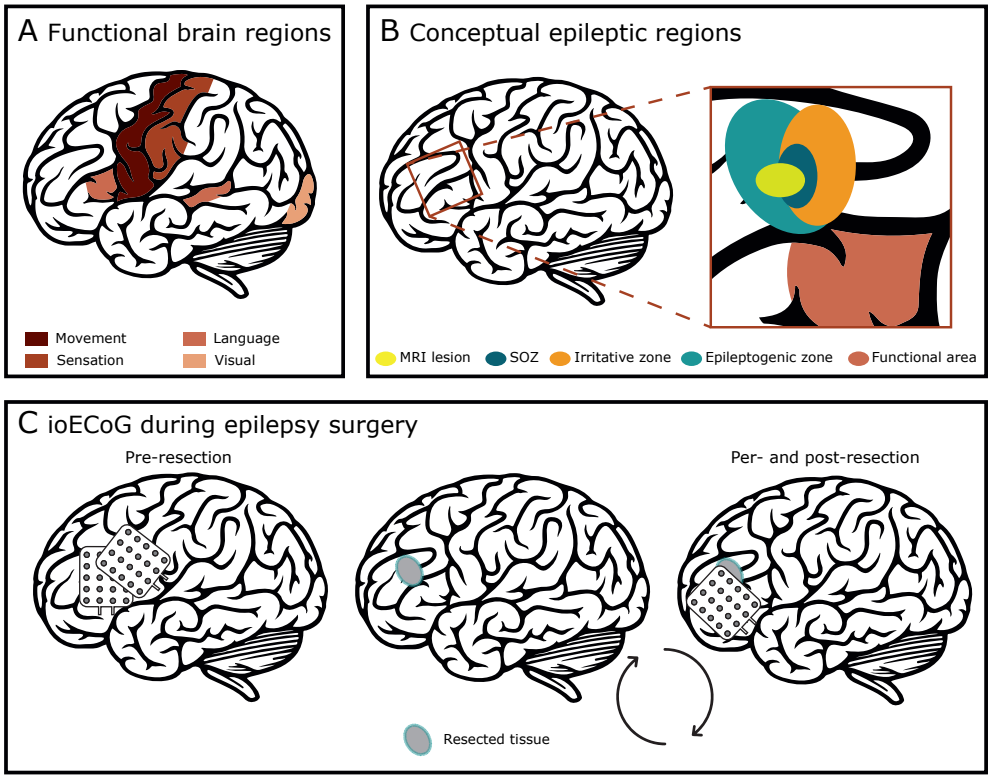


Figure 1: Schematic patient example of functional regions, key zones and the resulting ioECoG tailored surgical resection during epilepsy surgery. A) Schematic visualization of several functional brain regions not to be harmed during epilepsy, e.g. movement, sensation, language, and visualization. B) Key zones that construct the conceptual epileptogenic zone: MRI lesion: the structural lesion visible on the MRI that is presumably related to the epilepsy; the seizure onset zone (SOZ): the area where the seizures starts; the irritative zone: the zone where spikes and/or high-frequency oscillations occur; functional areas: explained in Figure 1A; the epileptogenic zone the minimal tissue that needs to be resected to achieve seizure freedom. As shown in this figure, these zones might (partly) overlap. C) The ioECoG-based tailoring procedure. Before resection, a recording is made: the pre-resection recording. After initial resection, another recording is made and, if needed, additional tissue can be resected. These last two steps – recording and additional resection – are repeated until the final resection is done.
Abbreviations: ioECoG = intraoperative electrocorticography, SOZ = seizure onset zone.

A challenge in the use of these traditional biomarkers intraoperatively is their often focal characteristics, which may not be adequately captured by conventional grid electrodes with relatively low spatial resolution, so-called low-density grids. High-density grids have the potential to overcome this limitation by providing higher spatial sampling, potentially improving the detection and localization of epileptiform abnormalities.[13]

Advanced signal analysis

Traditional visual analysis of ioECoG data – for spikes and/or HFOs – is inherently subjective and may miss clinical important patterns. Moreover, not all patients show clear interictal spikes or HFOs during surgery, limiting the applications of these biomarkers.[14] To overcome these limitations, the field is increasingly exploring advanced signal analysis methods and machine learning techniques.[15-21] In this thesis, we explore the possibilities of an entropy measure, spectral entropy, and decision-tree based machine learning techniques. Spectral entropy quantifies the irregularity or complexity of the frequency components within a signal.[22,23] Machine learning models can be trained on a labeled dataset to detect patterns. These models are capable of learning from large datasets and making predictions on unseen data, offering a data-driven approach to extract new information from our data. Their black box nature poses challenges in clinical acceptance. Explainable artificial intelligence can give insight in the decision-making processes of machine learning models.[24,25] This transparency can offer clinicians understanding and trust to integrate machine learning models into clinical care.[26]

Structural underlying lesional pathologies that can cause focal epileptic seizures[2]

Cavernoma	A vascular malformation composed of abnormally dilated capillary vessels without intervening normal brain tissue.
Focal cortical dysplasia (FCD)	A developmental malformation of the cortex characterized by disorganized cortical architecture and abnormal neurons. FCD is a common cause of drug-resistant focal epilepsy. On MRI the lesions may be visible, but they are often subtle.
Mesial temporal sclerosis (MTS)	Sclerotic and atrophic tissue in the mesial temporal lobe. The hippocampus, amygdala and parahippocampal gyrus can all be affected.
Gliosis	Reactive scar tissue of the brain, resulting from trauma, infection or prior surgery.
Low grade tumors	Slow growing, often benign, brain tumors, such as: dysembryoplastic neuroepithelial tumor (DNET), gliomas, gangliogliomas, pleomorphic xanthoastrocytoma (PXA).
Tuberous sclerosis complex (TSC)	A genetic disorder that causes benign tumors in different parts of the body, especially in the brain, skin, heart and kidneys. Cortical tubers are the main cause of epilepsy in these patients.

Aims and outline of the thesis

The debate on the use and clinical relevance of spikes and HFOs remains ongoing.[14,27,28] Spikes might be more useful in particular patient cohorts and HFOs in others.[14] There is a continued need to investigate both biomarkers, how they behave by different pathologies, and how they can be applied effectively in ioECoG-guided resection strategies. In parallel, there is a growing interest in identifying and validating novel signal-based biomarkers.

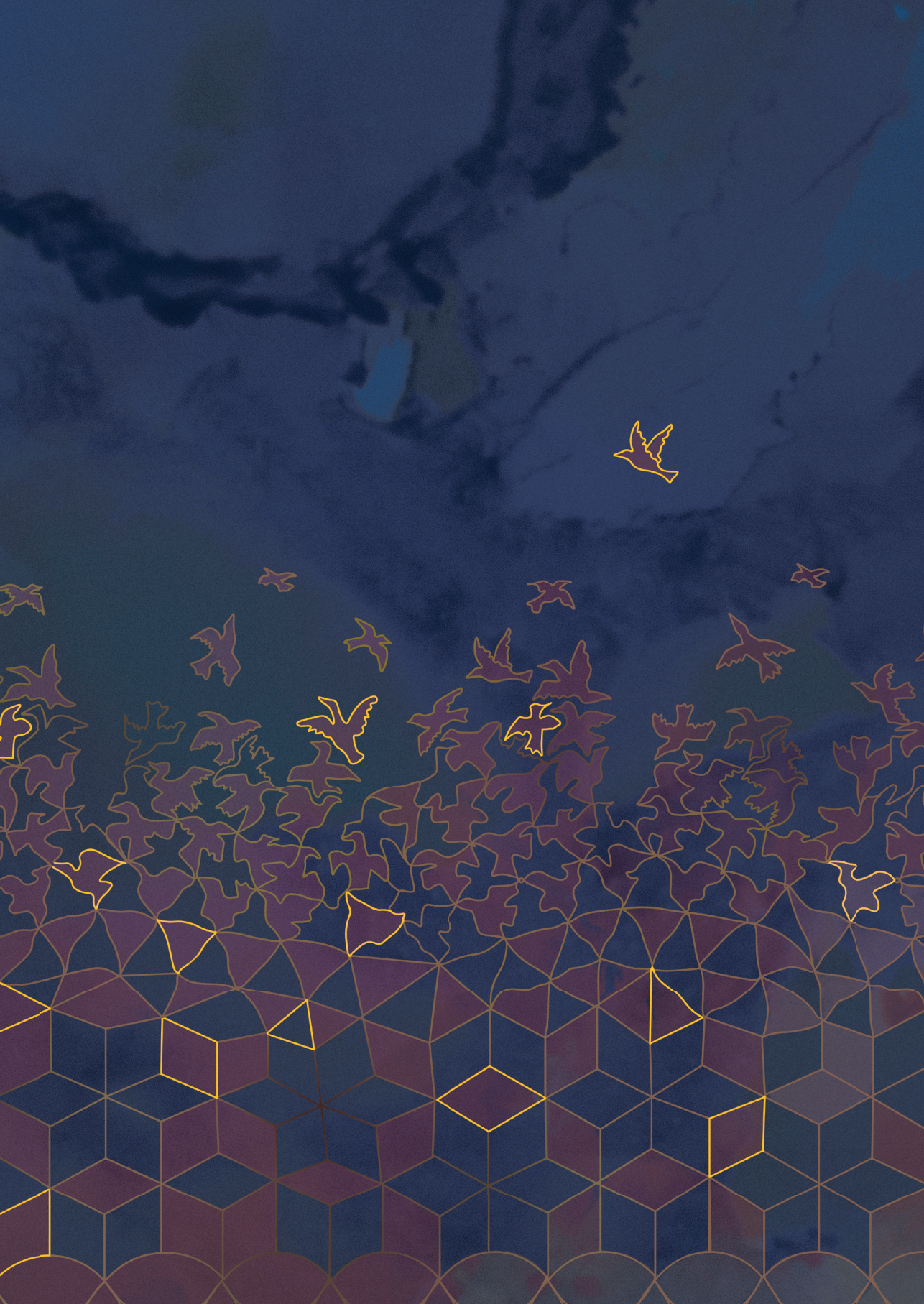
Other challenges lie in the practical use of ioECoG: how we visualize, interpret and record the signal. Visualization is determined largely by the chosen montage, the interpretation depends heavily on the clinician's experience, pre-surgical findings, and presumed underlying pathology. Recording is traditionally done by low-density grids, which may miss focal epileptiform activity. High-density grids have demonstrated their potential in research settings, but their clinical implementation introduces new challenges.

This thesis explores the potential of ioECoG beyond traditional visual interpretations and aims to contribute to more precise, efficient, and automated delineation of the epileptogenic zone. The work focuses on two complementary aspects: advanced signal analysis of ioECoG (Part I) and the interpretation of ioECoG and clinical implementation of high-density grids (Part II). Together, these efforts aim to support more accurate, reproducible, and data-driven surgical decision in epilepsy care.

Part I – Spikes to Spectra
The first part focuses on advanced analytic methodologies applied on ioECoG. **Chapter 2** explores the spatial and temporal characteristics of ripples and spikes in a seizure-free patient population with one particular underlying pathology: focal cortical dysplasia. In **chapter 3**, patients with focal cortical dysplasia (both seizure free patients and patients with recurring seizures) are included and we observe the variability of spectral entropy in epileptic tissue and the possibility to predict post-surgical outcomes. **Chapter 4** describes the use of explainable artificial intelligence of power spectra features in seizure free patients with a wide range of underlying pathologies.

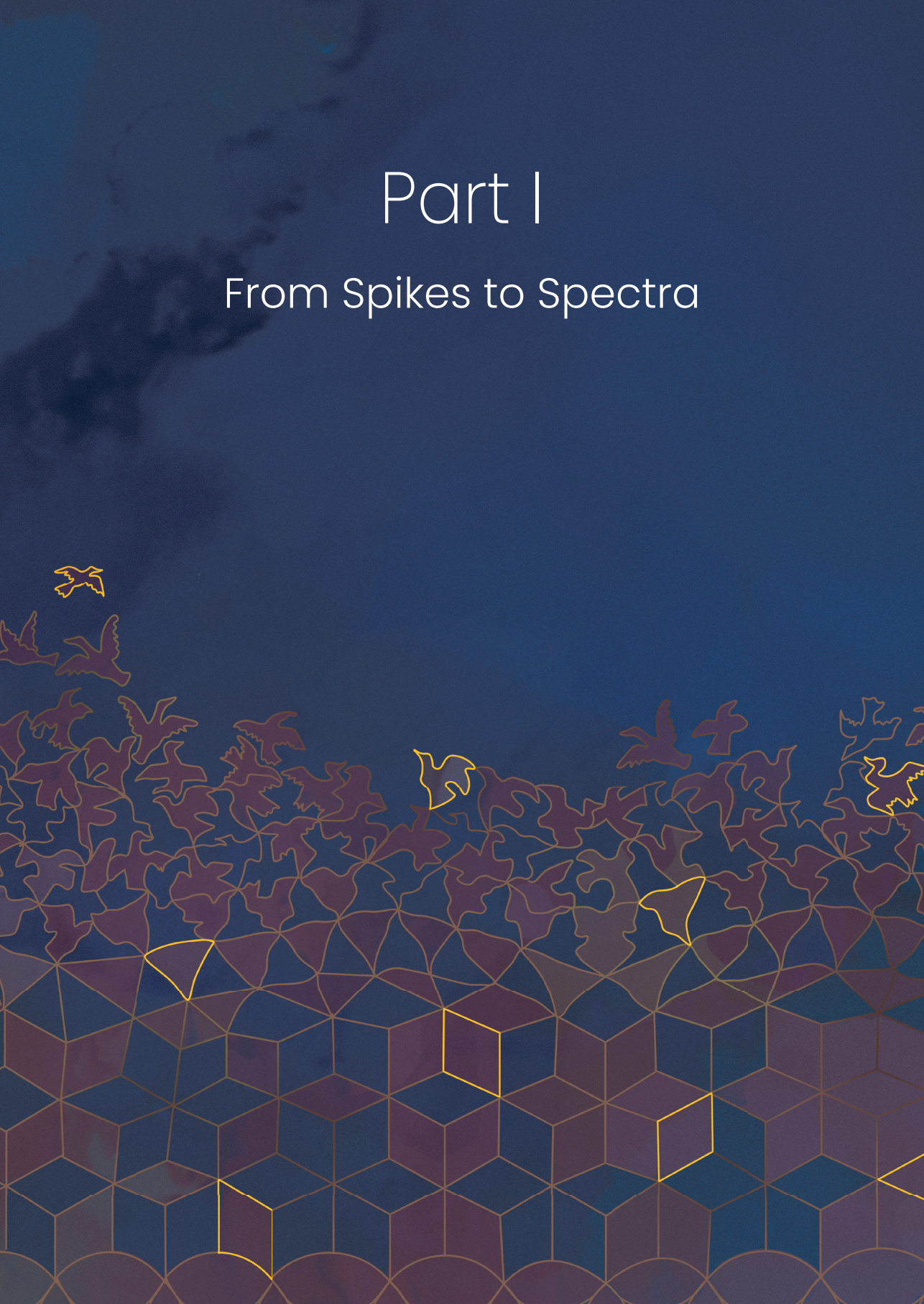
Part II – Interpretation to Innovation
The second part examines innovative intraoperative recording techniques aimed at improving interpretability and utility of ioECoG. **Chapter 5** describes a systematic evaluation of different montages to identify the most effective configuration for visualizing epileptic activity in intraoperative recordings. **Chapter 6** demonstrates that the distance between interictal activity recorded from the cortical surface and the MRI lesion is dependent on the specific pathology, emphasizing the importance of individualized interpretation strategies. **Chapter 7** presents the clinical implementation of high-density ioECoG grids and discusses their potential to increase spatial resolution, along with the associated technical and workflow-related challenges.

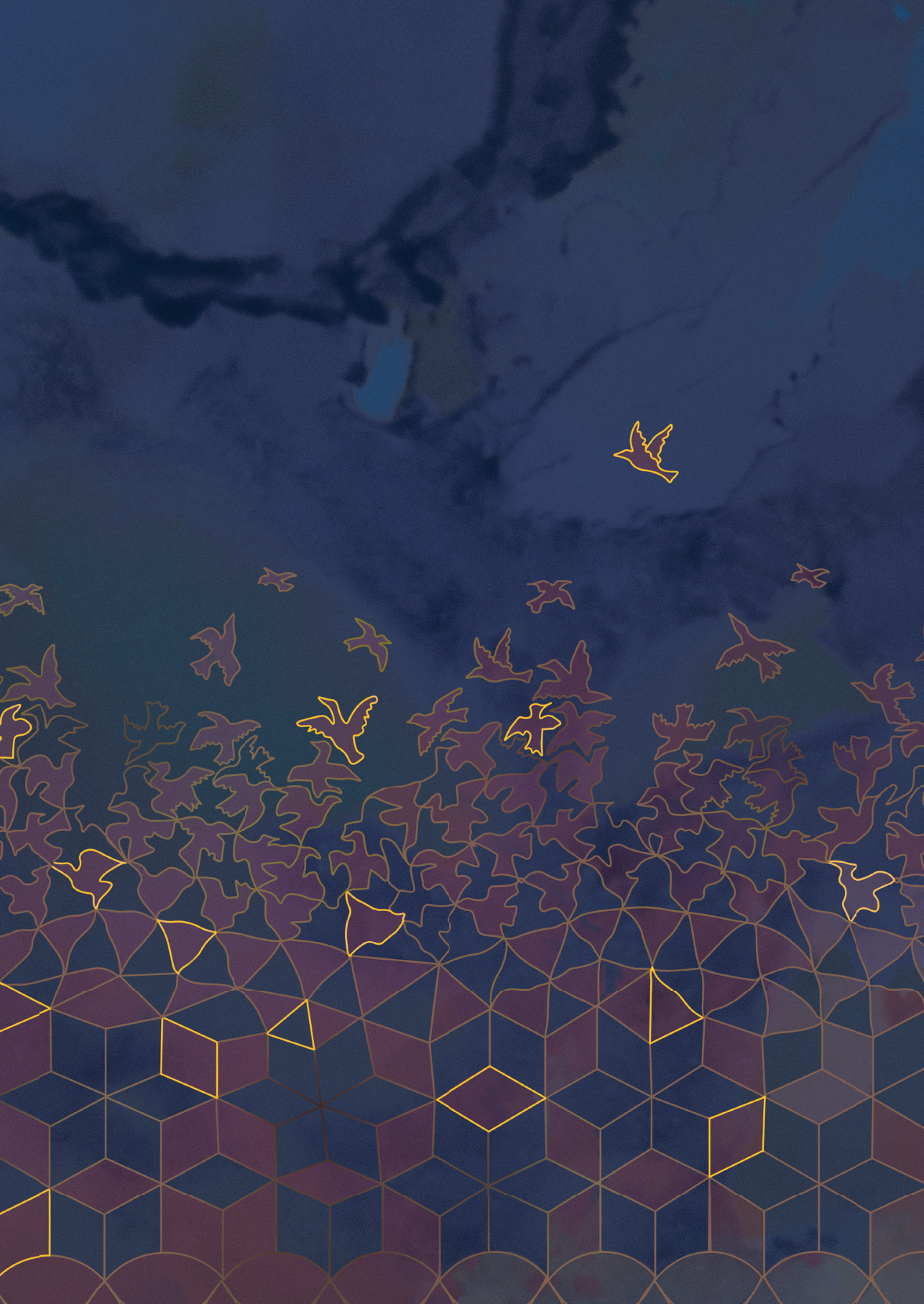
Chapter 8 summarizes the main findings of this thesis and discusses them from a clinical and technical perspective. The results highlight both the potential and the limitations of current biomarkers and intraoperative techniques in accurately guiding resection. Finally, directions for future research are proposed, with a focus on translating analytic advances into practical tools that support real-time clinical decision-making in epilepsy surgery.



Part I

From Spikes to Spectra





Chapter 2

Spatial and temporal properties of intraoperatively recorded spikes and high frequency oscillations in focal cortical dysplasia



Eline V. Schaft, Dongqing Sun, Maryse A. van 't Klooster, Dorien van Blooijs, Paul L. Smits, Willemiek J.E.M. Zweiphenning, Peter H. Gosselaar, Cyrille H. Ferrier, Maeike Zijlmans on behalf of the RESPect database study group

Published in Clinical Neurophysiology, Volume 162, June 2024

Abstract

Objective

Focal cortical dysplasias (FCD) are characterized by distinct interictal spike patterns and high frequency oscillations (HFOs; ripples: 80-250Hz; fast ripples: 250-500Hz) in the intraoperative electrocorticogram (ioECoG). We studied the temporal relation between intraoperative spikes and HFOs and their relation to resected tissue in people with FCD with a favorable outcome.

Methods

We included patients who underwent ioECoG-tailored epilepsy surgery with pathology confirmed FCD and long-term Engel IA outcome. Spikes and HFOs were automatically detected and visually checked in 1-minute pre-resection-ioECoG. Channels covering resected and non-resected tissue were compared using a logistic mixed model, assessing event numbers, co-occurrence ratios, and time-based properties.

Results

We found pre-resection spikes, ripples in respectively 21 and 20 out of 22 patients. Channels covering resected tissue showed high numbers of spikes and HFOs, and high ratios of co-occurring events. Spikes, especially with ripples, have a relatively sharp rising flank with a long descending flank and early ripple onset over resected tissue.

Conclusion

A combined analysis of event numbers, ratios, and temporal relationships between spikes and HFOs may aid identifying epileptic tissue in epilepsy surgery.

Significance

This study shows a promising method for clinically relevant properties of events, closely associated with FCD.

Introduction

Epilepsy occurs in about 65 million people worldwide.[29] Epilepsy surgery can cure focal epilepsy. intraoperative electrocorticography (ioECoG) might improve the surgical outcome by delineating epileptic tissue based on display of interictal biomarkers to guide the neurosurgery on the extent of the resection.[30] Although removal of all tissue showing interictal spikes has been related to good outcome, other research shows that seizure freedom is also achieved by incomplete removal of tissue showing spikes.[31,32] Residual high frequency oscillations (HFOs), a newly proposed biomarker, may predict seizure recurrence better than residual spikes.[33,34] HFOs are subdivided into ripples (80-250Hz) and fast ripples (FR; 250-500Hz). A recent double-blinded randomized-controlled trial demonstrated non-inferiority of HFOs to spikes in extra-temporal lobe epilepsies and not in temporal lobe epilepsies[14]. Co-occurring events, like ripples and fast ripples (FR) on spikes (RoS; FRoS) are thought to be more specific for the epileptogenic focus than spikes or HFOs on their own.[35,36] A study in scalp EEG suggests that RoS discriminate between clinically important sharper spikes and irrelevant propagating spikes.[37]

Focal cortical dysplasia (FCD), the underlying pathology in 20% of people with focal epilepsy, could generate characteristic electrophysiological patterns with continuous spiking. Alternatively, spikes can be completely absent.[38] HFOs are often prominently present in FCD and higher HFO rates occur in patients with FCD type II compared to FCD type I.[34,39,40] Epilepsy surgery is successful in about 62% of people with FCD.[41] Since the border of an FCD lesion can be hard to distinguish on MRI images, more knowledge is needed to delineate the extent of resection. Improving our understanding of the relation between HFOs and spikes might increase knowledge about which tissue to resect and, thus, increase surgery success. We investigated the spatial and temporal relations of intraoperative spikes and HFOs in people with FCD with a good post-surgical outcome. The aim of this study was to find distinctive differences between resected and non-resected tissue.

Methods

Patient selection

We retrospectively selected patients from the UMCU RESPect database[42], a database consisting of patients who underwent epilepsy surgery from 2008 till now. Patients were selected if they met the following inclusion criteria: 1) epilepsy surgery with pre-resection ioECoG (pre-ioECoG), 2) FCD pathology confirmed by histology, 3) seizure free (Engel IA) ≥1 year after surgery, allowing us to assume that all epileptogenic tissue was incorporated in the resected area. Exclusion criteria were: 1) participant in randomized control trial 'the HFO study' [14] 2) ioECoG sample frequency <1000Hz, 3) long-term ECoG or sEEG monitoring performed during pre-surgical work-up.

Our institutional ethics committee waived the need for informed consent for all retrospectively collected data before 2018 – as of 2018 informed consent is required and obtained – and approved the use of pseudonymized data in the RESPect database for the purpose of retrospective research.

Clinical information

We collected clinical characteristics, including sex, age at epilepsy onset, age at surgery, anti-epileptic drugs (AED) before and after surgery, side of the lesion (left/right), anatomical location of the lesion, from RESPect database electronic

data capturing system (Castor, Amsterdam, The Netherlands) – data originates from the electronic patient database (HiX, Chipsoft, Amsterdam, The Netherlands) –. Histology reports were screened, and we used the 2011 ILAE classification of FCD subtypes to classify pathology.[43] Post-surgical follow-up was performed by the treating neurologist on a yearly basis. Seizure outcome was classified by the Engel classification[8], and seizure freedom was defined as Engel IA. Seizure outcome at the longest follow-up, with a minimum of 1 year, was used.

Intraoperative ECoG recordings

ioECoG was recorded during surgery with a 2x4 grid, 4x5 grid and/or 1x8 strip (AD-Tech) placed directly on the cortex. The grids and strips had platinum electrodes, which were embedded in silicon, with a contact surface of 4.2 mm^2 and 10 mm inter-electrode distance. Recordings were made with a 64-channel EEG system (Systemplus, Micromed, Treviso, Italy) sampled at 1024Hz or 2048Hz using a common reference montage. During recordings, propofol anesthesia was temporarily paused to avoid burst-suppression patterns in the ioECoG and to avoid suppression of epileptic activity. To make reliable clinical decisions based on the ioECoG recording, we wait until the burst-suppression is gone and then we record for an additional 2-3 minutes. We selected the last minute of each recording to minimize the propofol effect, and thus burst-suppression, in the recordings. Included recordings were selected after cessation of burst-suppression patterns.[44,45] Multiple recordings were done by placing the grid on different locations on the cortex before (pre-ioECoG) and after the resection. Tailoring was based on interictal spikes in the ioECoG. Per patient, the following three data pre-processing steps were taken: 1) we selected the pre-ioECoG recording where the grid covered the resected and the non-resected tissue. We chose to select one grid location – including both resected and non-resected channels without taking into account anatomical location nor functional areas – instead of all available grid locations, because many patients have grids placed on multiple locations during pre-ioECoG recording outside the ultimately resected tissue. Including all these grid locations would have merely led to an increase in the number of non-resected channels, recorded in different time epochs, while we wanted to directly compare resected and non-resected channels. 2) we selected the last minute of the pre-ioECoG recording to limit bias due to burst suppression and 3) converted the data to the Brain Imaging Data Structure (BIDS) format.[42]

Channel labels

We matched the intraoperatively taken photos of the grid location on the cortical surface with a photo of the final resected tissue (Figure 1A). The researcher identified channels covering resected and non-resected tissue while being blinded for identified ioECoG events. Subsequently we labelled all the unipolar pre-resection grid channels as follows : 1.) *resected* (covering the resection), 2.) *edge* (within 5mm of the resection border), or 3.) *non-resected* (>5mm from the resection border). Bipolar labels, required for HFO analysis, were derived from the unipolar channel labels as follows (Figure 1B):

- *resected,* in case both channels were labeled resected, or one resected and the other on edge;
- *edge,* in case both channels were on edge, or one was on edge and the other non-resected, or one was resected and the other non-resected;
- *non-resected,* in case both channels were labeled non-resected.

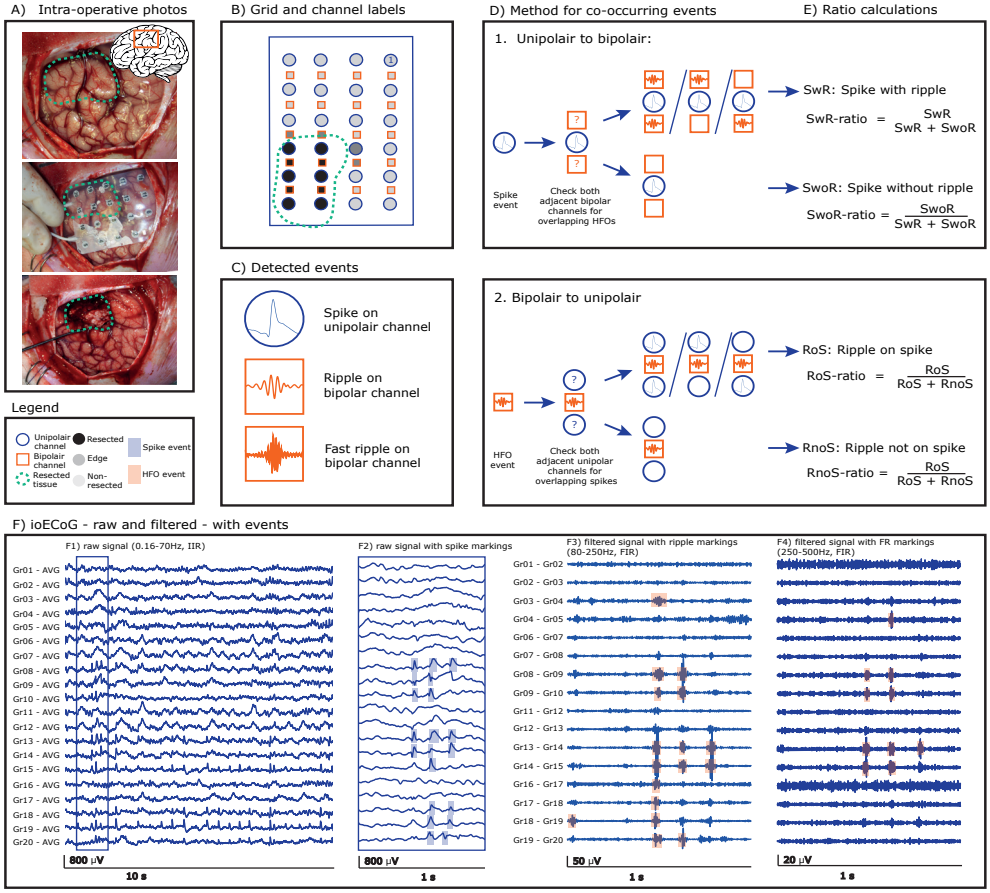


Figure 1: Method for channel labeling and event detection. A) intraoperative photos are used to determine channel positions and resected tissue. B) Visualization of the grid with unipolar and bipolar channels with channel labels for each channel: resected, edge or non-resected. Detected events are spike in unipolar channels, HFO (ripples and fast ripples) on bipolar channels. D) Visualization of the method to find co-occurring events for 1. Unipolar to bipolar (SwR as example) and 2. Bipolar to unipolar (RoS as example). Note that the number of unipolar channels is different from the number of bipolar channels and the number of spikes is different than the number of HFOs, which causes a different number of SwR and RoS. E) Equations of the calculation of the ratios per channel. F) Patient example (Pat. nr. 6, FCD subtype 2B) of raw and filtered ioECoG data; F1) Ten seconds of raw data in AVG montage (0-70Hz, IRR filtered) F2) Spike markings in one-second zoom of data in AVG montage (0-70Hz, IRR filtered). F3) Ripple markings in bipolar montage (80-250Hz FIR filtered), F4) FR markings in bipolar montage (250-500Hz FIR filtered).
Abbreviations: HFO = high frequency oscillation, SwR = spike co-occurring with a ripple, SwoR = spike not co-occurring with a ripple, RoS = ripple co-occurring with a spike, RnoS = ripples not co-occuring with a spike, ioECoG = intraoperative electrocorticography

Event detection

We used an algorithm[46] to automatically detect spikes and an HFO detector[13,47] to automatically detect ripples and FRs in Matlab 2021b (The MathWorks, Inc., Natick, Massachusetts, United States). We used a train set consisting of four patients from the total population to determine the required thresholds to optimize both detectors for our ioECoG data. A unipolar referential montage was used for spikes (settings: 0.16-80Hz IIR filter, 800µV amplitude, 15sec/page) and a bipolar montage for ripples (settings: 80-1000Hz FIR filter, 50µV amplitude, 1sec/page)

and FRs (250-1000Hz FIR filter, 20μV amplitude, 1sec/page). FR detection could not be performed in recordings with a sample frequency of 1024Hz and/or those recorded with an LTM 64 Express headbox (these yielded high-frequency noise). The output of the spike detector was the time point of the peak of the spike on the channel of occurrence per detected event. The output of the HFO detector included the start and end time on the channel of occurrence per detected HFO. All automatically detected events were visually checked in BrainQuick (Micromed, Treviso, Italy) by two expert reviewers (ES, MvtK). Missing (e.g., false negative) events were added and false positive detections were discarded.

We evaluated the following co-occurring events, defined as overlap in time of occurrence: spikes with ripples (SwR), spikes with FRs (SwFR) ripples on spikes (RoS), and FRs on spikes (FRoS). We calculated the events not occurring with another event by subtracting the number of co-occurring events from the total number of events. This resulted in spikes without ripples (SwoR), spikes without FRs (SwoFR), ripples not on spikes (RnoS), and FRs not on spikes (FRnoS). We checked unipolar channels for spikes and their co-occurrence with the HFO on the adjacent bipolar channels (Figure 1D). In case of two unipolar spikes that co-occurred during the same bipolar HFO, the first in time occurring spike was considered most relevant and was therefore used. SwR/spike- and SwoR/spike-ratios per unipolar channel were calculated by: SwR / (SwR + SwoR) per channel and SwoR / (SwR + SwoR) per channel (Figure 1E). RoS/ripple- and RnoS/ripple-ratios per bipolar channel were calculated by: RoS / (RoS + RnoS) per channel and RnoS / (RoS + RnoS) per channel.

Event timing

We visually marked the start time, end time, and time of the maximum for all spikes. We calculated time-based properties of the spike: the duration of the spike – defined as the time between the start of the spike and the end of the spike –, the duration of the rising flank – defined as the time between the start of the spike and the peak –, and the duration of the descending flank – defined as the time between the peak and the end of the spike –. We calculated time-based properties of the HFOs: the duration of HFOs – defined as the time between the start and the end time –. We calculated time-based properties of the co-occurring events: the percentages of co-occurring HFOs before the onset of spike, on the rising flank, on the descending flank and after the spike offset.

Statistical analysis

Medians and interquartile ranges (IQR) were calculated for continuous variables. We calculated the following spatial properties: the total number of events (spikes, ripples, FR, RoS, RnoS, FRoS, FRnoS) on channels covering resected and non-resected tissue and the median and IQR of number of events per channel. We compared total numbers, spike- and ripple-ratios and time-based properties between all channels covering resected and non-resected tissue using a logistic mixed model:

$$log(resection_{patient}) = \alpha + \beta x_{property} + \alpha_{patient} + \gamma_{patient} x_{property} + \delta_{patient} electrode + \varepsilon_{patient}$$

$resection_{patient}$ was the binary dependent variable (resected / non-resected), $x_{property}$ the spatial or time-based property, α the fixed intercept, β the average relation between the dependent variable and the $x_{property}$. $\alpha_{patient}$ and $\gamma_{patient} x_{property}$ represented the random intercept and slope for each patient. The random

effect ($\delta_{patient}electrode$) was added when analyzing time-based properties. $\varepsilon_{patient}$ represented the residuals. We performed subgroup analyses, only when ≥ 10 patients, for anatomical location of the resection and FCD subtypes using afore mentioned statistics. Statistics were performed in RStudio 2021.09.1 (R Core Team, 2021). We considered a p-value <0.05 as significant. We corrected for multiple comparison by the false discovery rate (FDR) method.[48]

Patient-wise tailoring

We evaluated the clinical usability of the analyzed event detections and time-based properties, per patient. For all properties in which we found a difference between the resected and non-resected tissue at group level, we calculated the differences per patient. If the directionality of the difference matched the direction at group level, it was a matching property for that patient. For example; number of RoS is positively associated with resected tissue, for each patient with a positive association between RoS and resected tissue, this is a matching property. Subsequently, we calculated the percentage of matching properties per patient and the percentage of patients with a match for each property.

Results

Clinical characteristics

A total of 22 patients (9 female) met the inclusion criteria. Median age at surgery was 14 (range 0-55), median age at epilepsy onset was 2 years (range 0-20 years). Two patients used AED after surgery, the rest was seizure free (Engel IA) with complete AED withdrawal. The anatomical region of the resection was frontal in ten, parietal in five and temporal in seven patients. Four temporal lobe resections included hippocampectomies, but histopathology revealed no hippocampal abnormalities. Based on histopathology results, two patients had FCD subtype 1A, six had FCD subtype 2A, 14 had FCD subtype 2B (Table 1).

Event numbers

A total of 3344 spikes were found in 21 out of 22 patients, in 291 out of 416 unipolar channels (11 (4) spikes per channel in resected tissue and 1.5 (5) in non-resected tissue). SwR, 20% of all spikes, were found in 19 out of 22 patients, in 78 out of 416 channels (0 (1) SwR per channel in resected tissue and 0 (0) in non-resected tissue). SwoR , 80% of all spikes, were found in 21 out of 22 patients, in 286 out of 416 channels (3 (8) SwoR per channel in resected tissue and 1 (5) in non-resected tissue). A total of 1296 ripples were found in 20 out of 22 patients, in 134 out of 321 bipolar channels (0 (5) ripples per channel in resected tissue and 0 (1) in non-resected tissue). RoS ,77% of total number of ripples, were found in 20 out of 22 patients, in 97 out of 321 channels (0 (2) RoS per channel in resected tissue and 0 (0) in non-resected tissue). RnoS, 23% of total number of ripples, were found in 19 out of 22 patients, in 95 out of 321 channels (0 (1) RnoS per channel in resected tissue and 0 (0) in non-resected tissue).

Differences between the number of events in channels covering resected and non-resected can be found in Table 2. A positive association was found between resected tissue and total numbers of events for all events (spikes: β=0.042, p=.008; SwR: β=0.200, p<.001; SwoR: β=0.046, p=.01; ripples: β=0.037, p<.001; RoS: β=0.036, p<.001; RnoS: β=0.073, p=.006) (Figure 2). A positive association was found between resected tissue and the SwR/spike- and RoS/ripple-ratios, and a negative association for SwoR/spike- and RnoS/ripple-ratio (SwR/spike-ratio: β=5.051, p<.001; RoS/ripple-ratio: β=0.036, p<.001; SwoR/spike-ratio: β=-0.232, p<.001; RnoS/ripple ratio: β=-1.249, p<.001).

FR detection could not be performed in eleven patients (three with sample frequency of 1024Hz, eight with LTM64 headbox). A total of 214 FR were found in seven out of the eleven analyzed patients, in 21 out of 182 channels. These eleven patients and channels were included in further analysis. All FRs were found in resected channels. FRoS and FRoR were found in all seven patients with FRs. 94% of FRs co-occurred with spikes. Of these, on average 76% of the fast ripple span preceded the spike peaks (Figure 3). Subsequent mixed model statistics could not be performed due to low FR counts.

Table 1: Clinical characteristics per patient: age at surgery, age at epilepsy onset, anti-epileptic drugs (AED) used before and after surgery, sex, anatomical location of the surgery, FCD subtype, mean number of events per channel in resected and non-resected tissue.

									Resected tissue					Non-resected tissue			
Pat.nr	**Surgery age**	**Onset age**	**AED before**	**AED after**	**Sex**	**Locati-on**	**Side**	**FCD type**	**Spikes**	**SwR**	**Ripples**	**RoS**	**FR**	**Spikes**	**SwR**	**Ripples**	**RoS**
Pat. 1	12	11	CLB, LEV, OXC	No AED	F	Frontal	L	2A	8,60	0,50	1,38	0,80	0,63	11,13	0,00	0,25	0,00
Pat. 2	41	0	CLB,CBZ,TPM	No AED	M	Frontal	R	2B	0,50	0,00	0,00	0,00	0,00	0,93	0,00	0,00	0,00
Pat. 3	8	0	LEV	No AED	M	Frontal	L	2A	3,05	0,16	0,94	0,11	*NA*	2,60	0,00	6,25	0,20
Pat. 4	21	18	CLB,CBZ,LEV,LTG,TPM	No AED	F	Temporal	R	2B	2,57	0,50	1,13	1,00	*NA*	4,25	1,25	3,00	1,63
Pat. 5	17	10	CLB,LEV,LTG	No AED	F	Frontal	R	2A	4,25	0,00	0,50	0,00	*NA*	8,58	0,00	0,42	0,25
Pat. 6	14	1	LTG,VPA	No AED	M	Frontal	R	2B	35,25	16,50	28,82	18,67	5,82	4,77	0,62	2,30	0,69
Pat. 7	1	0	CBZ,LEV,VPA	LEV	F	Frontal	R	2A	4,40	0,10	1,45	0,30	*NA*	7,00	0,33	1,67	0,67
Pat. 8	17	12	LTG,OXC	No AED	M	Parietal	R	2B	78,75	67,00	56,83	76,25	19,83	3,13	1,31	1,30	0,31
Pat. 9	13	3	CLB,CBZ	No AED	M	Frontal	R	2B	0,43	0,00	0,13	0,00	0,00	0,10	0,10	0,09	0,07
Pat. 10	10	4	OXC,VPA	No AED	F	Temporal	R	2B	3,50	0,50	0,25	0,25	*NA*	14,70	0,00	0,38	0,10
Pat. 11	14	5	CBZ	No AED	M	Frontal	L	2B	0,00	0,00	0,33	0,17	*NA*	4,64	0,36	0,90	0,36
Pat. 12	16	12	OXC	No AED	M	Parietal	R	2B	46,67	4,00	3,40	5,33	*NA*	5,27	0,33	0,73	0,27
Pat. 13	11	1	LTG,OXC	No AED	F	Temporal	R	2B	9,74	6,16	6,05	5,11	1,05	4,00	0,00	2,00	0,00
Pat. 14	55	0	LTG,VPA	No AED	M	Temporal	R	1A	5,90	0,60	0,40	0,40	0,00	1,00	0,00	0,00	0,00
Pat. 15	0	0	CBZ,LEV,VGB	VGB	M	Parietal	L	2B	24,17	4,33	5,13	6,67	*NA*	11,85	1,54	1,88	1,15
Pat. 16	3	1	CBZ	No AED	F	Frontal	R	1A	5,00	0,25	0,67	0,50	*NA*	4,20	0,07	1,33	0,47
Pat. 17	3	1	LEV	No AED	M	Frontal	R	2B	4,67	1,33	4,17	1,83	*NA*	9,00	0,38	0,70	0,38
Pat. 18	17	1	CLB,LCM,PER	No AED	F	Parietal	L	2B	61,00	31,00	38,33	56,50	5,00	8,06	3,76	0,62	0,41
Pat. 19	9	1	CLB,OXC	No AED	F	Temporal	R	2B	3,88	0,75	1,88	1,88	0,38	4,82	1,45	1,13	0,64
Pat. 20	47	3	CBZ,LTG,PER	No AED	M	Temporal	R	2A	0,00	0,00	0,00	0,00	*NA*	0,00	0,00	0,00	0,00
Pat. 21	45	20	BZT,CLB,CBZ,LCM	No AED	M	Parietal	R	2A	5,00	1,29	1,88	0,71	0,00	1,00	0,00	0,29	0,00
Pat. 22	25	9	LTG	No AED	M	Temporal	R	2B	6,71	1,50	1,26	1,08	0,35	5,25	0,00	0,00	0,00

Abbreviations: AED = anti-epileptic drugs, BVT = brivaracetam, CLB = clobazam, CBZ = carbamazepine, LCM = lacosamide, LEV = levetiracetam, LTG = lamotrigine, OXC = oxcarabazepine, PER = perampanel, TPM = topiramate, VGB = vigabatrin, VPA = vaproic acid, Pat.nr. = patient number, F = female, M = male, NA = not available, L = left, R = right, SwR: spike co-occurring with ripple RoS = ripple co-occurring with spike, FR = fast ripple

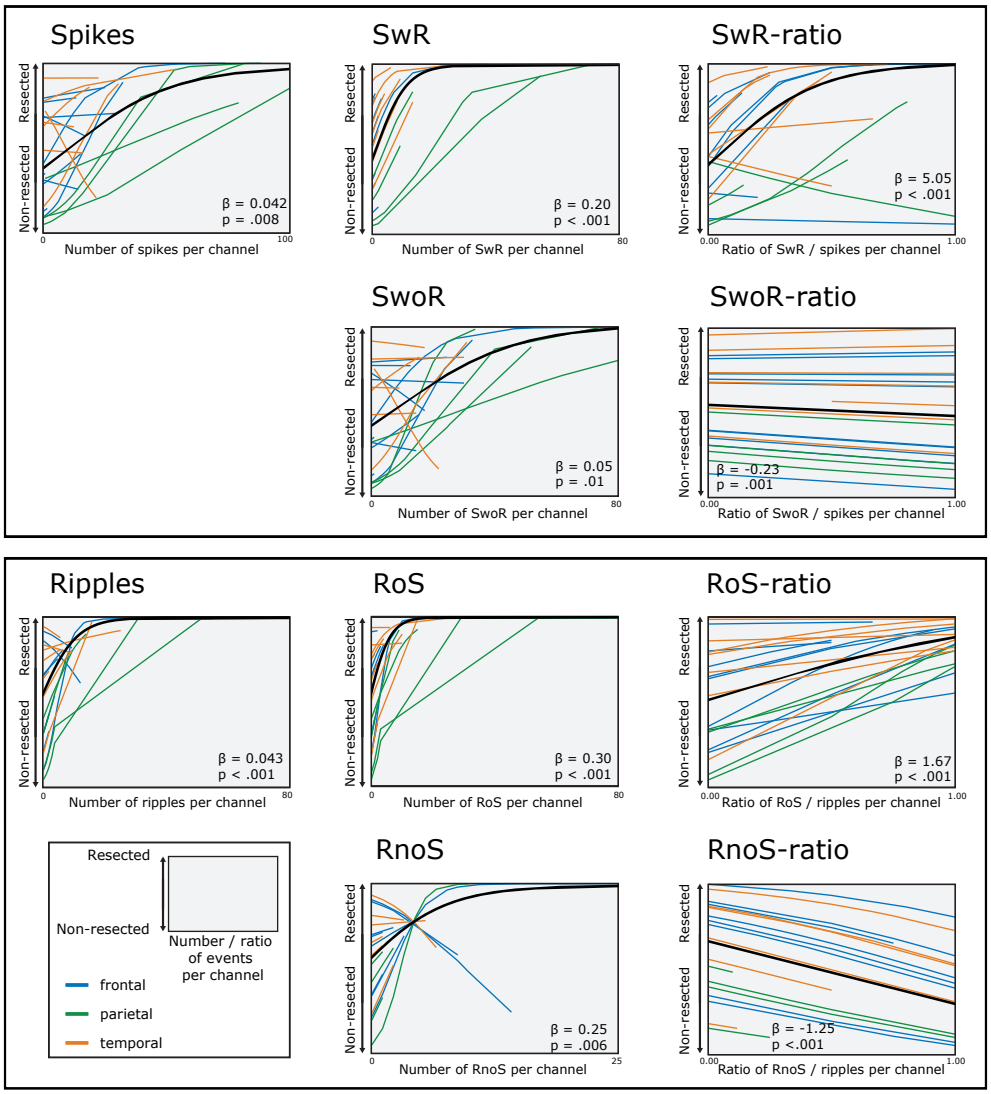


Figure 2: Relation between total number of events or ratio and resected tissue. Colored lines are the patient specific logistic regression lines. The bold black line represents the fixed effect of the model. The fixed coefficient β represents the average relation between the dependent variable and resected channels. What can be seen is that especially the ratio of ripples on spikes compared to all ripples and the ratio of ripples not on spikes compared to all ripples are related to resected/non-resected channels in all individual patients. p-values are the FDR adjusted p-values. Abbreviations: RoS = ripples co-occurring with a spike, RoS-ratio = RoS / ripples per channel, RnoS = ripples not co-occurring with a spike, RnoS-ratio = RnoS / ripples per channel.

Event timing

The differences in total durations of spikes and the rising and descending flanks of spikes can be found in Table 3. For all spikes, a non-significant negative trend was observed between the duration of the rising flank and resected tissue (β=-12.07, p=.07), and a positive association was seen between the descending flank and resected tissue (β=17.41, p<.001). For SwR, a negative association was observed between resected tissue and total duration (β=-75.97, p<.001) and duration of the rising flank (β=-102.77, p<.001). A positive association was observed between resected tissue and duration of the descending flank (β=11.88, p<.001). Comparing SwR and SwoR, we found a shorter total duration (Wilcoxon, p<.001) and shorter duration of the rising flank (Wilcoxon, p<.001) in SwR than SwoR. No difference was observed for the duration of the descending flank in SwR and SwoR (Wilcoxon, p=.47).

The median duration of ripples was 47.0 (21.0) ms in resected and 44.0 (18.8) ms in non-resected tissue (β=3.85, p=.70; Table 3). The duration of RoS was longer than the duration of RnoS (Wilcoxon, p<.001). A positive association was observed between resected tissue and the start time of the ripple minus the start time of the spike (β=5.25, p<.001). A positive association was observed for the duration of RoS and resected tissue (β=3.63, p=.008), while a negative association was observed for the duration of RnoS and resected tissue (β=-5.71, p<.001). The averaged time span of ripples preceded the spike peak with 62% for the resected and 56% for the non-resected tissue (Figure 3). A positive trend was observed between resected tissue and percentage of the ripple before the spike started, while a negative association was observed between resected tissue and percentage of the ripple after the spike ended.

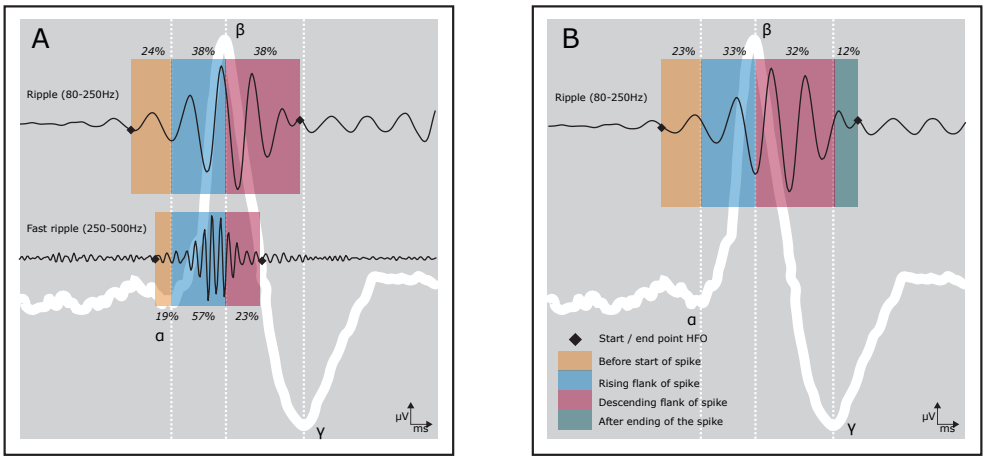


Figure 3: The averaged percentages of the time span of the ripple (top) and fast ripple (bottom) with respect to the time span of the co-occurring spike. A) resected tissue, B) non-resected tissue. Note that there were no fast ripples present in non-resected tissue.
Abbreviations: α = start of the spike, β = peak of the spike, γ = end of the spike. HFO = high frequency oscillation.

Table 2: Logistic mixed model results for the analysis of the total population and subgroup analysis frontal lobe and FCD 2B. Light grey box: positive significant association between resected channels and property. Dark grey box: negative significant association between resected channels and properties. β is the fixed effect of the mixed model for that type of event. p-values are the FDR adjusted p-values.

		Spikes	SwR	SwR ratio	SwoR	SwoR ratio	Ripples	RoS	RoS ratio	RnoS	RnoS ratio
Total population (n = 22)	Resected	11 (4)	0 (1)	0 (0.06)	3 (8)	0.64 (0.43)	0 (5)	0 (2)	0 (0.75)	0 (1)	0 (0.14)
	Non-resected	1.5 (5)	0 (0)	0 (0)	1 (5)	0.61 (0.47)	0 (1)	0 (0)	0 (0)	0 (0)	0 (0)
	Mixed model (β , p-value)	β = 0.042 p = .008	β = 0.20 p < .001	β = 5.05 p < .001	β = 0.05 p = .01	β = -0.23 p = .0011	β = 0.043 p < .001	β = 0.30 p < .001	β = 1.67 p < .001	β = 0.25 p = .006	β = -1.25 p < .001
Anatomical location Frontal (n = 10)	Resected	3 (9)	0 (0)	0 (0)	2 (8)	0.58 (0.46)	0 (4)	0 (1.25)	0 (0.5)	0 (2)	0 (0.5)
	Non-resected	1 (4.5)	0 (0)	0 (0)	1 (4)	0.50 (0.50)	0 (1)	0 (0)	0 (0)	0 (1)	0 (0.5)
	Mixed model (β , p-value)	β = 0.06 p = .003	β = 2.66 p = .05	β = 24.68 p = .03	β = 0.05 p = .009	β = -0.36 p = .009	β = 0.16 p = .03	β = 0.78 p < .001	β = 2.37 p < .001	β = 0.24 p = .03	β = -1.50 p < .001
FCD subtype 2B (n = 14)	Resected	4 (11)	0 (2)	0 (0.26)	3 (10)	0.58 (0.42)	1 (7.5)	0 (5.5)	0 (0.88)	0 (2)	0 (0.2)
	Non-resected	1 (6)	0 (0)	0 (0)	1 (5)	0.56 (0.47)	0 (1)	0 (0)	0 (0)	0 (0)	0 (0)
	Mixed model (β , p-value)	β = 0.02 p = 0.48	β = 0.16 p < .001	β = 2.97 p = .006	β = 0.03 p = .42	β = -0.27 p = .10	β = 0.16 p < .001	β = 0.28 p < .001	β = 1.57 p < .001	β = 0.39 p < .001	β = -0.70 p < .001

Abbreviations: SwR = spike co-occurring with ripples, SwR ratio = SwR / spikes per channel, SwoR = spikes not co-occurring with ripple, SwoR ratio = SwoR / spikes per channel, RoS = ripples co-occurring with a spike, RoS ratio = RoS / ripples per channel, RnoS = ripples not co-occurring with a spike, RnoS = RnoS / ripples per channel.

Subgroup analysis

Event numbers

Subgroup analysis for anatomical location (10 frontal lobe epilepsies) showed merely the same results as the total population: a positive association between resected tissue and total number of spikes, SwR (trend), SwR/spike-ratio, SwoR, ripples, RoS, RoS/ripple-ratio, and RnoS and a negative association between resected channels and SwoR/spike-ratio and RnoS/ripple-ratio. (Table 2) For 14 patients with FCD subtype 2B, we found a positive association between resected tissue and SwR, SwR/spike ratio, ripples, RoS, RoS/ripple-ratio, and a negative association for RnoS.

Event timing

Subgroup analysis of anatomical location frontal lobe epilepsy (N=10) showed results that were different from the total populations: significantly negative associations between resected tissue and the duration of the rising flank of all spikes, the duration of ripples and the duration of RnoS. The associations for the durations of SwR that were all in a different direction compared to the total population (Table 3). Subgroup analysis for FCD subtype 2B (N= 14) were mostly alike the total group, showing a negative association between resected tissue and total durations of SwR and RoS, and the duration of the rising flank of SwR, while a positive association was found for descending flank of SwR, the total duration of RnoS and the start time of the ripple minus the start time of the spike. (Table 3).

Patient-wise tailoring

The properties used to evaluate clinical per-patient usability were the total number of spikes, SwR, SwoR, RoS/ripple-ratio, RnoS/ripple-ratio, duration of the rising flank of spike, duration of the descending flank of spike, duration of RoS, duration of RnoS, and the time between the start of the ripple and the peak of the spike. The highest percentage of matching properties per patient was 90.0% (Median: 40%, IQR: 28%)). 14 out of 22 patients had at least four matching properties. In 20 patients (91%) we found at least one matching property. The percentage of patients with a match was highest for RoS/ripple-ratio (14 patients; 64%).

Table 3: Logistic mixed model results for the analysis of the total population and subgroup analysis frontal lobe and FCD 2B. Light grey box: positive significant association between resected channels and property. Dark grey box: negative significant association between resected channels and properties. β is the fixed effect of the mixed model for that time-based property. p-values are the FDR adjusted p-values.

		Spikes			SwR			SwoR			Ripples	RoS		RnoS
		Total duration	Rising flank duration	Descending flank duration	Total duration	Rising flank duration	Descending flank duration	Total duration	Rising flank duration	Descending flank duration	Total duration	Total duration	Start time ripple - time peak	Total duration
Total population (n = 22)	Resected	54.1 (19.9)	20.7 (10.3)	32.1 (15.4)	49.7 (22.7)	15.9 (10.7)	32.1 (18.6)	55.7 (17.8)	21.9 (9.3)	32.1 (14.8)	47.0 (21.0)	48.5 (22.5)	-28.9 (18.0)	40.5 (15.5)
	Non-resected	54.3 (19.1)	22.4 (10.9)	30.3 (14.6)	46.9 (24.0)	17.2 (10.4)	25.2 (20.4)	54.9 (19.0)	22.9 (10.6)	30.4 (14.0)	44.0 (18.8)	47.9 (25)	-29.1 (21.9)	42.5 (13.0)
	Mixed model (β , p-value)	β=4.05 p=.69	β=-12.07 p=.11	β=17.41 p<.001	β=-75.97 p<.001	β=-102.77 p < .001	β=11.88 p<.001	β=5.11 p=.47	β=-8.50 p=.09	β=16.48 p=.09	β=3.85 p=.70	β=3.63 p=.008	β=5.25 p<.001	β=-5.71 p<.001
Anatomical location Frontal (n = 10)	Resected	57.17 (15.47)	22.50 (9.47)	33.15 (13.34)	56.83 (23.68)	21.31 (10.66)	35.52 (13.57)	57.19 (15.38)	22.50 (8.45)	31.97 (13.12)	42.8 (12.5)	44.0 (13.0)	-34.0 (12.9)	40.5 (10.5)
	Non-resected	56.27 (17.37)	23.68 (9.86)	30.28 (13.48)	50.91 (20.44)	18.78 (11.93)	27.23 (16.52)	56.27 (16.99)	23.82 (9.67)	30.28 (13.37)	42.0 (13.8)	42.0 (14.0)	-26.9 (17.5)	41.5 (13.0)
	Mixed model (β , p-value)	β=-6.34 p =.75	β=-21.00 p<.001	β=3.33 p=.83	β=90.32 p<.001	β=271.40 p<.001	β=-278.00 p<.001	β=-0.70 p=.96	β=-15.32 p<.001	β=6.38 p=.74	β=-45.11 p<.001	β=20.92 p=.47	β=9.60 p=.17	β=-34.61 p<.001
FCD subtype 2B (n = 14)	Resected	53.66 (19.08)	19.54 (10.79)	32.80 (15.46)	49.7 (23.07)	15.88 (10.35)	31.97 (18.66)	55.14 (17.66)	21.31 (9.12)	32.80 (14.19)	47.0 (20.8)	48.0 (21.9)	-28.7 (18.0)	42.5 (13.0)
	Non-resected	53.59 (20.18)	22.15 (11.12)	29.77 (15.06)	46.72 (23.91)	17.00 (10.32)	24.86 (21.09)	54.06 (19.48)	22.53 (10.84)	30.30 (14.06)	45.0 (23.2)	51.0 (23.5)	-29.8 (24.4)	39.0 (13.5)
	Mixed model (β , p-value)	β=-4.64 p=.71	β=-23.66 p=.12	β=13.50 p=.39	β=-51.90 p=.02	β=-89.86 p=.009	β=16.70 p<.001	β=-4.68 p=.69	β=-21.04 p=.06	β=10.92 p=.47	β=8.33 p=.15	β=3.41 p<.001	β=3.46 p=.01	β=27.21 p<.001

Abbreviations: SwR = spike co-occurring with ripples, SwoR = spikes not co-occurring with ripple, RoS = ripples co-occurring with a spike, RnoS = ripples not co-occurring with a spike.

Discussion

A combination of spatial and time-based properties of ripples co-occurring with spikes, seems to distinguish best between resected and non-resected tissue in people with FCD. Where other research focuses on the individual numbers of HFOs[34,39,49], we concentrate on the number and time-relations of ripples co-occurring with spikes. Van Klink et al.[37] demonstrated a first time-relation between ripples and spikes in scalp EEG and Shi et al.[50] showed that the majority of spike ripples were removed in implanted intracranial EEG. We are the first to explore this phenomenon in ioECoG recordings in patients with FCD. We found more RoS, earlier starts of the ripples co-occurring with the spikes, and longer ripple durations in resected tissue compared to non-resected tissue. We found that non-resected tissue contained higher SwoR/spike-ratio and RnoS/ripple-ratio than resected tissue. Subgroup analysis revealed that these properties are clearly distinctive in patients with FCD subtype 2B. These results suggest that combining spikes and HFO properties can help delineate resected tissue, which could help to achieve seizure freedom in people with FCD.

This study emphasizes the importance of the rising flank of the spikes with a co-occurring ripple. RoS occurred earlier on the spike in resected tissue compared to non-resected tissue. The morphology of the spike can be explained by the duration of rising and descending flank. Building on literature acknowledging distinct morphologies[51], our findings align with shorter rising and longer descending flanks in resected tissue, i.e. sharper spikes are more specific for the epileptogenic zone. The earlier manifestation of RoS within resected tissue, prompts a hypothesis that ripples and spikes originate from independent neural networks[52]. The temporal disparity between resected and non-resected tissue may be attributed to the faster spread of spikes. While spreading dynamics were not explicitly explored, this avenue holds promise for future investigations into underlying neurobiological mechanisms. While most research on RoS was conducted in scalp EEG[35,36], one study in intracranial stereo-EEG similarly showed that RoS have a higher correlation with seizure onset zone (SOZ) than ripples or spikes alone.[53] A study on ictal onset patterns suggested that spikes preceded by FR occur more often in the SOZ.[54] A post-hoc analysis confirmed that 13 out of 17 FRnoS precede a spike within 300ms. Another post-hoc analysis showed that all FR co-occur with a ripple within 100ms. Thus, spikes superimposed simultaneously with ripples and FR provide no additional information to SwFR.

It is often indicated in literature[51] that RnoS should be considered as physiological and have a longer duration than pathological ripples. We found a negative association between resected tissue and RnoS/ripples-ratio. In other words, the more RnoS were seen compared to RoS in one channel, the more likely it is that the tissue underneath that channels was non-resected. We found longer durations of RoS than RnoS. This contrasts with the assumption that RnoS are physiological ripples and have a longer duration. The RnoS were shorter in resected tissue than in non-resected tissue and part of RnoS might thus be pathological ripples as well.[55] The process of selecting both resected and non-resected tissue was deliberately conducted without being influenced by any knowledge of anatomical location or functional areas, but researchers could not be totally blinded. While we aimed to minimize biases associated with these factors, it is important to acknowledge that our data selection methodology may have inadvertently introduced biases in the pursuit of achieving statistical significance.

In all patients with FCD type 2B that were included for analyzing FR, FR were present. We found low numbers of ripples and no FR in patients with FCD type 1A. These results are similar to findings in long-term intracranial EEG, where higher numbers of HFOs were found in FCD types 2 than FCD types 1.[39] It is important to note that our study cohort includes a limited number of patients with FCD type 1, which might impact the generalizability of this comparison. A study by Abdijadid et al.[56] investigating the mechanisms of epileptogenisis and its electrographic correlates, in FCD type I and II, demonstrated that not the balloon cells, but the dysmorphic and immature neurons play a crucial role in initiation and spread of epileptic spikes. It is interesting what the role of these neurons play in the initiation and spread of HFOs. The lack of specific histological findings beneath each electrode in this retrospective study hinders this extra analysis. Our intraoperative recordings, and thereby potentially also the number of HFO events, were influenced by propofol anesthesia. Anesthesia reduces the number of HFOs in comparison to HFOs during non-REM sleep, while it does not reduce the number of interictal spikes.[44,57] This could explain the fewer occurrences of HFOs, compared to other long-term intracranial studies.[39,58]

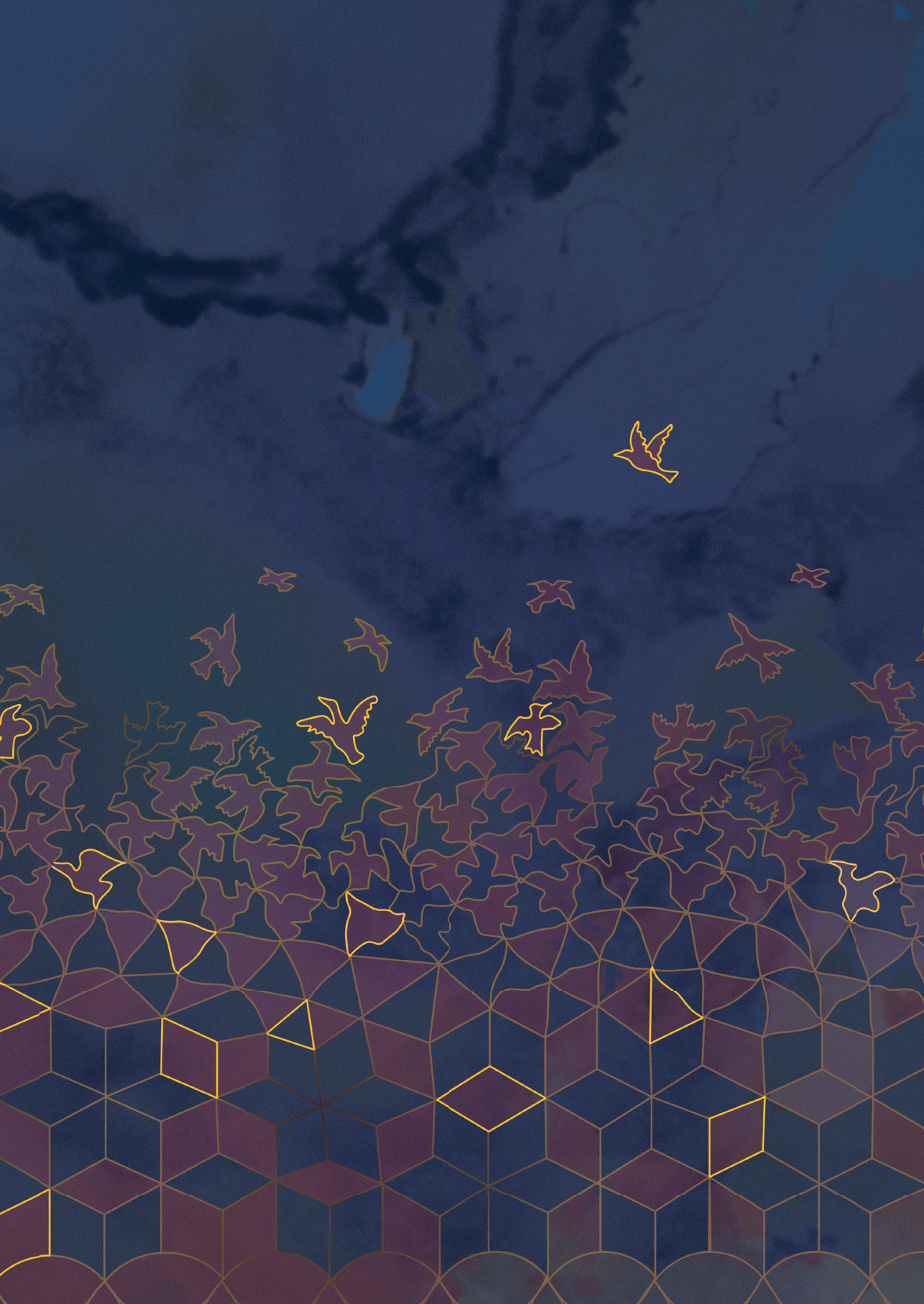
Whereas in most intracranial EEG studies the events are compared to the SOZ, we compared the events to the resected tissue. Labelling the SOZ requires ictal information and subject to non-objective interpretation by the epileptologists, and it's value as gold standard is debated as complete removal of SOZ tissue is no guaranty for seizure freedom.[59] Similar to the rationale of Cimbalnik et al.[60] we labeled resected tissue as epileptic tissue, which represents the most practical method to label epileptic tissue in our study population in absence of SOZ information. By selecting a population based on a strict definition of seizure freedom, we assumed that all epileptic tissue was incorporated in the resected tissue. A consequence of this choice is that resected tissue might contain both epileptogenic and non-epileptogenic tissue. Channels could be labeled as resected, even if there is no epileptogenic tissue underneath. This inclusion of resected non-epileptogenic channels in our results may have an impact. According to our anticipation, these channels may possess properties similar to non-resected tissue, thereby complicating the differentiation between resected and non-resected regions. Another limitation of our study is the exclusion of patients with unfavorable outcome. In our patient selection, with 91% of patient long-term Engel IA without any AED, strengthens our hypothesis that the epileptic tissue was incorporated in the resected tissue.

A limitation is that we could not analyze FR in all patients, because of the high frequency noise produced by the LTM64 headbox (Micromed, Italy). This is an example of problems that can be encountered in clinical practice. A lot of devices are present in the operation room, which yield noise in the ioECoG recordings. It is imported to be aware of this to accurately interpret findings in the recordings. Another limitation is the choice of one recording per patient. With this choice, we lowered the number of channels covering non-resected tissue, and thus improved the resected versus non-resected channels ratio.

Although our included patients with resections of FCD still yield a heterogeneous group with differences in the anatomical location of the resection, subgroup analysis (n>10) could be performed for frontal-lobe resection. The HFO trial, a randomized controlled trial, suggests that extra-temporal resections might benefit more from HFO analysis than temporal resections.[14] We confirm the results of use

of HFOs in the subgroup of frontal-lobe resections (n=10), but not for temporal lobe resections due to a too small group size (n=7). Please note that the HFO trial was conducted in the same center, but there was no overlap in patients for this study. In this retrospective study, we have defined anatomical locations based on the position of the FCD lesion as identified on the MRI. It is crucial to note that the exact electrode positions were not determined in accordance with gyrus anatomy due to the inherent retrospective nature of our study. As we move forward, the development of an intraoperative HFO atlas could potentially address these challenges, and we remain vigilant about incorporating such advancements in future studies.

In clinical practice, the underlying pathology is rarely confirmed prior to the surgery. Often, an FCD pathology is suggested by the radiologist based on MRI imaging pre-surgery. A next step would be to see if the pathology can be predicted by the ioECoG signal, a recent study did this on stereo-EEG data.[61] This knowledge about the underlying pathology might help the neurosurgeon during epilepsy surgery. Future research focusing on biomarkers in ioECoG should examine variations in the fundamental pathologies causing epilepsy. Pathology-specific biomarkers in the ioECoG could further help delineate the epileptic tissue during epilepsy surgery.



Chapter 3

Spectral entropy variability of intraoperative electrocorticography predicts outcome after epilepsy surgery in patients with focal cortical dysplasia

Eline V. Schaft, Sem Hoogteijling, Dongqing Sun, Cyrille H. Ferrier, Pieter van Eijsden, Wim M. Otte, Galia Anguelova, Nick F. Ramsey, Maryse A. van 't Klooster, Maeike Zijlmans on behalf of the RESPect database study group

Accepted in Epilepsia, January 2026

Abstract

Objective

Epilepsy surgery in people with focal cortical dysplasia (FCD) requires accurate removal of all epileptogenic tissue, and outcome is difficult to predict. We explored whether spectral entropy, a fast computable electroencephalographic (EEG) feature, could estimate epileptic activity in intraoperative electrocorticography (ioECoG) and forecast post-surgical outcomes.

Methods

We included people with FCD pathology who underwent ioECoG-assisted resective surgery. We analyzed ioECoG recordings acquired before and after resection. We computed spectral entropy across eight frequency bands (1-500,1-4,4-8,8-12,12-20,20-80,80-250,250-500Hz) in 2s-epochs during 1 minute, and the mean and SD per electrode. The pre-resection features were the input for a random forest machine learning model to classify channels covering resected from non-resected tissue. Explainable artificial intelligence was used to select features that positively influenced the model predicting resected tissue. We then related these markers measured after the resection to postsurgical outcome using trend analysis (Jonckheere-Terpstra) across outcome groups Engel IA without medication, Engel IA-ID, Engel II, Engel III and Engel IV.

Results

We analyzed ioECoG data from 37 patients (age range 0-61 years, 21 patients were ≤16 years), including 2270 pre-resection and 1278 post-resection channels. The random forest model discriminated between resected and non-resected cortex (validation fold AUC=0.84; 95%-CI: [0.74-0.95]). Features with the strongest positive Shapley Additive exPlanations values (SHAP) included high spectral entropy variability (SEV) in the 80-500Hz bands. In post-resection recordings, higher mean SEV and greater spatial variability of SEV were associated with poorer Engel outcome across several frequency bands. After multiple comparison correction, the positive relationship between high mean SEV ($p=0.004$) and high spatial variability ($p=0.001$) in 250–500Hz with poor seizure outcome remained statistically significant.

Conclusion

SEV is a real-time computable invasive EEG marker that represents persisting epileptic activity after resection. SEV may be used to evaluate resection adequacy directly or may reflect residual epileptic activity. This would enable epilepsy surgery guidance and post-surgical counseling and decision making.

Introduction

Resective surgery is a potential cure for focal epilepsy, which requires precise identification and resection of epileptogenic tissue. intraoperative electrocorticography (ioECoG) may enhance surgical outcomes by tailoring of the resection, traditionally based on interictal epileptiform discharges.[10,30,64] Focal cortical dysplasia (FCD) is the underlying pathology in 20% of people with focal epilepsy and is associated with postoperative seizure freedom rates of 62%.[41] Optimizing intraoperative delineation of epileptic tissue through advanced ioECoG signal analysis techniques may improve the precision of the resection and thereby clinical outcomes.

Among advanced EEG signal analysis techniques applied in the past decades, entropy-based measures quantify the temporal variability and spectral irregularity of cortical activity, i.e., the degree of synchrony versus asynchrony in the underlying neuronal population. Entropy measures have been successfully applied on EEG signals to detect seizures[16], to monitor anesthesia depth[17], and to diagnose dementia[18]. There is a wide variety of entropy-based measures and they can be calculated from the signal in the time or frequency domain. Spectral entropy reflects the distribution of power across frequencies.[22,23] Low spectral entropy values indicate concentrated energy in one frequency, suggestive of synchronous neuronal firing. High values reflect an evenly spread distribution of power, indicative of asynchronous activity.[98] Different theories exist on synchronous and asynchronous firing patterns in relation to epileptic tissue. One theory suggests that regularity, i.e., low entropy, of interictal gamma oscillations and the presence of high-frequency oscillations (HFOs) are correlated with the epileptogenic tissue.[27,34,99,100] The underlying mechanisms of HFOs involve pathological synchrony, as well as asynchrony at the cellular and network levels.[101] This combination of synchronous and asynchronous firing patterns may lead to temporal fluctuations in spectral entropy.[102] Mooij and colleagues[103] showed that the standard deviation, i.e., variability, of wavelet entropy in the 80-200Hz range in stereo EEG recordings was a predictor for epileptic tissue.[103] Spectral entropy is suitable for online real-time ioECoG analysis during surgery due to its fast computation. Machine learning approaches can be applied to automatically classify features that distinguish epileptogenic from non-epileptogenic tissue.[104] Moreover, explainable artificial intelligence techniques provide an opportunity to open the black box of these models by highlighting the most relevant frequency bands and measures, thereby offering a transparent, data-driven framework to support surgical decision-making.[105,106]

We wanted to test if readily calculable spectral entropy features like variability may serve as a predictor for epileptic tissue in ioECoG recordings. We focused on patients with underlying FCD pathology to create a relatively homogeneous cohort with a considerable potential to improve surgical outcomes. The aims of this study were twofold: 1) to investigate whether spectral entropy in different frequency bands of pre-resection ioECoG distinguishes between resected and non-resected tissue; 2) to explore the potential of spectral entropy in post-resection ioECoG to predict post-surgical outcome at individual patient-level.

Methods

Patient selection

We retrospectively included people from the University Medical Center Utrecht and SEIN RESPect database[42]. This database contains patients who underwent epilepsy surgery from 2008 till 2023. We included patients when they: 1) underwent tailored epilepsy surgery with ioECoG recordings pre- and post-resection, 2) had FCD pathology confirmed by histopathology. We excluded patients based on the following criteria: 1) prior brain surgery, since the cortex is not intact at the start of the surgery; 2) ioECoG sample frequency <1000Hz, since we want to analyze up to 500Hz (Nyquist frequency) and thus the sample frequency needs to be twice this Nyquist frequency; 3) participant in randomized control trial 'the HFO study'[14], since the tailoring method (spikes versus ripples) was randomized in this study.

The UMCU and SEIN institutional ethics committee waived the need for informed consent for all retrospectively collected clinical data in the RESPect database before 2018. As of 2018 informed consent was required and obtained. Accordingly, pseudonymized data usage for the purpose of retrospective research was approved.

Clinical data

We collected the following clinical characteristics from the RESPect database (Castor eCDF, Amsterdam, The Netherlands): gender assigned at birth, age at epilepsy onset, age at surgery, duration of epilepsy (age at surgery - age at epilepsy onset), lesion laterality (left/right), anatomical location of the lesion on MRI, FCD subtype, and post-surgical seizure outcome. The FCD subtypes were based on the 2011 ILAE classification.[43] Post-surgical seizure outcome was evaluated and classified using the Engel classification on a yearly basis by the treating neurologist.[8] Longest available seizure outcome was used, with a minimum of 1 year. Patients were divided in five groups based on seizure outcome: 1) Engel IA+: complete seizure freedom with successful withdrawal of all antiseizure medications; 2) Engel IA-D: free of disabling seizures; 3) Engel IIA-D: rare disabling seizures; 4) Engel IIIA-B: worthwhile improvement of seizures; and 5) Engel IVA-C: no worthwhile improvement.

Intraoperative recordings

ioECoGs were recorded with grids and/or strip electrodes (AD-Tech or Dixi Medical) placed directly on the cortical surface of the brain. The grid and strips consisted of platinum electrodes with 4.2 mm^2 contact surface (AD-Tech) or 12.6mm^2 contact surface (Dixi Medical). Recordings were acquired with a 64-channel EEG system (Systemplus, Micromed, Treviso, Italy) sampled at 1024Hz or 2048Hz using a common reference, behind the ear on the mastoid. Propofol anesthesia was used in combination with an analgesics at the start of the surgery. Propofol starting dose was patient-specific. Propofol was temporarily paused during recording to avoid suppression of epileptic activity and burst-suppression patterns in the ioECoG.[107] Average duration of the propofol pause is 9±5 minutes in our center. The standardized protocol for anesthesia and propofol pausing was described in detail by Sun et al.[107] Intraoperative tailoring was based on interictal spikes. Location of ioECoG recordings were chosen by the neurologist and neurosurgeon based on location of the MRI abnormality, anatomical possibilities (e.g. bridging veins can prevent the grid from being placed in a certain location), and findings

in ioECoG recordings during the surgery (e.g. if interictal spikes are found on the border electrodes of the grid, the grid will be replaced so the border electrodes of the previous recording are centered in the new recording). After opening of the skull and dura mater, one or more pre-resection ioECoG recordings were acquired in different positions on the intact cortex. After the initial resection, ioECoG was performed to evaluate residual epileptiform activity. Recordings acquired after the final resection, i.e., when no further surgical intervention was planned, were defined as post-resection recordings. During surgery photos were taken of the exposed cortex without grids, of each grid position, and of the final resection cavity. (Figure 1A)

Electrode locations and channel labels

We determined individual electrode locations on the cortex based on the intraoperative photos. Photos of pre-resection grid positions were matched with a pre-resection photo of the exposed cortex without grids. Photos of the pre- and post-resection grid positions were matched with a photo of the cortex showing the final resection cavity. As a next step this resection cavity was projected onto the pre-resection grid to label its channels into two categories: 1) resected, i.e., channels covering the resection cavity and/or a 5 mm border around the resection cavity; 2) non-resected, i.e., all other channels at least 5 mm distance from the resection border.[108] (Figure 1A)

ioECoG post-processing

To facilitate signal post-processing, each ioECoG recording was converted into the Brain Imaging Data Structure (BIDS) format, which involves a standardized data organization, anonymization and artifact annotation.[42] We included all pre- and post-resection recordings of each patient when at least 50 seconds of artifact free data was available. We excluded recordings containing motor or sensory stimulation. We selected 50-60 seconds of artifact-free segments from the end of each recording to avoid burst-suppression patterns, which often occurred at the beginning of the recording due to discontinuation of propofol. The ioECoG signals were notch-filtered at 50Hz to remove line noise and subsequently divided into non-overlapping epochs of 2 seconds.

Spectral entropy analysis

We calculated the spectral entropy (Supplementary Materials) in eight conventional frequency bands: broadband (1-500Hz), delta (1-4Hz), theta (4-8Hz), alpha (8-12Hz), beta (12-20Hz), gamma (20-80Hz), ripple (80-250Hz), and fast ripple band (250-500Hz). Spectral entropy values range between 0 and 1. A value close to 0 indicates regularity within the frequency band, i.e., the signal contains one dominant frequency. A value close to 1 indicates irregularity within the frequency band, i.e., the signal contains a variety of frequencies within the selected frequency band.[23] The toolbox Entropyhub was used to calculate spectral entropy.[109] We calculated spectral entropy over all two seconds non-overlapping epochs, resulting in 25 to 30 spectral entropy values per channel per frequency band.

Machine learning to classify resected channels

We used a machine learning approach to explore differences in spectral entropy between resected (i.e. epileptic tissue) and non-resected channels (i.e. non-epileptic tissue) in pre-resection recordings. We included only patients with good outcome in this explorative analysis, since all epileptic tissue in these patients is included in the resected channels. We calculated a set of 16 features per channel for pre-resection recordings; the mean and standard deviation (SD) of the spectral entropy over all epochs per frequency band. This mean and SD represented the average and variability of the spectral entropy over time per channel. We refer to the average as the mean spectral entropy per channel and we refer to the standard deviation as the spectral entropy variability (SEV) per channel. The set of 16 spectral entropy features per channel were used as input and the channel labels – resected or non-resected – were used as output. We trained a random forest model with leave-one-subject-out cross validation. To determine the best hyperparameters for the random forest, we executed a grid search, we selected the parameters with the highest area under the curve (AUC) value.[110,111] Accuracy, sensitivity, specificity, positive and negative predictive values were calculated for the validation fold. Shapley Additive exPlanations (SHAP) was used to evaluate the contribution of each feature to its performance.

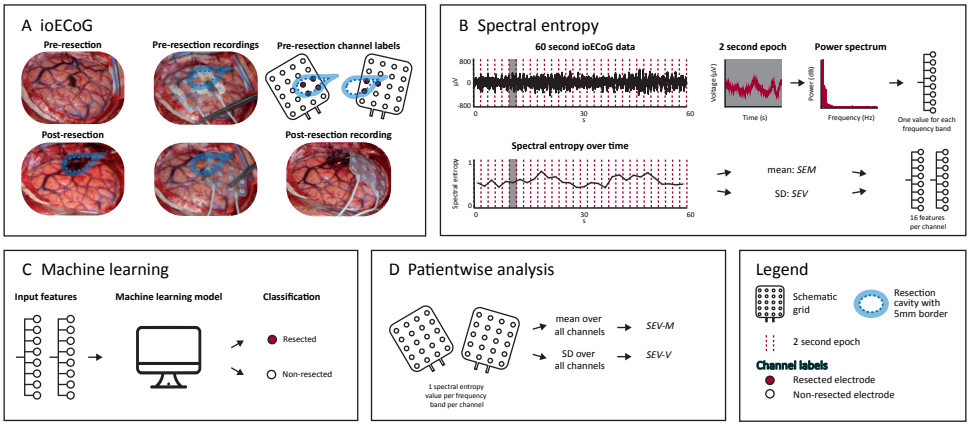


Figure 1: Methodology of the classification of channel labels and the computation of spectral entropy. A) intraoperative photos taken during surgery were used to label all channels of the pre-resection recordings into channels covering resected and non-resected cortex. B) Spectral entropy was calculated over 2s epochs via the normalized power spectrum. This resulted in a spectral entropy over time-curve for each frequency band. The mean and standard deviation were calculated over this curve to compute the mean and SD of spectral entropy for each channel in each frequency band. C) These features were used as input for the machine learning models to distinguish channels covering resected and non-resected cortex. D) Per patient, the mean and standard deviation of SEV over all channels was calculated. These features were associated with post-surgical seizure outcome.
Abbreviations: ioECoG = intraoperative electrocorticography, mm = millimeter, SD = standard deviation, SEV = spectral entropy variability.

Spectral entropy variability as a predictor for surgical outcome

To investigate whether spectral entropy was associated with post-surgical outcome, we used a patient-wise analysis where SEV measures were aggregated per patient using the mean and the standard deviation across all channels. Features were calculated independently for all post-resection recordings. Features per patient were plotted against the five seizure outcome groups. We fitted a second-degree polynomial to the data for visualization purposes only, to illustrate the direction of observed associations. The statistical significance of these associations were assessed separately using the Jonckheere-Terpstra test, which evaluates whether there is a monotonic increase or decrease in entropy variability across the five seizure outcome groups.[112] We applied the false discovery rate (FDR) method for multiple comparison correction.

Statistical analysis for clinical variables and software

For all continuous clinical variables, we calculated the median and interquartile range (IQR). We used Kruskal-Wallis test for continuous variables and χ^2-test for categoric variables to determine group differences. To assess whether age at epilepsy, age at surgery, and duration of epilepsy duration acted as a confounder, a separate linear regression analysis was performed for spectral entropy values in each frequency band for non-resected channels in the pre-resection recordings and all post-resection recordings. The potential confounder was entered as the independent variable. Model fit was evaluated using the coefficient of determination (R^2), and statistical significance was evaluated using the omnibus F-test of the regression model.

All machine learning training, testing, and SHAP analyses were performed in Python 3.12 (Spyder version 5.5.1). All other pre- and post-processing analyses were performed in Matlab R2024a (The MathWorks, Inc., Natick, Massachusetts, United States). We considered a p-value <0.05 significant. We showed results with and without FDR correction.

The code for spectral entropy calculation can be found on Github: https://github.com/UMCU-EpiLAB/umcuEpi_ioECoG_SpectralEntropy.

Results

Patient selection and clinical data

92 patients underwent ioECoG-guided surgery between 2008 and 2023 with FCD pathology confirmed with histopathological examination. We excluded 25 patients with previous surgeries, 9 with recordings <1000Hz and 21 people included in the HFO trial. We thus included 37 patients (18 female; median age at surgery 14 (IQR 17) years, 21 patients ≤16y; median age at epilepsy onset 3 (IQR 11) years) that underwent ioECoG-tailored surgery. Seventeen patients were seizure free with complete withdrawal from antiseizure medication (Engel score IA+), eleven had Engel score IA-D, four had Engel score IIA-D, two had Engel score IIIA-B and three had Engel score IVA-C. Histopathology revealed FCD type I in eight patients (Ia: 4 patients; Ib: 3 patients; no further classification: 1 patient), and FCD type II in 29 patients (IIa: 7 patients; IIb: 21 patients; no further classification: 1 patient). Anatomical locations of the intraoperative recordings were frontal (n=15), temporal (n=12), parietal (n=3), fronto-parietal (n=1), temporo-parietal (n=2), temporo-occipital (n=2), parieto-occipital (n=1), temporo-parieto-occipital (n=1). There were no differences in age at surgery (p=0.08), age at epilepsy onset (p=0.51) and epilepsy duration (p=0.09) between the five outcome groups. There was a significant difference between follow-up time between the five outcome groups (p=0.03). In post-hoc testing, no group differed significantly from another, indicating an overall between-group variation. Another significant difference in clinical characteristics between the five outcome groups was found in FCD subtypes (p=0.02). All patients within outcome group with Engel score III have a FCD type Ib. (Table 1)

Intraoperative recordings

Five patients had recordings with a sample frequency of 1024Hz. The median of included pre-resection ioECoG recordings was three different locations on the cortex per patient (IQR 2; range 1-7) and the median of included post-resection recordings was two (IQR 1; range 1-6). A total of 291 channels were excluded from further analyses, 242 due to poor signal quality and 49 due to less than 50s of artefact-free data. This resulted in a total of 2270 pre-resection channels (864 resected and 1406 non-resected) and 1278 post-resection channels for further analysis. (Table 1) The median number of pre-resection channels per patient was 52 (IQR 33) and the median number of post-resection channels per patient was 27 (IQR 24).

Machine learning approach to classify resected channels

The random forest model showed a performance of AUC is 0.84 (95%-CI: [0.74-0.95]) on the cross-validation fold (Figure 2A). The accuracy was 0.72, the sensitivity 0.56, the specificity 0.95, the positive predictive value 0.92, the negative predictive value 0.85. Feature importance analysis using SHAP revealed that mean spectral entropy and in several frequency bands contributed substantially to the model's predictions. As a general trend, lower mean spectral entropy in the broad and ripple bands, a higher mean spectral entropy in the alpha band and higher SEV in the gamma, ripple and fast ripple bands contributed to the prediction of resected channels in the model. (Figure 2B&3)

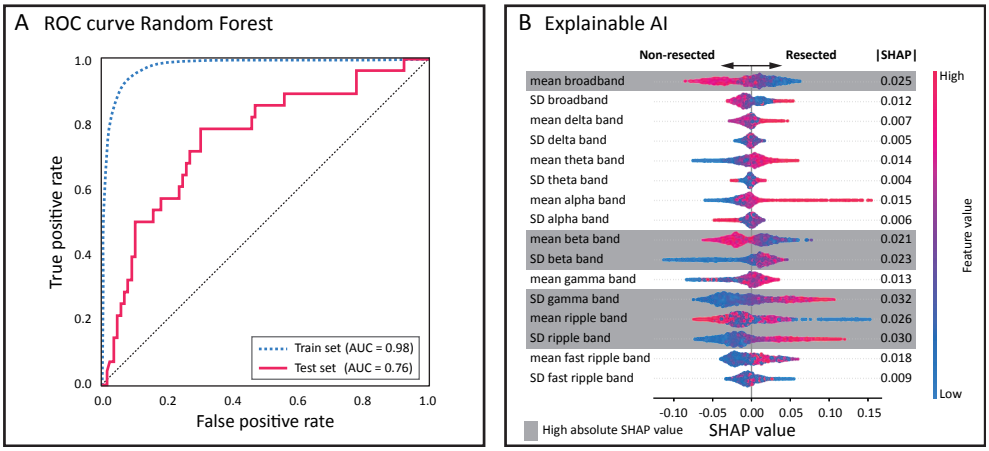


Figure 2: The ROC curve and explainable AI findings of the random forest model trained to distinguish channels covering resected and non-resected cortex. A) The ROC curve with an AUC of 0.98 on the training set and an AUC of 0.84 on the cross-validation fold B) SHAP analysis revealed the input features that have the highest contribution to the performance of the model. The features with the highest absolute SHAP values are highlighted in grey. Out of these, mean alpha band, SD gamma band, SD ripple band and mean fast ripple band showed a positive direction of influence (high feature value influence the model to resected tissue). SHAP dependence plots of the six key features are available in the Supplementary Materials (Figure S2).
Abbreviations: AI = artificial intelligence, AUC = area under the curve, ROC = receiver operating characteristic, SHAP = Shapley Additive exPlanations, SD = standard deviation.

Table 1: Study population characteristics. Group differences for continuous variables were not found (Kruskal-Wallis test), age at epilepsy debute (p=0.51), age at surgery (p=0.08), and number of included pre- (p=0.23) and post-resection (p=0.80) channels. Group differences for categorical variables were only found within FCD subtype (p=0.02; only patients with FCD type Ib with Engel score III), not for the other categorical variables, gender (p=0.65), side of the lesion (p=0.08), and anatomical location of the lesion (p=0.53).

Engel score	Pat.nr	Gender	Age at epilepsy debute	Age at surgery	Side of the lesion	Anatomical location of the lesion	Number of included pre-resection channels	Number of included post-resection channels	FCD subtype
	1	F	1	3	R	Fr	40	16	I
	2	M	3	13	R	Fr	56	19	Ia
	3	F	0	1	R	Fr	54	37	IIa
	4	F	11	12	L	Fr	57	69	IIa
	5	M	9	25	R	T	44	37	IIa
	6	F	18	21	R	T	52	28	IIb
	7	M	1	14	R	Fr	51	69	IIb
	8	F	4	10	R	T	60	46	IIb
IA+	9	M	12	17	R	TP	80	108	IIb
	10	M	5	14	L	Fr	59	16	IIb
	11	M	12	16	R	T	36	15	IIb
	12	F	1	11	R	T	52	19	IIb
	13	M	20	45	R	T	52	29	IIb
	14	M	14	33	R	TO	40	33	IIb
	15	M	1	3	R	Fr	90	52	IIb
	16	F	1	17	L	Fr	20	19	IIb
	17	F	1	9	R	TPO	77	14	IIb

IA-ID	18	F	1	2	R	T	118	73	Ia
	19	M	0	55	R	T	50	18	Ia
	20	M	3	47	R	P	16	4	II
	21	M	15	47	R	TO	64	32	IIa
	22	F	10	17	R	Fr	31	42	IIa
	23	M	0	41	R	Fr	120	43	IIb
	24	M	0	0	L	FP	51	75	IIb
	25	F	25	45	R	Fr	45	11	IIb
	26	F	0	13	L	Fr	89	26	IIb
	27	M	11	59	L	Fr	22	16	IIb
	28	F	15	61	L	T	106	19	Ib
II	29	M	0	8	L	Fr	76	108	IIa
	30	F	1	8	R	T	52	25	IIa
	31	F	7	25	R	TP	39	27	IIb
	32	M	0	12	R	P	59	15	IIb
III	33	F	12	25	L	T	47	19	Ib
	34	F	0	0	R	Fr	129	33	Ib
	35	F	0	3	L	T	78	19	Ia
IV	36	M	3	8	L	P	43	16	IIb
	37	M	3	5	L	PO	115	31	IIb

Abbreviations: Engel score IA+= seizure freedom with successful withdrawal of all antiseizure medications; IA-D= free of disabling seizures; II= rare disabling seizures; III= worthwhile improvement of seizures; and Engel IV= no worthwhile improvement, F = female, FP = fronto-parietal, Fr = frontal, FCD = focal cortical dysplasia, L = left, M = male, Pat. nr. = patient number, P = parietal, PO = parieto-occipital, R = right, T = temporal, TO = temporo-occipital, TP = temporo-parietal, TPO = temporo-parieto-occipital

Spectral entropy variability as a predictor for surgical outcome

In post-resection recordings, we found a positive association between mean SEV and poor seizure outcome for theta (p=0.048) and fast ripple band (p=0.004) and a positive association between the spatial variability of SEV and poor seizure outcome for the delta (p=0.01), theta (p=0.04), beta (p=0.04), ripple (p=0.03) and fast ripple band (p=0.001). After multiple comparison correction, the positive relationship between high mean and variability of SEV in the fast ripple band in post-resection recordings remained statistically significant. (Table 2; Figure 4) There was no significant effect of any of the confounders (age at surgery, age at epilepsy onset, and epilepsy duration) on the mean spectral entropy and SEV values for non-resected pre-resection recordings and all post-resection recordings.

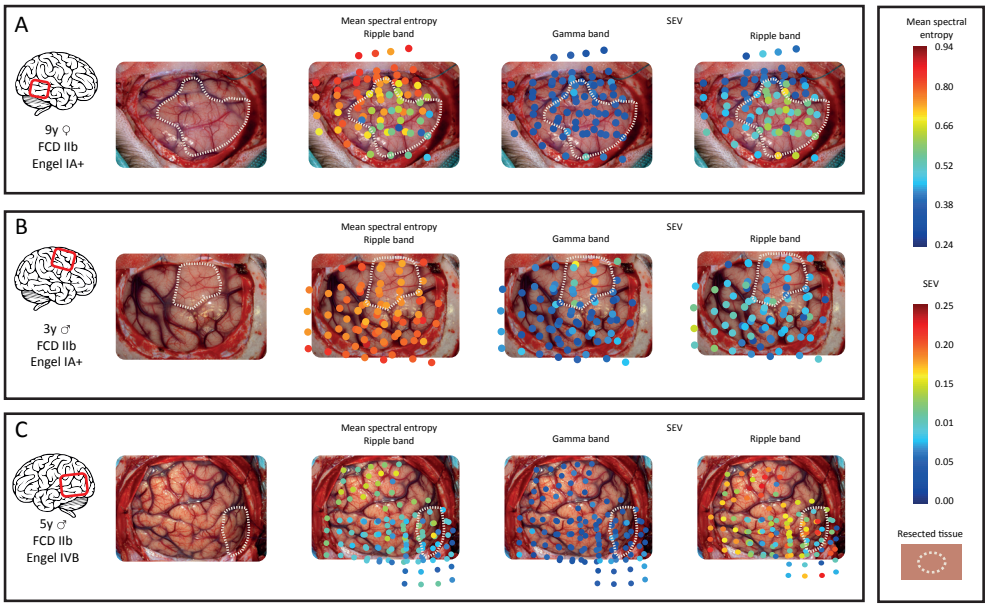


Figure 3: Spectral entropy features with highest absolute SHAP values of all pre-resection channels projected on intraoperative photo with resection cavity for three patients: mean spectral entropy in ripple band, and SEV in gamma and ripple band. Two patients with good outcome (A and B) show deviating values within the resected tissue, whereas a patient with poor outcome (C) shows deviating values both within and outside the resected tissue. For all patients, age at surgery (years), FCD subtype, and Engel seizure outcome are shown. A) pt. nr 17 had good post-surgical outcome (Engel IA+). We observed lower values of mean spectral entropy in the ripple band and high values of SEV in the ripple band within resected tissue. B) pt. nr 15 had good post-surgical outcome (Engel IA+). We observed high values of SEV in the gamma band within the resected tissue. C) pt. nr 37 had poor post-surgical outcome (Engel IVB). We observed high values of mean spectral entropy in the ripple band and deviating values of SEV in the ripple band all over the exposed cortex.
Abbreviations: IA+ = Engel score IA with complete withdrawal of medication, FCD = focal cortical dysplasia, y = year, SEV = spectral entropy variability.

Table 2: Patient-wise analysis between the mean SEV and variability of SEV and the seizure outcome groups. These analyses were performed for all channels from the post-resection recordings.

Features	Mean SEV		Variability of SEV	
Broadband	JT = 278.3	p = 0.12	JT = 249.6	p = 0.33
1-4Hz	JT = 226.6	p = 0.44	JT = 318.6	p = 0.01*
4-8Hz	JT = 297.9	p = 0.048*	JT = 302.5	p = 0.04*
8-12Hz	JT = 245.0	p = 0.38	JT = 270.3	p = 0.17
12-20Hz	JT = 253.0	p = 0.30	JT = 302.5	p = 0.04*
20-80Hz	JT = 224.3	p = 0.417	JT = 246.1	p = 0.36
80-250Hz	JT = 296.7	p = 0.05	JT = 307.1	p = 0.03*
250-500Hz	JT = 335.8	p = 0.004*♦	JT = 361.1	p = 0.001*♦

** p-value of 0.05 considered significant, ♦ remains significant after multiple comparison correction. Abbreviation: JT = Jonckheere-Terpstra effect size.*

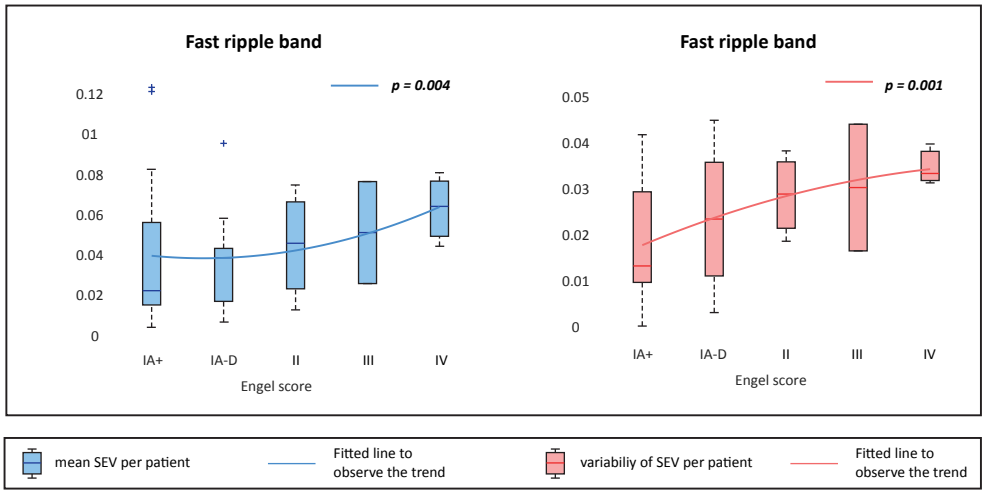


Figure 4: Mean and variability of SEV per patient in fast ripple band versus outcome groups. The fitted line is a second-degree polynomial to show the association between entropy values and seizure outcome. The statistical test used was the Jonckheere-Terpstra test to evaluate whether the association was significant.
Abbreviations: IA+ = Engel score IA with complete withdrawal of medication, SEV = spectral entropy variability.

Discussion

We demonstrated that low mean spectral entropy and high SEV distinguished resected tissue from non-resected tissue in people with FCD. We found an association between SEV and post-surgical seizure outcome with a stepwise increase across Engel outcome groups: the higher the mean and variability of SEV, the poorer the seizure outcome. The fast ripple band exhibited this phenomenon most, followed by the ripple and theta bands (and delta for only the variability of SEV). The ease of calculating spectral entropy directly makes it a promising biomarker for real-time intraoperative display, with the potential to improve resection precision and to be used as an associated measure for seizure outcome for optimal post-surgical counseling.
Explainable AI revealed that resected channels were characterized by high SEV in the gamma and ripple bands. These results align with prior studies on entropy and HFOs in stereo-EEG recordings, showing that wavelet and relative entropy in the ripple frequency band can differentiate epileptic tissue from non-epileptic tissue.[103,113] Wavelet and relative entropy may capture non-linear or time-frequency dynamics in greater detail, but these features are complex with a high computational burden. Spectral entropy offers a significant advantage in terms of computational efficiency and simplicity. This makes it particularly well-suited for real-time intraoperative application, as rapid analysis is essential for intraoperative signal interpretation.

The biological basis of the selected spectral features lies in the underlying neuronal dynamics: ripples are thought to arise from tightly synchronized interneuron-pyramidal circuits, whereas fast ripples reflect asynchronous microcircuit discharges due to local disinhibition.[101,114] Rapid alternations between these oscillatory modes produces fluctuations in the power spectrum which are captured by spectral entropy. Our results extend insights in these dynamics by showing that high variability in spectral entropy not only could support delineation of epileptic tissue for resection, but also associates with poor surgical outcomes when present in non-resected tissue.

The inclusion of post-resection recordings enabled us to assess residual epileptogenic electrophysiological activity after complete resection. The clinical relevance of post-resections spikes remains a subject of ongoing debate, with some studies questioning their predictive value for long-term outcome.[67,115] However, our findings suggest that post-resection recordings do contain prognostic information, although not necessarily in the form of traditional biomarkers such as spikes. Instead, we demonstrated that high spatial variability of SEV in the fast ripple band was associated with poor surgical outcome when present in unresected cortex. This is in line with prior work showing that residual ripples and fast ripples are associated with seizure recurrence.[33,89] Visual interpretation of ioECoG, including assessment of interictal spikes and high-frequency oscillations, remains the clinical gold standard for surgical guidance. The present study did not aim to replicate visual ioECoG assessment, but to evaluate spectral entropy variability as an automated, objective, and real-time computable marker derived from short intraoperative recordings. Future studies should directly relate SEV to visually and/or automatically quantified spike and HFO metrics to determine its complementary value in intraoperative decision-making.

Most studies focusing on post-surgical outcome dichotomize patients into favorable (Engel IA-B or Engel I) versus unfavorable (Engel higher than IC or Engel II-

IV) groups, which may overlook important clinical relevant differences within these categories. By using the Engel scores as a scale, we observed a monotonic relationship between variability in spectral entropy and seizure outcome: patients with Engel score IV have the highest value of spatial variability of SEV in non-resected tissue, whereas patients with Engel II or III showed intermediate values. Refining analysis for these seizure outcome subgroups in this way emphasizes spectral entropy's relative predictive potential and suggests that it may capture the extent to which residual networks remain capable of generating seizures. This approach may have pre- and postoperative counseling value, by offering more nuanced expectations beyond a simple favorable or unfavorable dichotomy. For example, rare but non-disabling seizures (Engel score II) may have considerably less impact on quality of life than a lack of improvement in seizure frequency (Engel score IV), underscoring the importance of individualized outcome prediction.

Besides the high frequency bands, we identified associations between SEV in slower frequency bands in non-resected tissue and poorer outcome. These instabilities in the slower frequencies may reflect persistent large-scale network dysfunction in non-resected tissue. Given that the standard deviation is used to quantify the variability, it is unlikely that one single abnormal channel (i.e., one outlier) causes this high variability. It rather suggests distributed irregularities across multiple channels. This supports the idea that poor outcome may be linked to broader, unresolved network pathology beyond the margins of the resection. Previous work has implicated beta and gamma connectivity and full-spectrum synchrony in epileptic networks.[116-118] Our findings add that delta band spectral complexity also carries prognostic information and might indicate pathological circuit rewiring after resection.

Our choice of 2 seconds epoch length balanced the need for sufficient temporal resolution in 50-60 seconds data and the minimal epoch length for adequate sampling for low frequency analysis. Travnicek and colleagues explicitly tested relative entropy values in epoch lengths ranging from 0.5s to 10s and found no significant differences in relative entropy values between epoch lengths.[113] Similarly, Richman and Moorman demonstrated that spectral entropy values stabilize for time series longer than 100 data points.[119] Thus with our high sample frequency of 1024Hz or higher corresponding to epochs of at least 2048 data points, variability in our spectral entropy data due to undersampling is not expected. It is important to note that SEV in the present study reflects short-timescale fluctuations, as ioECoG cannot capture slower physiological rhythms that evolve over hours or days, such as sleep–wake transitions or circadian excitability cycles. The SEV method here is used as a marker of rapid cortical variability relevant within the surgical timescale.

Several clinical and surgical variables are known to influence seizure outcome after epilepsy surgery, including resected lobe, extent of resection, and MRI-visible lesions. Seizure freedom rates differ across lobes, with temporal resections generally yielding better outcomes than extratemporal resections, and more complete resection of epileptogenic tissue is consistently associated with improved outcome, particularly in FCD.[64,120-122] In the present cohort, anatomical lesion location was heterogeneous but did not differ across Engel outcome groups ($\chi 2$-test, $p=0.53$). Potential confounding effects of age at surgery, age at epilepsy onset, and epilepsy duration were explicitly evaluated and showed no association with spectral entropy measures. All included patients had MRI-visible

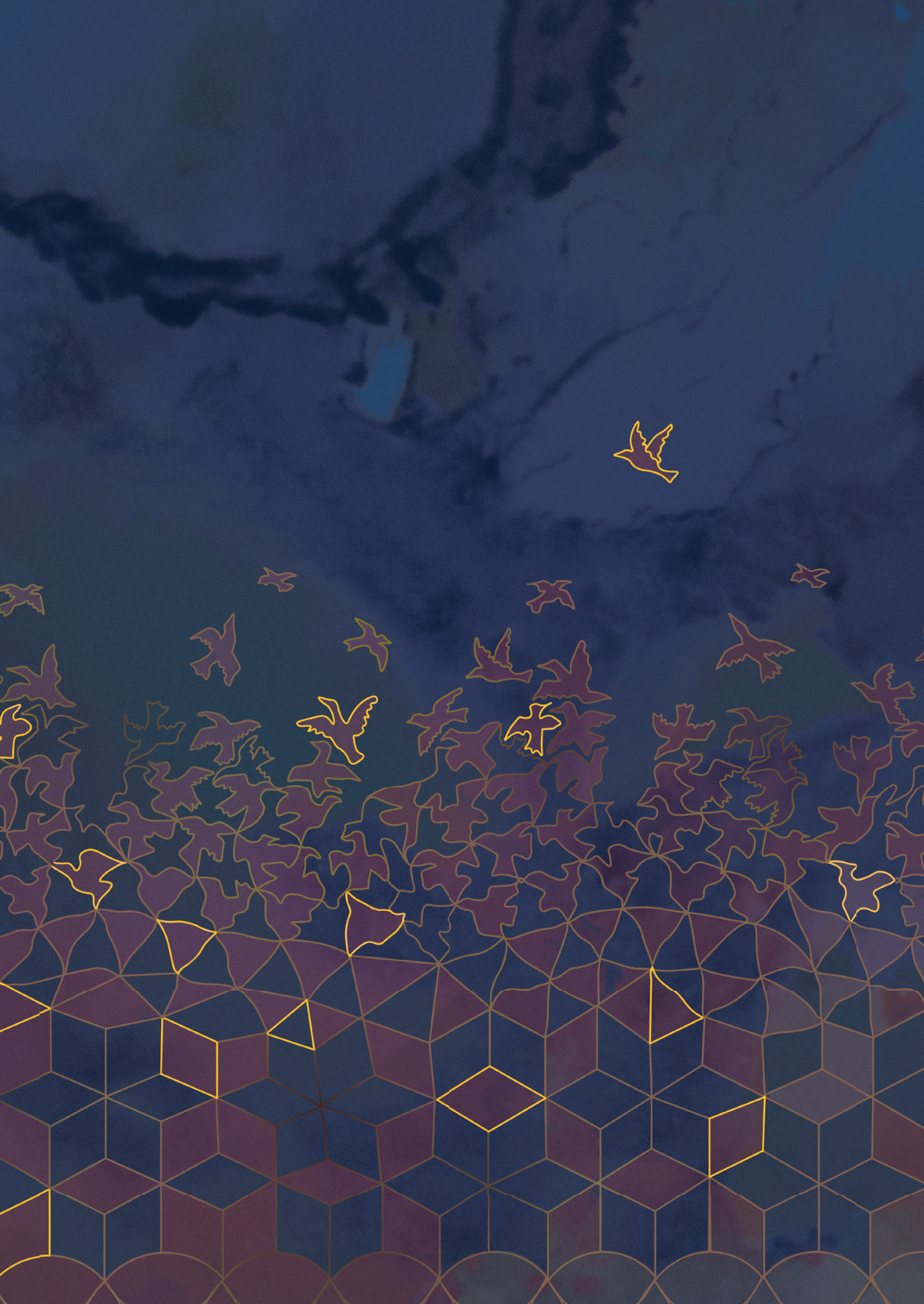
structural abnormalities and histopathological confirmed FCD, limiting variability in lesions. Quantitative measures of resection extent were not available in this cohort and could therefore not be included. A major strength of this study is the relatively homogeneous patient population consisting exclusively of patients with FCD pathology. This minimizes confounding by etiology and enhances the interpretability of the findings within this specific pathology. All histopathological classifications in this cohort (<2023) were made using the 2011 ILAE scheme. Applying the newer 2022 classification[123] would require reassigning some cases to newer subtypes but would not affect the primary classification. Since we did not use FCD subtypes in our analyses, we expect no impact of this updated scheme on the conclusions of the present study. Furthermore, we applied multiple comparison correction to control for false positives across frequency bands, which resulted in the loss of statistical significance for several findings. This approach safeguards analytical rigor and ensures that our conclusions are based on effects that withstand correction for the number of tests performed. Although the frequency bands we analyzed have limited spectral overlap, we deliberately applied correction to maintain the methodological integrity of the study and to ensure that our main findings are robust.

A limitation is the limited number of patients with poor surgical outcomes (Engel III and IV, n=5), reducing the robustness of the subgroup analyses. Another potential source of bias lies in signal quality. It is conceivable that recordings were noisier in the more complex patients in whom poor outcome was achieved, due to longer procedures or more electrode repositioning. This can have introduced additional artifacts that may have affected the spectral characteristics of the signal and, in turn, spectral entropy. Since spectral entropy is derived from the power distribution across frequencies, deviations in the overall shape or stability of the power spectrum could be mistakenly interpreted as physiological variability. To mitigate this, we systematically selected artifact-free segments based on visual inspection and excluded recordings with insufficient noise-free data. This ensured that variability in spectral entropy reflected underlying neuronal dynamics rather than technical differences. A third limitation is that post-resection ioECoG signals, and therefore the calculated SEV, may be influenced by acute surgical effects such as cortical injury, edema, or transient ischemia. Studies have shown that post-resection injury-spikes and focal suppression-burst patterns can arise from local tissue disturbance rather than intrinsic epileptogenicity.[124-126] We minimized these effects by inclusion of all post-resection channels, including electrodes remote from the resection margin, which are effected the least by acute surgical effects.

Conclusion and future perspectives

We demonstrated that spectral entropy is a promising intraoperative biomarker for both delineation of epileptic tissue during surgery and post-operative outcome prediction and thus counseling for people with epilepsy and underlying FCD pathology. Spectral entropy is easy to calculate and may improve the precision of the resection, enhancing the clinical outcomes in this patient group. In our implementation, entropy across all bands can be calculated in less than a minute for one minute of 'artifact-free' data. The calculation time for clinical use depends on the possibilities of the EEG acquisition system: 1.5-3 minutes for a system with plug-in for advanced processing and 3.5-10 minutes if the data needs to be exported from the system. (Supplementary Materials, Figure S1) To our knowledge, this is the first study to stratify post-surgical outcome as a scale and to demonstrate an association between an advanced signal analysis biomarker, in

this case spectral entropy, and scaled seizure outcomes. Future research should focus on the validation of these types of advanced signal analysis techniques in clinical practice by developing real-time computation algorithms integrated in the clinical EEG systems, and exploring entropy dynamics across patients with other underlying pathologies.



Chapter 4

Explainable artificial intelligence unveils (non-)epileptiform spectral powers in intraoperative electrocorticography

Sem Hoogteijling, **Eline V. Schaft**, Evi H.M. Dirks, Sven Straumann, Matteo Demuru, Pieter van Eijsden, Tineke A. Gebbink, Willem M. Otte, Geertjan M. Huiskamp, Maryse A. van 't Klooster, and Maeike Zijlmans, on behalf of the RESPect database group

Published in Clinical neurophysiology, Volume 167, November 2024

Abstract

Objective

Clinical visual intraoperative electrocorticography (ioECoG) reading intends to localize epileptic tissue and improve epilepsy surgery outcome. We aimed to understand whether machine learning (ML) could complement ioECoG reading, how subgroups affected performance, and which ioECoG features were most important.

Methods

We included 91 ioECoG-guided epilepsy surgery patients with Engel IA outcome. We allocated 71 training and 20 test set patients. We trained an extra trees classifier (ETC) with 14 spectral features to classify ioECoG channels as covering resected or non-resected tissue. We compared the ETC's performance with clinical ioECoG reading and assessed whether patient subgroups affected performance. Explainable artificial intelligence (xAI) unveiled the most important ioECoG features learnt by the ETC.

Results

The ETC outperformed clinical reading in five test set patients, was inferior in six, and both were inconclusive in nine. The ETC performed best in the tumor subgroup (area under ROC curve: 0.84 [95%-CI: 0.79-0.89]). xAI revealed predictors of resected (relative theta, alpha, and fast ripple power) and non-resected tissue (relative beta and gamma power).

Conclusions

Combinations of subtle spectral ioECoG changes, imperceptible by the human eye, can aid healthy and pathological tissue discrimination.

Significance

ML with spectral ioECoG features can support, rather than replace, clinical ioECoG reading, particularly in tumors.

Introduction

Tailored epilepsy surgery uses pathological activity in the intraoperative electrocorticogram (ioECoG), including spikes, sharp waves and ictiform spike patterns, to localize epileptic brain tissue.[62,63] The value of tailoring based on these epileptiform ioECoG markers is debated, since it has been associated with increased post-operative seizure freedom by some[38,64-66], but not by others[67-69]. Additionally, not all people with epilepsy show epileptiform interictal markers in the ioECoG[14], possibly due to the stochastic occurrence of these events. Distilling more subtle aberrant patterns in the ioECoG background activity is difficult for human observers, due to the vast variety of normal ioECoG activity. Recent advancements towards high-density ioECoG recordings[13] and high frequency activity (>80Hz)[12] present further challenges for human review. Previous studies showed that complex ioECoG signal analyses can aid epileptic tissue detection, but in specific subgroups.[15,70] There is a need to identify novel accurate epileptiform ioECoG background patterns to aid epileptic tissue localizing and therewith improve epilepsy surgery outcomes.

Artificial intelligence is increasingly introduced in clinical practice and computer-aided pattern recognition algorithms, i.e., machine learning (ML) models, have been developed to evaluate EEG signals e.g., automatic detection of interictal epileptiform discharges.[20] To date, ML approaches have not been applied to ioECoG data for epileptic tissue localization, since well-documented ioECoG data is scarce and many data are required for ML models to learn generalizable patterns. From a ML perspective, ioECoG-based epileptic tissue localization is a binary classification task between channels covering epileptic versus healthy tissue. Recently, it was shown that power differences in canonical EEG frequency bands (delta: 1-4Hz, theta: 4-8Hz, alpha: 8-13Hz, beta: 13-30Hz, and gamma: 30-80Hz) and high frequencies (80-500Hz) differ between epileptiform and non-epileptiform intracranial EEG signals.[14,71] We hypothesized that a ML model can predict epileptic tissue even from basic canonical and high frequency ioECoG band powers.

A drawback of most ML approaches is a lack of transparency. Explainable artificial intelligence (xAI) can mitigate this ML's black-box nature by providing an interpretable explanation along with a ML model's decision-making process.[24] Recently, xAI revealed a ML model detecting seizures in EEG, mainly used the 30-60Hz frequency range for detection.[25] Unravelling the patterns learned by a ML model that classifies ioECoG signals as epileptiform or not may illuminate novel epileptiform background patterns.

We aimed to optimize insights on how ML could aid ioECoG guidance in epilepsy surgery. As starting point, we used basic spectral band powers and trained and tested a ML model on a unique and heterogeneous ioECoG data set of 91 post-operative seizure-free patients to classify ioECoG signals as covering epileptiform or non-epileptiform tissue. We evaluated the added clinical value of the ML model by comparing its performance to clinical ioECoG reading. We assessed whether patient subgroups affected the ML model performance. Subsequently, we used xAI to explore the patterns learned by the ML model.

Methods

Cohort

We retrospectively included people who underwent ioECoG guided lesionectomy from the Registry for Epilepsy Surgery Patients (RESPect database[42]) of the University Medical Center Utrecht (UMCU) and Stichting Epilepsie Instellingen Nederland (SEIN). This database consists of adults and children who underwent epilepsy surgery from 2008 onward in the UMCU, Utrecht, the Netherlands.

Inclusion criteria were: (1) ioECoG recorded at 2048Hz, (2) photographs of ioECoG electrode positions and resected area were available, (3) at least 1-year post-surgical seizure outcome was available, and (4) seizure free (ILAE 1 or Engel IA) at latest follow-up, allowing us to assume that the non-resected tissue was devoid of epileptic tissue. We excluded patients who had multiple epileptic foci, dual pathology, or a surgery involving an amygdala-hippocampectomy, frontal disconnection, or hemispherectomy to minimize the presence of healthy tissue within the resected area. Patients with a prior brain surgery were also excluded.

From the RESPect database, we collected patients' demographic and clinical characteristics including age, sex, duration of epilepsy, presence of MRI lesions (MRI+ vs. MRI-), anatomical ioECoG location, histopathology results, and seizure outcome after surgery at latest follow-up (≥1 year after surgery). We divided the histopathology results into four categories: malformations of cortical development (MCD, e.g. focal cortical dysplasia, tuberous sclerosis), tumors (e.g. glioma, ependymoma), other (e.g. cavernomas, gliosis), and no abnormalities.

The institutional medical ethical committee waived the need for informed consent for all retrospectively collected data before 2018, provided that data were handled (pseudo)anonymously. From 2018, all patients - and/or parents or legal representatives of patients younger than 17 years - signed informed consent for data use.

Procedures and data acquisition

All patients received standard presurgical work-up, which includes at least MRI, video-EEG and neuropsychological testing. Additional investigations as high-resolution EEG, magnetoencephalogram, EEG-functional MRI, 7T MRI, PET, or ictal SPECT were performed if deemed necessary. Generally, the surgical resection plan and initial placement of the ioECoG electrodes were based on the presence of MRI lesions, ictal and interictal epileptiform activity in the video-EEG, and the concordance with the results of other non-invasive investigations.

The ioECoG was recorded relative to a mastoid reference electrode using a 32 or 64-channel EEG system (MicroMed LTM Express, SD64 or SD PLUS Flexi, MicroMed, Veneto, Italy) with 2048Hz sampling rate and 538Hz antialiasing filter. We used 4×5, 4×4, 2×8, 1×8, and/or 1×6 electrode grids or strips with 4.2mm2 platinum contact surface electrodes embedded in silicone and 1cm interelectrode distance (AD-Tech, Racine, WI). Propofol anesthesia was stopped during the recording to avoid burst suppression. The ioECoG was recorded at different locations to cover all putative epileptic brain tissue (Figure 1A). Photos and sketches were made during surgery to identify ioECoG electrode positions. In all patients, routine ioECoG tailored surgery was performed with conventional ioECoG display settings (common reference montage; 70Hz low-pass filter; 10-15s/page). The ioECoG tailoring was based on the presence of interictal spikes

and ictiform spike patterns before and after resection, to determine the extent of the resection. In ten patients, tailoring was based on HFOs as they participated in the HFO-trial.[14] The surgical team always weighted the ioECoG information against other pre-surgical diagnostic information, like MRI, video-EEG, semiology, and neuropsychological testing.

Data preparation

We used the pre-resection ioECoG in common average montage and assumed that channels covering later-on resected tissue showed epileptiform signal characteristics, whereas channels covering later-on non-resected tissue did not. This assumption was based on (1) previous work showing that epileptic tissue has different ioECoG characteristics and (2) the postoperative seizure free outcome of all included patients, indicating that the resected tissue contained all epileptic tissue. We assigned ioECoG channels to the epileptiform ($chan_{epi}$) or non-epileptiform ($chan_{non\text{-}epi}$) class based on digitally aligned photos of the pre-resection ioECoG and the resected area (Figure 1B). We excluded channels situated near the resection margin (<0.5 cm) but outside the resected area to prevent the ML model from training with erroneous labels caused by small photo alignment errors. We visually assessed the channels for the presence of seizures and artifacts, and divided seizure and artifact free segments into non-overlapping epochs of 20 seconds. We filtered the 20-second epochs with an infinite impulse response notch filter to remove the 50Hz powerline artifact and a third-order 0.16Hz high-pass Butterworth filter to remove the drift artifact. We computed the power spectral density per epoch using Welch's method with a 2 second Hamming window and 80% window overlap. We extracted the absolute and relative (i.e. absolute power divided by full band [0.5-500Hz] power) spectral band power in seven frequency bands: delta (0.5-4Hz), theta (4-8Hz), alpha (8-13Hz), beta (13-30Hz), gamma (30-80Hz), ripple (80-250Hz) and fast ripple (250-500Hz). This yielded 14 spectral features (Figure 1C). We separated the patients into two sets: 80% of patients for training and 20% for testing, stratified for histopathology. All ioECoG channels of one patient were either in the training or test set.

Machine learning model and performance

We trained an Extra Tree Classifier (ETC) to classify ioECoG channels as $chan_{epi}$ or $chan_{non\text{-}epi}$ based on their spectral features. Similar to other tree-based algorithms like random forests, an ETC builds multiple decision trees and averages their predictions as final output. The ETC introduces variability by randomly selecting features and thresholds to split, which improves diversity among decision trees and often leads to better generalization performances. We used the ETC with 100 decision trees and 45% randomly selected features evaluated per split. We assessed the ETC's generalizability performance in five-fold cross-validation. This validation divides patients in the training set into five subsets, then trains five times an ETC on ioECoG data from four subsets, and evaluates the performance of the trained ETC on the fifth subset, i.e. the validation subset (Figure 1D). We normalized all features in the training and validation subsets to zero mean and unit variance based on the training subsets. Once trained, the ETC assigns class ($chan_{epi}$ and $chan_{non\text{-}epi}$) probabilities to every 20-second epoch, ranging from 0 to 1. To address variations in the total number of 20-second epochs per patient, we computed the mean probability assigned to a channel for model performance evaluation (Figure 1C). We aimed at a high specificity to minimize the risk that the ETC would recommend resecting healthy tissue. Hence, we chose an arbitrary probability classification threshold based on a 95% specificity in the training subsets to calculate the following performance metrics for classification of ioECoG channels as $chan_{epi}$ or $chan_{non\text{-}epi}$: accuracy, sensitivity, specificity,

positive predictive value, negative predictive value, and area under the curve (AUC) of the receiver operating characteristic. The ETC that obtained the highest specificity in five-fold cross-validation was evaluated on the test set (Figure 1D). Similar as described above, we used the mean probability per channel for test set performance evaluation.

Patient-wise tailoring

To investigate whether subgroups of patients influenced the ETC performance, we assessed for every patient the probabilities given to all $chan_{epi}$ and $chan_{non\text{-}epi}$ channels in relation to the patient's age, histopathology category and ioECoG location. Additionally, we evaluated the ETC's performance when trained and tested on data from one histopathology or ioECoG location category (only when n≥20 patients) and compared this to the performance when the ETC was trained on the entire training set but tested on that specific subgroup.

Clinical ioECoG reading

We used the clinical ioECoG reports to identify which pre-resection channels exhibited epileptiform activity (spikes, ictiform spike patterns, periodic lateralized epileptiform discharges [PLEDs], or ictiform spike patterns plus HFOs in the patients who participated in the HFO study[14], as reviewed by experienced epileptologists. We computed the sensitivity, specificity, positive predictive value, and negative predictive value for classifying a channel as $chan_{epi}$ when the clinical ioECoG report noted epileptiform activity. We evaluated the 2x2 contingency table of the ETC's and clinical ioECoG reading predictions to compare performance on group level. We evaluated the ETC's added clinical value for decision making at the individual patient level by comparing its performance to clinical ioECoG reading on patient level. Per patient, we constructed schematic overviews illustrating the different pre-resection ioECoG recording locations, akin Figure 1B, with the channels' electrographic information from the clinical ioECoG report and mean probability given by the ETC. Four (technical) physicians (SH, ES, MvtK and MZ) visually assessed the schematic overviews to determine superiority between the clinical ioECoG reading and ETC in representing the resected area.

At last, we created for each channel a dichotomous variable indicating the presence or absence of epileptiform activity and evaluated how the ETC performed when this variable was added as an extra feature to the ETC.

Explainable artificial intelligence

We used Shapley Additive exPlanations (SHAP) to explain the ETC's classifications in the test set, as SHAP has a stronger concordance with human explanations compared to alternative xAI methods.[72] SHAP calculates a SHAP value for each feature per 20-second epoch, representing the feature's average incremental contribution to the ETC's output across all possible feature combinations. Positive SHAP values suggest that the feature value was beneficial for the classification as $chan_{epi}$, whereas a negative SHAP value indicates that the feature value was beneficial for the classification as $chan_{non\text{-}epi}$. The SHAP value's magnitude reflects the degree of contribution. For example, a SHAP value of +0.05 reflects that the feature value increased the $chan_{epi}$ probability with 5%. For all features, we plotted and visually assessed the feature values and their corresponding SHAP value.

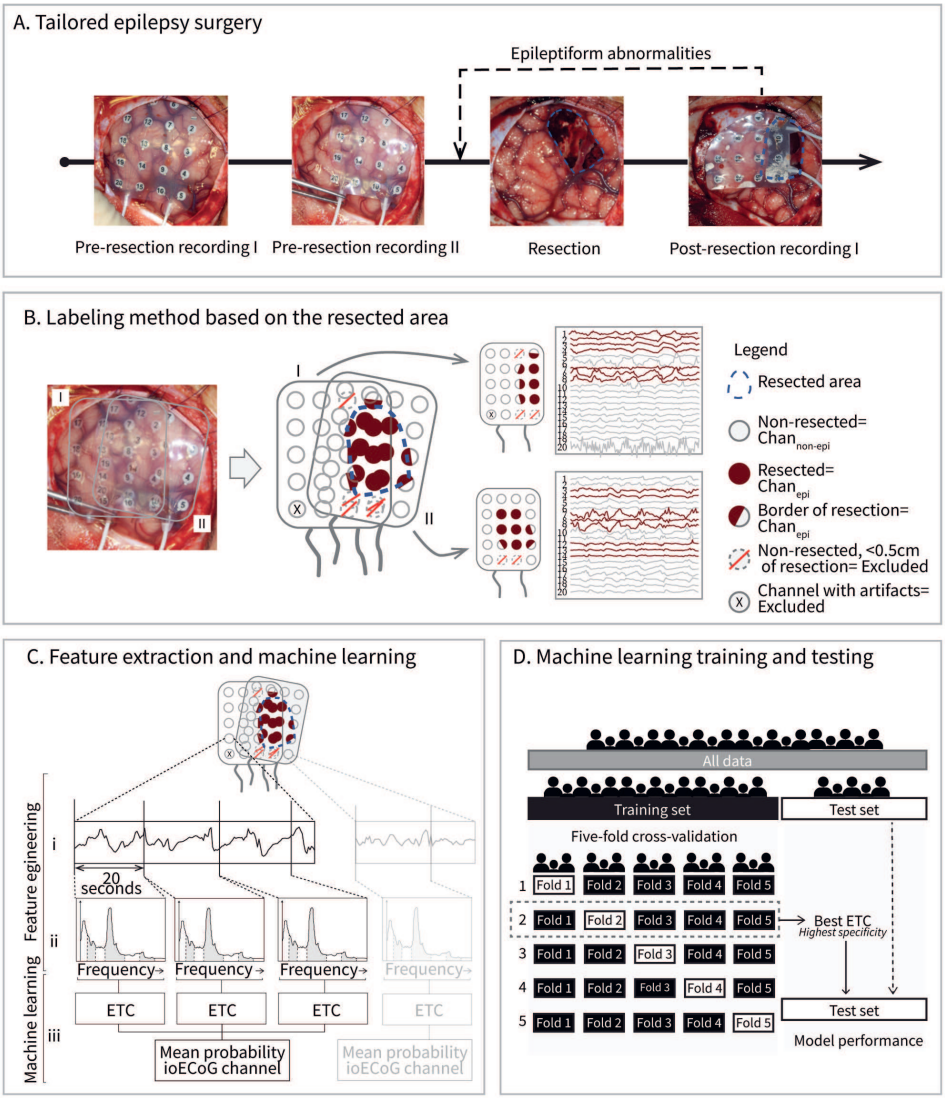


Figure 1: Schematic overview of ioECoG tailored epilepsy surgery, the labeling method, feature extraction and machine learning approach. (A) The different pre-resection ioECoG recordings are acquired by relocating the ioECoG grid every few minutes (i.e. recording locations) to cover all putative epileptic tissue. After resection, a post-resection ioECoG is acquired, which can be repeated until no epileptiform abnormalities persist. Here, only the pre-resection ioECoG is used (pre-resection recording I and II in this example). (B) Labeling approach of pre-resection ioECoG channels in common average montage as $chan_{epi}$ or $chan_{non\text{-}epi}$ based on the performed resection. Channels covering the resection margin are labeled as $chan_{epi}$. Channels covering non-resected tissue within 0.5 cm of the resection margin are excluded to avoid erroneous labels caused by small photo alignment errors. Channels containing artifacts are excluded. (C) For every pre-resection recording location and for each 20 second epoch of a single channel, spectral band powers are computed from the power spectrum density. To account for differences in recording length among recording locations, the mean probability per channel is used for model performance evaluation. (D) Patients are allocated to an 80% training or 20% test set. In five-fold cross-validation, the patients are divided into five subsets, the ETC is trained five times on the data of four subsets, and validated on the fifth subset (i.e., validation subset, white subset in this Figure). The ETC that obtains the highest specificity on the validation subset is evaluated on the test data (model 2 in this example).
Abbreviations: ETC = Extra trees classifier, ioECoG = intraoperative electrocorticography.

Statistical analysis

For the training and test set, we computed summary statistics i.e., absolute and relative frequencies for categorical data and the median (interquartile range [IQR]) for continuous data. As patients had different total amounts of 20-second epochs, we also computed summary statistics at epoch level. At patient level, categorical variables and continuous variables were compared between the training and test set using the Chi-square test and Wilcoxon rank sum test.

We computed the mean (standard deviation [SD]) of the ML performance metrics in five-fold cross-validation. For performance evaluation in the test set, we calculated 95% confidence intervals (CI) with the Clopper-Pearson exact method for accuracy, sensitivity and specificity, standard logit CI given by Mercaldo et al.[73] for the negative and positive predictive value, and DeLong's method[74] for the AUC. Per patient, we compared the average probability between $chan_{epi}$ and $chan_{non\text{-}epi}$ channels with a one-tailed independent t-test, or a one-tailed one-sample t-test when a patient had only one $chan_{epi}$ channel. The AUC of different models (ETC trained with and without clinical ioECoG report information, and ETC trained on patient subgroups) were compared with DeLong's method.[74] For performance comparison between the ETC and clinical ioECoG reading, we evaluated the 2x2 contingency table with the McNemar test.[75]

For all analyses, we considered a p-value ≤ 0.05 significant. We did not correct for multiple comparisons. All ML, xAI and statistical analyses were performed in Python 3.9.

Data and code availability statement

The aggregated dataset of the ioECoG spectral band power data and the source code are publicly available on DataverseNL (dataverse.nl/privateurl.xhtml?token=4bb2a72a-e7cb-48d0-9006-8c8ca9d354c1) and GitHub (github.com/UMCU-EpiLAB/umcuEpi_explainable_AI). The raw ioECoG data are available upon reasonable request via the corresponding author.

Results

Cohort

We included 91 patients (median age 14 years; 40 females; Table 1). All showed MRI abnormalities. Pathology revealed MCD in 35, tumor tissue in 34, other pathology in 18, and no abnormalities in 4. There were 47 patients with a resection in the frontal lobe, 31 in the temporal lobe, 10 in the parietal lobe and 3 in the occipital lobe. The median (IQR) seizure outcome follow-up period was 24 (12-41) months. There were no group differences between the training (n=71; median age 14 years; 31 female) and test set (n=20; median age 13.5 years; 9 female) except for the number of patients with a parietal resection (6% vs. 30%, p=0.008, χ^2- test).

Data acquisition and preparation

The training set comprised 201 different pre-resection ioECoG recording locations with a median (IQR) of 3 (2-4) recording locations per patient. Per recording location, we recorded for a median (IQR) of 199.5 (139-309) seconds with a median (IQR) of 20 (20-26) channels. We excluded a median (IQR) of 1 (0-3) channel per recording location as they were within 0.5 cm of the resection margin but outside the resected area, and 0 (0-1) channels due to artifacts. We labeled a median (IQR) of 6 (2-10) channels as $chan_{epi}$ per recording location. This yielded 44231 epochs of 20-seconds in the training set. The test set comprised 59 different pre-resection ioECoG recording locations with a median (IQR) of 2.5 (2-4) per patient. Per recording location, we recorded for a median (IQR) of 187 (126-287) seconds with a median (IQR) of 20 (20-20) channels. We excluded a median (IQR) of 1 (0-2) channels per recording location due to artifacts and labeled a median (IQR) of 4 (2-8) channels per recording location as $chan_{epi}$. This yielded 12604 epochs of 20-seconds in the test set. No seizures were recorded in the training and test set.

Machine learning model performance

The ETC obtained on the test set a 74.1% (95%-CI: 71.4-76.7%) accuracy, 19.0% (95%-CI: 14.5-24.2%) sensitivity, 92.4% (95%-CI: 90.4-94.2%) specificity, 45.5% (95%-CI: 37.2-54.1%) positive predictive value, 77.4% (95%-CI: 76.4-78.5%) negative predictive value, and AUC of 0.68 (95%-CI: 0.64-0.71) (Table 2; Figure 2A). During five-fold cross-validation, the average performance metrics seemed slightly higher on the training set than on the validation set (Table 2; mean AUC [±SD] 0.74 [±0.01] versus 0.63[±0.06]). Clinical ioECoG reading slightly outperforms the ETC (p=0.03, McNemar), as was also suggested by the performance evaluation metrics, except for specificity (Table 2).

Table 1. Cohort characteristics

	Total data set		**Train set**		**Test set**		
	Participants	Epochs	Participants	Epochs	Participants	Epochs	Participants
	n = 91	n = 56835	n = 71	n = 44231	n = 20	n = 12604	*p-value*
Female (n(%))	40 (44%)	21166 (37%)	31 (44%)	15908 (36%)	9 (45%)	5258 (42%)	1.0‡
Children (n%))	61 (67%)	40558 (71%)	46 (65%)	30276 (68%)	15 (75%)	10282 (82%)	0.56‡
Age at surgery (years, median (IQR))	14 (10-23)	13 (10-20)	14 (10-23)	13 (10-22)	13.5 (10-18)	14 (9-16)	0.54§
Children (<18 years)	12 (8-14)	12 (9-14)	12 (7-14)	12 (8-14)	12 (9-15)	12 (9-16)	0.80§
Adults	33 (23-40)	30 (23-41)	33 (22-40)	30 (22-41)	25 (25-36)	36 (25-36)	0.81§
Duration of epilepsy (months, median (IQR))	57 (20-130)	55 (20-122)	52 (20-142)	52 (20-128)	67 (13-103)	67 13-103)	0.71§
Follow-up period (months, median (IQR))	24 (12-41)	29 (13-57)	25 (12-42)	33 (14-58)	24 (12-32)	25 (12-44)	0.72§
MRI lesion (n(%))	91 (100%)	56835 (100%)	71 (100%)	44231 (100%)	20 (100%)	12604 (100%)	1.0‡
Pathology (n(%))							
Malformations of cortical development	35 (38%)	24142 (42%)	28 (39%)	19527 (44%)	7 (35%)	4615 (37%)	0.92‡
Focal cortical dysplasia	29 (32%)	17983 (32%)	22 (31%)	13368 (30%)	7 (35%)	4615 (37%)	0.95‡
Tuberous sclerosis	4 (4%)	5189 (9 %)	4 (6%)	5189 (12%)	0 (0%)	0 (%)	0.64‡
Other malformations	2 (2%)	970 (2%)	2 (2%)	970 (2%)	0 (0%)	0 (%)	1.0‡
Tumors	34 (37%)	19529 (34%)	28 (39%)	15021 (34%)	6 (30%)	4508 (36%)	0.61‡
Neuronal and mixed neuronal-glial tumors	25 (27%)	15016 (26%)	20 (28%)	11334 (26%)	5 (25%)	3682 (29%)	1.0‡
Diffuse gliomas	8 (9%)	3301 (6%)	6 (8%)	2475 (6%)	1 (5%)	826 (7%)	0.97‡
Other glioma	1 (1%)	798 (1%)	1 (1%)	798 (2%)	0 (0%)	0 (0%)	1.0‡
Ependymal tumor	1 (1%)	414 (1%)	1 (1%)	414 (1%)	0 (0%)	0 (0%)	1.0‡
Other	18 (20%)	11003 (19%)	12 (17%)	7855 (18%)	6 (30%)	3148 (25%)	0.33‡
Cavernoma	8 (9%)	4341 (8%)	5 (7%)	2945 (7%)	3 (15%)	1396 (11%)	0.51‡
Gliosis scars	5 (5%)	2444 (4%)	4 (6%)	1863 (4%)	1 (5%)	581 (5%)	1.0‡

Arteriovenous malformation	1 (1%)	258 (0%)	1 (1%)	258 (1%)	0 (0%)	0 (0%)	1.0‡
Other	4 (4%)	3960 (7%)	2 (3%)	2789 (6%)	2 (10%)	1171 (9%)	0.44‡
No abnormality	4 (4%)	2161 (4%)	3 (4%)	1828 (4%)	1 (5%)	333 (3%)	1.0‡
Anatomical ioECoG location (n(%))							
Frontal	47 (52%)	30689 (54%)	40 (56%)	26416 (60%)	7 (35%)	4273 (34%)	0.15‡
Temporal	31 (34%)	19472 (34%)	26 (37%)	16557 (37%)	5 (25%)	2915 (23%)	0.48‡
Parietal	10 (11%)	5211 (9%)	4 (6%)	1167 (3%)	6 (30%)	4044 (32%)	**0.008*‡**
Occipital	3 (3%)	1463 (3%)	1 (1%)	91 (0%)	2 (10%)	1372 11%)	0.23‡

‡Chi-square test.
§Wilcoxon rank sum test.
** p < 0.05.*
Abbreviations: ioECoG = intraoperative electrocorticography, IQR = interquartile range, MRI = magnetic resonance imaging

Patient-wise tailoring

In 37 patients in the training subset, the ETC assigned significantly higher probabilities to $chan_{epi}$ than to $chan_{non\text{-}epi}$ (patients with $p<0.05$, independent t-test, Figure 3). In both the training and test set, the ETC seemed to perform better in patients with a tumor and temporal lesions compared to patients with other pathology types or lesion locations (Figure 3). This could not be observed for age subgroups and resulted in a good model performance when tested in tumors (AUC 0.81) and temporal lesions (AUC 0.81) subgroups. Subgroup training increased the test set performance in tumors (AUC [95%-CI] 0.84 [0.79-0.89] vs. 0.81 [0.76-0.86], p=0.04, deLong), decreased test set performance in temporal (AUC [95%-CI] 0.70 [0.63-0.77] vs. 0.81 [0.77-0.86], p<0.001, deLong) and frontal lesions (AUC [95%-CI] 0.48 [0.41-0.55] vs. 0.66 [0.60-0.73], p=0.01, deLong), and did not significantly affect test set performance in MCD (AUC [95%-CI] 0.60 [0.55-0.66] vs. 0.66 [0.60-0.71], p=0.09, deLong) (Figure 2B).

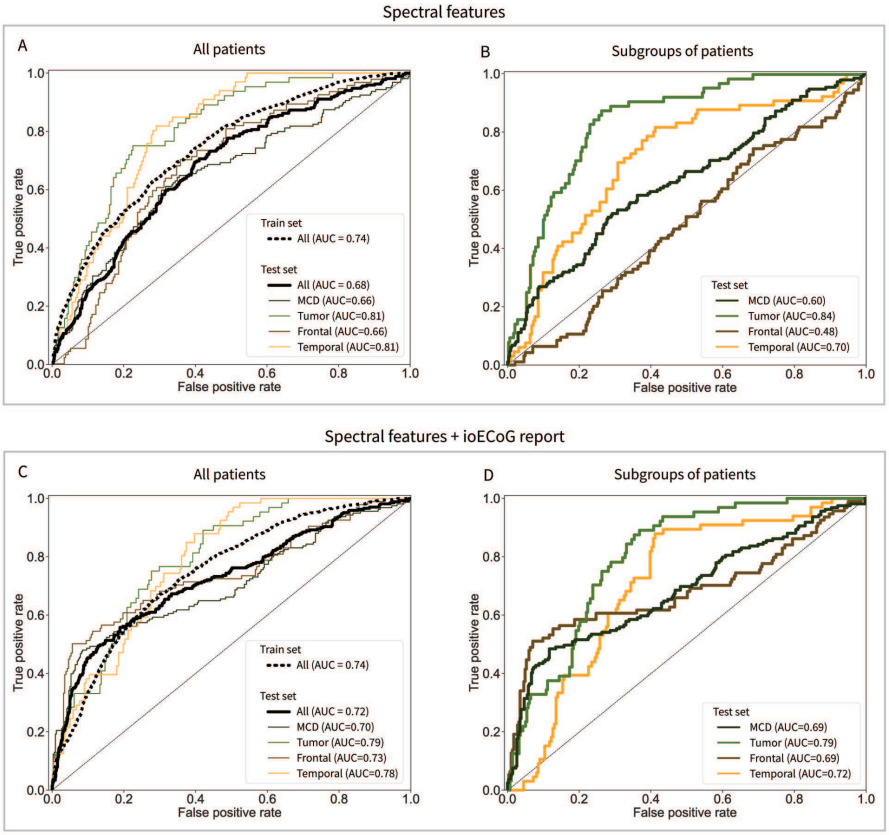


Figure 2: Receiver operating characteristic of ETC performance. (A) The ETC seems to perform slightly better in the training set compared to the test set (AUC_{train} [95%-CI] 0.74 [0.72-0.76] vs. AUC_{test} 0.68 [0.64-0.71]). (B) When trained and tested on subgroup of patients, the ETC obtains an AUC of 0.60 (95%-CI 0.55-0.66) in patients with MCD, 0.84 (95%-CI 0.79-0.89) in patients with tumors, 0.48 (0.41-0.55) in patients with frontal lesions, and 0.70 (95%-CI 0.63-0.77) in patients with temporal lesions. (C,D) When information from clinical ioECoG reading is added to the model, the ETC shows improved test set results in all patients (AUC [95%-CI] 0.72 [0.68-0.75] vs. 0.68 [0.63-0.72], p=0.01, deLong).
Abbreviations: ETC = Extra trees classifier, ioECoG = intraoperative electrocorticography, AUC = area under the curve, MCD = Malformation of cortical development

Clinical ioECoG reading

In the test set, the schematic overviews illustrating the different ioECoG recording locations showed high ETC probabilities of $chan_{epi}$ centered around the resected area in five patients (three temporal tumors), and no clusters of high probabilities in 15 patients (Figure 4). The ETC probabilities represented the resected area better than clinical ioECoG reading in these five patients, whereas clinical ioECoG reading represented the resected area better in six patients (four MCD). Both the ETC probabilities and clinical ioECoG reading failed to identify the resected area in nine patients. When epileptiform activity information from the clinical ioECoG report was added as feature, the ETC represented the resected area well in eight patients. This superior performance was also reflected in different proportions of errors in the test set compared to clinical reading (p=0.003, McNemar) and in higher performance metrics, except for the sensitivity and negative predictive value (Table 2). Adding information from the clinical ioECoG reading increased performance when trained and tested on the whole group (Figure 2; $AUC_{spectral\ features+ioECoG\ report}$ [95%-CI] 0.72 [0.68-0.75] vs $AUC_{spectral\ features}$ 0.68 [0.63-0.72]; p=0.01 deLong).

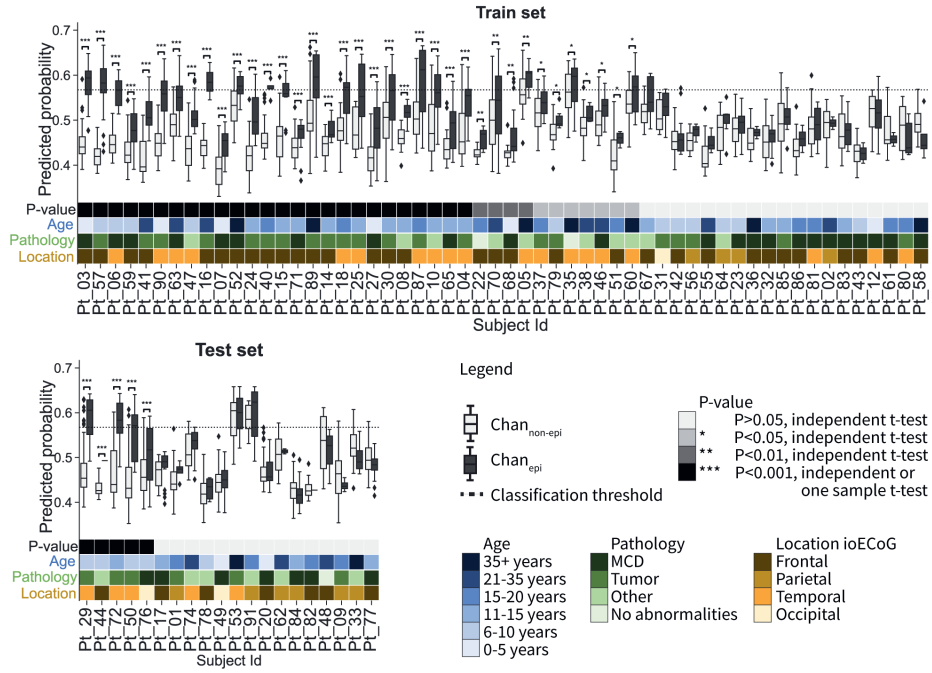


Figure 3: ETC performance in individual patients. The boxplots reflect the probability given to the $chan_{epi}$ and $chan_{non-epi}$ channels per patient. Patients are ranked from left to right based on their p value. The ETC shows superior performances during training and testing in patients with tumors and temporal ioECoG compared to other pathology types and ioECoG recording locations. No such effects are observed for age subgroups.
Abbreviations: MCD = Malformation of cortical development, ETC = Extra trees classifier.

Table 2. Performance metrics of the ETC model.

ETC – spectral features				
	Training set		Test set	
Metric	ETC – training *Mean (SD)*	ETC – validation *Mean (SD)*	ETC* *Value (95% CI)*	Clinical ioECoG reading*/** *Value (95% CI)*
Accuracy	72.3 (1.4)%	69.6 (5.1)%	74.1 (71.4-76.7)%	77.4 (74.8-79.8)%
Sensitivity	24.4 (2.3)%	19.0 (5.5)%	19.0 (14.5-24.2)%	39.9 (34.0-46.1)%
Specificity	95.0 (0.0)%	92.7 (5.4)%	92.4 (90.4-94.2)%	89.8 (87.5-91.8)%
PPV	69.6 (1.4)%	60.6 (13.3)%	45.5 (37.2-54.1)%	56.6 (50.3-62.7)%
NPV	72.7 (1.5)%	71.0 (4.2)%	77.4 (76.4-78.5)%	81.8 (80.3-83.3)%
AUC	0.74 (0.01)	0.63 (0.06)	0.68 (0.64-0.71)***	*NA*
ETC – spectral features + ioECoG report				
	Training set		Test set	
Metric	ETC + ioECoG report – training *Mean (SD)*	ETC + ioECoG report - validation *Mean (SD)*	ETC + ioECoG report** *Value (95% CI)*	
Accuracy	71.0 (2.1)%	68.5 (2.9)%	79.2 (76.7-81.6)%	
Sensitivity	20.4 (4.6)%	15.8 (5.1)%	37.3 (31.5-43.4)%	
Specificity	95.0 (0.0)%	92.7 (3.0)%	93.2 (91.2-94.8)%	
PPV	65.1 (3.3)%	52.3 (10.1)%	64.5 (57.4-71.0)%	
NPV	71.6 (2.1)%	70.3 (3.2)%	81.7 (80.3-83.1)%	
AUC	0.76 (0.01)	0.68 (0.05)	0.72 (0.68-0.75)***	

**McNemar test $ETC_{spectral\ features}$ vs clinical ioECoG reading: p=0.03. **McNemar test $ETC_{spectral\ features\ +\ ioECoG\ report}$ vs clinical ioECoG reading: p=0.003. ***DeLong test AUC $ETC_{spectral\ features}$ vs $ETC_{spectral\ features\ +\ ioECoG\ report}$: p=0.01.*
Abbreviations: ETC = Extra trees classifier, ioECoG = intraoperative electrocorticography, SD = Standard deviation, CI = Confidence interval, PPV = Positive predictive value, NPV= Negative predictive value, AUC = Area under the curve, NA = Not applicable.

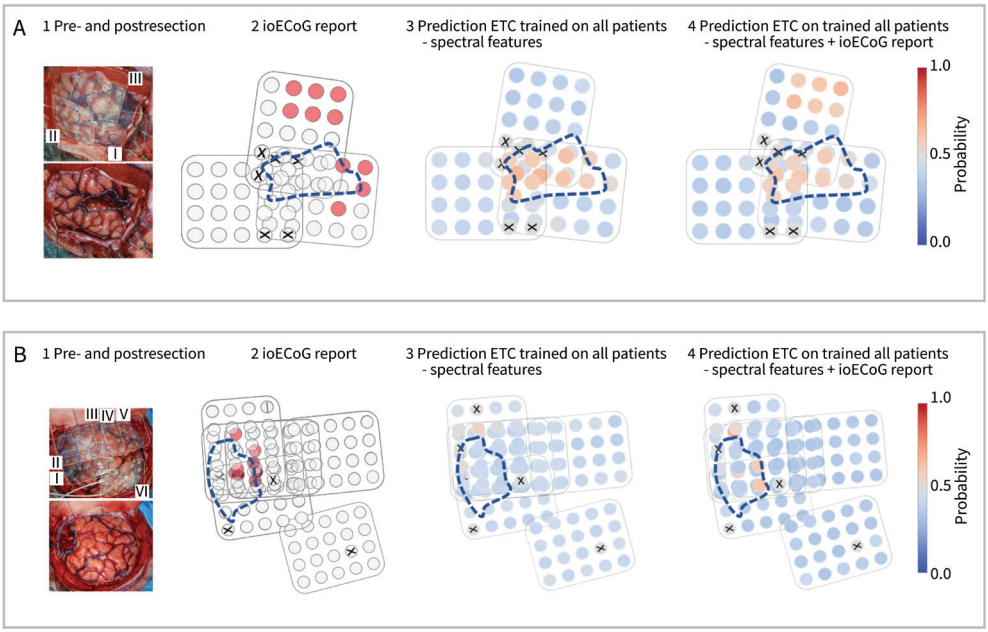


Figure 4: Examples of ETC performance in individual patients. (A) Example of a patient (9 years) with a temporal tumor dysembryoplastic neuroepithelial tumor) and three pre-resection ioECoG locations. For identification of the resected tissue, the clinical ioECoG reading represents resected tissue poorly and the ETC represents this tissue well, as channels covering later-on resected tissue are assigned high probabilities and channels outside the resected area low probabilities of chanepi by the ETC. When information from the clinical ioECoG report is added as a feature to the ETC, it assigns high probabilities to the area showing spikes outside the resected area. (B) Example of a second patient (5 years) with an occipital MCD (focal cortical dysplasia type IIB) and six pre-resection recording ioECoG locations. For identification of the resected tissue, clinical ioECoG reading represents the resected tissue decent and the ETC represents the resected tissue poorly, since channels inside and outside the later-on resected area are both assigned low probabilities of chanepi by the ETC. Adding information from clinical ioECoG reading improves ETC representation as some channels within the later-on resected area show high probabilities of chanepi.
Abbreviations: MCD = Malformation of cortical development, ETC = Extra trees classifier, ioECoG = intraoperative electrocorticography.

Explainable artificial intelligence

The xAI analyses with SHAP showed positive SHAP values for high values of relative theta, alpha and fast ripple power (Figure 5). This indicates that the ETC tends to classify channels as $chan_{epi}$ when they show high values for these features. We observed negative SHAP values for high values of relative beta or gamma power, indicating that the ETC tends to classify a channel as $chan_{non\text{-}epi}$ when high relative beta or relative gamma power is present.

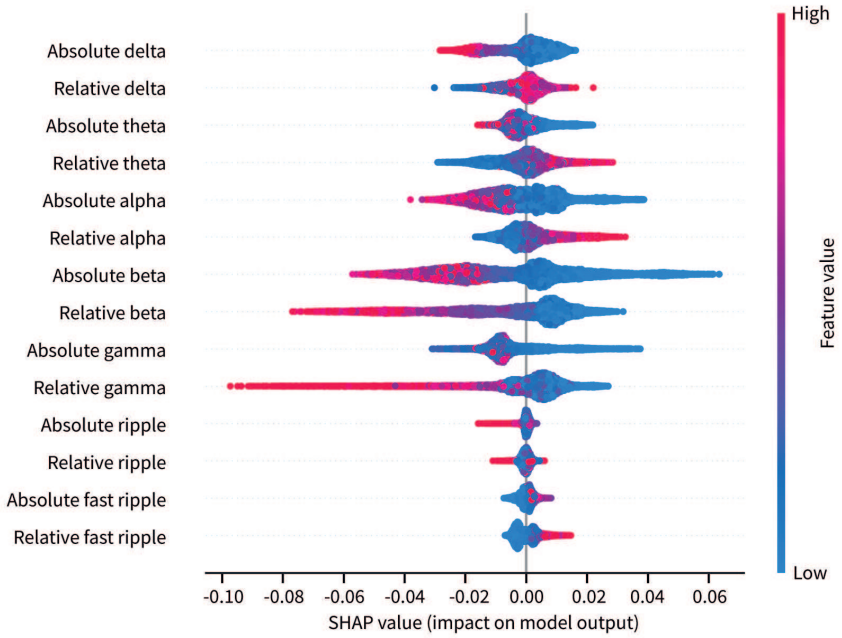


Figure 5: xAI analyses of the test set with SHAP. Overview of SHAP values and the corresponding feature values where two clear patterns are observed. SHAP values are positive for relatively high feature values of the relative theta (4-8Hz), alpha (8-13Hz), fast ripple (250-500Hz) power. Similarly, SHAP values are negative for relatively high feature values of relative beta (13-30Hz) or gamma (30-80Hz) power. Abbreviation: SHAP = Shapley Additive exPlanations.

Discussion

We examined the potential of ML for ioECoG based epileptic tissue identification beyond clinical reading in a ML combined with xAI approach. The ML model ETC classified pre-resection ioECoG channels with 19.0% sensitivity, 92.4% specificity, and an AUC of 0.68 using basic spectral features derived from ioECoG background activity. The ETC was superior to clinical ioECoG reading in five out of 20 test patients and was outperformed by clinical ioECoG reading in six patients. Combining the ETC with clinical ioECoG reading yielded superior performances compared to using either one alone. The ETC performances varied per patient, with the best performances observed in patients with tumors. With xAI, using SHAP, we revealed relative theta, alpha, and fast ripple power as important for the characterization of epileptic tissue by the ETC and the relative beta and gamma power as important for characterizing non-epileptic tissue (the relative beta and gamma power). Our findings, based on basic spectral features, suggest an untapped richness of ioECoG in epilepsy surgery. The ML and xAI analysis presented here forms a touchstone for future ML approaches for ioECoG based epileptic tissue localization.

Previous ML studies with predefined intracranial EEG features for epileptic tissue identification showed comparable or slightly better results.[60,76-80] A fair comparison is difficult as all prior studies used long-term intracranial EEG and different labeling approaches (seizure onset zone vs. resected area) and/or recording types (ictal vs. interictal, depth electrodes vs. electrocorticography). For example, Varatharajah et al.[80] showed slightly better results (AUC 0.73 vs. 0.68 here) but focused on seizure onset zone identification using 90-minute interictal recordings. Other researchers successfully used ML to automatically detect existing stochastic epileptiform ioECoG biomarkers e.g., interictal epileptiform discharges[81] and HFOs[21]. This will speed up visual ioECoG reading but will not necessarily increase the predictive value of the ioECoG. Two prior studies used ML techniques as deep learning to extract intricate features automatically - a promising approach as explicitly designing epileptiform ioECoG features is challenging.[82,83] Their generalizability remains however uncertain, as they used a selected and small sample size of five patients with temporal lobe epilepsy. Previous studies often used leave one (patient) out cross-validation or cross-validation with data from the same patients to evaluate a ML model's generalizability, probably due to limited patient numbers.[21,60,76-80,82,83] These approaches have shortcomings: leave-one-out risks high performance variance while cross-validation with data from the same patients will affect the reliability of the generalization assessment.[26] We kept a separate test set and included a heterogenous study population (i.e., different ages, anatomical locations, and etiologies) to obtain a fair and robust generalizability assessment. We presented results for individual patients and showed that the ML performances varied among patients. This underlines that ML performances cannot directly be generalized to other patients with epilepsy. Recognizing the inherent complexity of ioECoG data – recorded from different brain regions of patients with varied demographics and etiologies – is essential for advancing ML models applied to it.

Data-driven insights from ML combined with xAI approaches may lead to novel biomarkers or refinements of biomarkers[21], but there is no consensus in literature on how xAI methods should be exploited.[24] SHAP highlighted ioECoG features that contributed to the classification, but did not explain the underlying reasons, as was also encountered in a previous EEG study using SHAP.[84] Here, SHAP revealed that high relative theta, alpha, and fast ripple power increased the probability that a channel had epileptiform characteristics. Aberrant activity in the theta and alpha band was observed in people with epilepsy in earlier EEG and magnetoencephalography studies.[85-87] In a prior ioECoG study, alpha band alterations were related to distance of the resected tissue.[88] Previous studies

focusing on the fast ripple frequency band have mainly studied the fast ripple as stochastic event.[12,14,27,89] In line with recent work[90], our findings suggest that not only the events, but also the power in the background activity within the fast ripple frequency band contains predictive value for epileptic tissue identification.

SHAP showed that the presence of relative high beta and gamma activity was important for the classification of channels with non-epileptiform characteristics. This finding aligns with Claus et al.[91], who reported increased beta and gamma activity following diazepam administration but not in epileptic tissue. The patients in our study received propofol anesthetics, which acts through positive modulation of the GABA type A receptor, similar to diazepam.[92] Hence, high beta and gamma power may indicate a normal response to propofol anesthetics, reflecting non-epileptic tissue. Our finding also aligns with a previous study in mice where alterations in gamma power were hypothesized to reflect a local inhibitory network that suppresses seizures in the surrounding area and thus to be predictive of non-epileptic tissue.[93] As clinicians and researchers tend to focus on pathological (i.e. epileptiform) patterns[14,15,21,89], the revelation of ioECoG patterns indicative of healthy brain tissue opens opportunities to explore such patterns further. These patterns can enhance tailored epilepsy surgery, especially in cases where stochastic epileptiform markers are absent.

Strength and limitations

A strength of this work is that we presented results for individual patients from a heterogeneous cohort. Training on ioECoG recording location subgroups did not improve the ETC performance, meaning that the ETC was able to learn patterns generalizable across anatomical locations. On the contrary, adding information from the clinical ioECoG report to the ETC improved performances for patients with MCD, but not for patients with tumors. These findings indicate that interpatient ioECoG variability, caused by different underlying pathologies, hampered the ETC in learning generalizable patterns across etiologies. While our ETC shows the potential of ML for ioECoG based epileptic tissue localization with a high specificity (92.4%) and decent negative predictive value (77.4%), its performance is not adequate yet for clinical implementation. To increase the ETC's robustness, more data or additional synthetically created data is needed, especially for underrepresented subgroups, e.g., patients with occipital lesions. Models optimized for a specific subgroup or incorporating clinical characteristics into a ML model may improve epileptic tissue detection performances and can lead to a personalized ioECoG tailored epilepsy surgery. Training the ETC on ioECoG data from multiple centers would enhance robustness for ioECoG variability introduced by OR-settings, EEG recording systems, and patient populations.

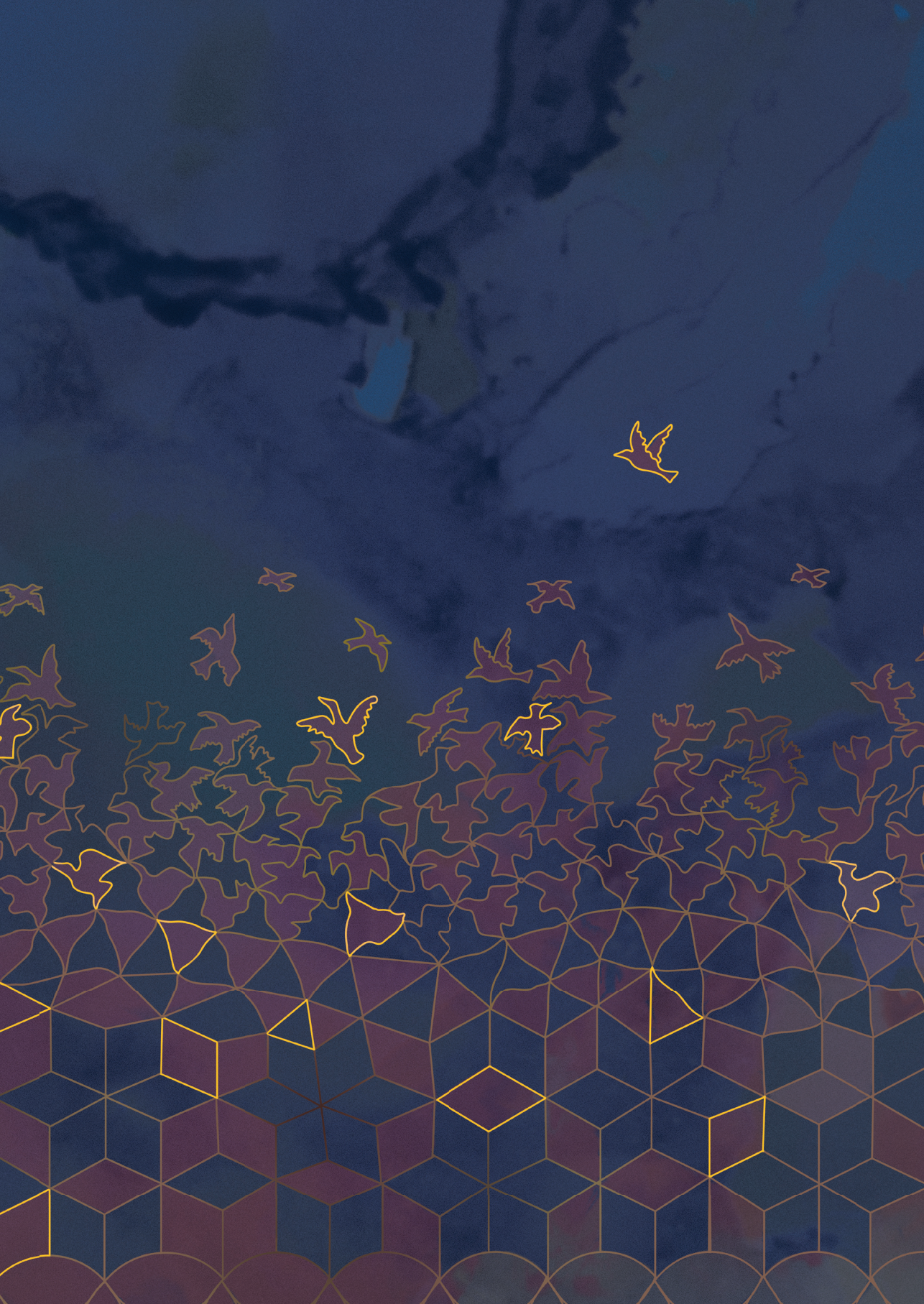
In contrast to previous work, we assessed ML performances in relationship with clinical ioECoG reading. The finding that our ETC can complement clinical ioECoG reading in some cases holds clinical implications. Using ML with quantitative features has benefits such as objectivity, convenience, and rapid assessment - our ETC classifies a 20s ioECoG within 1 second. In addition, it allows for identification of subtle patterns that might be overlooked by visual ioECoG reading. Our results open opportunities for developing a fully automated tool for aiding clinical ioECoG based epileptic tissue detection.

A limitation is the labeling method. Labeling tissue as epileptic is difficult as there is no direct measure for it. Labeling based on the resected area in patients who attained post-surgical seizure freedom seemed the only option but could have led to survival bias. In addition, the reliability of post-surgical outcomes increases over time and depends on anti-seizure medication usage.[94] The assumption that all channels covering the resected area contained epileptiform abnormalities may have yielded false positives given that the resected area may have comprised

non-epileptic tissue as well. Although it was shown that AI models can mitigate labeling errors[95], the ETC may have learned patterns not only specific for epileptic tissue but for peri-epileptic tissue as well. Novel ML techniques, specifically multi-instance learning, may address this labeling issue by considering that not all resected tissue may be epileptic.

Our ioECoG input for the ML model was limited. The ioECoG is a non-stationary multivariate time series with varying channel numbers and configurations.[96,97] This makes it difficult to define a standardized ML model input. We opted for single ioECoG channels of 20 seconds to create a ML baseline for ioECoG-based epileptic tissue localization and to align with a previous ML approach using intracranial EEG for epileptic tissue localization.[82] Nonetheless, the optimal epoch length warrants further investigation. While epilepsy is regarded a network disease, our spectral features do not hold information about network dynamics. Incorporating information about brain activity propagation or connectivity may improve ML performances.[60] For example by using network measures as input or a multi-dimensional ioECoG representation and learning techniques that can automatically extract features (e.g., deep learning). Likewise, information from post-resection ioECoG and other modalities, like MRI-findings, could be integrated.

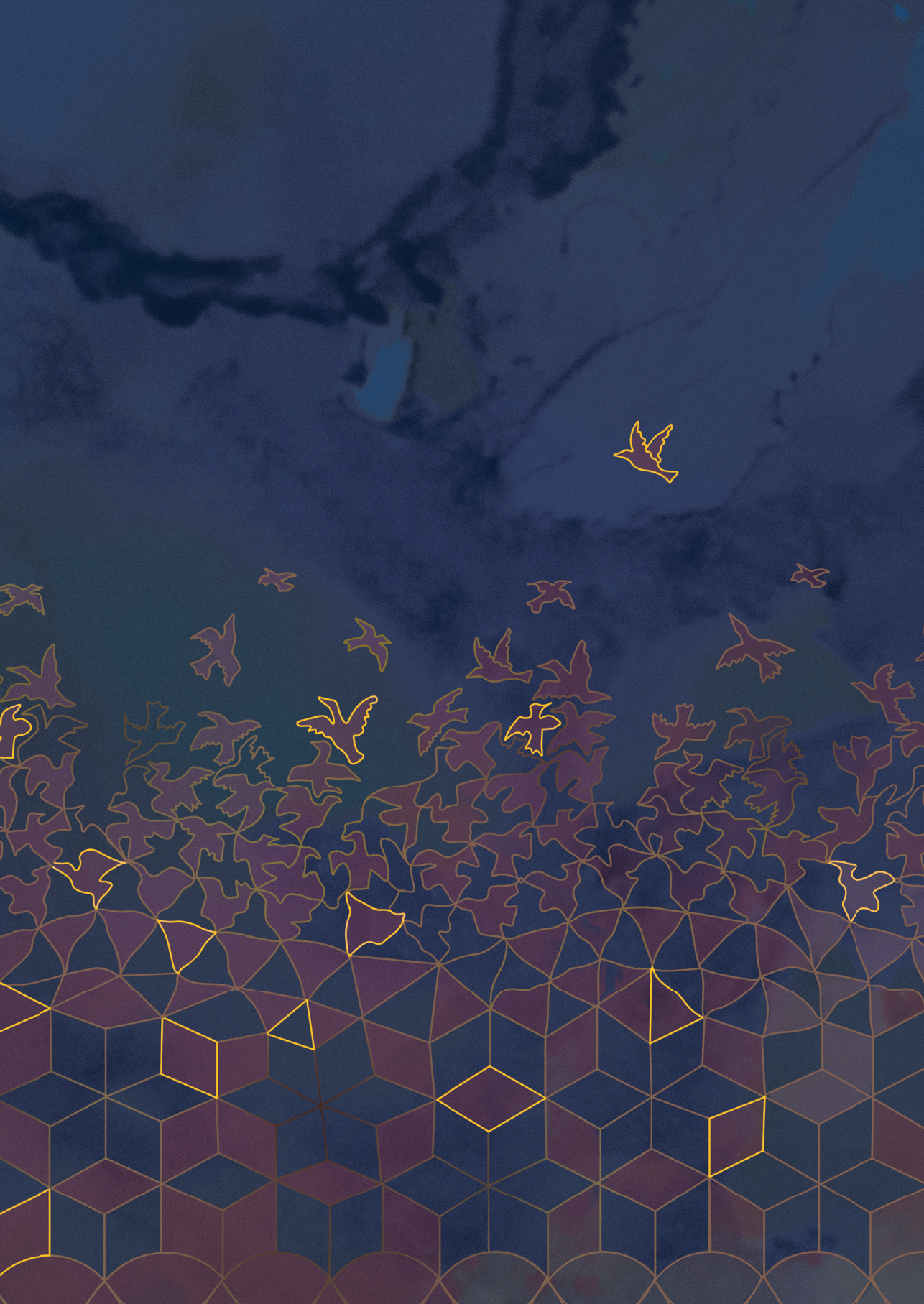
We applied ML for direct intraoperative epileptic tissue localization based on the ioECoG. Our analyses showed that the ioECoG holds a richness which is yet to be explored. With xAI we established ioECoG patterns important for tissue classification as (non-)epileptic. Our ML performances based on basic signal properties form a touchstone for future research and suggests high potential of advanced ML applied on the ioECoG in epilepsy surgery. Next steps are to include ioECoG network measures and features derived from clinical information in ML models. We made our (explainable) AI source code publicly available and endorse its application to continue this AI research in the field of epilepsy surgery.



Part II

From Interpretation to Innovation





Chapter 5

The optimal montage to mark epileptiform discharges and high frequency oscillations in intraoperative electrocorticography

Ziyi Wang*, Jiaojiao Guo*, **Eline V. Schaft**, Sem Hoogteijling, Cyrille H. Ferrier, Gerhard H. Visser, Dongqing Sun, Friso W.A. Hoefnagels, Taku Inada, Sandra M.A. van der Salm, Geertjan M. Huiskamp, Nicole E.C. van Klink, Maryse A. van 't Klooster, Maeike Zijlmans, on behalf of the RESPect database study group

* These authors contributed equally

Published in Clinical Neurophysiology Practice, Volume 10, July 2025

Abstract

Objective

In intraoperative electrocorticography (ioECoG), interictal epileptiform discharges (IEDs) and high frequency oscillations (HFOs; ripples 80-250Hz, fast ripples (FRs) 250-500Hz) can be identified in average or bipolar montage. We studied how montage choice affects event identification.

Methods

Two reviewers independently marked IEDs and HFOs across three montages (average, horizontal- and vertical bipolar) from 13 patients who were seizure free after ioECoG-guided surgery. We analyzed the number of channels with events, total events count, events morphology (maximum amplitude, duration, frequency), number of instances with overlapping events across multiple channels (event instance), concordance of event instances over montages, and percentage of channels with events in the resected area.

Results

Bipolar montages yielded more channels with events, higher counts, and greater maximum amplitude of IEDs and ripples compared to average montages. Average and horizontal bipolar montages yielded more IED instances than vertical bipolar montages. Average montages detected the highest percentage of event instances occurring only in this montage. Event duration, frequency, and percentage of channels with events in the resected area did not differ across montages.

Conclusions

All three ioECoG montages are clinically useful to find epileptic events. The bipolar montage detects more events with greater amplitude, while the average montage uncovers a wider variety of unique events. Combining montages provides complementary information.

Significance

This study quantitatively revealed how different montages capture epileptiform events.

Introduction

Epilepsy surgery offers a chance for cure for people with refractory epilepsy.[7,127] Surgical effectiveness hinges on precise delineation and complete resection of epileptogenic tissue.[7] Intraoperative electrocorticography (ioECoG) directly measures activity from the cortex and enables repeated recordings, enhancing surgical precision by identifying electrophysiological abnormalities.[64,128]
Conventional interictal epileptiform discharges (IEDs) are well-established biomarkers of epilepsy.[129] IEDs are defined as transient events characterized by a 'spike' or sharp waveform lasting 20-70 ms, distinctively standing out from the background brain activity.[130,131] High frequency oscillations (HFOs), subdivided into ripples (80-250 Hz) and fast ripples (FRs; 250-500 Hz), have been proposed as a novel biomarker to more precisely localize the source of the epilepsy than IEDs.[12,27,33,34,89,132] HFOs are defined by their morphology, defined as at least four consecutive oscillations with an amplitude clearly above the baseline signal, and a duration of less than 200 ms.[133-135]

Various EEG display montages are used to capture seizures and epileptiform events in clinical EEG practice.[136,137] The most prevalent montages are: a common (external) referential, a standard average, and a bipolar montage.[138] Similar to surface EEG, a common referential montage is used for both recording and clinical review purpose during ioECoG monitoring.[139] It involves a reference electrode that is often placed on the contralateral mastoid. This hardware setup, with the considerable distance between the reference point and the electrodes on the grid, is susceptible for noise or artifacts. This issue can be addressed by transforming the raw data into standard average or bipolar montage for a clearer display.[13,140,141]

An average montage generally preserves the broader shape and amplitude distribution of IEDs across its coverage, allowing for better visibility of electrical activity.[138] Yet on the downside, the averaging process can smooth out the sharp features of IED waveforms. Further, artifacts in one channel can contaminate all other channels when using an uncorrected average montage.[138,142] Stereo EEG is often reviewed in a bipolar montage and it enables direct channelwise localization of epileptic activity.[143,144] In line with the pioneering stereo EEG studies[58,145], we and other centers used bipolar montages for the detection of HFOs on ioECoG.[13,57,128] In an ioECoG grid configuration, both horizontal and vertical directions along the grid are possible (Figure 1A). The bipolar configuration depends on potential differences between two adjacent recording electrodes [142] and has the advantage of eliminating common noise, but might also mask identical events occurring on two neighboring electrodes.[139]

Marking intraoperative events can be done in any aforementioned montage configuration, but it is an unanswered question whether different montages capture equivalent or akin IEDs and HFOs. This work compared IEDs and HFOs marked in ioECoG recordings using three types of montage configurations: average montage (AVG), horizontally oriented bipolar montage (HBIP), and vertically oriented bipolar montage (VBIP). Our main research purpose was to pinpoint the methodological issues related to diverse ioECoG montages, and how these influence the accurate identification and interpretation of IEDs and HFOs.

Methods

Study design and patient selection

We retrospectively selected 13 people with refractory focal epilepsy characterized by a neocortical lesion who were part of the Registry for Epilepsy Surgery Patients (RESPect) database of the University Medical Center Utrecht (UMC Utrecht) and Stichting Epilepsie Instellingen Nederland (SEIN). Those 13 people underwent ioECoG tailored epilepsy surgery between 2008 and 2018, and achieved seizure freedom (Engel IA) at ≥ 1y. We assumed that seizure freedom signified complete resection of the presumed epileptogenic tissue. Our aim was to assess various aspects of the aforementioned montages in a diverse population, ensuring representation across: 1) all anatomical regions of the brain (i.e. temporal, frontal, parietal, and occipital), excluding patients with mesial temporal lobe epilepsy due to the inability to visualize grid placement; 2) common underlying histopathologies associated with epilepsy (e.g. malformations of cortical development (MCD) and central nervous system (CNS) tumors.

The RESPect database was approved by the institutional ethical committee of UMC Utrecht, who exempted the requirement for written informed consent till 2018 due to the research's retrospective nature, whereas explicit informed consent is requested from 2018 onwards (non-WMO; METC18-109C). All collected data were coded to maintain (pseudo)anonymity.

Surgical procedure and ioECoG recordings

Epilepsy surgery was performed under general intravenous propofol anesthesia. The neurosurgeon exposed the cortex intended to be removed and a few centimeters of the surrounding tissue. We recorded ioECoG with standard 4x5 grid electrodes (AD-Tech, Racine, WI), featuring platinum surfaces encased in silicone with a contact area of 4.2mm² and an interelectrode distance of 10 mm. The ioECoG was recorded using a 32 or 64 channel EEG system (Micromed, Treviso, Italy) at 2048Hz sampling rate, with an 538Hz antialiasing filter. Recorded signals were referenced to an external electrode positioned on the contralateral mastoid. To reduce the potential interference of burst suppression, we temporarily halted the administration of propofol before ioECoG monitoring. [107]

ioECoG recordings composed three stages: 1) Pre-resection recordings: grids were positioned in multiple locations before the planned resection to encompass all suspected epileptogenic tissue; 2) Intermediate-resection recordings: if epileptic activity persisted after the initial resection, the resection was extended if not limited by eloquent cortex or too distant locations; 3) Post-resection recordings: following the finalized resection, ioECoG was recorded from cortex around the cavity. The ioECoG was recorded in each position for 2-5 minutes, consistent with our previous work.[14,89,146]

Intraoperative photographs and crafted sketches were used to document the ioECoG position on the cortex. ioECoG electrode placement was guided by surgical practicalities and was not standardized across patients. For example, the neurosurgeons tend to place electrode grids in a way that maximizes contact with regions suspected of epileptogenic activity, while fitting within the boundaries of the craniotomy, thus not typically oriented parallel or perpendicular to the gyri configurations. In temporal lobe epilepsy, the grid was often placed first directed towards the temporal pole and then towards dorsotemporal. In those situations, the horizontal configuration generally follows the natural pattern of the temporal

gyri. ioECoG guided surgical resection of the epileptogenic tissue was based on preoperative MRI findings and IEDs. One patient was enrolled in a RCT "the HFO trial"[128] and assigned to the HFO guided tailoring arm, meaning that HFOs instead of IEDs were used to guide the surgeon.

Montage configurations, artefacts and channel labels

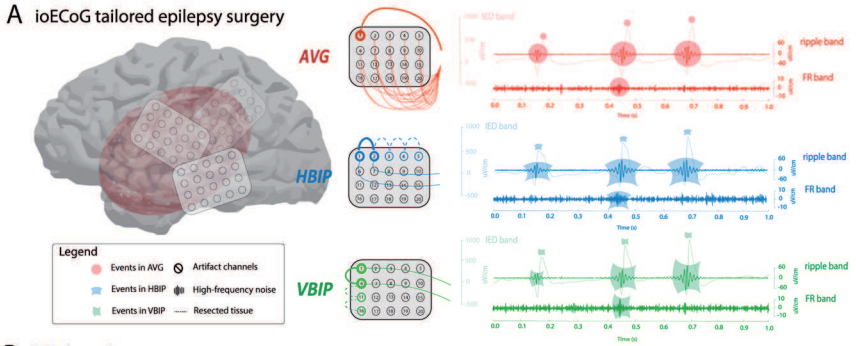
We rereferenced the raw data offline to AVG, HBIP, and VBIP montages (Figure 1A). Channels in each montage that exhibited continuous artefact interference or no cortical signal were excluded from further analysis.

We used custom made software to align pre- and intermediate-resection photographs to post-resection photographs, identifying which unipolar grid electrodes in pre- and intermediate-resection recordings covered the eventually resected area (Figure 1Bii, 1Cii, and 1Dii). We categorized unipolar channels into two groups: i) Resected, covering the complete post-resection cavity, which encompassed tissue ≤5mm inward from the edge of resection cavity; ii) Non-resected, covering the tissue >5mm from the edge of the resection cavity. Based on these unipolar labels, we derived bipolar labels: i) Resected, if at least of one of the two unipolar channels were resected; ii) Non-resected, if both unipolar channels were non-resected. In both intermediate- and post-resection recordings, we excluded all unipolar channels located above the resection cavity and their corresponding bipolar channels.

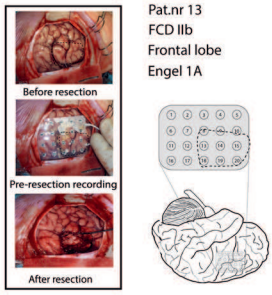
IED and HFO markings

We selected one-minute epochs at the end of each recording to minimize propofol effects.[44,107] All events were marked in BrainQuick Software (Micromed, Treviso, Italy) in three montages (i.e. AVG, HBIP, and VBIP). The reviewers were restricted to using only one montage during the marking process. IEDs were marked independently, blinded for HFOs. IEDs were marked using the consistent settings across three montages: 80Hz lowpass IIR filter, gain 800 μV/cm, 15 s/page. We defined IEDs as transient and stereotype waveforms (< 80Hz) distinctly standing out from the baseline with an evident epileptiform pattern, including single spikes (<80ms), shape waves (>80ms), periodic spikes/ sharp waves, polyspikes, and spike/sharp wave and slow wave complexes. IEDs were marked separately by two reviewers (ZW, JG) and checked by two experts (MvtK, CF).

HFOs were initially marked in the three montages by an automated HFO detection algorithm[13,47]. Consistent settings across montages were used: ripple: 80-1000Hz bandpass FIR filter, gain 50μV/mm, 1s/page; FR: 250-1000Hz bandpass FIR filter, gain 10μV/mm, 1s/page). All automated marked events were visually inspected separately by two reviewers (ZW, JG) on two 22-inch wide screens. One screen displaying ripples and the other showing FRs, both time locked for simultaneous viewing. Three HFO experts (MvtK, MZ, NvK) checked the marked HFOs.

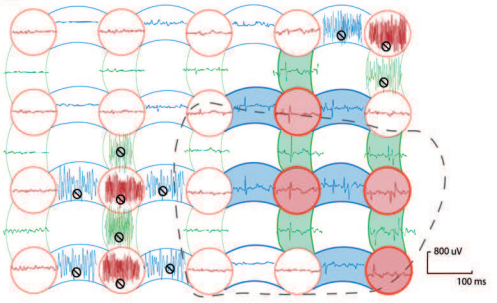


B IED band (80 Hz low-pass IIR filter, gain 800 µV/cm, 15 s/page)

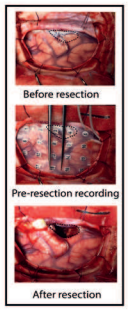


B ii)

Pat.nr 13
FCD IIb
Frontal lobe
Engel 1A

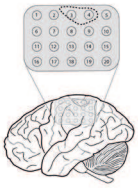


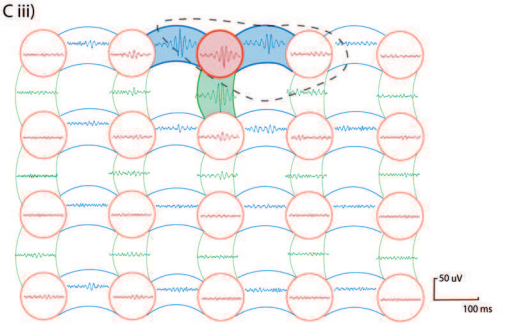
C Ripple band (80-1000 Hz band-pass FIR filter, gain 50 µV/mm, 1 s/page)



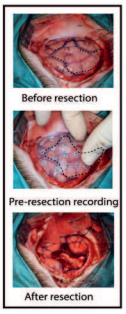
C ii)

Pat.nr 02
FCD IIb
Parietal lobe
Engel 1A



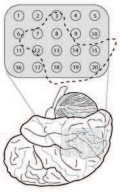


D FR band (250-1000 Hz band-pass FIR filter, gain 10 µV/mm, 1 s/page)



D ii)

Pat.nr 01
FCD IIb
temporal-parietal-occipital lobes
Engel 1A



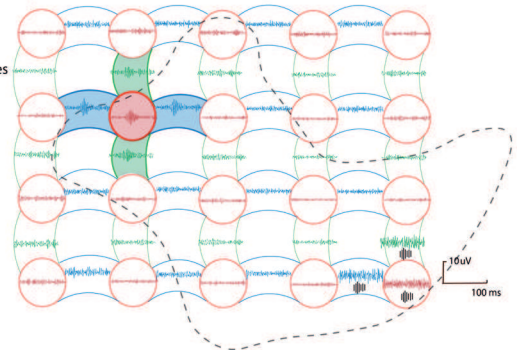


Figure 1: Schematic illustration of the ioECoG recording situations, the three montages with their corresponding channels, and three representative patient examples. A) Schematic representation of a standard electrode grid configured with AVG, HBIP, and VBIP montages. After opening the dura, the grid is placed in various positions per stage, and ioECoG is recorded in each position for 2-5 minutes. Based on the standard 4x5 grid configuration, the AVG consist of 20 channels, the HBIP of 16 channels, and the VBIP of 15 channels. An example of data from a single channel, showing events in the IED, ripple, and FR band, is presented for each montage. AVG (in red): average reference signal is calculated by summing the voltages from all electrodes (excluding the mastoid reference, and bad channels) and dividing this by the total number of electrodes. The potential for each electrode is calculated by subtracting the average reference signal from the voltage recorded at that electrode. HBIP (in blue): for each neighboring pairs of adjacent electrodes that are transversely aligned – left to right in horizontal direction over the grid–, the bipolar potential is calculated as the voltage recorded at the left electrode subtracted from the voltage recorded at the right electrode (e.g., 01-02, 02-03, 03-04, 04-05). VBIP (in green): for each neighboring pair of adjacent electrodes that are longitudinally aligned – top to bottom in vertical direction over the grid – , the bipolar potential is calculated as the voltage recorded at the lower electrode subtracted from the voltage recorded at the upper electrode (e.g., 01-06; 06-11; 11-16). B) Patient example (Pat.nr 13) showing IEDs in the frontal lobe for the three montages. Bi) intraoperative photographs (unresected cortex, pre-resection recording, and after final resection) are matched to determine channel positions and resected tissue (also for Ci and Di). Bii) patient characteristics (Pat.nr, histopathology, anatomical location, 1y seizure outcome) and schematic visualization of the pre-resection grid position including the resected area to label channel as either resected or non-resected (also for Cii and Dii). Biii) in the pre-recording, IEDs were observed on AVG channel 09, 14, 15 and 20; on HBIP channel 08-09, 09-10, 13-14, 14-15, and 19-20; on VBIP channel 04-09, 09-14, 14-19, 10-15, 15-20. Instantaneous artifacts were observed on AVG channel 05, 12, 17; on HBIP channel 04-05, 11-12, 12-13, 16-17, 17-18; on VBIP channel 05-10, 07-12, 12-17. C. Patient example (Pat.nr 02) showing ripples in the parietal lobe for the three montages. Ciii) in the pre-recording, ripples were observed on AVG channel 03; on HBIP channel 02-03, 03-4; on VBIP channel 03-08. D) Patient example (Pat.nr 01) showing FRs in the temporal-parietal-occipital region for the three montages. Diii) in the pre-recording, FRs were observed on AVG channel 07; on HBIP channel 06-07, and 07-08; on VBIP channel 02-07, 07-12. Instantaneous high-frequency noise were observed on AVG channel 20; on HBIP channel 19-20; on VBIP channel 15-20. Abbreviations: AVG = average montage, HBIP = horizontally-oriented bipolar montage, VBIP = vertically-oriented bipolar montage, IED = interictal epileptiform discharge, FR = fast ripple, ioECoG = intraoperative electrocorticography, Pat.nr = patient number, FCD = focal cortical dysplasia, Engel IA = seizure free ≥ 1 year after surgery.

Interrater agreement

The interrater agreement between the two reviewers (ZW, JG) was calculated using Cohen's Kappa coefficient (κ-value) for the visually marked IEDs and HFOs per 1-minute segment across all three montages.[147] A $\kappa<0$ reflects that the agreement was made by chance; $\kappa=0.5$ reflects moderate agreement; $\kappa=1$ indicates complete agreement. We defined $\kappa>0.5$ as the threshold of sufficient concordance.[148]

Agreed events (IEDs, ripples, and FRs) were defined as events marked by both reviewers (ZW, JG). Recordings with more agreed events had a greater influence on the calculation of the κ-value for that montage compared to recordings with fewer agreed events. To address this imbalance, we calculated the overall weighted average κ-value as a proxy for IED and HFO marking quality across the three montages. For example, the overall weighted average κ-value for the IED in AVG equals

$$\frac{(\kappa_1 * \text{Nr. Agreed IED}_1) + (\kappa_2 * \text{Nr. Agreed IED}_2) + (\kappa_3 * \text{Nr. Agreed IED}_3) + \ldots}{\text{Nr. Agreed IED}_1 + \text{Nr. Agreed IED}_1 + \text{Nr. Agreed IED}_1 + \ldots}$$

(*1,2,3…* represented the recording numbers)

All agreed events, onwards termed events, were retained for subsequent montage performance analysis, while events marked by only one reviewer (ZW or JG) were rejected.

Montage performance and analysis

All events were extracted from the BrainQuick .trc files and imported into Matlab (version 2022, The MathWorks Inc, Natick, MA) for further analysis. We assessed the montage performance as follows: 1) number of channels with events; 2) total event counts; 3) number of event instances; 4) concordance of event instance over montages; 5) events morphology; 6) percentage of channels with events located within the resected area. The assessments were performed independently for IEDs, ripples, and FRs, and subsequently compared across the three montages.

1. *Number of channels with events*: we normalized for the variance in the total number of artefact free channels across the montages by using the number of artefact free channels in *AVG* montage as reference. Based on this reference, we proportionally adjusted the channel counts in the *HBIP* and *VBIP* montages. We first calculated the normalized number of channels with events for each recording (pre-, intermediate-, and post-resection) at the recording group level. We further summed these number across all recordings for each patient, obtaining patient group level data.
2. *Total events count*: following the same proportional adjustment based on channel normalization, we calculated the normalized event counts at the recording and patient group levels.
3. *Number of event instances*: an event instance is defined as a duration in which at least one event occurred in a single montage. If multiple events had overlap in time, the event instance covers the duration of all overlapping events. We calculated the number of event instances at the recording group level.
4. *Concordance of event instances*: we compared if event instances had overlap in time between montages. These simultaneous event instances in at least two montages were classified as concordant event instances. In contrast, event instances that were detected solely in one montage were classified as unique event instances. Venn plots were used to illustrate the concordant and the unique event instances between the montages.
5. *Event morphology*: we calculated the following properties for each event: i) the maximum amplitude (in μV), defined by the highest absolute value within the duration of the event based on Hilbert transform envelope; ii) the duration (in ms): the time from start to stop of the marking of an event; iii) the frequency (in Hz), by counting the number of times an event crosses the zero horizontal axis (zero crossing rate). For comparisons between montages, we used the averaged morphologies, weighted at the recording group level. The event count for each recording represented its relative importance, with recordings containing a higher event count carrying greater statistical weight.
6. *Percentage of channels with events located within the resected area*: we calculated the amount of channels with events located inside the resection margin, for each pre- and intermediate-recording. We then compared the percentage as following:

$$\textit{The percentage channels with events within resected area} = \frac{\textit{The amount of channels with events in the resected area}}{\textit{Total amount of channels in the resected area}}$$

Statistical analysis

We calculated and compared the following variables among three montages: i) weighted average κ-values; ii) number of channels with events; iii) total events count; iv) number of event instances; v) event morphology (maximum amplitude, duration, frequency); vi) percentage of channels with events in the resected area.

These variables contained three level nested data, namely several recordings (*i*) within multiple recording stages (e.g pre-, intermediate-, and post-recordings; *R*) per patient (*P*). Two generalized linear mixed models (GLMM) were utilized to account for these dependencies:

- Model 1 used for the analysis of i) and v):
  $log(E[Y_{miRP}]) = \alpha + \alpha_R + \alpha_P + \beta_1 X_{Hm} + \beta_2 X_{Vm} + \beta_3 X_{iRP} + \varepsilon_{mRP} + \varepsilon_{RP} + \varepsilon_P)$

- And Model 2 used for the analysis of ii), iii), iv), and vi):
  $log(E[Y_{miRP}]) = \alpha_0 + \alpha_R + \alpha_P + \beta_1 X_{Hm} + \beta_2 X_{Vm} + (\varepsilon_{mRP} + \varepsilon_{RP} + \varepsilon_P)$

where $log(E[Y_{miRP}])$ is the logarithmic transformation to the calculated variable for *recording i* in *recording stage R* in *patient P* on *montage m*, α the overall intercept; α_R the fixed effect for *recording stage R*; α_P the fixed effect for *patient P*; X_{Hm} & X_{Vm} variables for the variables in the *HBIP* and *VBIP* montage (*AVG* was selected as the reference category); X_{iRP} (weighted power) the count of events for *recording i* in *recording stage R* in *patient P*; $\varepsilon_{mRP}$the residual error *for recording i* in *recording stage R* in *patient P* on *montage m*; ε_{RP} the residual error for *recording stage R* in *patient P*; ε_P the residual error for *patient P* β_1, β_2, and β_3 represent the variable coefficients.

We reported continuous variables as medians with interquartile ranges (IQR). Continuous variables were assessed using either the χ^2-test or Fisher's exact test with Bonferroni correction (p_{Bonf}). Due to the non normal distribution of the event counts at the patient group level, we employed non-parametric Friedman tests to examine differences across the three aforementioned montages. Post-hoc Nemenyi test (p_{Nem}) was conducted following the Friedman test for pairwise comparisons. In the context of GLMM, the regression coeffecients (β_1, β_2) were reported as Estimate values (EST), representing the log-transformed difference between montages relative to the reference montage (AVG). Exponentiated estimates (exp(EST)) were used to express the effects as multiplicative changes in the expected outcome. Positive values indicate an increase and negative values indicate a decrease, relative to the reference montage. Tukey adjustment (p_{Tuk}) was applied following the GLMM model to account for multiple comparisons and control family-wise error rates. All statistical analyses were performed using RStudio software 4.1.0 version. Results were considered significant if p-values were <0.05.

Results

Patient population and ioECoG recordings

We included 13 patients (6 females, median age at surgery 10 years [range: 1- 53y]; Table 1) of whom four had an epileptic focus located in the frontal lobe, two in the temporal lobe, and seven at the intersection of these regions. Nine patients underwent a single stage resection, four underwent multiple stages resection with intermediate-recordings. The two most common underlying pathologies were MCDs and CNS tumors. A total of seventy-nine recordings (40 pre-, 10 intermediate-, and 29 post-resection recordings) from 13 patients were analyzed. Across these recordings, 1373 artifact free channels in the AVG montage, 1041 in the HBIP montage, and 967 in the VBIP montage were included. (Table 2) Three representative ioECoG examples displaying each of the three epileptiform events (IEDs, ripples, and FRs) were chosen from three individual patients to illustrate consistencies and discrepancies among montages (Figure 1Biii, 1Ciii, and 1Diii).

Agreed events and interrater agreement

In the AVG montage, 9555 (69.6%) agreed IEDs, 1791 (68.9%) agreed ripples, and 42 (57.1%) agreed FRs were retained. (Table 2) In the HBIP montage, 9003 (66.0%) agreed IEDs, 2098 (63.8%) agreed ripples, and 44 (60.7%) agreed FRs were retained. In the VBIP montage, 7624 (68.6%) agreed IEDs, 1814 (55.2%) agreed ripples, and 45 (53.0%) agreed FRs were retained.

The overall weighted average κ-value for the AVG montage was 0.70 (IEDs: 0.69, ripples: 0.71, FRs: 0.75); for the HBIP 0.66 (IEDs: 0.66, ripples: 0.67, FRs: 0.71); and for the VBIP 0.68 (IEDs: 0.69, ripples: 0.60, FRs: 0.65). All κ-values exceeded the predefined threshold of 0.5, indicating reliable interrater agreement between the two reviewers (ZW, JG). After Tukey's adjustment, the GLMM pairwise comparisons showed that the two reviewers achieved a higher κ-value on ripple marking in AVG and HBIP compared to the VBIP montage (AVG vs. VBIP EST=0.19, $p_{Tuk}<0.0001$; HBIP vs. VBIP EST=0.12, $p_{Tuk}=0.01$). There was no difference in κ-value for IEDs and FRs marking among the three montages (all $p_{Tuk}>0.05$).

More channels with ripples were observed in both bipolar montages compared to AVG montage (HBIP vs. AVG $p_{Bonf}<0.0001$, VBIP vs. AVG $p_{Bonf}<0.0001$). No difference in the number of channels with IEDs and FRs was found. There were no differences among the three montages in the number of patients with events (IEDs & HFOs), nor in the number of recordings with events (Table 2).

Montage performance

Number of channels with events

After channel normalization, both bipolar montages yielded more channels with ripples compared to AVG montage at recording- and patient group levels (GLMM: HBIP vs. AVG EST=0.33, $p_{Tuk}<0.0001$, VBIP vs. AVG EST=0.37, $p_{Tuk}<0.0001$; Friedman: HBIP vs. AVG $p_{Nem}=0.003$, VBIP vs. AVG $p_{Nem}=0.005$; Figure 2A). We found no difference in the count of channels with ripples between the HBIP and VBIP montages. (Figure 2A) Moreover, no differences were found in the numbers of channels with IEDs or FRs among the three montages.

Table 1: Patient population

Pat.	Sex	Age at surgery	Anatomical Location (side)	Histopathology (type)	Number of recordings per recording stage			Post-surgical follow-up time (years)
					Pre	Inter-mediate	Post	
1	F	9	TPO (R)	MCD (FCD IIb)	4	4	1	1
2	F	17	Fr (L)	MCD (FCD IIb)	1	NA	1	2
3	M	3	Fr (R)	MCD (FCD IIb)	4	NA	3	1
4	M	7	TP (R)	CNS tumor (Neuronal and mixed-neuronal-glial tumor)	1	1	1	3
5	M	10	TP (L)	CNS tumor (Neuronal and mixed-neuronal-glial tumor)	5	NA	4	4
6	M	14	Fr (L)	MCD (FCD IIb)	4	NA	4	2
7	F	13	T (L)	CNS tumor (Neuronal and mixed-neuronal-glial tumor)	3	2	1	2
8	F	10	FP (R)	Others	1	NA	1	1
9	M	5	PO (L)	MCD (FCD IIb)	6	NA	3	7
10	F	16	Fr (L)	MCD (FCD IIa)	2	NA	1	1
11	F	53	FP (R)	Others	2	NA	1	7
12	M	10	T (R)	CNS tumor (Neuronal and mixed-neuronal-glial tumor)	3	NA	3	2
13	M	1	FP (L)	MCD (FCD IIb)	4	3	5	2

Abbreviations: CNS = central nervous system, FCD = focal cortical dysplasia, Fr = frontal, FP = fronto-parietal, L = left, MCD = malformations of cortical development, NA = not available, Pat. = the number of patient, PO = parieto-occipital, R = right, T = temporal, TP = temporo-parietal, TPO = temporo-parieto-occipital.

Total event counts

Both bipolar montages yielded more IEDs and ripples compared to AVG montage at the recording group level (GLMM: HBIP vs. AVG IEDs EST=0.23, p_{Tuk}=0.0001, ripples EST=0.45, p_{Tuk}<0.0001; VBIP vs. AVG IEDs EST=0.17, p_{Tuk}=0.008, ripples EST=0.40, p_{Tuk}<0.0001; Figure 2Bi)). At the patient group level, HBIP montage yielded more IEDs compared to AVG montage (Friedman: p_{Nem} =0.02); both bipolar montages yielded more ripples compared to an AVG montage (Friedman: HBIP vs. AVG p_{Nem}=0.002, VBIP vs. AVG p_{Nem}=0.02; Figure 2Bii). We found no differences in IED and ripple counts between the HBIP and VBIP montages (Figure 2B) and in FR counts among the three montages.

Number of event instances

Both AVG and HBIP montages yielded more IED instances compared to a VBIP montage (GLMM: AVG vs. VBIP EST =0.24, p_{Tuk}=0.0002; HBIP vs. VBIP EST=0.14, p_{Tuk}=0.05; Figure 2C). We found no difference in the number of IED instances between HBIP and AVG montages and in the number of ripple- or FR instances among the three montages.

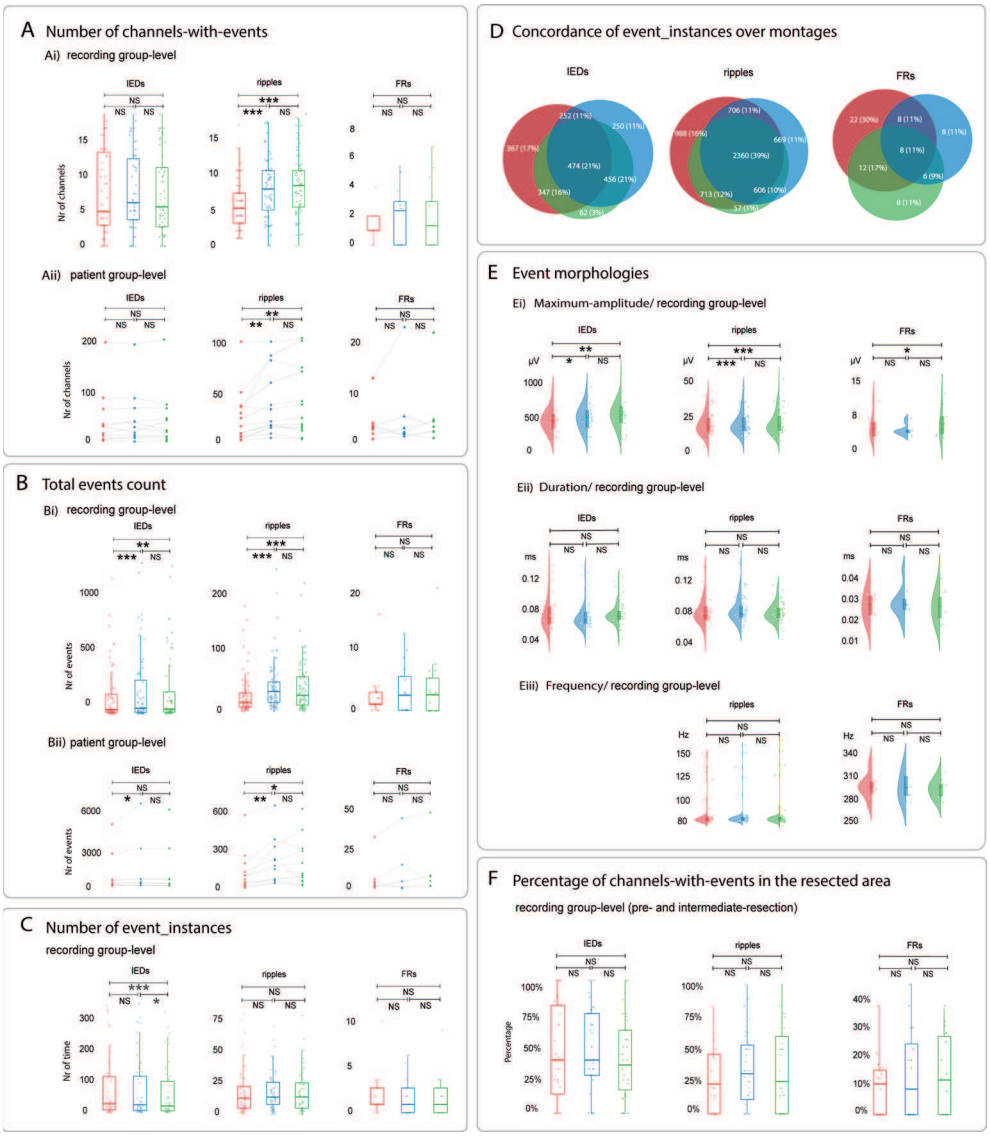


Figure 2: Comparison of montage performance across AVG, HBIP, and VBIP montages. A) Number of channels with events. Ai) at recording and Aii) patient group level, both BIP montages yielded significantly more channels with ripples than an AVG montage. (recording group-level: HBIP vs. AVG p<0.0001, VBIP vs. AVG p<0.0001; patient group level: HBIP vs. AVG p=0.003, VBIP vs. AVG p=0.005). B) Total events count. Bi) at recording group level, both BIP montages yielded significantly more IEDs and ripples compared to an AVG montage (HBIP vs. AVG IEDs p=0.0001, ripples p<0.0001; VBIP vs. AVG, IEDs p=0.008, ripples p<0.0001); Bii) at patient group level, both BIP montages yielded more significantly ripples compared to an AVG montage (HBIP vs. AVG p=0.002, VBIP vs. AVG p=0.02); an HBIP montage yielded significantly more IEDs compared to an AVG montage (p=0.02). C) Number of event instances. At recording group level, both AVG and HBIP montages yielded significantly more IED instances compared to a VBIP montage (AVG vs. VBIP p=0.0002; HBIP vs. VBIP p=0.05). D) Concordance of event instances over montages. Scaled Venn plots per event type displaying the number

(% of total event instances) of concordant event instances at each inter- and divergence section across the three montages. An AVG montage yielded the highest percentage of unique event instances: 17% IEDs, 16% ripples, and 30% FRs. A VBIP montage yielded the lowest percentage of unique event instances with 3% IEDs, and 1% ripples. E)Event morphology. Ei) at recording group-level, both BIP montages yielded a significantly higher maximum amplitude for IEDs and ripples than those in an AVG montage (HBIP vs. AVG IEDs p=0.02, ripples p=0.0001; VBIP vs. AVG IEDs p=0.0003, ripples p=0.003); A VBIP montage yielded a significantly higher maximum amplitude for FRs in comparison to those in an AVG montage (p=0.002). Eii) duration and Eiii) frequency analysis showed no significant differences for IEDs and HFOs among the three montages at recording group level. F) Percentage of channels in pre- and intermediate-resection recordings with events located within the resected area: There were no significant differences in IEDs and HFOs among the three montages. Statistical significances at the patient group levels (Aii and Bii) were determined using the Friedman test, with the Nemenyi test applied as a post-hoc analysis. Statistical significances at the recording group levels were determined by a GLMM (model 1 for panel E; model 2 for panel Ai, Bi, C, F) with Tukey adjustment. The inner horizontal line marks the median, and the inner box indicates the interquartile range (25th to 75th percentiles).
Abbreviations: AVG = average montage, HBIP = horizontally oriented bipolar montage, VBIP = vertically oriented bipolar montage, IED = interictal epileptiform discharge, FR = fast ripple, GLMM = generalized linear mixed model, HFOs = high frequency oscillations, NS = not significant.

Concordance of event instances

The percentage of concordant event instances that occurred simultaneously across all three montages was 21% for IED, 39% for ripple, and 11% for FR. The percentage of unique event instances in AVG montage was 17% for IEDs, 16% for ripples, and 30% FRs, in HBIP montage 11% for IEDs, 11% for ripples, and 11% for FRs and in VBIP 3% for IED, 1% for ripple, and 11% for FR. (Figure 2D)

Event morphology

Figure 2E shows the differences in event morphology across the three montages at the recording group level. The amplitudes of IEDs and ripples were higher in both HBIP and VBIP montages compared to AVG montage. (GLMM: HBIP vs. AVG IEDs EST=0.09, p_{Tuk}=0.02, ripples EST=0.11, p_{Tuk}=0.0001; VBIP vs. AVG IEDs EST=0.13, p_{Tuk}=0.0003, ripples EST=0.09, p_{Tuk}=0.003); A VBIP montage yielded higher FRs amplitudes than an AVG montage (GLMM: EST=0.17, p_{Tuk}=0.002). There were no differences in the amplitudes of IEDs, ripples, or FRs between HBIP and VBIP montages. No differences in durations and frequency were observed among the three montages for IEDs, ripples, and FRs.

Percentage of channels with events located within the resected area

We found no differences in the percentage of channels with events (IEDs, ripples and FRs) covering the resected tissue during pre- and intermediate-resection recordings among the three montages. (Figure 2F)

Table 2: Patients, recordings and channels with agreed events and the percentages of the total groups.

	AVG	HBIP	VBIP	p-value#
IEDs				
Patients with IEDs / all patients	11/13 (84.6%)	10/13 (77%)	11/13 (84.6%)	1.00
Recordings with IEDs / all recordings	50/79 (63.2%)	50/79 (63.2%)	53/79 (67.1%)	1.00
Channels with IEDs / all channels	441/1373 (32.1%)	341/1041 (33.2%)	302/967 (31.2%)	0.76
Total number of IEDs	9555	9003	7624	*NA*
Ripples				
Patients with ripples / all patients	13/13 (100%)	13/13 (100%)	13/13 (100%)	*NA*
Recordings with ripples / all recordings	72/79 (91.1%)	72/79 (91.1%)	72/79 (91.1%)	1.00
Channels with ripples / all channels	405[a]/1373 (29.4%)	431[b]/1041 (41.4%)	409[b]/967 (42.3%)	<0.0001*
Total number of ripples	1791	2098	1814	*NA*
FRs				
Patients with FRs / all patients	5/13 (38.4%)	4/13 (30.7%)	5/13 (38.4%)	1.0
Recordings with FRs / all recordings	14/79 (17.7%)	9/79 (11.4%)	11/79 (11.4%)	0.52
Channels with FRs / all channels	21/1373 (1.53%)	25/1041 (2.40%)	23/ 967 (2.48%)	0.36
Total FRs	42	44	45	*NA*

Pairwise comparisons were conducted using the χ^2-test with Bonferroni correction, except when the expected frequency in one or more cells was less than 5, in which case Fisher's exact test was applied.
** A p-value of $p<0.05$ is considered significant, with directionality b is significantly higher than a.*
Abbreviations: AVG = standard average montage, HBIP = horizontally oriented bipolar montage, VBIP = vertically oriented bipolar montage, NA = Not applicable, IED: interictal epileptiform discharge, FR = fast ripple.

Discussion

We investigated the optimal montage in marking ioECoG biomarkers (i.e., IEDs and HFOs) and came up with three main findings: 1) Bipolar montages, regardless of electrode connection direction, yielded more channels, higher counts, and greater amplitudes of ripples and IEDs compared to average montages. 2) Average montages showed most unique IEDs- and HFOs instances which were not identified in one of the bipolar montages. 3) The percentage of IEDs and HFOs channels covering the epileptogenic tissue was similar in average and bipolar montages.

During ioECoG tailored epilepsy surgery, prompt decision making is required. An average montage may provide a faster and straightforward overview, whereas bipolar montages may require more time for detailed analysis. We observed that an average montage yielded greater raw counts of IEDs and ripples than an bipolar montage (Table 2). Given the configuration by us used 4x5 electrode grids, an average montage comprised more channels (20 channels) than an bipolar montage (16 channels in horizontal orientation and 15 in vertical). This emphasizes the importance of conducting comparisons on an equal basis, accounting for differences in the number of channels between montages. After channel normalization, the results reversed: higher counts of IED and ripple channels, and greater event numbers were found in the bipolar montages. A possible explanation is that an electrode pair in a bipolar montage records both the input and output sides[142,149], resulting in the same event being marked twice. Two duplicate events, observed as phase reversals in adjacent channels of a bipolar montage, are often optimal for marking due to their distinct localization and prominence.[138,139]

We found that bipolar montages displayed more distinct amplitudes of IEDs and ripples, which may facilitate visual discrimination, compared to the average montage. This is probably because the bipolar montage emphasized local voltage differences between two adjacent electrodes, reducing the influence of widespread distant noise.[139] In contrast, an average montage computes the mean voltage across all channels. During this procedure channels contaminated with artefacts need to be removed.[138] The averaging method may dilute extensive IEDs or oscillations, often resulting in lower amplitude signals that might cause them to fail to meet the strict criteria for event marking. The other way around, focal high amplitude events can be reflected on other channels. Above reasons may make the bipolar montage superior to average montage for subtle event analysis where clean, localized signals are crucial.

In our center, we are used to review the ioECoG using a horizontal orientation bipolar montage for research purposes[33,34,89,107,132,146], but when needed we create an average montage to confirm whether the observed events are truly present and to rule out distortions from bipolar subtraction. For clinical evaluation of IEDs during the surgical procedure, we most often use the average montage. In this study, we found an average montage added some new information to the horizontally oriented bipolar montage (17% unique IED instances, 16% unique ripple instances, 30% unique FR instances), while the vertically oriented bipolar montage added less (3% unique IEDs instances, 1% unique ripple instances, 11% unique FR instances). One interpretation might be that some events are canceled out in a bipolar montage if they occur relatively synchronously at the two paired electrodes which may be picked up by the average montage. Another interpretation is that if an electrode in the middle of the grid is noisy, one channel will be

excluded from further analysis in an average montage, whereas two channels will be excluded in a bipolar montage. Moreover, electrodes positioned in the middle of the grid benefit from having neighboring electrodes on all sides, enabling multiple bipolar pairs in two or more traces for each electrode. In contrast, the edges and corners electrodes lack this advantage, making it difficult to discern whether the electrical activity originates from one electrode or is equally shared between both. The vertically oriented configuration can preserve events on the lateral and corner channels when the horizontally oriented channels are contaminated with artifacts and vice versa. This is illustrated in Figure 1Biii; as channel 17 is contaminated by high frequency noise, events displayed by channel 16 are also missed in the horizontally oriented bipolar configuration; whereas the bipolar channel 11-16 channel in vertically oriented bipolar montage still captures these events.

Brain activity can propagate differently across sulci due to differences in cortical connectivity. Placing electrodes on the same gyrus allows for a clearer understanding of localized IEDs and HFOs because neighboring electrodes are sampling the same cortical area. Nonetheless, in 15 out of 79 recordings, particularly those involving the temporal lobe, the grids were often aligned with the direction of gyri. This alignment resulted in pairs of channels from the vertically oriented bipolar montage to go across sulci and detect events from different gyri. A region of HFOs rather covers a single gyrus than multiple adjacent gyri; This could be reflected by multiple consequential channels showing HFOs in horizontal direction and just single channels in vertical direction. The ambiguity about the precise origin of the vertically detected ripple may have made it more challenging for both reviewers (ZW, JG) to confidently mark the events. This likely contributed to lower agreement on whether the ripple was truly present and distinct (κ-value 0.60 for ripples in VBIP). Consequently, fewer unique event instances (3% IEDs, 1% ripples) were detected in the vertical configuration.

Calculating the percentage of channels with IEDs or HFOs inside the assumed epileptogenic zone is a widely adopted approach to evaluate their predictive value in epilepsy surgery research.[34,50,130] Complete resection of areas generating IEDs and the absence of residual IEDs after resection has been associated with favorable seizure outcome.[38,64] A recent meta-analysis showed that fully HFOs removal, especially that of FRs, correlates with good seizure outcome.[27] Would different montages change the distribution of channels with events and in turn affect the diagnostic value for locating epileptogenic tissue? This study answered that question by showing no significant differences between the average and bipolar montages in the percentage of channels with IEDs and HFOs covering the epileptogenic tissue. In other words, the distribution of channels showing IEDs and HFOs in the epileptogenic tissue was robust and unaffected by the choice of the ioECoG montage.

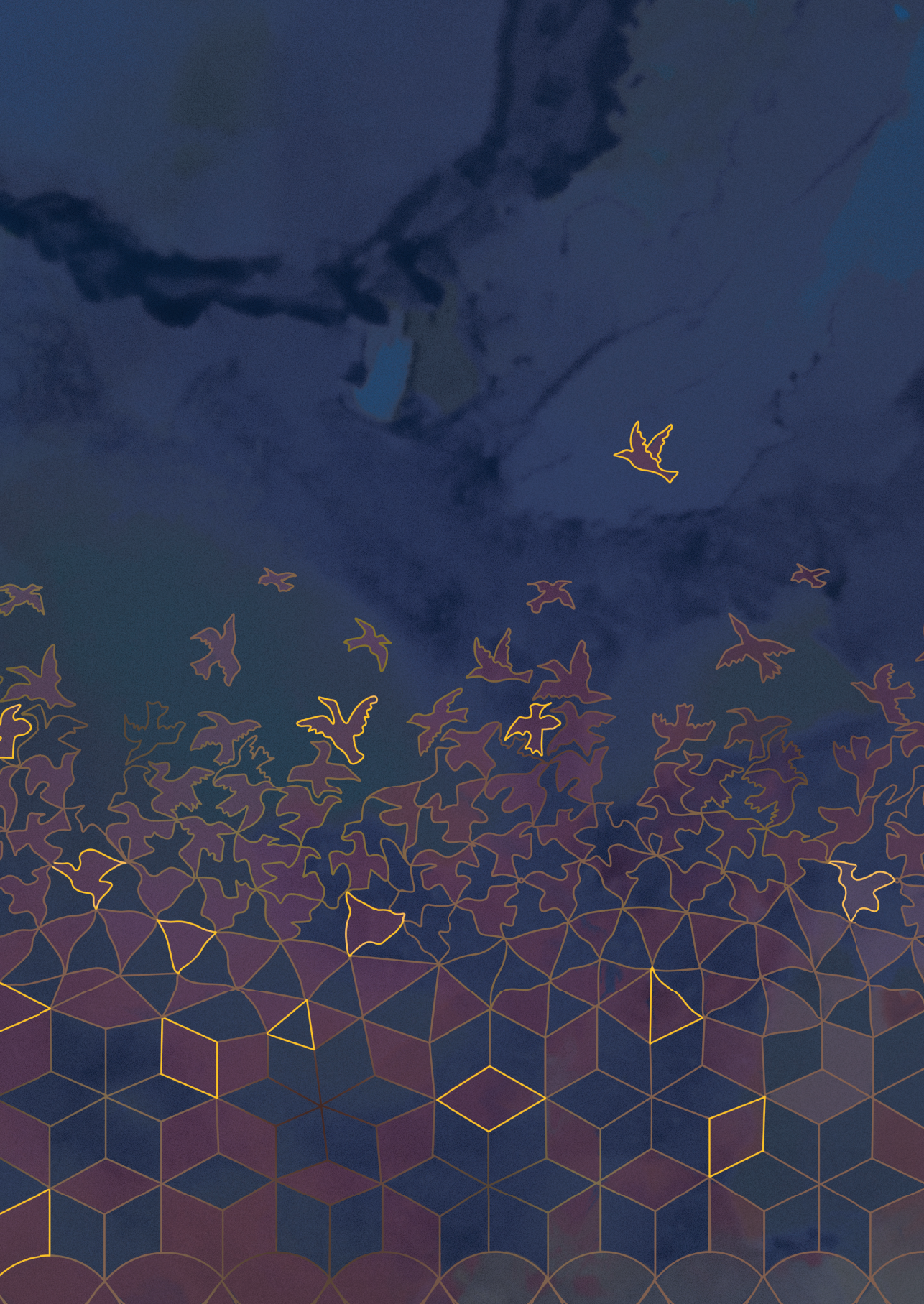
A strength of our study is its contribution to bridge practical research gap in investigating which ioECoG montage is optimal for marking IEDs and HFOs. We provided quantitative data to evaluate these differences addressing a broad spectrum of aspects for its use in clinical practice (e.g. number of channels with events, total events count, event morphology, concordance of event instances over montages, and percentage of channels with events in the resected area). Another strength is that the IEDs and HFOs analyzed in this study were marked by two observers. The acceptable κ-value (all >0.60) confirms the reliability of these events. Finally, we evaluated an alternative vertically oriented bipolar

montage and demonstrated that it added less unique information than the other two montages.

The study's limitations include the small sample size for FRs identification and the definition of epileptogenic tissue. The rarity of FRs and the low sensitivity of standard equipment resulted in their small size[34], necessitating optimized marking strategies by multiple montages. Determining the exact boundaries of the epileptogenic zone is difficult even if postoperative seizure freedom was achieved. It is possible that some channels within the assumed epileptogenic tissue were covering non-epileptic, but resected tissue. The number of patients was low to rule out a small difference in the value to localize the epileptic tissue. As our initial goal was to find an optimal montage for identifying specific events, we deliberately did not compare the localization accuracy of IEDs to that of HFOs. In addition, we did not take the event threshold into account: regardless of whether a channel had one event or a dozen, it was classified as a channel with events in present work. In clinical practice, channels with only one or very few abnormalities might be less relevant identifier of the seizure focus than channels with frequent events. Future studies should focus on setting a specific threshold to determine whether a channel should be considered for resection, rather than simply labeling it as abnormal based on the presence of IEDs or HFOs.

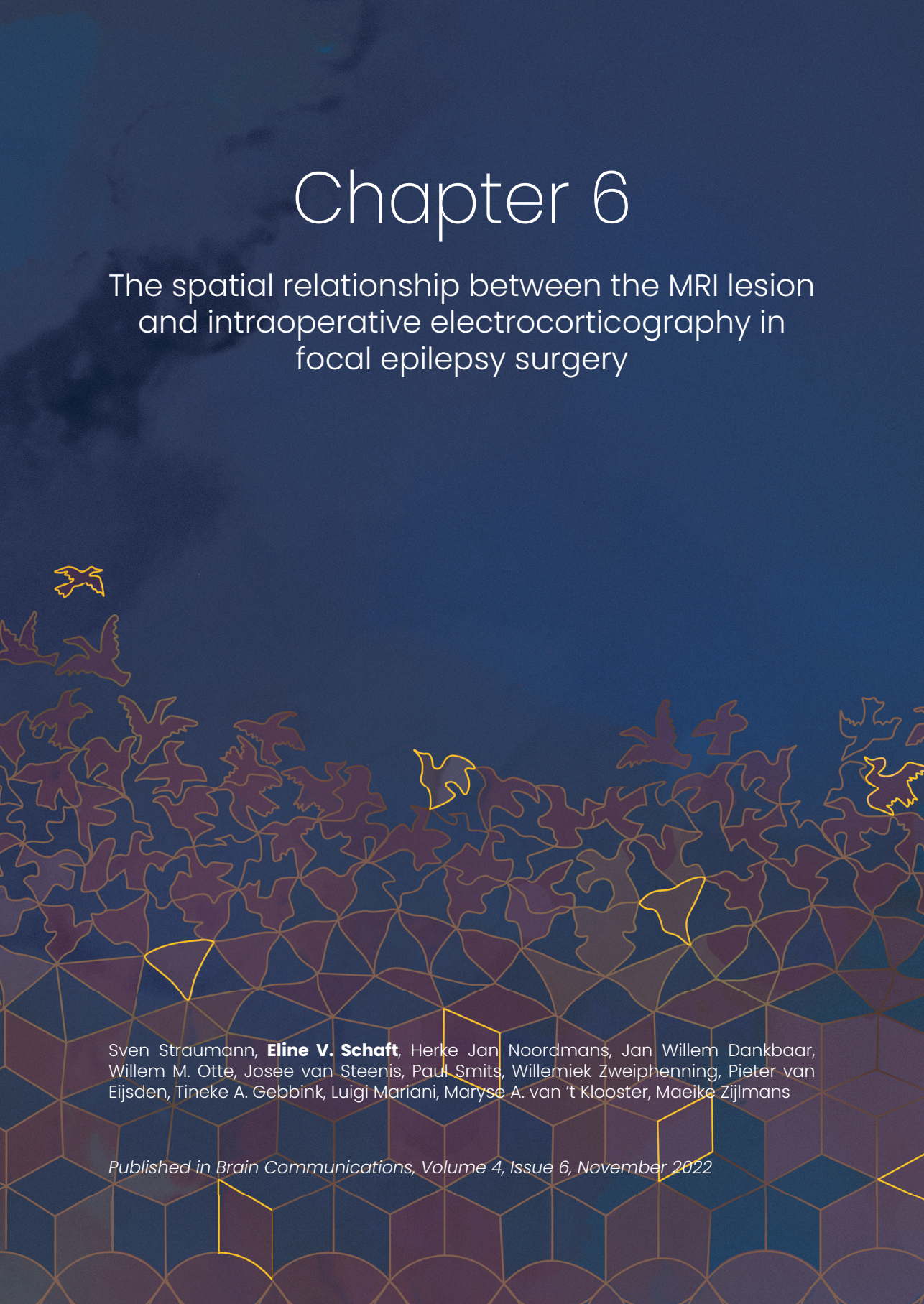
Conclusion and future recommendations

All three ioECoG montages hold value in clinical utility to find epileptic events. The bipolar montage excels at detecting a higher number of events with greater amplitude, and the average montage reveals a broader spectrum of unique events. Rather than favoring one montage over the others, the choice to review the ioECoG between bipolar or average montage should align with specific goals, data nature, and personal preferences. Notably, combining these montages offers complementary insights. Future advancements in automated systems could integrate data from both bipolar and average montages, enabling comprehensive analyses across multiple approaches. This progression would unify information, reduce the effort for manual review, and enhance localization accuracy. Furthermore, it has been suggested that high density recordings could enhance the signal-to-noise ratio and increase the possibility of HFO detections. Further research is needed to investigate whether current results for standard grids can be generalized to high density grids.



Chapter 6

The spatial relationship between the MRI lesion and intraoperative electrocorticography in focal epilepsy surgery



Sven Straumann, **Eline V. Schaft**, Herke Jan Noordmans, Jan Willem Dankbaar, Willem M. Otte, Josee van Steenis, Paul Smits, Willemiek Zweiphenning, Pieter van Eijsden, Tineke A. Gebbink, Luigi Mariani, Maryse A. van 't Klooster, Maeike Zijlmans

Published in Brain Communications, Volume 4, Issue 6, November 2022

Abstract

MRI and intraoperative electrocorticography are often used in tandem to delineate epileptogenic from healthy tissue in resective surgery for focal epilepsy. The aim of this study was to find the spatial relationship between MRI lesions and electrographic discharges on electrocorticography, e.g., spikes (<80Hz) and high-frequency oscillations (80-500Hz).

We retrospectively included 33 pediatric and adult patients with lesional neocortical epilepsy who underwent electrocorticography-tailored surgery (14 female, median age 13.4 years, range 0.6-47.0 years). Mesiotemporal lesions were excluded. We used univariate linear regression to find correlations between spike/high-frequency oscillation rates on an electrode and its distance from the MRI lesion. We tested straight lines to the centre and the edge of the MRI lesion, and the distance along the cortical surface to determine which of these distances best reflects the actual generation and propagation of spikes/high-frequency oscillations. A simple slopes moderator analysis was used to investigate the influence of the underlying pathology type and lesion volume on our results.

We found spike and high-frequency oscillation rates to be spatially linked to the edge of the MRI lesion. The underlying pathology type influenced the spatial relationship between spike/high-frequency oscillation rates and the MRI lesion (p_{spikes}<0.0001, $p_{ripples}$<0.0001), while lesion volume did not (p_{spikes}=0.64, $p_{ripples}$=0.89). A higher spike rate was associated with a shorter distance to the lesion for cavernomas (F(1,64)=-1.37, p<0.0001, η^2=0.22), focal cortical dysplasias (F(1,570)=-0.25, p<0.0001, η^2=0.05), and pleomorphic xanthoastrocytomas (F(1,66)=-0.18, p=0.01, η^2=0.09). In focal cortical dysplasias, a higher ripple rate was associated with a shorter distance (F(1,570)=-0.35, p<0.0001, η^2=0.05). Conversely, low-grade gliomas showed a positive correlation; the further an electrode was away from the lesion, the higher the rate of spikes (F(1,75)=0.65, p<0.0001, η^2=0.37) and ripples (F(1,75)=2.67, p<0.0001, η^2=0.22).

We conclude that pathophysiological processes specific to certain pathology types seem to determine the spatial relationship between the MRI lesion and electrocorticography results. Our data support the notion that non-tumorous lesions (focal cortical dysplasias, cavernomas) intrinsically generate spikes and high-frequency oscillations, while low-grade gliomas preferentially cause epileptogenicity in the peritumoral tissue. This suggests that a one-size-fits-all interpretation for intraoperative electrocorticography may not exist; The underlying pathology and its influence on the generation of spikes and high-frequency oscillations should be considered.

Introduction

Up to 30-40% of people with focal epilepsy cannot achieve adequate seizure control despite optimised drug treatment.[4,150,151] In many of these cases, the surgical resection of the presumed seizure focus is an effective and safe treatment option.[4,151,152] The accurate localisation of epileptogenic tissue is paramount for a good surgical outcome.[4,30,153,154] Rosenow and Lüders[155] defined the minimal theoretical resection area to ensure seizure freedom as the epileptogenic zone (EZ). More recent evidence has led to an emerging view of the EZ not as a static area of tissue but an interconnected network within the epileptic brain.[156-161]

During pre-surgical workup, MRI scans form a vital basis for the localisation of structural lesions associated with epilepsy.[4,152,162,163] Patients with a clearly defined MRI lesion are two to three times more likely to achieve postoperative seizure-freedom than patients without structural abnormalities on MRI.[4] But not all epileptogenic pathologies are readily visible on structural MRI scans.[163] Moreover, even a clearly defined MRI lesion is not necessarily the sole substrate for epileptogenic processes.[156] Tissue around or at a distance from an MRI lesion may be more epileptogenic than the lesion itself.[89,164,165] This implies that MRI lesions, which are often the primary target of surgical resection, may be only part of a broader epileptogenic network.[156] Additional diagnostic techniques are needed to delineate parts of this network that cannot be detected through MRI alone.

Intraoperative electrocorticography (ioECoG) can assist the localisation of the EZ beyond the margins of MRI lesions,[30,153,166-168] particularly in patients with neocortical lesions.[32,153] A surgical strategy that combines a complete resection of the MRI lesion and resecting epileptogenic tissue identified through ioECoG has been linked to a better surgical outcome than lesionectomy alone.[153,168] Limitations of ioECoG include the limited time available to gain accurate recordings during surgery, its dependency on interictal rather than ictal biomarkers, and its susceptibility to anaesthesiologic agents.[30,153,166,168]

Epileptiform spikes are the most commonly used ioECoG biomarkers to identify epileptogenic tissue.[155,168] The cortical area where spikes are found is thought to be larger than the EZ.[153] Patients often display multiple areas of spike generation, from which spikes are thought to propagate throughout the brain along the epileptogenic network.[157,158,169-171] In recent decades, high-frequency oscillations (HFOs) have been described as promising electrographic biomarkers, though their clinical application is not yet as widespread as that of spikes.[12,154,172,173] HFOs represent prominent, burst-like events with a frequency of >80Hz. They can be subclassified into ripples (80-250Hz) and fast ripples (250-600Hz).[12,166,172] HFOs, particularly fast ripples[132,174], have been shown to be more specific for epileptogenic tissue than spikes.[11,175] Their complete removal has been linked to a better outcome than the complete removal of spikes.[34,176] Other studies have put the reliability of HFOs as a biomarker into question.[7,89,173,177]

Structural MRI scans and ioECoG are often used in tandem to localize the EZ. However, no studies have yet investigated the direct relationship between the visible lesion on MRI and electrographic biomarkers recorded on ioECoG. It is generally assumed that the generation of spikes and HFOs are spatially linked to MRI lesions, but to what extent is unclear.

We hypothesised that the spike and HFO rates on a given ioECoG electrode correlate with its distance from the MRI lesion. We tested three distances as different models to link ioECoG findings to the MRI lesion. We hypothesised that the distance that best reflects the actual generation and propagation of electrographic discharges within the epileptogenic network would strongly correlate with the recorded spike and HFO rates. Additionally, we investigated the influence of the underlying pathology type and lesion volume on the relationship between MRI and ioECoG.

Materials & methods

Study design and patients

We selected patients from the cohort of participants of the HFO trial, a randomized controlled trial comparing the use of spikes and HFOs for intraoperative neurosurgical guidance.[178] The results of the HFO trial will be published separately. Our institute's medical ethical committee approved the trial protocol and subsequent data analysis. The trial was performed by the principles of the Declaration of Helsinki. All patients and the parents or legal representatives of eligible patients provided written informed consent before enrolment.

We retrospectively included pediatric and adult patients who underwent ioECoG-tailored neurosurgery for focal lesional epilepsy at our institution between October 2014 and January 2020 as a part of the HFO trial that fulfilled the following criteria: (1) Good postsurgical seizure outcome, defined as Class Ia on the Engel Outcome Scale at the 1-year follow-up visit[179]; (2) Availability of a post-operative structural MRIs with no radiographic signs of residual lesional tissue; We excluded (3) patients who had repeated surgery and (4) patients with mesiotemporal lesions. We included neocortical temporal lesions that did not affect the mesiotemporal structures.

Intraoperative electrocorticography

ioECoG recordings

The surgical approach and placement of ioECoG electrodes were based on the standardized presurgical workup at our institution. ioECoG recordings were performed directly on the cortex using standard 4x5 or 4x4 electrode grids and 1x8 electrode strips (AD-Tech, Racine, WI, USA). Grids and strips consisted of platinum electrodes with a 4.2 mm^2 contact surface and an interelectrode distance of 1 cm. We used a 64-channel (Micromed LTM Express) or 32-channel (Micromed Flexi) EEG system at a sampling rate of 2048Hz with an anti-aliasing filter at 538Hz. The neurosurgical strategy was to remove the MRI lesion based on Brainlab neuronavigation (Brainlab, Munich, Germany) and further intraoperative tailoring of the resection with ioECoG. The intravenous application of propofol was stopped for 5-10 minutes during each recording until a continuous background pattern was confirmed to minimize the influence of propofol on the ioECoG recordings.[44] Patients remained unconscious throughout the entire surgical procedure. The ioECoG was reviewed intraoperatively for spikes or HFOs in Stellate Harmonie *Viewer* (Natus Medical Inc., Montreal, QC, Canada) to guide the resection. Intraoperative photographs of the ioECoG grid positions on the cortex were taken.

ioECoG data selection and detection of biomarkers

We included all ioECoG recordings that were taken prior to the start of the resection. ioECoG recordings were retrospectively visually assessed using Brain

Quick Software (Micromed SpA). Artefactual channels were excluded. One-minute epochs near the end of each recording were selected to detect spikes and HFOs. Spikes and fast ripples were visually marked by the main author (SS) in a bipolar montage. We used conventional settings to identify spikes (1.6-80.0Hz FIR filter, 500-900μV/cm gain, 5-10 seconds/page) and fast ripples (250-1000Hz FIR filter, 10-30μV/cm gain, 1 second/page). Ripples were automatically detected in a bipolar montage using a MATLAB-based detector adapted to our data.[13,47,180,181] All one-minute epochs were subsequently visually checked for missing and false positive ripples by the main author (SS) using conventional settings (80-1000Hz FIR filter, 40-60μV/cm gain, 1 second/page). All spike, ripple and fast ripple markings were independently verified by two additional researchers (MZ and ES).

Pathology type
The underlying pathology type of all lesions was determined using intraoperatively obtained tissue samples as part of their routine histopathological analysis after surgery.

MRI

MRI acquisition
All patients underwent structural 1.5T or 3T MRI brain scans using a dedicated epilepsy protocol pre- and postoperatively (including a 3D T1-weighted and either a T2-weighted or Fluid Attenuated Inversion Recovery (FLAIR) image).

MRI lesion segmentation
We segmented the MRI lesions as binary volumes using the *A*ctive Contour Segmentation Mode in ITK-SNAP[182]. Different brain and lesion tissue types were manually marked in the *Classification* pre-segmentation mode based on differences in signal intensities in T1, T2, and FLAIR weighted scans, followed by a semi-automated segmentation of the MRI lesion.

All segmentations were visually verified (and manually corrected, if needed) by the main author (SS) and a board-certified neuroradiologist (JD). Lesion volumes were calculated in ITK-SNAP based on the MRI lesion segmentations.

ioECoG electrode coordinates in MRI space
We performed an automatic whole-brain segmentation of the original MRI in *FreeSurfer*[183]. This segmentation was then imported into the custom written image analysis software Java Navigation (release 2021),[184] developed by HK and adapted for this study.

We used prominent anatomical features (such as sulci, gyri, and blood vessels) to visually match photographs taken during surgery to the cortical reconstruction in Java Navigation. We then manually placed markers for ioECoG electrodes visible on the photographs onto the cortex. An automated extrapolation process, which took the fixed between-electrode distance of 1 cm and the curvature of the cortical surface into account, was used to arrive at the position of any electrodes that were hidden under the skull. This allowed us to obtain coordinates in MRI space for all ioECoG electrodes. (Figure 1)

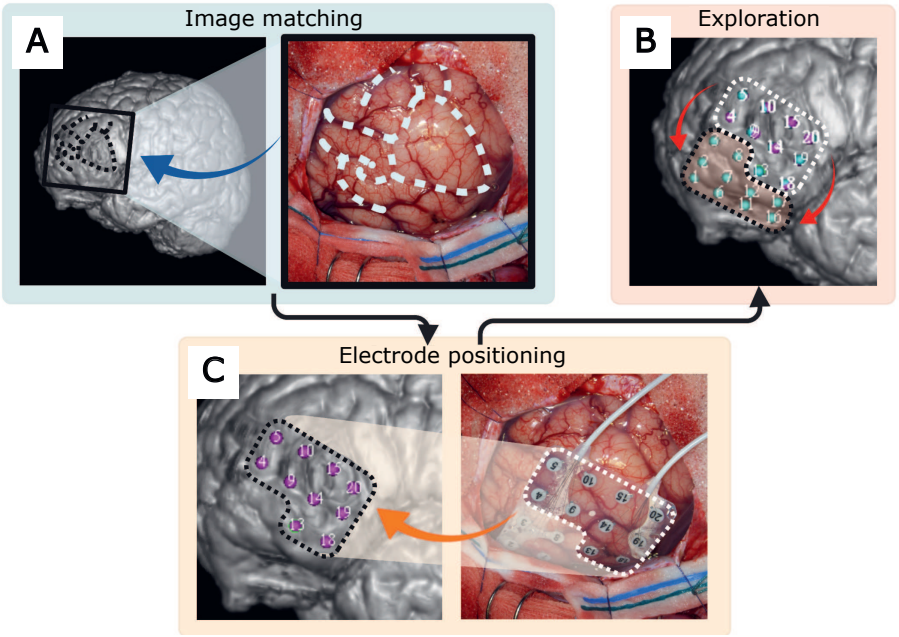


Figure 1: The determination of ioECoG electrode coordinates in MRI space. An ioECoG recording of the left frontal lobe is used as an example (patient 23). (A) Intraoperative photographs were visually matched to a cortical reconstruction in Java Navigation using prominent anatomical features (such as gyri, sulci, and blood vessels). (B) Markers (magenta) were manually placed for all visible electrodes. (C) In an automated step, the positions of all remaining electrodes were extrapolated (cyan) taking the fixed between-electrode distance of 1 cm and the curvature of the cortical surface into account.
Abbreviations: ioECoG = intraoperative electrocorticography, MRI = magnetic resonance imaging

Distances

Distances between ioECoG electrodes and MRI lesions

Lesion segmentations, whole-brain segmentations, and ioECoG electrode coordinates were imported into *MATLAB* (The MathWorks Inc., Natick, MA, USA). The bipolar montage used to mark spikes and HFOs was recreated by defining the exact spatial midpoint between two neighbouring electrode coordinates as the bipolar electrode coordinate. We then calculated the following distances:

1. The Euclidian distance between each bipolar electrode and the closest edge of the lesion.
2. The Euclidian distance between each bipolar electrode and the centre of mass (COM) of the lesion.
3. The geodesic distance between each bipolar electrode and the COM of the lesion, consisting of the shortest possible straight line from the COM to the cortical surface and the shortest line from that point along the cortical surface to the electrode.

The geodesic distance was calculated using the Image Processing Toolbox and the open-source MatImage Library[185]. For an illustration of the three distances, see Fig. 2. We then determined which distance showed the strongest correlations with ioECoG biomarker rates. We used this distance for additional analyses.

Distance to the electrode with most events

We determined the electrode with the highest spike, ripple, and fast ripple rate for each patient. The distance to this electrode is called D_{max}*(spikes),* D_{max}*(ripples),* D_{max}*(fast ripples)*, respectively.

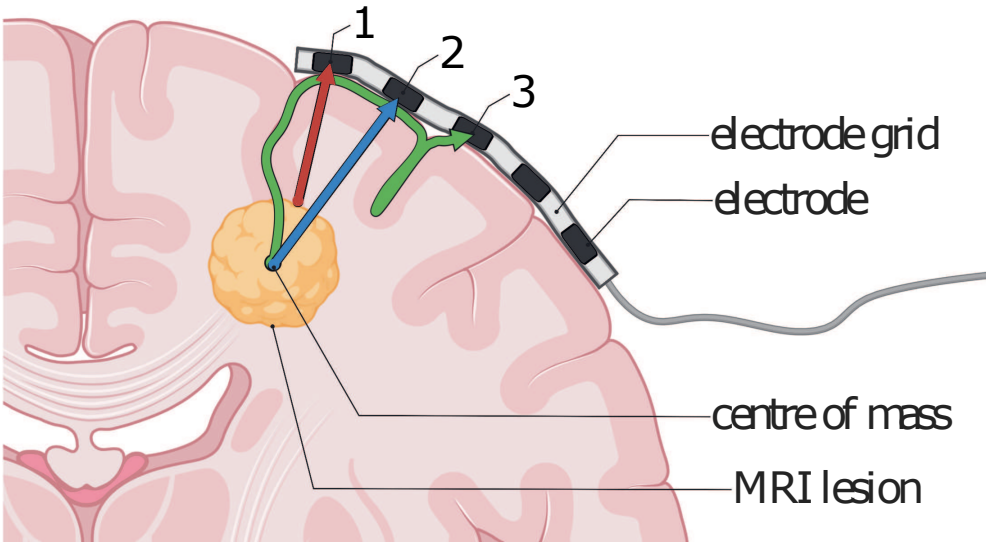


Figure 2: An illustration of the three different distances between the MRI lesion and ioECoG electrodes. 1. The Euclidian distance to the closest edge of the lesion (red), 2. The Euclidian distance to the COM of the lesion (blue), 3. The geodesic distance to the COM of the lesion along the cortical surface (green). Abbreviations: COM = centre of mass, ioECoG = intraoperative electrocorticography, MRI = magnetic resonance imaging

Statistical analyses

We performed all statistical analyses in IBM SPSS Statistics 20 (IBM Corp., Armonk, NY, USA). We calculated means and standard deviations if data were normally distributed and medians and ranges if data were not normally distributed.

We used heteroscedasticity consistent (HC) standard errors (using an HC3 Davidson-MacKinnon estimator) in all of our regression models and moderator analyses. For this reason, we report eta-squared (η^2) as the effect size. It should be noted that, in our models, η^2 is numerically equivalent to R^2.[186] To our knowledge, no results of comparable analyses have been published to date to serve as comparison for the effect sizes of our models. Therefore, we used Cohen's[187] original classification for effect sizes: $\eta^2 \leq 0.01$ as small, $\eta^2 \leq 0.06$ as moderate, and $\eta^2 \geq 0.14$ as large. A p-value of <0.05 was considered statistically significant. We did not correct for multiple comparisons as we tested complementary hypotheses with interdependent variables.

The correlation between spike/HFO rates and distance

We used separate univariate linear regression to determine the relationship between the three distances (dependent variable) and spike, ripple, and fast ripple rates (independent variable*).* Linear regression was performed for the entire population and for subgroups based on the underlying pathology. Bootstrapping based on 1000 samples was performed for all our linear regression models. Based on the effect sizes of these linear regressions, we determined which of the three distances illustrated in Fig. 2 best reflects the spatial link between the MRI lesion and ioECoG findings. The distance which showed the strongest correlations to spike/HFO rates was assumed to most likely represent the actual generation and propagation of electrographic discharges. This distance was used for all additional analyses.

Visual slope comparison
To test whether the results of our linear regressions may have been caused by within-subject rather than between-subject effects, we used a visual slope comparison. We plotted the highest spike and ripple rate as a single data point per patient against the distance to that electrode (D_{max}*(spikes)*/ D_{max}*(ripples)*). We then visually compared the resulting slopes (negative vs positive) per pathology with those of our linear regression models. We interpreted a mismatch to indicate that within-subject effects may have caused the regression results.

Comparison of distances to the electrode with most events
We compared the mean D_{max}*(spikes)*, D_{max}*(ripples)*, and D_{max}*(fast ripples)* using a one-way analysis of variance (ANOVA).

Moderator analysis of pathology type and lesion volume
We hypothesised that the underlying pathology type and/or lesion volume might influence the spatial relationship between the MRI lesion and ioECoG results. To test this, we conducted a simple slope moderator analysis developed by Hayes.[188] Pathology type was tested as a categorical moderator and lesion volume as a continuous moderator.

Data availability
The custom Java scripts required for the placement and extrapolation of electrode markers on the cortical surface in Java Navigation (release 2021) can be accessed via the Supplementary material. The entire software and the data that support our findings can be made available upon reasonable request to the corresponding author.

Results

Patients and descriptive statistics

We included 33 patients (14 female, median age=13.4 years, range=0.6-47.0 years). FCDs and gangliogliomas were the most frequent pathologies. Baseline characteristics and mean lesion volumes are outlined in Table 1a. Between one and five pre-resection ioECoG recordings were performed for each patient, resulting in the initial inclusion of 1578 bipolar ioECoG electrodes. Two 1x8 strips had to be excluded because no photograph of their placement was available to reconstruct their coordinates in MRI space. We further excluded 168 bipolar ioECoG electrodes due to artefacts, which left a total of 1396 electrodes for our analyses.

We marked a total of 3519 spikes, 1975 ripples, and 181 fast ripples. The mean distance of all bipolar electrodes to the edge of the lesion was 18.9 mm (±13.9mm), electrodes on which spikes were found had a mean distance of 17.9 mm (±12.5mm), electrodes with ripples 18.7 mm (±12.2 mm), and with fast ripples 15.6 mm (±12.0 mm). For additional descriptive statistics refer to Table 1b.

Evaluation of the three distances

All patients combined

The distance to the edge of the lesion showed a negative correlation with spike rates ($F(1,1394)=-0.10$, $p=0.03$, $\eta^2=0.004$) and ripple rates ($F(1,1394)=-0.14$, $p=0.04$, $\eta^2=0.003$). The distance to the centre of the lesion showed a negative correlation only with ripple rates ($F(1,1394)=-0.22$, $p=0.003$, $\eta^2=0.01$). The geodesic distance along the cortical surface showed no correlations with ioECoG biomarker rates. None of the three distances showed a correlation with fast ripple rates.

Stratified by pathology type

The distance to the edge of the lesion showed a correlation with spike rates for cavernoma, FCDs, low-grade glioma, and PXAs. Ripple rates correlated for FCDs and low-grade gliomas. Fast ripple rates correlated for gangliogliomas. The results of these linear regressions are discussed in more detail below.

The distance to the centre of the lesion showed correlations for the same pathology types as the distance to the edge, except that it did not correlate with spike rates for PXAs. Effect sizes were either similar for the distance to the centre and the edge of the lesion, or larger for the distance to the edge. The geodesic distance showed only few correlations: spike rates correlated for DNETs and PXAs, and fast ripple rates correlated for PXAs.

Conclusion

In summary, the distance to the edge of the lesion showed the strongest correlations to ioECoG biomarker rates. Hence, this distance was used for all following, additional analyses and figures. For all linear regression results please refer to Supplementary Table 1.

Table 1a: Baseline patient characteristics and mean lesion volumes (cm^3)

Sex (number of patients)	
Male/female	19 / 14
Age at surgery (years)	
Median [range]	13.4 [0.6 - 47.0]

Underlying pathology	**Number of patients (%)**	**Mean volume [SD] (cm^2)**
FCD	12 (36%)	2.5 [3.0]
of which subtype 2a	1	2.1
of which subtype 2b	8	3.1 [3.4]
of which subtype not conclusively identifiable	3	1.0 [0.6]
Ganglioglioma	9 (27%)	10.6 [9.7]
DNET	5 (15%)	12.6 [9.4]
Low-grade glioma (WHO Grade I)	3 (9%)	20.8 [28.6]
PXA	2 (6%)	7.0 [8.2]
Cavernoma	2 (6%)	2.1 [0.01]
Anatomical location of surgery (number of patients, %)		
Temporal	18 (55%)	
Frontal	11 (33%)	
Frontal and temporal	1 (3%)	
Central	2 (6%)	
Parietal	1 (3%)	

Table 1b: Total number and rates of ioECoG biomarkers, and distance characteristics.

ioECoG characteristics	**Number of included bipolar channels**	**Total spikes [mean spikes/ min, SD][a]**	**Total ripples [mean ripples/ min, SD][a]**	**Total fast ripples [mean fast ripples/min, SD][a]**
All patients	1396 (100%)	3519 [8.3, SD 11.2]	1975 [5.7, SD 7.7]	181 [3.7, SD 7.0]
FCD	572 (41%)	1870 [9.4, SD 12.8]	1224 [6.0, SD 7.8]	154 [4.4, SD 8.2]
Ganglioglioma	368 (26%)	884 [8.7, SD 10.1]	521 [6.6, SD 7.3]	22 [2.0, SD 1.7]
DNET	245 (18%)	230 [3.7, SD 3.3]	125 [3.7, SD 4.7]	- [c]
Low-grade glioma	77 (6%)	299 [10.0, SD 11.9]	35 [3.9, SD 3.8]	- [c]
PXA	68 (5%)	167 [13.9, SD 15.3]	54 [4.2, SD 4.4]	2 [1.0, SD 0.0]
Cavernoma	66 (5%)	69 [4.1, SD 4.9]	16 [2.3, SD 1.7]	- [c]

Distance characteristics[b] (mm)	**Mean distance to all bipolar electrodes, SD**	**Mean distance to electrodes with spikes, SD**	**Mean distance to electrodes with ripples, SD**	**Mean distance to electrodes with fast ripples, SD**
All patients	18.9, SD 13.9	17.9, SD 12.5	18.7, SD 12.2	15.6, SD 12.0
FCD	20.0, SD 13.6	16.8, SD 12.1	17.9, SD 12.8	15.5, SD 13.2
Ganglioglioma	20.4, SD 12.6	20.0, SD 11.0	21.4, SD 11.8	15.4, SD 9.3
DNET	14.3, SD 14.9	11.9, SD 9.9	15.6, SD 9.1	- [c]
Low-grade glioma	15.6, SD 14.6	20.0, SD 16.0	28.6, SD 11.5	- [c]
PXA	17.5, SD 12.4	13.0, SD 7.4	17.1, SD 8.3	15.5, SD 6.3
Cavernoma	26.8, SD 15.0	23.4, SD 16.4	18.1, SD 12.8	- [c]

[a]Mean spike, ripple, and fast ripple rates were calculated for channels on which at least one of the respective biomarkers was recorded. [b]Euclidian distance to the edge of the lesion. [c]No fast ripples were recorded for these pathologies.
Abbreviations: DNET = dysembryoplastic neuroepithelial tumor, FCD = focal cortical dysplasia, PXA = pleomorphic xanthoastrocytoma, SD = standard deviation, WHO = world health organization

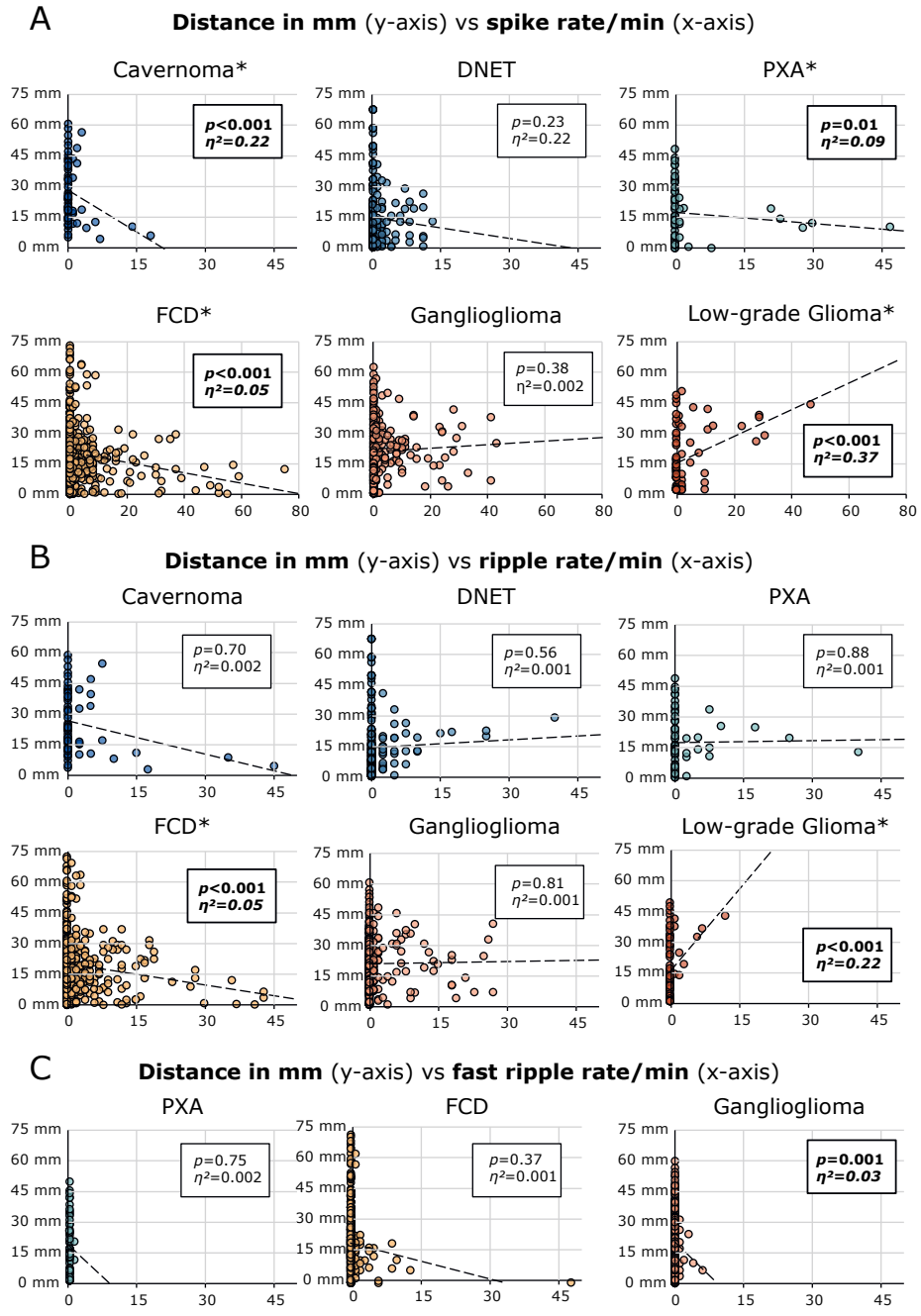


Figure 3: Scatterplots of distance against spike, ripple, and fast ripple rates with linear regression lines. (A) spike rates, (B) ripple rates, and (C) fast ripple rates per minute (x-axis) are plotted against the distance to the edge of the lesion in mm (y-axis). Linear regression lines and their respective p-value and effect size η^2 are provided. Significant correlations are marked in bold and with an asterisk (*). It should be noted that the scale of the x-axis differs from the first to the second row of plots in (A) and (B). No fast ripples were recorded for cavernoma, DNETs, and low-grade glioma.
Abbreviations: DNET = dysembryoplastic neuroepithelial tumor, FCD = focal cortical dysplasia, PXA = pleomorphic xanthoastrocytoma

Correlations between spike/HFO rates and distance for different pathology types

Spike rates

A higher spike rate was associated with a shorter distance to the lesion for cavernomas, FCDs, and PXAs. The effect sizes for these negative correlations were: large for cavernomas (η^2=0.22), small for FCDs (η^2=0.05), and moderate for PXAs (η^2=0.09). Conversely, we found a positive correlation between spike rate and distance for low-grade gliomas. The effect size of this correlation was large (η^2=0.37). Spike rates did not correlate with distance for DNETs and gangliogliomas. (Figure 3A)

HFO rates

We found correlations for two pathologies between ripple rates and distance: FCDs showed a negative correlation with a small effect size (η^2=0.05), and low-grade gliomas showed a positive correlation with a large effect size (η^2=0.22). Ripple rates did not correlate with distance for cavernomas, DNETs, gangliogliomas, and PXAs. (Figure 3B) No fast ripples were recorded for cavernomas, DNETs, and low-grade gliomas. Gangliogliomas showed a negative correlation between fast ripple rates and distance with a small effect size (η^2=0.03). No correlation was found for FCDs and PXAs. (Figure 3C)

Distance to the electrode with the maximum event rate

Visual slope comparison

All correlations we found through linear regression were consistent with the slopes in this visual analysis, except for PXAs. We found a positive slope for PXAs with single data points per patient, while our linear regression results indicated a negative correlation between spike rate and distance for PXAs. (Figure 4A, 4B)

Mean distances

A one-way Welch's ANOVA revealed no significant differences between the mean distance to the electrode with the highest rate of spikes, ripples, and fast ripples ($F(6, 2283)=0.98$, $p=0.41$). (Figure 4C)

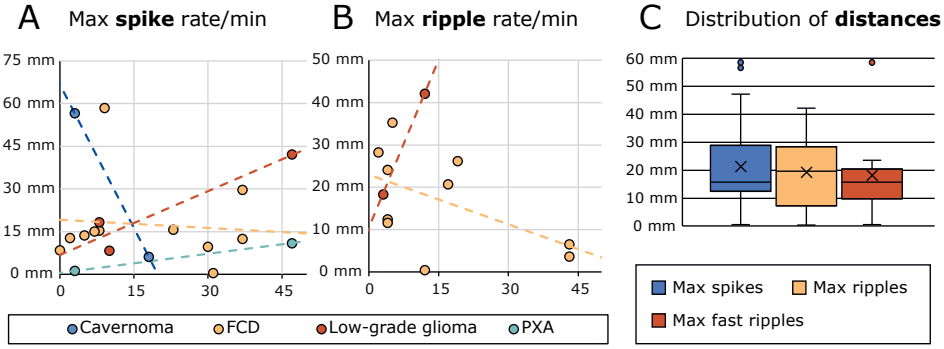


Figure 4: Distances to electrodes with the highest event rates. Scatterplots of the maximum recorded (A) spike rate in spikes/min and (B) ripple rate in ripples/min (x-axis) and the distance of that electrode to the lesion edge in mm (y-axis). Every patient is represented by a single dot to visually compare the resulting slope to the linear regression results in Fig. 3. Except for the result for PXAs, all slopes matched those of our earlier results. (C) Boxplots of the distribution of the D_{max}(spikes), D_{max}(ripples), D_{max}(fast ripples).

Abbreviations:FCD = focal cortical dysplasia, PXA = pleomorphic xanthoastrocytoma

The influence of pathology type and lesion volume

Mean lesion volumes

Gliomas (20.8±28.6 cm^3) tended to have the largest lesion volumes. FCDs (2.5±3.0 cm^3) and cavernomas (2.1 ± 0.01 cm^3) tended towards relatively small lesion volumes on MRI. (Figure5A)

Moderator analysis of pathology type and lesion volume

A moderator analysis revealed the underlying pathology type to have a significant effect on the correlation between spike rates and distance ($F(5, 1382)=14.98$, $p<0.0001$) while lesion volume did not ($F(1,1382)=0.21$, $p=0.64$). (Fig. 5, B-D) We also found pathology type to influence the relationship between ripple rates and distance ($F(5,1382)=8.65$, $p<0.0001$), while lesion volume did not ($F(1,1382)=0.02$, $p=0.89$). Neither pathology type ($F(2,1000)=0.07$, $p=0.93$) nor lesion volume ($F(1,1000)=0.22$, $p=0.64$) influenced the relationship between fast ripple rates and distance.

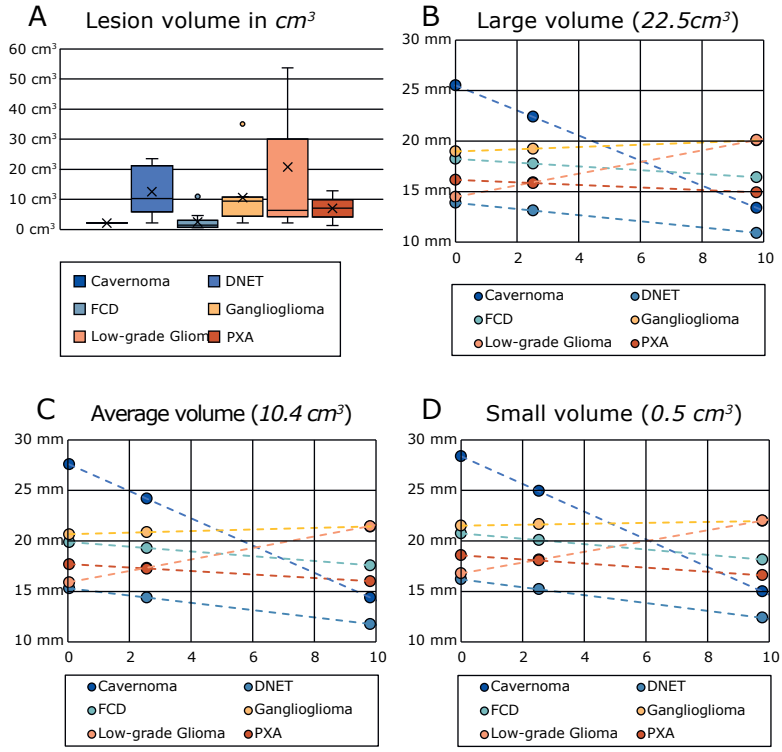


*Figure 5: Illustration of the simple slopes moderator analysis. (A) Boxplots of the lesion volumes stratified by pathology types. FCDs and cavernoma tended to have the smallest, low-grade gliomas the largest lesion volumes. (B-D) An illustration of the influence of pathology type and lesion volume on the relationship between spike rates and distance. B-D show scatterplots of the mean distance to the edge of the lesion in mm (y-axis) against the mean spike rate per minute at that distance (x-axis). Regression lines are provided for different pathology types (coloured slopes). Different lesion volumes are represented in the three scatterplots: (C) mean lesion volume (10.4cm^3), (B)large lesion volume (mean+1*SD=22.5cm^3), (D) small lesion volume (mean-1*SD=0.5cm^3). The regression slopes differ markedly between pathology types within the three scatterplots (B-D). However, slopes of the same pathology type vary only insubstantially when compared at large (B), average (C), and small lesion volumes (D). This illustrates the fact that pathology type has a significant influence on the relationship between spike rates and distance ($p<0.0001$), while lesion volume does not influence that relationship ($p=0.64$). It should be noted that the small, average, and large volume categories are only exemplary. Lesion volume was treated as a continuous moderator in our analysis.*

Discussion

We found spike and HFO rates to be spatially linked to the edge of the MRI lesion in patients with focal epilepsy. The nature of this link depended on the underlying pathology type. High spike rates correlated with a shorter distance to the edge of the lesion for cavernomas, FCDs, and PXAs. High ripple rates also correlated with a shorter distance for FCDs. Conversely, both high spike and high ripple rates correlated with a longer distance to the lesion for low-grade gliomas.

The spatial link between spike/HFO rates and the edge of the MRI lesion

The geodesic distance along the cortical surface showed a much weaker correlation with spike and HFO rates than the two Euclidian distances we tested. This suggests that a structural lesion causes high spike and HFO rates radially in all directions rather than exclusively along horizontal cortico-cortical connections. This is in line with earlier findings that epileptiform ECoG patterns recruit different areas of non-continuous neocortex at the same time, suggesting subcortical rather than purely cortico-cortical pathways of propagation.[189,190] The Euclidian distance to the edge of the lesion was more strongly correlated with spike and HFO rates than the distance to the centre of the lesion. This indicates that spike/HFO generation is most likely spatially linked to the lesion edge, which has also been proposed in earlier studies.[191]

In FCDs, electrodes close to the edge of the lesion showed a higher rate of spikes and ripples than those further away from the lesion. This is consistent with earlier findings suggesting the epileptogenic zone is often congruent with the extent of the lesion in FCDs.[192-194] It is also in line with the fact that FCDs, particularly type 2, likely generate epileptic activity intrinsically.[39,165,194,195] We found the opposite correlation for low-grade gliomas; the further an electrode was away from the lesion, the higher the rate of spikes and ripples it recorded. This is consistent with earlier findings suggesting that epileptic activities may not be intrinsically generated inside low-grade gliomas but preferentially arise in surrounding peritumoral tissue.[196-198] The epileptogenicity of tissue surrounding low-grade gliomas may be due to infiltration processes by glioma cells,[196,197] though neurotransmitter and receptor imbalances, blood-brain barrier disruption, acidosis, and hypoxia have also been proposed as possible pathomechanisms.[198]

Previous studies attribute ambivalent properties to other low-grade tumours in generating epileptic activity. Similar to low-grade gliomas, they can also generate epileptic activity at a distance from the lesion itself,[199] possibly due to similar invasion processes of the peritumoral tissue.[196] On the other hand, low-grade tumours like DNETs and gangliogliomas have also been shown to generate seizure activity intrinsically.[198] This suggests these tumour types may generate epileptic activity both in- and outside the structural lesion. This may explain why we found neither a conclusive positive nor negative correlation between HFO/spike rates and the distance to the radiographic lesion for DNETs and gangliogliomas, while low-grade gliomas showed a positive and FCDs a negative correlation.

Low-grade tumours (low-grade gliomas, DNETs, gangliogliomas, and PXAs) tended to have larger lesion volumes than non-tumorous lesions (FCDs and cavernomas). The results of our moderator analysis, however, indicate that lesion volume is not an independent moderator of the spatial relationship between the MRI lesion and spike/HFO rates. Our results suggest that pathophysiological processes specific to

the underlying pathology type most likely determine this relationship, independent of the size of the lesion.

Overall, spike rates showed a stronger correlation with the distance to the lesion than HFO rates. This implies that the generation of HFOs is less strongly spatially linked to the MRI lesion than the generation of spikes. This is consistent with the fact that HFOs are often incongruent with radiographic lesional areas and instead correlate with areas involved in seizure generation.[165,200]

We visually compared our linear regression results to slopes based on single data points per patient. The type of slope (positive vs negative) was consistent for FCDs, cavernomas, and low-grade gliomas. This suggests that the correlations we found through linear regression for these pathology types are based on genuine between-subject effects. However, the slope did not match the correlation type for PXAs. This indicates caution should be exercised in interpreting the linear regression results for PXAs, as they may have been caused by within-subject effects.

Clinical relevance of our findings

We found a striking difference between different pathology types in terms of correlation between spike/HFO rates and distance. This indicates that a simple, one-size-fits-all solution may not exist for the intraoperative tailoring of epilepsy surgery using ioECoG. Pathomechanisms specific to certain pathology types likely influence the spatial relationship between the MRI lesion and spike/HFO generation. This suggests that high spike or HFO rates on ioECoG may not warrant the same surgical action for different underlying pathologies.

We illustrate this finding in Figure 6 using the case of a FCD and a low-grade glioma patient. Aligning with the results of our linear regressions, high spike and HFO rates are located close to the edge of the radiographic lesion in the FCD patient (left). Because FCDs most likely generate epileptic activity intrinsically,[39,165,194,195] these high spike/HFO rates likely indicate residual lesional tissue in their vicinity. This strongly argues for the resection of the tissue underneath these electrodes, as a complete lesionectomy has repeatedly been shown to be a good predictor of post-surgical seizure freedom.[201] This is in line with earlier studies that have found ioECoG tailored lesionectomy to be linked to a better surgical outcome than lesionectomy alone for both FCDs[193,202] and cavernomas.[203]

Congruent with our linear regression results, electrodes with high spike and ripple rates lie far outside the radiographic lesion in the exemplary low-grade glioma patient (right). Whether the removal of such distant foci is also related to good surgical outcomes is debated. Some studies have found that ioECoG tailored resections yield better seizure control for tumour-related focal epilepsy than lesionectomy alone,[204,205] while others have not.[68,206]

This illustrates that the pathology type should be taken into account when ioECoG results are interpreted clinically, where the precise location of the radiographic lesion is not always immediately apparent due to brain shift and other uncertainties. One should be aware that high spike/HFO rates correlate well with proximity to the edge of the MRI lesion for some pathology types, but not for others. Frauscher et al.[207] recently proposed an atlas with normative values for physiological HFO rates according to different anatomical locations. This is a promising way to tailor

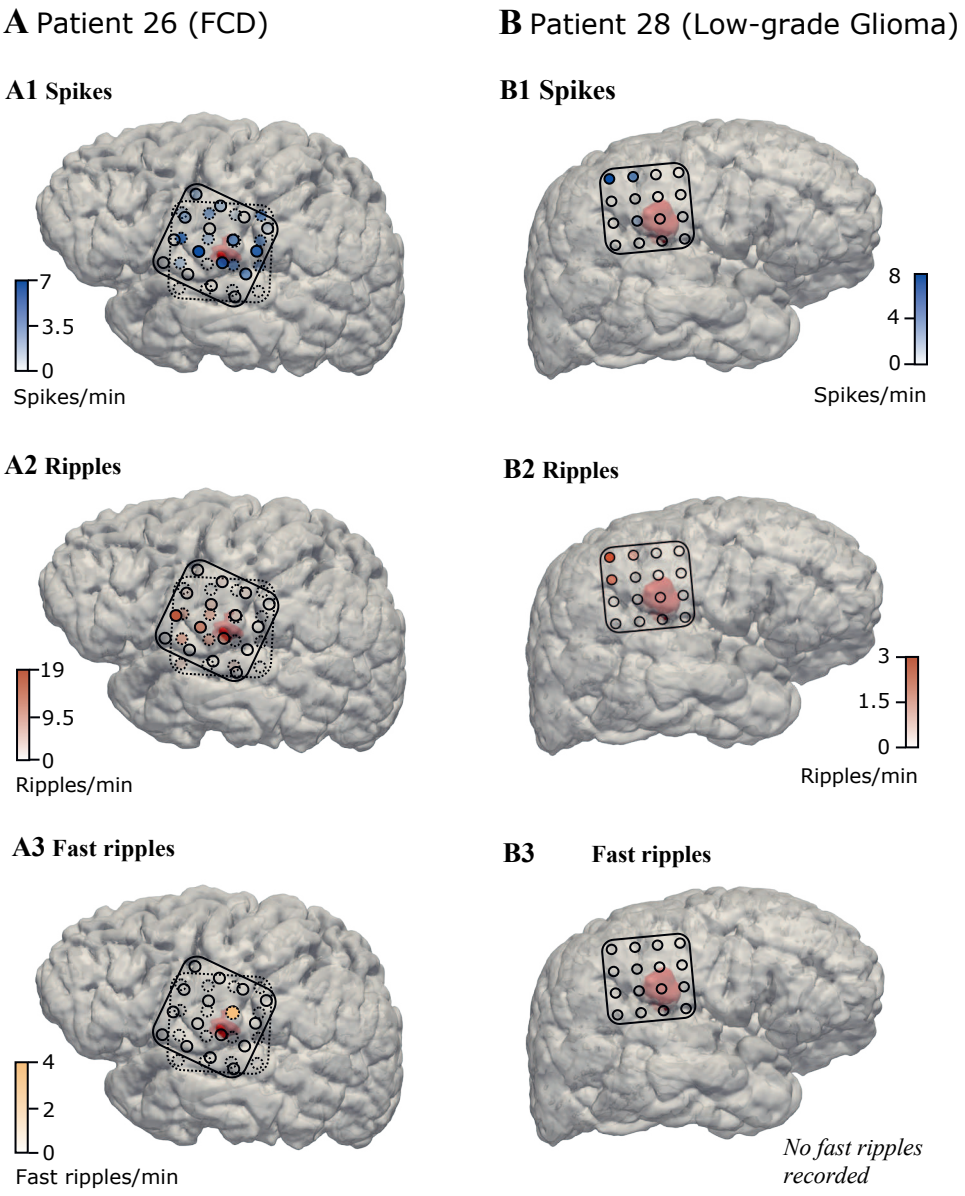


Figure 6: Illustrative FCD and low-grade glioma cases. (A) Patient 26 (FCD, left) and (B) patient 28 (low-grade glioma, right) are portrayed to illustrate the typical ioECoG findings for these pathology types in our study. Two pre-surgical ioECoG recordings were taken for patient 26 (solid and dashed lines), one was taken for patient 28 (solid line). Electrodes with high spike, ripple, and fast ripple rates are located close to the MRI lesion (red segmentation) for the FCD patient. Conversely, electrodes with high spike and ripple rates are far away from the MRI lesion for the low-grade glioma patient. No fast ripples were recorded for patient 28.
Abbreviations: FCD = focal cortical dysplasia, min = minute, MRI = magnetic resonance imaging

the interpretation of ioECoG results to the anatomical site of resection. The results of our study suggest that the influence of pathology types on ioECoG results may be a useful addition to such an atlas.
Furthermore, high spike or ripple rates on ioECoG are sometimes used clinically to determine the site of corticotomy at the beginning of resection in lesional epilepsy surgery. It is important to note that while this practice may target the area of highest epileptogenicity, it may not necessarily target the underlying MRI lesion for low-grade tumours, especially not for low-grade gliomas.

Strengths and potential limitations of this study

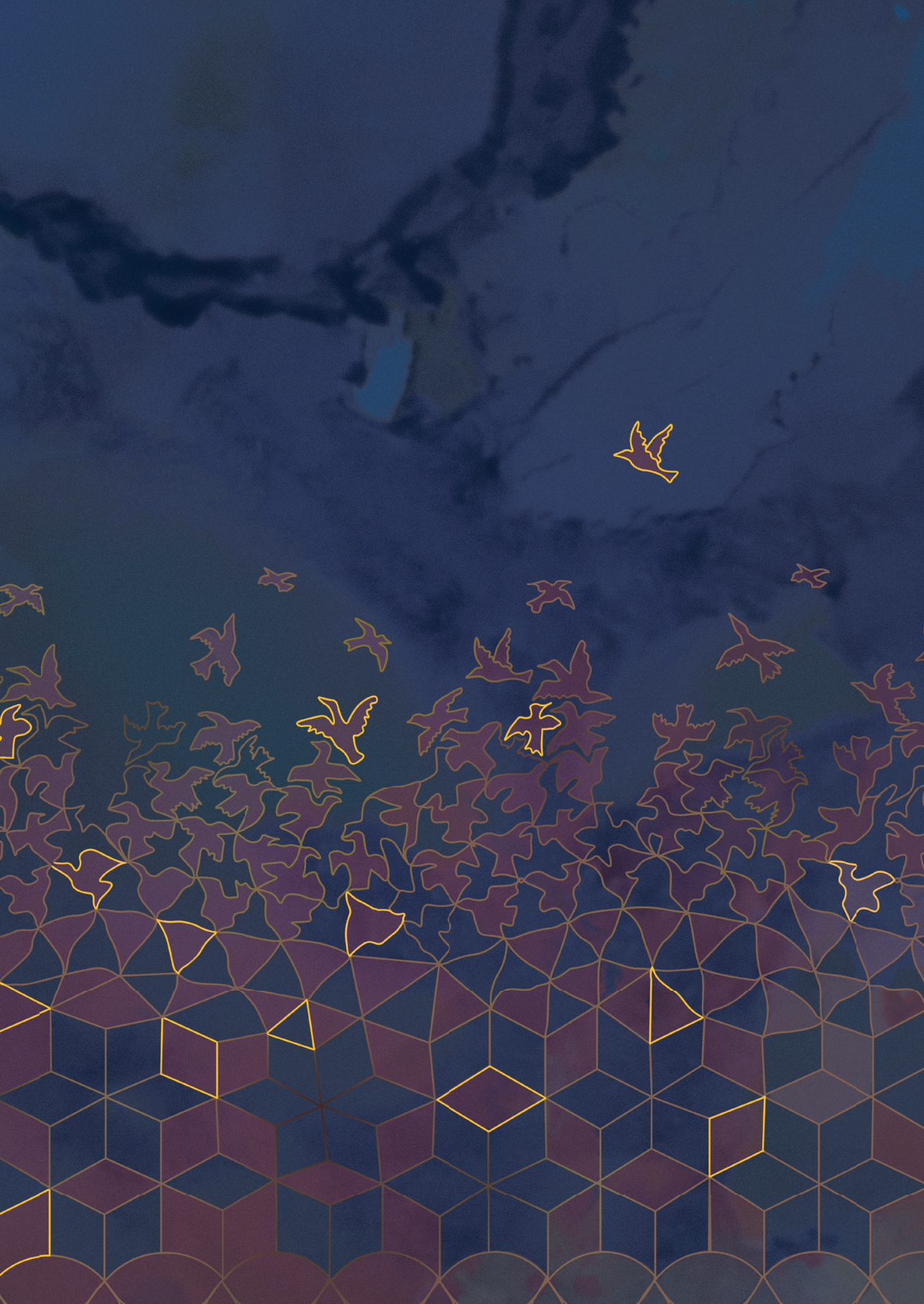
A strength of our study is its novelty. To our knowledge, this is the first study investigating correlations between neocortical spike/HFO rates and distance as a measure of their spatial relationship to MRI lesions. We hope future studies can benefit from our methods to overcome similar technical hurdles in fusing MRI and ioECoG data.

A limitation of our study is its retrospective design and the relatively small number of included patients. These small numbers are in part due to our strict inclusion criteria to minimise confounding factors. We excluded all patients with non-optimal surgical outcome, incomplete resections, and repeated surgeries because these factors might indicate that the EZ extended further than the area on which ioECoG was performed. We furthermore excluded patients with mesiotemporal lesions because mesiotemporal structures have been shown to display higher HFO rates than superficial lesions,[89] possibly due to physiological HFOs being recorded along with pathological HFOs.[89,132]

We did not correct for multiple comparisons for our linear regression results. However, the application of a Bonferroni correction would not have significantly altered our results.
Another potential limitation is that we recorded relatively few fast ripples, and none for three pathology types. This may have limited the capacity of our analyses to uncover existing correlations between fast ripples rates and distance. There is growing evidence that fast ripples, if captured, are excellent predictors for epileptogenic tissue. The use of high-density ioECoG grids or additional depth electrodes in future studies may increase the detection of fast ripples.[13,33]

It should also be noted that our retrospective process of marking spikes and HFOs differs from clinical practice in ioECoG-tailored surgery, where spikes and HFOs are marked prospectively and according to general occurrence rather than exact rates. We focused solely on spike and HFO rates as indicators of epileptogenicity in this study, with no further classification. Several studies indicate that tailoring the resection to tissue generating leading instead of propagated spikes might be favourable to removing all tissue where spikes are recorded.[65,153,206,208] HFOs are also thought to propagate from their area of generation[160], and the resection of leading ripples may similarly be associated with better post-surgical seizure control than the resection of propagated ripples.[175] It would be interesting to investigate the spatial relationship specifically between leading spikes/ripples and the MRI lesion in a future study.

We would like to encourage future studies on spikes and HFOs to perform subgroup analyses stratified by pathology type. This may advance our understanding of the influence of pathology type, particularly tumorous versus non-tumorous lesions, on ioECoG results.



Chapter 7

Implementing intraoperative high-density electrocorticography during epilepsy surgery

Eline V. Schaft*, Dongqing Sun*, Sem Hoogteijling, Ziyi Wang, Frans S.S. Leijten, Pieter van Eijsden, Nick F. Ramsey, Pierre A.J.T. Robe, Maryse A. van 't Klooster, Maeike Zijlmans on behalf of the RESPect database group

* These authors contributed equally

Published in Epilepsia, Volume 66, Issue 5, February 2025

Abstract

Objective

In intraoperative electrocorticography (ioECoG) tailored epilepsy surgery, standard low-density (LD) electrode grids (16-20 electrodes,; 10mm inter-electrode distance) are used, covering ±20cm^2 cortex. High-density (HD) grids have shown advantages in basic research. We wanted to evaluate clinical use of HD-grids during epilepsy surgery. We assessed how often HD-ioECoG might have altered the presurgical hypothesis by recording highly localized epileptic spikes and high frequency oscillations (HFOs) and by facilitating spike onset localization.

Methods

Patients undergoing HD-ioECoG-tailored epilepsy surgery (64 electrodes, 5 mm inter-electrode distance; 2048Hz sampling) were selected from our registry (2021-2023). We assessed clinical reports to evaluate impact on surgical strategy. Intraoperative decision making was guided mainly by interictal spikes. We visually marked spikes, and HFOs (ripples 80-250Hz and fast ripples [FR] 250-500Hz) in 1-minute artefact-free epochs. We assessed number of events, and compared channels covering the resected and non-resected tissue and surgical outcome with logistic mixed models. We assessed focal events which occurred in few channels and could be missed on LD grids. We analyzed spike onset localization with Granger's causality.

Results

We included 36 HD-grid positions from 20 patients. HD-ioECoG would have confirmed the original surgical plans in 11 patients and adapted it in 6. We found 41-5485 spikes, 0-2243 ripples (1 patient none), and 0-1008 FR (3 patients none) per patient. More FR occurred in channels covering the resected areas than outside ($p<0.001$), particularly in people who became seizure free ($p<0.001$). Of the spikes, ripples, and FR, 6.1%, 19.5%, and 46.7% occurred on one or two channels. 58.3% of the HD spike onset locations might be localized differently with standard LD-grids.

Significance

HD-ioECoG can be used clinically for epilepsy surgery guidance. HD-ioECoG captures increased detail when identifying focal epileptic events, especially FR, and pinpointing spike onsets, which may be missed with LD-ioECoG.

Introduction

Epilepsy surgery offers a potentially curative treatment for people with focal epilepsy. Precise delineation of epileptogenic tissue is crucial to achieve postsurgical seizure freedom.[209,210] Intraoperative electrocorticography (ioECoG) is employed to identify epileptogenic tissue by recording interictal epileptiform discharges directly from the cortex and guide surgical decision making during the surgical procedure. This technique is known as surgical 'tailoring'.[32,211] The ioECoG electrode grids commonly used in clinical practice typically have a 4x4 or 4 x 5 electrode configuration with a 10 mm inter-electrode distance, which we classify here as low-density (LD). New high-density (HD) grids, with smaller inter-electrode distance, and thus higher resolution, have been developed. Recent studies have shown advantages of HD grids in research, but not yet in clinical routine.[212]

ioECoG is based on the detection of interictal epileptiform transients. Due to the low resolution of LD grids, entire gyri, along with critical epileptiform transients over anatomical structures, can be completely missed, potentially leading to significant gaps in detection. Traditionally, these epileptiform transients comprise of spikes, the established EEG biomarkers of epileptogenic tissue. Interictal spikes are events that either occur in isolation or propagate from the spike onset area to neighboring regions.[213] The ability to distinguish onset spikes from propagated spikes is crucial since the removal of the spike onset area is associated with favorable seizure outcome[35], whereas propagated spikes do not need to be included in the resection plan.[214-216] Interictal high frequency oscillations (HFOs) have emerged as EEG biomarkers with greater specificity for the epileptogenic tissue than spikes [11,12]. These fast oscillations, ranging between 80 and 500Hz, are further subclassified into ripples (80-250Hz) and fast ripples (FRs, 250-500Hz).[11] The absence of HFOs after the resection has been associated with seizure freedom.[33,175]

HFOs are focal phenomena that could be missed when using LD electrodes.[13,14,217] With increased spatial resolution, HD-grid may record HFOs more effectively. In addition, HD-grid may better distinguish onset spikes and propagated spikes and facilitate reconstruction of propagation patterns. Recent studies have shown that HD grids provide advantages over LD grids in detection of intraoperative microseizures [218] and HFOs [13], and in connectivity analysis.[217] We aimed to evaluate the clinical use of HD grids during epilepsy surgery. We studied 1) implementation of HD-ioECoG and looked if this adapted the surgical plan, 2) the amount of detected events in the resected area in people who became seizure free, and 3) whether HD grids facilitated detection of focal epileptic events and spike onset localization.

Materials & methods

Patient cohort

Patients of all ages were considered eligible for clinical HD-ioECoG recordings when they were candidates for ioECoG tailored epilepsy surgery, with a few exclusion criteria: 1) presumed epileptic focus in the occipital lobe, as this is associated with the presence of physiological HFOs;[207] 2) the presumed epileptic focus was difficult to reach by the relatively rigid HD-grid (e.g. interhemispheric, orbito-frontal); and 3) if the primary purpose of ioECoG was to decide on the necessity of a hippocampectomy.[45]

We retrospectively selected patients from this clinical HD-ioECoG cohort in the period September 2021 till August 2023. Exclusion criteria for further analyses were 1) HD-ioECoG recording under awake conditions, since HFO occurrence under awake conditions differ from those under anesthesia,[58] and 2) HD-ioECoG recorded with the MicroMed LTM Express amplifier (MicroMed, Veneto, Italy) due to its low signal-to-noise ratio for frequencies above 100Hz.

Ethical approval

All data were collected from the Registry for Epilepsy Surgery Patients in the UMC Utrecht and Stichting Epilepsie Instellingen Nederland (RESPect database). The collection of data in the RESPect database is approved by the institute's Medical Research Ethical Committee under protocol number 18-109. Participants included after 2018 gave consent in accordance with Declaration of Helsinki 2013 for collection and use of their data for research purposes.

Clinical data

We collected clinical characteristics, including sex, age at surgery, epilepsy duration, previous brain surgery, anatomical location of resection, MRI diagnoses, histopathological diagnoses, seizure outcome and follow-up time, from the RESPect database electronic data capturing system (Castor, Amsterdam, The Netherlands). One year postsurgical seizure outcome was determined based on the ILAE classification[219].

High density intraoperative electrocorticography recordings

All patients underwent surgery under general anesthesia using propofol.[107] Propofol infusion was interrupted during HD-ioECoG-recordings to achieve a continuous background pattern with minimal propofol effect.[44] HD-ioECoG was recorded with 8×8 silicone grids with 2 mm platinum electrodes (exposed surface 4.2mm^2) with 5 mm interelectrode distance (FG64C-SP05X-000, AD-Tech, Racine, WI, USA), placed directly on the cortex. HD-ioECoG has four times more electrodes than our standard LD-ioECoG, while the individual electrode contact surface area is the same (4.2mm^2). Recordings were made with a 64-channel EEG-system (MicroMed LTM PLUS, MicroMed, Veneto, Italy) at 2048Hz sampling frequency. A unipolar ECG was included in the recordings, resulting in HD-ioECoG recordings of channel 1 to 63. HD-ioECoG was recorded from multiple positions on the cortex during different stages of surgery. Pre-resection recordings were performed to investigate the epileptic characteristics in the signal and to assist in defining the resection border. Recordings were performed at moments indicated by the surgeon to examine whether the resection of the epileptic area was completed or should be extended. The final recording, after the completion of the resection, was named the post-resection recording. Intraoperative tailoring is based on interictal spikes

and ictal discharges. If an HFO expert (E.V.S./D.S.) was available, intraoperative HFO analysis was also incorporated in the tailoring of resection plan. When analyzing HFOs intraoperatively, data were transferred to a separate computer to visualize HFOs. The settings used are described below in the next section. Based on the epileptic events (either spikes alone or spikes in combination with ictal discharges and HFOs), advice was given by the clinical neurophysiologist to the neurosurgeon on the extent of the tissue to be resected in relation to the surgical plan. In the absence of any relevant events, the resection was performed based on the presurgical hypothesis of the epileptogenic zone, which is based on preoperative MRI, scalp electroencephalography (EEG) and long-term intracranial EEG if available. The added value of HD-ioECoG to the presurgical hypothesis, was determined post-hoc based on the clinical reports and divided into three categories: 1) confirmation of surgical plan, defined by the presence of epileptic activity before resection, and absence of epileptic activity after resection; 2) adaptation of surgical plan, defined by adaptation and/or extension of the resection; 3) no added value, defined by the absence of epileptic activity before and after resection.[14]

Visual marking of interictal events

We included all pre-resection HD-ioECoG recordings (HD-ioECoG$_{pre}$) in our analyses. We only used visual analyses of interictal events without automated analysis methods during clinical workup or the study, because of the short recording times and the great amount of intraoperatively recorded artefacts. We selected an artefact-free one-minute epoch of each HD-ioECoG$_{pre}$ recording that had minimal propofol effects (i.e., excluding burst suppression patterns). In these HD-ioECoG$_{pre}$ epochs interictal spikes (by EVS) and HFOs, ripples and FR, (by DS) were visually marked independently using BrainQuick (v1.01.0012, MicroMed, Veneto, Italy). In case of uncertainty, expert reviewers (MZ, MvK) were consulted to reach consensus. Spikes were marked in an average montage with conventional EEG filter settings (0.16Hz high pass infinite impulse response filter, 70Hz low pass infinite impulse response (IRR) filter, gain of 800μV/cm and timescale of 15s/page). HFOs were defined as oscillatory events with at least four oscillations (to avoid marking solely the ringing effect of bandpass filtering sharp spikes) and were marked in a bipolar montage with the following settings; a) Ripples (80-250Hz): high pass finite impulse response (FIR) filter at 80Hz, gain of 50μV/cm and timescale of 1s/page, and b) FRs (250-500Hz): high pass FIR filter at 250Hz, gain of 10μV/cm and timescale of 1s/page) (Figure 1B). We reviewed the raw ioECoG signal next to marking HFOs to avoid marking false HFOs resulting from ringing effects due to the band pass filtering.

Channel labels

We retrospectively matched intraoperative photos of the HD-ioECoG$_{pre}$ positions on the cortical surface with photos of the final resection cavity. For each HD-ioECoG$_{pre}$ recording a researcher (ES, SH, ZW) - blinded to the marked HD-ioECoG events - categorized all unipolar channels as follows: 1) resected, channels covering the complete post-surgical resection cavity and channels covering the cortex around the resection margin (5mm); or 2) non-resected, channels covering the cortical tissue more than 5 mm distance away from the border of the resection cavity. In case that a channel partially covered the resection cavity and its 5mm edge, this channel was considered resected if >50% of the channel covered the resection cavity including 5mm edge (Figure 1A). Bipolar channels, required for HFOs analysis, were categorized using the unipolar channel categorization as follows:

1) resected*:* if both unipolar channels were labeled resected, or if one was labeled as resected and the other as non-resected
2) non-resected*:* if both unipolar channels were labeled as non-resected.

We quantified in how many cases the resected channels of HD-ioECoG recorded interictal epileptic events. We repeated this measure for the four simulated LD-ioECoG by calculating the mean frequency that LD-ioECoG would record interictal epileptic events in the resected channels and compared this to the HD-ioECoG.

Focality of interictal epileptic events

In order to assess focality of interictal epileptic events, we retrospectively counted the number of channels with simultaneously occurring events over time for each event type. We classified events into three groups: focal, semi-focal or scattered. A focal event was defined as occurring in one channel only, a semi-focal event as one occurring in 2 channels, and a scattered event if more than 2 channels were involved. We counted the number of focal and semi-focal events, as we assume that these are the type of highly localized events which might have been missed if recording with an LD grid.

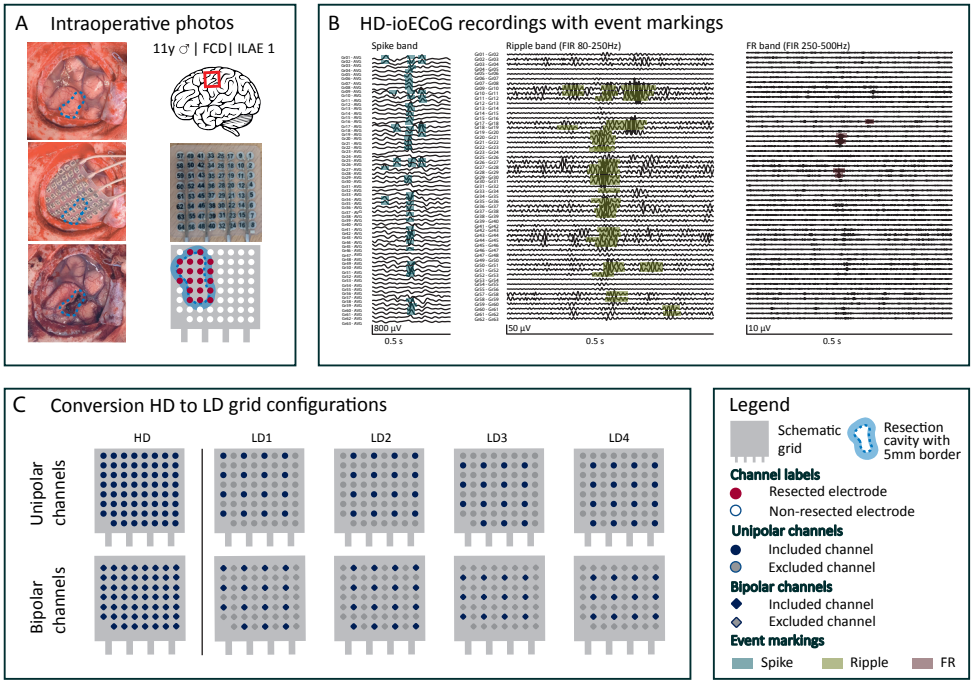


Figure 1:Schematic representation of methodological aspects of channel labeling, event detection and HD vs LD grid configurations. A. A patient example (pat nr. 4) of the intraoperative photos that were used to determine channel positions and resected and non-resected channels. B. The patient's corresponding HD-ioECoG signals including marked events; 0.5 second of raw data with marked spikes in common average montage (0-70Hz, IRR filtered) (left panel), ripples in bipolar montage (80-250Hz FIR filtered) (middle panel), and FRs in bipolar montage (250-500Hz FIR filtered) (right panel). C. Schematic illustration of conversion method form HD to LD grid configuration. HD grids have four times more electrodes than LD grids, so four different simulated LD grid configurations could be constructed to compare the HD grid findings to the corresponding hypothetical LD grid findings. Abbreviations: FCD = focal cortical dysplasia, FIR = finite impulse response, FR = fast ripple, HD = high-density, ioECoG = intraoperative electrocorticography, LD = low-density, µV = microvolt, s = seconds.

Spatial clustering of interictal epileptic events

In order to further evaluate which events might have been missed with LD grids, we retrospectively studied events on adjacent electrodes. We defined spatial clusters as ≥1 event(s) on adjacent channels. We counted the number of clusters consisting of 1, 2, or 3 channels, as we assume that these are the highly localized clusters which might have been missed if recorded with an LD grid. Spatial cluster analyses were repeated for four different simulated LD configurations (i.e. subsampled from HD grids to create LD configurations with 1cm inter-electrode distance) to create spatial clusters as they would have been with LD recordings (Figure 1C). We examined if the same spatial clusters occurred in the simulated LD configurations in comparison to those on the HD grid. This analysis is performed only on HD-ioECoG recordings with events.

Interictal spike onset localization

We retrospectively used the Granger's causality to analyze the propagation of interictal propagating spikes. Granger's causality is a bivariate measure, resulting in a NxN matrix, where N is the number of channels. This NxN matrix shows the causality of each channel to all other channels. We calculated outflow by applying the sum over one direction of the NxN matrix. This outflow represents propagation, since it shows the causalities of one channel to all other channels. The 1xN matrix was transformed back to the 8x8 grid configuration to display spike propagation. The spike onset channel was defined as the channel with highest outflow. We included HD-ioECoG recordings in this analysis if spike propagation was present, defined by spikes co-occurring on at least 1/3 of the grid (i.e., ≥21 channels). These spike onset localization analyses were repeated for 4 different simulated LD configurations, to create spike propagation patterns as they would have been with LD recordings (Figure 1C). We assumed spike onset location with LD grid might have been located differently if HD spike onset differed >0.5cm – the interelectrode distance between 2 electrodes – to LD spike onset.

Statistical analysis

Based on intraoperatively performed analysis, we counted the numbers of patients per category of clinical added value by HD-ioECoG. We calculated medians and interquartile ranges (IQR) for continuous clinical variables. All further analyses described were performed post-hoc and were not taken into account in the clinical decision making. We calculated the total number of events per interictal event type (spikes, ripples, FR) on channels covering resected and non-resected tissue and the mean and standard deviation (SD) of the number of events per channel. We compared numbers of events between channels covering resected and non-resected tissue using a logistic mixed model:

$$log(resection_{patient}) = \alpha + \beta x_{event\ type} + \alpha_{patient} + \gamma_{patient} x_{event\ type} + \varepsilon_{patient}$$

where $resection_{patient}$ was the binary dependent variable (resected / non-resected), $x_{event\ type}$ the type of interictal event, α the fixed intercept, β the average relation between the dependent variable and the $x_{event\ type}$. the effects $\alpha_{patient}$ and $\gamma_{patient} x_{event\ type}$ represented the random intercept and slope for each patient. $\varepsilon_{patient}$ represented the residuals. A $\beta>0$ indicates a positive association between number of events and resected tissue, where a $\beta<0$ indicates a positive association between number of events and non-resected tissue. These analyses were performed for the total population, good outcome (ILAE 1) and poor outcome (ILAE ≥2) subgroups.

To assess the focality of epileptic events, we calculated the numbers of focal, semi-focal and scattered events, the number of clusters per event type, and number, median and IQR of channels within each cluster. We calculated the percentage of focal and semi-focal events with respect to the total number of events as well as the percentages of clusters with 1, 2 or 3 channels with respect to the total number of clusters. To assess spike onset in HD-ioECoG, a spike propagation pattern was calculated for each patient showing spike propagation. The spike onset found in HD was compared with respect to resected and non-resected tissue. All data were processed and analyzed in Matlab 2023b (The MathWorks, Inc., Natick, Massachusetts, United States). All statistics were performed in RStudio 2023.12.1 (R Core Team, 2023). We considered a two-sided tested p-value ≤ 0.05 significant.

Results

Clinical data

Between September 2021 and August 2023, 27 patients underwent HD-ioECoG recordings. 7 patients were excluded for this study: 5 had LTM Express recordings and 2 had recordings under awake conditions. We included 20 patients (7 female). The median age at epilepsy onset was 6y (IQR 11y) and the median age at surgery was 24y (IQR 23.5y). One patient had prior brain surgery, two patients underwent stereo-EEG at 4 and 6 months preceding resection. The anatomical location of the resection was temporal in ten patients, frontal in seven patients, and parietal in three patients. Focal cortical dysplasia (MRI: n=8; histopathology: n=8) and central nervous system tumors (MRI: n=4; histopathology: n=6) were the most common MRI and histopathological diagnoses. One-year-seizure outcome was good (ILAE 1) in 13 patients and poor (ILAE ≥2) in 7 patients (Table 1).

High-density intraoperative electrocorticography recordings

Preresection HD-ioECoGs were recorded in 1 position in 8 patients, 2 different positions in 9 patients, and in 3 different positions in 4 patients. The median duration of each HD-recording in each position is 4 minutes 29 seconds [IQR 2 minutes 32 seconds-8 minutes 7 seconds]. The HD-ioECoG findings confirmed the surgical plan in 11 patients, adapted the surgical plan in 6 patients, and didn't have additional value in 3 patients. (Table 1) A total of 36 HD-ioECoG$_{pre}$ recordings were included for further analyses, consisting of 2188 unipolar channels (1006 resected and 1182 non-resected) vs. 1888 bipolar channels (981 resected and 907 non-resected). Intraoperative HFO analysis was performed in 11 out of 20 patients (7 with good outcome).

Visual marking of interictal events

No electrographical seizure were captured. A total of 21,358 spikes were found in all HD-ioECoG$_{pre}$ recordings in all patients. Mean (±SD) number of spikes per channel per minute was 9.95 (±13.83) in resected and 8.31 (±13.61) in non-resected tissue. Channels in the resected area captured spikes in 35 HD-ioECoGs (97%). In the simulated LD-ioECoG, channels in the resected area in 30 LD-ioECoGS (83%) captured spikes. This is 14% lower compared to HD-ioECoG.

A total of 8,288 ripples were found in 34 HD-ioECoG$_{pre}$ recordings in 19 patients. Mean (±SD) number of ripples per channel per minute was 4.02 (±5.68) in resected and 3.80 (±5.56) in non-resected tissue. Channels in the resected area captured ripples in 30 HD-ioECoGs. In the simulated LD-ioECoG, channels in the resected area in 27 LD-ioECoG captured ripples. This is 8% lower compared to HD-ioECoG.

A total of 2,610 FR were found in 29 HD-ioECoG$_{pre}$ recordings in 17 patients. Mean (±SD) number of FR per channel per minute was 1.24 (±2.47) in resected and 0.99 (±1.78) in non-resected tissue. Channels in the resected area captured FRs in 26 HD-ioECoGs. In the simulated LD-ioECoG, channels in the resected area in 19 LD-ioECoG captured FRs. This is 20% lower compared to HD-ioECoG.

Over the whole patient population, a significant positive association was found between resected tissue and numbers of events per channel for FR (β=0.021, $p<0.001$). In the good outcome group, a significant positive association was found between resected tissue and number of events per channel for FR (β=0.024, $p<0.001$), while this association was absent in the poor outcome group (β=0.018, $p=0.69$) (Table 2).

Table 1: Clinical patient characteristics

Pat. nr.	Sex	Epilepsy duration (in years)	Age at surgery	Pre-operative MRI lesion	Hemisphere	Anatomical location	Included number of grid positions	HD-ioECoG contribution to surgical plan	Intraoperative HFO analysis	Histopathology	Post-surgical outcome (ILAE class)
1	M	5	25	+	L	Parietal	1	Confirmation	No	Gangioglioma (WHO 1)	ILAE 4
2	M	41	52	+	L	Temporal	1	Confirmation	No	Gangioglioma (WHO 1)	ILAE 1
3	M	36	39	+	L	Temporal	2	Confirmation	No	Others	ILAE 3
4	M	4	11	+	L	Frontal	2	Adaptation	Yes	FCD 2A	ILAE 1
5	F	8	14	+	L	Parietal	1	Adaptation	No	Glioma (WHO 2)	ILAE 1
6	M	6	11	+	R	Temporal	3	Adaptation	No	TSC	ILAE 1
7	M	11	53	-	R	Temporal	3	Adaptation	Yes	FCD 2A	ILAE 5
8	M	12	28	+	R	Temporal	2	Adaptation	Yes	Gliosis	ILAE 3
9	M	4	12	+	L	Parietal	3	Confirmation	Yes	TSC	ILAE 1
10	F	31	31	+	R	Frontal	2	Confirmation	Yes	FCD 2A	ILAE 3
11	M	34	39	+	R	Frontal	1	Limitation	Yes	FCD 2A	ILAE 1
12	M	5	18	+	R	Temporal	3	Confirmation	Yes	DNET (WHO 1)	ILAE 1
13	F	19	23	+	L	Frontal	1	Confirmation	Yes	FCD 2A	ILAE 1
14	F	32	34	+	L	Frontal	2	Confirmation	No	FCD 2B	ILAE 1
15	M	4	6	+	R	Temporal	2	Confirmation	Yes	FCD 2A	ILAE 1
16	M	5	29	+	L	Temporal	2	Confirmation	No	DNET (WHO 1)	ILAE 1
17	M	5	7	+	L	Frontal	1	Adaptation	No	FCD 2A	ILAE 1
18	F	1	1	+	L	Frontal	2	Limitation	Yes	Others	ILAE 3
19	F	1	18	+	R	Temporal	1	Confirmation	Yes	Gangioglioma (WHO 1)	ILAE 1
20	F	31	39	+	R	Temporal	1	Limitation	No	TSC	ILAE 4

Abbreviations: F, female; FCD, focal cortical dysplasia; HD-ioECoG, high-density intraoperative electrocorticography; HFO, high frequency oscillation; ILAE, International League Against Epilepsy; L, left; M, male; MRI, Magnetic Resonance Imaging; Pat. nr., patient number; R, right; TSC, tuberous sclerosis complex; WHO, World Health Organization; +, positive MRI; -, negative MRI.

Table 2: Event numbers for interictal epileptic events in- and outside the resection and in relation to post-surgical outcome

	Total population (n = 20)			**ILAE 1 (n = 13)**			**ILAE ≥2 (n = 7)**		
	Resected channels	Non-resected channels	Resected vs non-resected	Resected channels	Non-resected channels	Resected vs non-resected	Resected channels	Non-resected channels	Resected vs non-resected
Spikes (n = 20)									
Total events	*10452*	*10906*		*6213*	*6428*		*4239*	*4478*	
Total events	522.6 (±726.2)	545.3 (±950.0)		443.8 (±459.1)	459.1 (±905.0)		706.5 (±737.6)	746.3 (±1019.6)	
# events per channel	10.0 (±13.8)	8.3 (±13.6)	β = 0.016 p = 0.69	10.4 (±15.8)	6.4 (±10.9)	β = 0.056 p = 0.31	9.1 (±8.9)	11.9 (±17.0)	β = -0.034 p = 0.60
# events per channel with events	13.18 (±13.83)	11.03 (±13.81)	β = 0.0324 **p = 0.003**	12.60 (±14.82)	8.87 (±10.49)	β = 0.0408 **p = 0.012**	14.42 (±11.29)	16.07 (±18.51)	β = 0.0352 p = 0.34
Ripples (n = 19)									
Total events	*4529*	*3759*		*2790*	*2343*		*1739*	*1416*	
Total events	226.5 (±373.4)	188.0 (±270.0)		199.3 (±338.4)	167.4 (±223.7)		289.8 (±438.0)	236.0 (±359.5)	
# events per channel	4.0 (±5.7)	3.8 (±5.6)	β = -0.015 p = 0.74	4.0 (±5.7)	2.9 (±3.1)	β = -0.017 p = 0.81	4.1 (±5.7)	5.5 (±8.2)	β = -0.009 p = 0.54
# events per channel with events	6.81 (±6.42)	6.90 (±6.69)	β = -0.0272 p = 0.19	5.99 (±5.63)	5.93 (±4.55)	β = -0.0363 p = 0.27	9.65 (±8.00)	9.64 (±10.11)	β = -0.0181 p = 0.80
Fast ripples (n = 17)									
Total events	*1370*	*1240*		*1085*	*1064*		*285*	*176*	
Total events	68.5 (±140.1)	62.0 (±132.2)		77.5 (±161.4)	76.0 (±154.0)		47.5 (±63.3)	29.3 (±37.0)	
# events per channel	1.2 (±2.5)	1.0 (±1.8)	β = 0.021 **p < 0.001**	1.6 (±3.0)	1.1 (±2.1)	β = 0.024 **p < 0.001**	0.7 (±0.8)	0.7 (±0.9)	β = 0.018 p = 0.69
# events per channel with events	3.42 (±3.39)	4.00 (±3.47)	β = -0.0022 p = 0.66	3.70 (±3.83)	4.34 (±3.92)	β = -0.0034 p = 0.52	2.73 (±1.77)	3.24 (±1.95)	β = 0.0395 p = 0.48

Note: ILAE 1 = good outcome, ILAE ≥2 = poor outcome, ξ = logistic mixed model, β>0 = positive association, β<0 = negative association. A p<0.05 is considered as a significant result (bold values).
Abbreviations: ILAE, International League Against Epilepsy; SD, standard deviation

Focality of interictal epileptic events

We found 669 (3.1%) focal spikes, 630 (3.0%) semi-focal spikes, and 20,059 (93.9%) scattered spikes. We found 924 (11.1%) focal ripples, 1,522 (18.4%) semi-focal ripples, and 5,842 (70.5%) scattered ripples. We found 683 (26.2%) focal FR, 534 (20.5%) semi-focal FR, and 1,393 scattered FR (53.3%). The number of highly localized events (i.e. focal and semi focal events) was thus 6.1% of the spikes, 19.5% of the ripples, and 46.7% of the FR (Figure 2A).

Spatial clustering of interictal epileptic events

We identified 88 spike clusters, ranging from 1 to 8 spike clusters per HD-ioECoG$_{pre}$ recording. The number of channels with spikes per cluster ranged from 1 to 63 channels with a median of 4 (IQR 17.75) channels in average montage. 29 (33.0%) clusters consisted of one channel, 5 (5.7%) clusters consisted of two channels, 9 (10.2%) clusters consisted of three channels, and 45 (51.1%) clusters consisted of more than three channels. We found a total of 43 out of 88 (48.9%) highly localized clusters with spikes. Comparing simulated LD clusters to HD clusters with events, similar cluster locations were found in 103 out of 144 LD configurations. Thus, 28.4% of the spike clusters might be missed with standard LD grids.

We identified 68 ripple clusters in 19 patients, ranging from 1 to 5 ripple clusters per HD-ioECoG$_{pre}$ recording. We found 0 to 10 clusters per patient (median 3). Each patient had 0 to 116 bipolar channels with ripples with a median of 35. Each cluster had 1 to 49 bipolar channels with ripples with a median of 6 (IQR 20.25). 7 (10.3%) clusters consisted of one channel, 10 (14.7%) clusters consisted of two channels, 4 (5.9%) clusters consisted of three channels, and 47 (69.1%) clusters consisted of more than three channels. We found a total of 21 out of 68 (30.9%) highly localized clusters with ripples. Comparing simulated LD clusters to HD clusters with events, similar cluster locations were found in 77 out of 136 LD configurations. Thus, 43.4% of the ripple clusters might be missed with standard LD grids.

We identified 74 FR clusters in 17 patients, ranging from 1 to 4 FR clusters per HD-ioECoG$_{pre}$ recording. This is 1 to 9 clusters per patient (median 4) and each patient have 0 to 89 bipolar channels with FR (median 12). Each cluster has 1 to 32 bipolar channels with FR (median 3 (IQR 3.75)). 19 (25.7%) clusters consisted of one channel, 17 (22.9%) clusters consisted of two channels, 10 (13.5%) clusters consisted of three channels, and 28 (37.9%) clusters consisted of more than three channels. We found a total of 46 out of 74 (62.1%) highly localized clusters with FR (Figure 2B). Comparing simulated LD clusters to HD clusters with events, similar cluster locations were found in 51 out of 116 LD configurations. Thus, 56.0% of the FR clusters might be missed with standard LD grids.

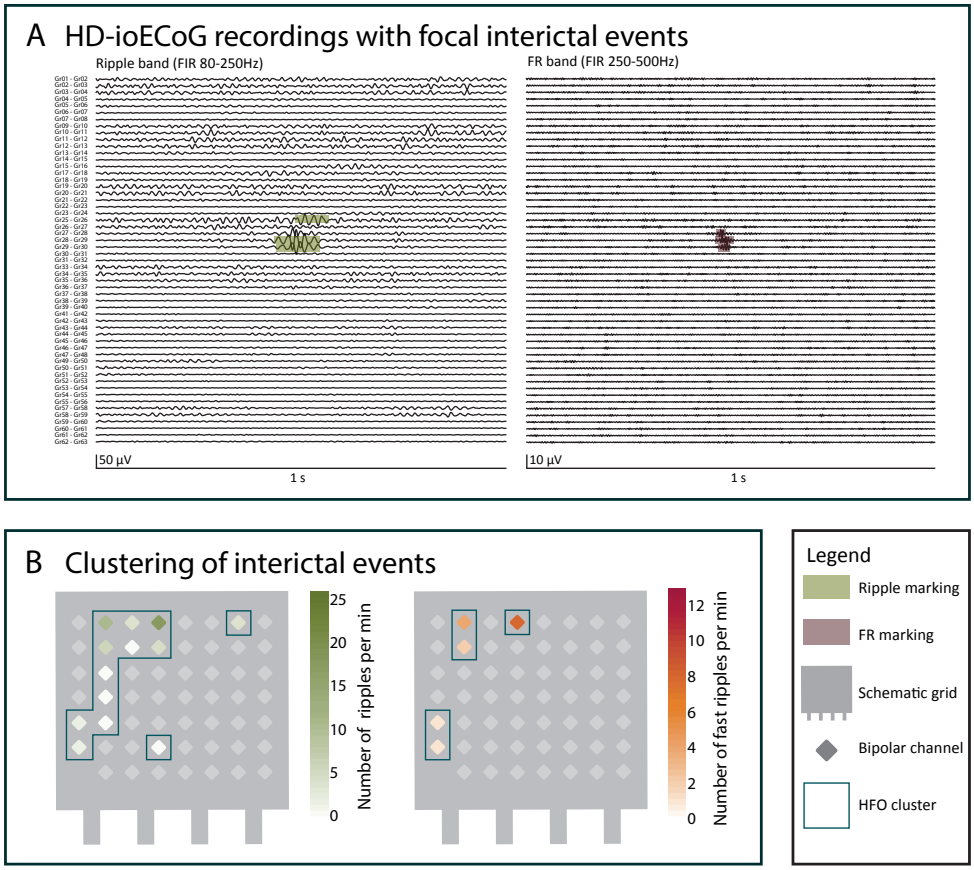


Figure 2: Two patient examples demonstrating highly localized events. A. Focality of interictal events. A patient example (pat nr. 6) showing one-second HD-ioECoG data in the ripple band (FIR 80-250Hz) and the FR band (FIR 250-500Hz). Note the simultaneous ripples on two neighboring bipolar channels and the FRs on three bipolar channels. These HFOs might have been missed without HD recordings, since HD recordings have four times more electrodes (Figure 1C). B. Clustering of interictal events. HD grid configuration (pat nr. 9), showing bipolar channels. Clusters are outlined with a dark blue line. In this patient, there are three ripple clusters: one cluster contained 10 channels with ripples and two clusters contained one channel with ripples, and three FR clusters: two clusters contained 2 channels with FR and one cluster contained one channel with FR. These HFOs might have been missed without HD recordings, since HD recordings have four times more electrodes (Figure 1C). Abbreviations: FIR = finite impulse response, FR = fast ripple, HFO = high frequency oscillation, µV = microvolt.

Interictal spike onset localization

We analyzed spike propagation patterns in 18 HD grid positions of 9 patients with Granger's causality (Figure 3). The onset spike was located in the resected area in 6 patients (4 were seizure free and 2 had recurrent seizures). The onset spike was located outside the resected area in 3 patients (2 were seizure free and 1 had recurrent seizures). Comparing HD onset spike to simulated LD onset spike, the location differed >0.5 cm in 42 out of 72 LD configurations. Thus, 58.3% of the spike onset locations might be located differently with standard LD grids.

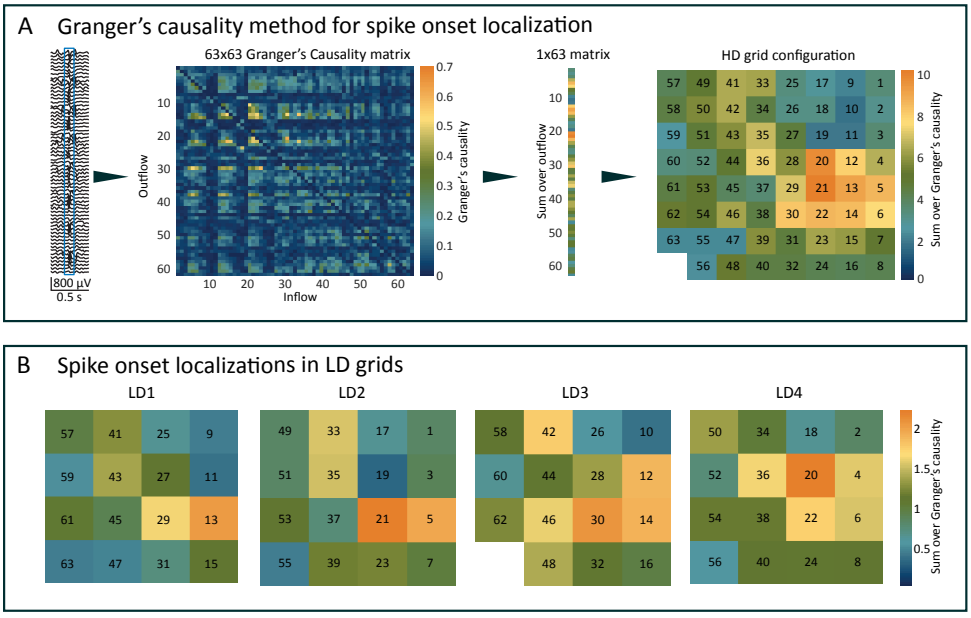


Figure 3: Spike onset localization with Granger's causality. A. Spike onset localization with Granger's causality is based on a tree step approach; Based on 63 HD-ioECoG channels with signal - channel 64 was used as a reference - (left-to-right panel 1), as a first step a 63x63 matrix was calculated (left-to-right panel 2) . In the second step the sum over the outflow of the Granger's causality matrix was taken. This outflow represents propagation, since it shows the causalities of one channel to all other channels. This resulted in a 1x63 matrix (left-to-right panel 3). In the final step this 1x63 matrix was transformed back into the 8x8 HD grid configuration to display spike propagation. The spike onset channel was defined as the channel with highest outflow (left-to-right panel 4). In this patient (pat nr. 4; see intraoperative photos in Figure 1A) the spike onset is located on grid 21. B. Spike onset localization calculated for the 4 LD grid configurations (Figure 1C). Note that due to the reduced resolution the spike onset location differs for the LD grid configurations, albeit they are all located within 0.5cm of the spike onset in the HD grid configuration.
Abbreviations: HD = high-density, LD = low-density, µV = microvolt, s = seconds.

Discussion

We investigated the potential added value of HD-ioECoG within the clinical context of epilepsy surgery. We assessed the ability of HD-ioECoG to record highly localized epileptic events and to contribute to the surgical plan. Our findings indicated that HD-ioECoG provided confirmation or adaption of the resection plan in 17 out of 20 patients (85%). Epileptic events, including FRs, were detected in the majority of patients. FRs were more present over the resected area, especially in people who were seizure free after surgery. Post-hoc analyses on the focality and spatial clustering of epileptic events revealed that a substantial number of highly localized events could potentially be missed with standard LD grids recordings. HD grid recordings can differentiate between onset spikes and propagated spikes, while our simulated LD grids would mislocate the onset spike in more than 50% of the cases.

We conducted HD-ioECoG recordings in 20 patients, with 17 patients (85%) showing FR. We did not record with LD grids in the same 20 patients. Based on our simulations, we argue that 46.7% of focal and semi-focal FRs and 56.0%-62.1% of localized FR-clusters may go undetected by LD grids. We compared our findings with the previous studies from our group using LD grids. In those studies, the electrode contact surface of LD and HD grids is the same (4.2 mm^2). Straumann et al.[40], who excluded mesiotemporal recordings in accordance with our exclusion criteria, found FR in 13 out of 33 patients (39.4%). Van 't Klooster et al.[34], who included 54 patients of whom 8 underwent mesiotemporal recordings, identified FR in 38 patients (70.7%). After excluding eight patients with mesiotemporal recordings from that study, 31 out of 46 patients (67.4%) showed FR. This suggests that HD-ioECoG recordings facilitate FR detection in a larger proportion of patients than LD recordings (increase of 17.5 - 45.6%). Our finding is in agreement with Boran et al. [13] which showed that increasing the electrode density of HD-ioECoG brings the electrodes closer to the FR generator and improves the probability of measuring the maximal intensity of FRs. HFO generators, particularly those responsible for FR, are characterized by their small size and high spatial signal attenuation.[101,220] Studies in rats have shown that FR generating areas do not exceed 1 mm^2.[221] Also in humans, recording techniques with high spatial density are crucial for capturing FR. This may suggest that optimal detection of FRs may require even higher-resolution grids. However, increasing grid resolution has associated limitations. To achieve similar cortical coverage with higher resolution, a larger number of electrodes is necessary, which complicates real-time interpretation of ioECoG during surgery. Reducing grid size to limit channels would increase recording time as different grid positions are needed to record whole area of interest. Our results showed that HD-ioECoG with a 5 mm interelectrode distance effectively records highly localized HFOs in most patients, while maintaining readablity in real-time.

FR were recorded more frequently in the resected area compared to the non-resected area in people who were seizure free after surgery, suggesting that presence of FR is indicative of seizure generating tissue. This association was not found in people with seizure recurrence. Even though we found a difference between FR in the resected and non-resected tissue, the effect size was limited. This limits the potential clinical impact. ioECoG recordings may not always measure HFOs, even if with a high density configuration. This may be due to types of pathologies or epileptic tissue in the depth. Recording with flexible electrode grids or adding depth electrodes to the surface recordings may improve the clinical value and needs further investigation.

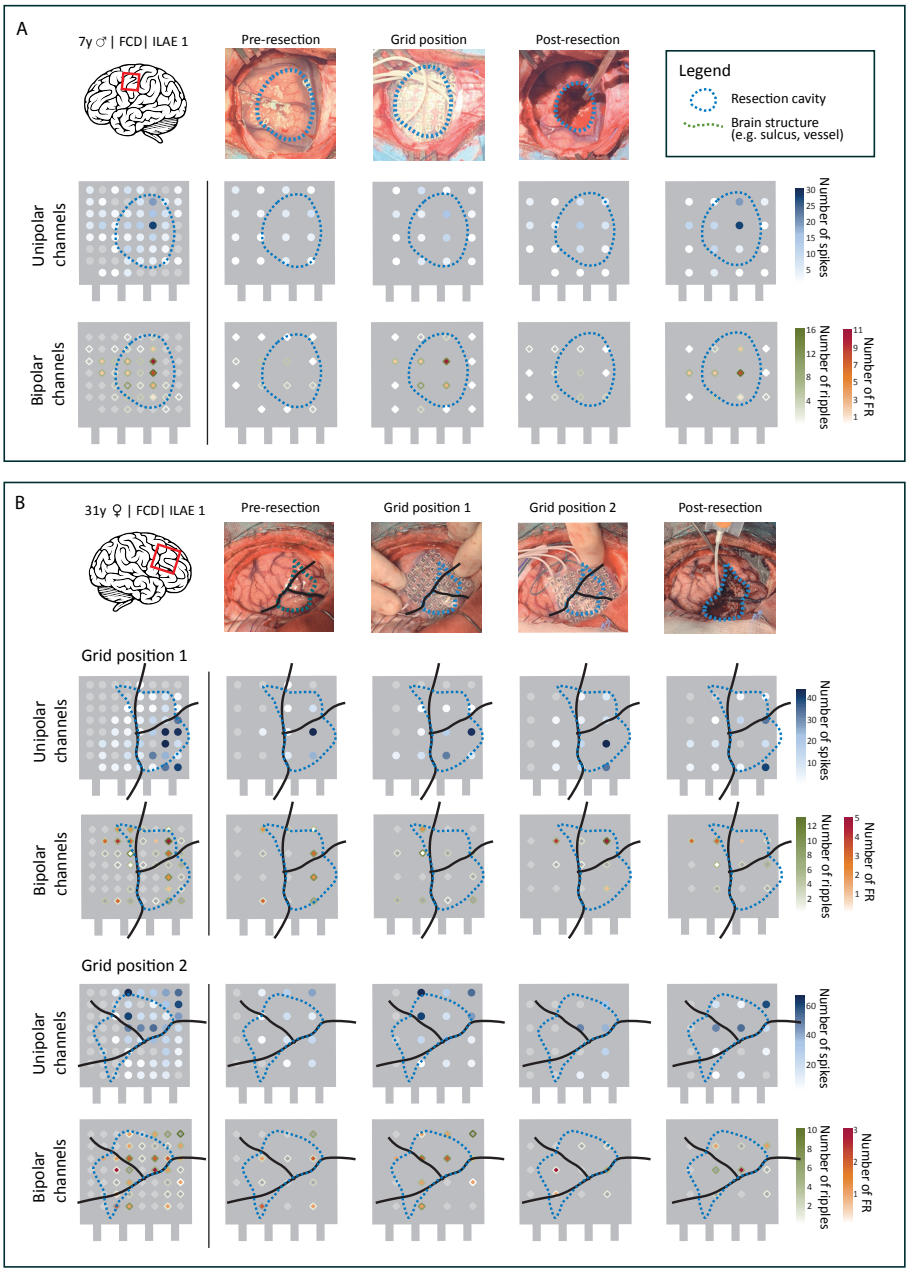


Figure 4: Two patient examples demonstrating the clinical benefits of performing HD-ioECoG to tailor epilepsy surgery. A. This patient example (pat nr. 17) demonstrates the ability of HD-ioECoG to record highly localized events. In contrast, if an LD grid had been used there would have been a high chance of missing these highly localized events, in particular ripples and FR. B. This patient example (pat nr. 10) demonstrates that the presence of anatomical brain structures (e.g. deep sulci, large blood vessels) impacts the amount of events that can be captured in the recorded signal. If these recordings would have been made with an LD grid, there is a high chance of putting only a few electrodes on top of these brain structures and thereby missing out on capturing interictal events of clinical importance. This emphasizes the importance of high resolution recordings for tailoring purposes in epilepsy surgery.
Abbreviations: FCD = focal cortical dysplasia; FR = fast ripple; y = year.

The specificity of spikes for the epileptic tissue and therefore the use of ioECoG has been debated.[32,222,223] Interictal spikes often extent beyond the epileptogenic tissue and are seen in multiple contacts due to rapid propagation, which limits its sensitivity for delineating epileptogenic tissue. Onset spikes are suggested to be more accurate predictors for epileptogenic tissue compared to interictal spikes alone but their specificity is not 100%.[214] Onset spikes in the non-resected area of seizure free patients in our study suggest low specificity but the numbers are too little to draw conclusions. Literature highlights the importance of intracranial recording of HFOs and spikes for seizure outcome. The resection of FR generating areas and overlapping spikes and ripple onset areas have been shown to be associated with favorable seizure outcome.[28,35] ioECoG-assisted surgery based on interictal spikes may be associated with extended resection beyond the true epileptogenic zone. That is why in clinical practice the ioECoG spikes should always be reviewed with the actual extension of the lesion, MRI, tissue appearance, and the expected pathology taken into consideration.

This study evaluated the clinical implementation of HD-ioECoG to tailor epilepsy surgery. Implementing HD-ioECoG in a clinical setting presents some challenges. First, epileptologists in our center are accustomed to perform real-time visual ioECoG analysis on 16-20 electrodes, whereas HD grids incorporate 64 electrodes. To assist epileptologists in the adjustment, we created different LD configurations (Figure 1C), that could be used real-time. We observed that after a learning curve of approximately one year, after approximately 15 HD-ioECoG recordings, our epileptologists began to prefer HD-ioECoG over standard LD recordings. Second, a neurosurgical challenge is the stiffness of the HD grid. The HD-grid's electrode characteristics were similar to those of standard LD-grids (both manufactured by AD-tech), with comparable diameter and contact surface. Therefore, we expect the signal-to-noise ratio (SNR) in the fast ripple band to be in line with previous literature. [224] However, these HD grids are made with a thicker silicon layer than that of LD grids, which might result in reduced pliability over the cortex, potentially introducing more noise. Recent studies have shown that flexible strips, such as the WISE Cortical Strip WCS® using novel thin-film technology, significantly improve SNR. These flexible strips, incorporating platinum nanoparticles in a polymer base, enhance the detection of small amplitude FR events.[224-226] The gains used in this HD study are similar to those used in our previous LD studies.[14,34,40] We observed no visually perceivable differences in the amplitudes of spikes, ripples, and fast ripples between the HD and earlier LD recordings. A direct comparison is difficult, as different amplifiers were used. We hypothesize that the choice of montage used for marking epileptic activity – different for spikes and HFOs in current study – may have a greater impact on observed amplitude differences than the grid itself. This will be subject of a future study. Third, these HD grids have limited transparency, which can impede the recognition of the cortical surface.

A unexpected advantage of using HD grids in clinical practice is the ability to rapidly recognize both epileptic and normal patterns, such as ictiform spike patterns and burst-suppression, because of the increased number of channels provided by HD grids compared to LD grids. We hypothesized that HD grids enhance the recording of focal phenomena, including highly localized interictal events and electrographic seizures detected on a limited number of electrodes. We did not record electrographic seizures, but we found highly localized interictal spikes and HFOs, especially FR, that could otherwise be missed. Another interesting finding is that, in some cases, the pattern of event clusters aligns with the distribution of

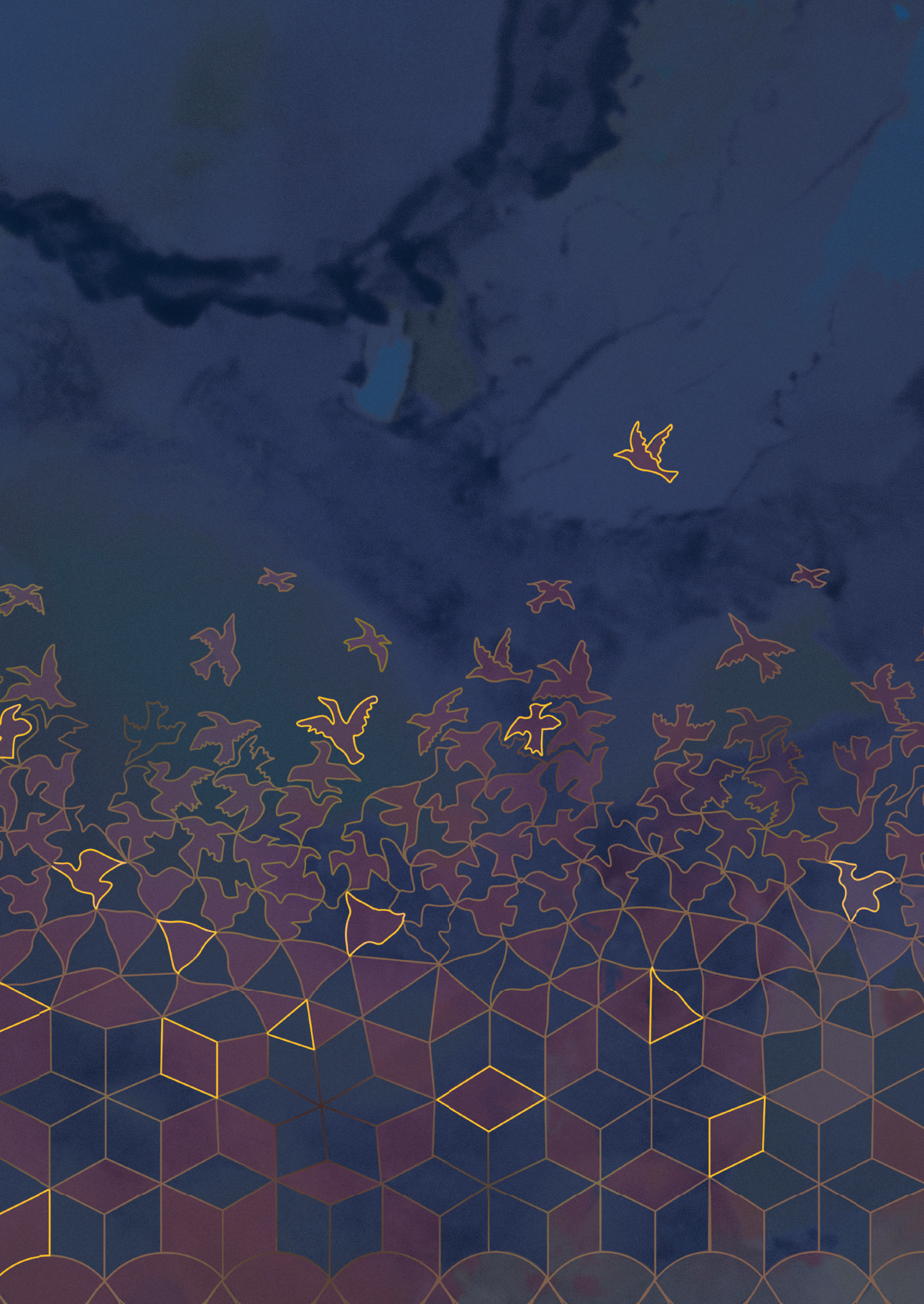
the anatomical gyrus-sulcus pattern, with events recorded only on the gyrus but not on the sulcus of the brain. (Figure 4B)

A limitation of our study is the absence of LD-ioECoG recordings in the same patients, which prevents a direct comparison between HD and LD recordings. We attempted to design our data analysis to draw conclusions as if LD recordings were available for the same patients. We reconstructed four simulated LD grid configurations of the electrode positions of the HD grid. (Figure 1C) Our reconstruction closely resembles 'real' LD grid recordings since it maintains the same characteristics of LD grid in terms of electrode size and inter-electrode distance. We analyzed epochs of one minute, while it is known from long-term invasive EEG that recordings of at least 5 minutes are needed to recognize a somewhat stable pattern[227] and that sleep and diurnal rhythms affect HFO occurrence[228]. Another limitation is the lack of long-term follow-up, which may restrict the conclusions we can draw regarding patient outcomes. Additionally, the patient population in our study is small and heterogeneous, with varying underlying pathologies. Despite that, this diverse sample demonstrates the potential applicability of HD-ioECoG across different cases.

Future recommendations and conclusion

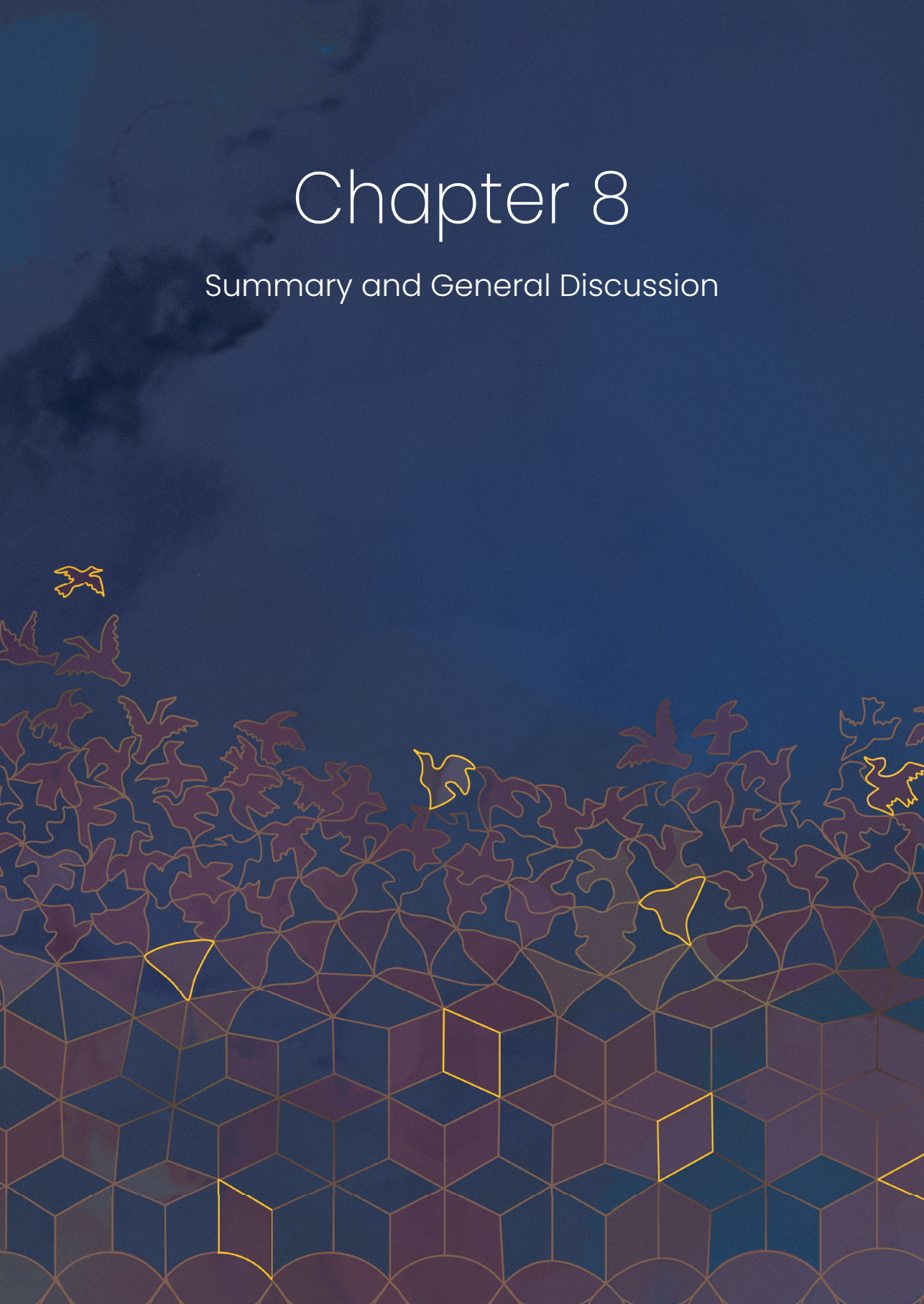
Future work should investigate using HFOs for clinical decision making and elaborate on pathology-specific signal characteristics. The development of flexible HD grids is currently ongoing.[212] Clinical implementation of these new grids should be evaluated, but these flexible grids are able to overcome some of the current clinical challenges. Grid designs should focus on enabling recording on different brain structures (gyri and sulci anatomy), and the possibility to record (partially) under the skull. Such grid may improve the signal-to-noise ratio, especially when the recording is facilitated by low-noise amplifier. Less noise facilitates fully automated HFO detection.[180] In addition, EEG software needs adaptation towards facilitating review of large numbers of channels, regardless of the montage of choice.

In conclusion, we provide strong indications that HD recordings can provide added value in clinical settings. Specifically, HD-ioECoG is able to 1) record highly localized interictal events, 2) identify FR in a larger number of patients compared to LD-ioECoG while ensuring they remain specific to the resected area in those who achieve seizure freedom, 3) record FR specifically over the resected area in people who are seizure free, and 4) characterize spike propagation and spike onset area.



Chapter 8

Summary and General Discussion



Summary

Approximately 50 million people worldwide have epilepsy. Epilepsy is caused by a disturbance of electrical activity in the brain, which can cause seizures. For a proportion of people with epilepsy, medication does not provide sufficient seizure control. For these patients, epilepsy surgery can be a potentially curative treatment. The goal of epilepsy surgery is to achieve lifelong seizure freedom. Currently, the reported proportion of patients who become seizure free after surgery ranges between 36 and 76%, indicating that there is room for improvement.

In epilepsy surgery, it is essential to completely remove the epileptogenic zone: the brain region responsible for seizure generation. Accurately localizing this zone is challenging and is performed prior to surgery using various diagnostic investigations, such as EEG, MRI, and sometimes additional advanced imaging techniques. Based on these investigations, a surgical plan is formulated. During surgery, this plan can be evaluated and, if necessary, adjusted using intraoperative electrocorticography (ioECoG), in which brain activity is recorded directly from the cortical surface. These signals are assessed in real time during surgery. Traditionally, attention is focused on two types of abnormal signals, referred to as biomarkers: interictal spikes and high-frequency oscillations (HFOs). Interictal spikes are brief, sudden discharges of neuronal activity that indicate increased excitability of brain tissue. HFOs are very fast rhythmic oscillations at high frequencies (above 80Hz), which can be subdivided into ripples (80-250Hz) and fast ripples (250-500Hz). Nevertheless, there is ongoing debate regarding the use and clinical relevance of spikes and HFOs. This debate concerns both which biomarker is most informative for different patient groups and practical questions related to how these signals should be recorded and interpreted.

This thesis investigates the potential of ioECoG beyond traditional visual assessment and aims to contribute to a more accurate, efficient, and automated delineation of the epileptogenic zone. The work focuses on two complementary themes: advanced signal analysis of ioECoG and the interpretation of ioECoG, including the clinical implementation of high-resolution grids.

In **Chapter 2**, we investigated the temporal relationship between interictal spikes and HFOs when they occur simultaneously. By studying only patients who became seizure free after surgery, the resected tissue could be considered representative of the tissue responsible for seizure generation. We found that concurrently occurring interictal spikes and ripples were more frequently present in resected, epileptic tissue. In addition, subtle temporal features of these signals, such as their timing relative to one another, were found to provide information about which brain tissue was epileptic.

In **Chapter 3** and **Chapter 4**, we examined whether specific signal characteristics of the ioECoG could support in identifying epileptic tissue. In **Chapter 3** we investigated whether variability in the complexity of the ioECoG signal, calculated as spectral entropy, was associated with surgical outcome. We found that this measure contains information both for distinguishing epileptic from healthy tissue and for estimating the likelihood of postoperative seizure freedom. In **Chapter 4**, artificial intelligence was used to investigate which frequency components of the ioECoG contribute to distinguishing epileptic from non-epileptic tissue. We found that certain changes in background activity, which are not readily visible to the naked eye, can nonetheless be informative. Whereas **Chapter 2** and

Chapter 4 focused on ioECoG recordings obtained prior to resection and included only patients who were seizure free, **Chapter 3** included ioECoG recordings acquired both before and after resection in patients with favorable as well as unfavorable surgical outcomes.

In **Chapter 5**, we investigated whether the way ioECoG signals are displayed influences the detection of interictal spikes and HFOs. We compared different visual representations of the same ioECoG recordings and assessed how well the various biomarkers could be identified. We found that the choice of montage has a major impact on what is observed, and that certain montages are more suitable than others for detecting specific biomarkers. This highlights that the interpretation of ioECoG depends not only on the signal itself, but also on how it is presented.

In **Chapter 6**, we examined the relationship between the location of abnormalities visible on MRI and the location of biomarkers detected with ioECoG. We found that this relationship differs depending on the underlying pathology, emphasizing the importance of a personalized interpretation of ioECoG. In **Chapter 7**, we describe the clinical implementation of high-resolution grids for ioECoG recordings. These grids contain four times as many electrodes as conventional low-resolution grids. Their use allows for the detection of a greater number of biomarkers, particularly fast ripples, and enables detailed visualization of the spatial spread of interictal spikes.

The results of this thesis demonstrate that ioECoG can provide valuable information during epilepsy surgery, but that no single biomarker or method is sufficient on its own to reliably identify epileptic tissue. The significance of interictal spikes, HFOs, and more subtle signal characteristics varies between patients and underlying pathologies. In addition, the interpretation of ioECoG is influenced by technical choices, such as recording and display methods, as well as by practical factors in the operating room. By combining advanced signal analysis with clinical expertise and by carefully implementing new recording techniques, such as high-resolution grids, ioECoG can evolve into a more objective and reproducible tool. These developments offer perspective for further improving epilepsy surgery, with the ultimate goal of increasing the likelihood of seizure freedom.

General discussion

The studies in this thesis investigated whether intraoperative electrocorticography (ioECoG), when supported by advanced analytical methods, can make a meaningful contribution to epilepsy surgery. These methods aim to overcome limitations of conventional visual inspection, reduce human bias, and enable more objective and reproducible decision-making. Specifically, I evaluated the potential of novel signal processing measures such as machine learning, spectral entropy, and explored the potential of high-density ioECoG.

This general discussion synthesizes the findings across this thesis and reflects on their methodological challenges, and their clinical impact in current and future clinical practice. To illustrate these issues, the discussion follows the path of a patient's epilepsy surgery journey: from presurgical evaluation throughout the surgery, and the postoperative follow-up.

Pre-surgical: from diagnosis to defined surgical plan

The ultimate aim of presurgical evaluation is to identify the epileptogenic zone (EZ) while safeguarding eloquent cortex. Standard assessment always includes high-resolution MRI, scalp EEG, and may include MEG, PET, SPECT, and neuropsychological testing depending on the individual patient case. Each test contributes unique information but remains incomplete in isolation: subtle focal cortical dysplasias (FCDs) may be visible or have indistinct margins on MRI, and functional modalities can be suggestive but non-specific unless interpreted alongside structural and electrophysiological information.[155,229] Presurgical evaluation is therefore best understood as an iterative process of hypothesis formulation and testing, in which successive investigations progressively refine a working model of the EZ.[6,230]

Crucially, assumptions and findings established during the presurgical evaluation shape the entire downstream process. The surgical team enters the operating room with a presurgical hypothesis about the EZ: typically anchored in the MRI-assumed pathology and its expected electrographic signatures. All intraoperative findings, both structural and electrophysiological, are then evaluated through that lens: which information is obtained, and how this information is processed and taken into clinical decision making. For the neurosurgeon, it may concern the tissue density he is inspecting and for the electrophysiological part, the hypothesis influences the sampled cortex and the interpretation of the signals. This underscores the importance of a well-established presurgical hypothesis about the EZ.

Although all signal analyses (Chapter 2-4) in this thesis were performed retrospectively with respect to histopathology-confirmed pathology, the ioECoG recordings themselves were guided by the presurgical hypothesis formulated for each patient. Electrode placement, sampling strategy, and analytic focus were all determined by this working model of the epileptogenic zone. Consequently, every ioECoG dataset reflects not only underlying pathology but also the assumptions embedded in the presurgical plan. The subsequent analyses used histopathological findings as the objective benchmark for validating the electrophysiological observations and for interpreting the patterns observed across pathologies (Chapters 2-4 and 6). This approach underscores that while histopathology provides the definitive ground truth, the data collected intraoperatively are fundamentally shaped by the hypothesis defined before surgery.[14,64,211]

In our HD-ioECoG cohort (Chapter 7), the presurgical hypothesis functioned as a dynamic, testable model during surgery: dense coverage was planned to assess whether epileptiform activity was confined to the MRI-defined lesion or extended into adjacent cortex, explicitly linking intraoperative findings to presurgical hypotheses. In this cohort, 11 out of 20 patients (55%) had intraoperative results that confirmed or adapted the presurgical plan, and 6 out of 20 patients (30%) required a substantive modification of the hypothesis, indicating that surgical strategy evolves through continuous feedback between preoperative reasoning and intraoperative evidence. While these observations derive from the HD setting studied, the broader implication is that the value of ioECoG – high-density or conventional – depends on a clear, testable presurgical hypothesis that guides electrode placement, focuses analysis, and enables meaningful interpretation of ioECoG signals.

Noninvasive clinical and neuroimaging data provide the foundation for formulating the presurgical hypothesis, offering early evidence that guides both patient selection and the decision to proceed with invasive evaluation. By assessing how clinical features, scalp EEG, and MRI findings converge on a single localization, these data help estimate the likelihood of seizure freedom and inform surgical planning. Favorable patterns such as unilateral interictal discharges and concordant localization across modalities are associated with better outcomes, whereas diffuse or bilateral ictal activity and focal-to-bilateral tonic-clonic seizures predict poorer results.[231,232] The presence of a structural lesion on MRI remains one of the strongest independent predictors of postoperative seizure freedom, while MRI-negative cases consistently show lower odds of achieving Engel I outcome.[233] Advances in computational analysis have further expanded the interpretive power of presurgical data. Machine learning models applied to short peri-ictal scalp EEG recordings have demonstrated the ability to predict postsurgical seizure outcomes with reasonable accuracy, suggesting that automated analyses could support clinical decision-making and reduce reliance on subjective interpretation.[234,235] Similarly, automated volumetric MRI analysis improves outcome prediction, with quantitative measures of hippocampal and extrahippocampal atrophy enhancing the ability of clinical models to distinguish patients who will or will not achieve seizure freedom after temporal lobe resection.[236] These developments indicate that even subtle, non-visually appreciable patterns in scalp EEG and MRI carry prognostic information that can be uncovered through computational pipelines. By integrating such approaches into presurgical evaluation, surgical teams could better identify patients most likely to benefit from resection and identify potential poor candidates. Additionally, they could provide clearer, individualized counseling about benefits and risks of the surgery. In turn, this may reduce long-term dependence on pharmacotherapy and improve overall outcomes and quality of life.

The surgery: from data to decisions

Intraoperative decision-making represents the critical translation of the presurgical hypothesis into surgical action. Once the cranium is opened and the cortex exposed, the surgeon and electrophysiologist must reconcile preoperative expectations with real-time physiological evidence. The goal is to confirm, refine, or adapt the presurgical hypothesis of the EZ based on ioECoG, neuronavigation, and – if applicable – functional mapping. In this phase, the earlier hypothesis determines how new data will be interpreted: a clear presurgical framework allows the team to recognize concordance, identify discrepancies, and decide whether adjustments

in resection strategy are warranted. Thus, intraoperative decision-making is not the beginning of exploration, but the verification and refinement of the presurgical hypothesis in real time.

Intraoperative navigation: from inertia to integration

Despite major advances in imaging and electrophysiology, intraoperative workflows still suffer from a certain inertia: ioECoG remains largely unaligned with real-time imaging data. In current practice, the navigation system is initialized using preoperative MRI, and once the skull is opened, this alignment rapidly deteriorates as brain shift occurs. Brain shift – caused by cerebrospinal fluid drainage, gravity, and tissue deformation - violates the rigid-body assumption of navigation systems and introduces spatial errors. Reviews of neurosurgical navigation report that displacements of several millimeters are common, and can accumulate during resection, reducing the reliability of targeting.[237,238] To mitigate this, intraoperative imaging modalities could be used to update the navigation framework. Among these, intraoperative ultrasound is a practical and increasingly popular solution: when co-registered, it provides real-time anatomical feedback, can detect residual pathology, and helps compensate for local deformation without the logistical constraints of intraoperative MRI. A high concordance can be reached between intraoperative ultrasound estimates of extent of resection and postoperative MRI.[239] However, even with intraoperative ultrasound updates, residual misregistration remains a challenge. Computational compensation models, such as finite-element simulations or data-driven deformation fields, offer a potential solution by predicting and correcting for brain shift within the navigation framework. Validation studies show that these approaches can reduce navigation error by several millimeters compared with uncorrected systems, and in some cases approach the accuracy of intraoperative imaging updates.[240-243]

This spatial uncertainty also affects the retrospective interpretation of intraoperative data, as electrode positions and resection margins may deviate from their preoperative references. In the studies presented in this thesis, this limitation was minimized through the use of intraoperative photographs taken at each surgical step, allowing precise documentation of electrode placement and resection boundaries. Electrode positions in pre-resection recordings, which formed the basis of analyses across all studies (Chapters 2-7), could be accurately localized relative to the pre-resection cortex. In contrast, post-resection recordings (Chapters 3 and 5) were more strongly affected by brain shift, as local deformation and cavity collapse introduced greater positional uncertainty. To address this, pre- and post-resection photographs were compared using anatomical landmarks, and electrode positions were linked to the post-resection photograph of the resection cavity, providing a consistent spatial reference for signal interpretation. Although navigation updates and computational corrections can substantially improve spatial fidelity, they are not yet part of standard clinical care. For now, reliable interpretation of ioECoG and other intraoperative data still depends on meticulous manual alignment between electrophysiology and anatomy, underscoring the need for improved integration between navigation, imaging, and signal analysis pipelines.

Electrode choice: from low-density to high-density

In standard clinical practice, ioECoG typically employs subdural strip or grid electrodes with relatively wide inter-electrode spacing 10 mm (low-density). These macroelectrode grids provide only coarse spatial resolution, which means

that epileptiform activity arising in areas between electrodes may be missed unless multiple recordings are performed. This requires prolonged anesthesia and additional surgical time. The choice of the spatial resolution also depends on the biomarker of interest: while interictal spikes can be detected reliably with standard grids, high-frequency oscillations (HFOs) often originate from smaller cortical domains and may therefore be undersampled.[12,13,244] HFO-rich regions have been shown to correlate more closely with the epileptogenic zone and surgical outcome than spike activity, emphasizing the need for higher spatial sampling when HFOs are used as intraoperative biomarkers.[217,244]

High-density ioECoG (HD-ioECoG) offers a substantial improvement in spatial sampling and can reveal epileptiform activity that would otherwise remain undetected. (Chapter 7) Denser electrode spacing improves the detection of fast ripples compared to standard grids.[13] . Similarly, microseizures – highly localized discharges invisible to conventional grids – can be recorded with HD micro-ECoG arrays during intraoperative monitoring.[218] These findings suggest that conventional grids may underestimate the true extent of the epileptogenic zone, especially in pathologies such as FCD.

Advances in material science have also enabled the development of thin, flexible HD arrays with very fine electrode spacing.[245,246] While such devices are technically promising, their value in clinical practice still needs to be demonstrated. Early clinical studies will have to show whether these flexible grids are both workable in the intraoperative setting and add meaningful diagnostic value. A first clinical study addressing this question is currently performed at the UMC Utrecht. Challenges such as mechanical fragility, sterility, and seamless integration into existing surgical workflows must be carefully addressed before these devices can be widely adopted.

Increasing electrode density and the number of electrodes brings practical challenges. In real-time intraoperative interpretation, too many channels can overwhelm the display: while 64-electrode grids remain manageable, 128-electrode grids often exceed what can be visualized effectively on a single screen, complicating the detection of spikes and HFOs. Higher channel counts also demand faster data acquisition and more robust automated analysis pipelines to extract meaningful information under time pressure. Furthermore, clinical evidence suggests that increasing electrode density yields measurable benefit: in intracranial EEG settings, higher densities have been linked to improved localization and diagnostic performance.[247]

Spikes and HFOs: from competition to complementary

The discussion about whether interictal spikes or HFOs serve as the better indicator of epileptogenic tissue is shifting from competition to complementarity. HFOs, particularly fast ripples, are spatially confined and closely linked to the epileptogenic cortex, whereas spikes reflect more distributed network excitability but remain robustly detectable even under intraoperative conditions. [12,244] Rather than representing distinct or competing biomarkers, spikes and HFOs capture different aspects of the same pathological process. Their co-occurrence reflects multi-scale neuronal activity, combining the macroscopic population discharges seen as spikes with the localized micro-synchrony reflected in HFOs. [50,248,249] These joint events consistently outperform isolated spikes or HFOs in delineating the epileptogenic zone and predicting surgical outcome. [250] Spikes co-occurring

with ripples were more specific for epileptogenic tissue than spikes without a co-occurring ripple in patients with FCD pathology (Chapter 2), underscoring that low- and high-frequency dynamics convey complementary pathological information. While resection of fast ripples correlates strongly with surgical success[33,251], co-occurring spikes and ripples remain detectable in nearly all patients and retain high predictive value even when fast ripples are absent.[250] (Chapter 2) Collectively, these findings emphasize that spikes and HFOs should not be interpreted in isolation but as interacting features of the same pathological network, where their co-occurrence offers the most reliable guide for surgical decision-making.

Interictal spikes and HFOs express differently across different epileptogenic pathologies, mirroring cortical architecture and network excitability. In FCD, particularly type II, spikes and HFOs cluster at the lesion margin. (Chapter 3) Both spikes and HFOs are more common in FCD type II than FCD type I.[39,200] Especially in FCD type II, continuous spike patterns are common.[38] In tumor-related epilepsy, both tumor and peritumoral cortex can generate interictal activity, but the strongest, most consistent spikes and HFOs typically lie at the tumor interface where gliosis and reorganization drive hyperexcitability.[89,252,253] In hippocampal sclerosis, spikes are dense and HFOs show region-specific clustering within mesiotemporal structures, aligning with classic hippocampal ripple and fast-ripple physiology in human epilepsy.[254] Cavernoma-related epilepsy is usually dominated by perilesional spikes, with HFOs occurring less consistently – though they can be present and clinically informative in individual cases – underscoring heterogeneity in HFO propensity across lesions.[255] Taken together, these interictal patterns argue for a pathology-aware interpretation of ioECoG in which the diagnostic weight of spikes, ripples, fast ripples, and their co-occurrence is adapted to lesion type and spatial context. We should move beyond single-feature heuristics toward signal fingerprints that may even predict pathology from interictal ioECoG patterns. (Chapter 2) Recent sEEG work supports this direction by showing that combined features of HFOs, spikes, and connectivity carry pathology-specific signatures.[61]

Recording challenges: from noise to knowledge

Intraoperative recordings are shaped by several methodological variables, and each choice can propagate into how the signal looks and thus how it is interpreted.

Filtering, sampling, and anti-aliasing

Noise can present itself in many forms, physiological background activity, interference with other surgical equipment, or artifacts introduced by the recording system. High-pass and band-pass settings can create spurious oscillations: sharp transients and non-sinusoidal waveforms may generate false ripples after filtering.[256] Sampling rate and anti-aliasing filter placement strongly influence automated HFO detection sensitivity and feature distributions; lower sampling may miss fast activity or distort event morphology, while aggressive anti-aliasing can attenuate true high-frequency content. To ensure that detected events truly reflect underlying neuronal activity rather than filter or sampling artifacts, centers must predefine and transparently report their acquisition parameters – including sampling rate, analog and digital filter characteristics, and detector settings – so that HFO metrics remain physiologically interpretable and comparable across studies.[257]

Influence of anesthesia
Different anesthetic agents influence ioECoG. Propofol tends to suppress HFOs more strongly than spikes, which may lead to underestimation of HFO-based markers when recordings are obtained under deep anesthesia.[44,57] Importantly, propofol can be safely paused for short periods.[107] Sevoflurane also affects both spikes and HFOs, though in a different manner, and can alter their rates and distribution.[258] Beyond these frequency-specific effects, anesthesia in general reduces overall cortical excitability, can introduce state-dependent variability in signal amplitude, and may increase background slowing. Together, these factors highlight the need to carefully consider anesthetic regimen and timing when interpreting ioECoG. A balance is required: recordings should be long enough to capture sufficient epileptic activity, but not so long that the pause in anesthesia and extended surgical time increase the risk of complications such as infections.

Montage and referencing
Bipolar derivations typically yield more channels with spikes and ripples and higher amplitudes than average-referenced signals; conversely, average reference can provide a faster overview but may dampen focal events and smear high-frequency content. Even when overall biomarker outcome associations appear robust across montages, patient-level decisions can shift with montage choice. Hence, there is a need to document and standardize the reference used for intraoperative decision-making. (Chapter 5)

Signal interpretation: from visual inspection to advanced signal analysis

Traditionally, ioECoG is analyzed visually by neurophysiologists. However, visual identification of spikes and HFOs is subjective, time-consuming, and inconsistent. Interrater variability is high, and under OR time pressure, subtle findings may be missed.[259,260] Automated detection algorithms offer a promising alternative by providing objective, reproducible, and real-time analysis.[47,261] Unfortunately, these algorithms have not been proven in multicenter studies and there is a lack of implementation in the clinical acquisitions systems.

Recent advances in signal analysis have moved beyond the counting of spikes or HFOs toward quantifying their morphology, frequency composition, and temporal coupling. By incorporating measures such as entropy (Chapter 3) , spike-ripple co-occurrence (Chapter 2), and spectral gradients (Chapter 4), we show that ioECoG has way more information in it that can be captured by just interictal spikes and HFOs. Quantitative characterization of patterns that involve both low- and high-frequency patterns in the signal enables objective and reproducible markers of epileptogenic tissue. Much of the progress in advanced signal analysis has so far been achieved in stereo EEG-recordings, where long, high-quality datasets allow for offline exploration of complex features. Translating these approaches to ioECoG is the next challenge. It requires the algorithms to give the same results, but also computationally efficient and robust to noise, anesthesia effects, and limited recording time. Real-time feasibility is essential: the clinical value of advanced analytics depends on delivering interpretable results within the surgical workflow, where decisions must be made within minutes rather than hours. Recent frameworks for real-time HFO detection have demonstrated proof-of-concept implementations capable of identifying epileptogenic tissue during ongoing recordings.[262] Meanwhile, the rapid wild grow of research involved in advanced signal analyses underscores the need for harmonized frameworks – like

BIDS structured databases[42] –, shared datasets, and standardized reporting, so that methods can transition from exploratory innovation to reliable clinical tools. Ultimately, real progress will come from uniting these computational pipelines with real-time anatomical imaging such as intraoperative navigation, enabling multimodal integration of structural and electrophysiological data in surgical decision-making.

Stop resecting: from experience to evidence

Determining when to stop resection remains one of the most challenging intraoperative judgments in epilepsy surgery. Traditionally, this decision has relied heavily on surgical and electrophysiological experience: a delicate balance between removing enough tissue to achieve seizure freedom and preserving eloquent cortex to prevent lasting deficits. Too little, and seizures may persist; too much, and postoperative impairments may follow. ioECoG offers a physiological compass, indicating whether residual epileptiform activity remains at the resection margin. Yet despite decades of use, there are no evidence-based thresholds defining how much residual spiking or HFO activity can be safely left behind.

Evidence increasingly suggests that complete removal of HFO-generating cortex correlates with improved seizure outcome. Patients in whom HFO-rich areas were fully resected achieved seizure freedom significantly more often than those with residual HFOs.[27,154,177,180] Residual spikes have been inconsistently linked to poorer outcomes, underscoring the variability of spike significance across pathologies and surgical settings.[115] The lack of standardized cut-offs reflects both technical heterogeneity and conceptual uncertainty: ioECoG remains interpreted largely through clinical experience rather than quantitative criteria. Bridging this gap requires multicenter, harmonized datasets that relate ioECoG features to long-term outcomes. As the recordings evolve toward high-density and computationally analyzed frameworks, ioECoG has the potential to transform from a descriptive tool into a quantitative, evidence-based tool.

Post-surgery: from resection to recovery

After resective surgery, the focus shifts to recovery and long-term outcomes. For patients, the immediate question is whether seizures recur. If they remain seizure-free after surgery, the main challenge is whether and when to withdraw antiepileptic drugs (AED). Benefits of AED withdrawal include reduction of cognitive and systemic adverse effects, drug interactions, and costs. Risks of AED withdrawal include seizure recurrence, with possible consequences like injuries, loss of driving license, work or social relapse. Evidence indicates that long-term seizure freedom is achievable for a substantial subset of surgical patients, but seizure recurrence can occur years later, which makes AED decisions hard.[263] Timing when to start tapering after surgery is crucial: early withdrawal is associated with high risk of seizure recurrence in adults[264] and a waiting period of at least six months is advised in children.[265] Other factors that are a predictor of seizure recurrence after withdrawal are post-operative seizures and high number of AED at the time of surgery.[264,265] Surveys among clinicians show that most would consider withdrawal in seizure-free patients, but practice varies widely: clinicians tend to overestimate recurrence risk in surgical cases relative to calculator estimates and weigh seizure consequences (e.g., driving) heavily in shared decisions.[266,267] In practice, many centers consider tapering after around 12 months of seizure freedom, one AED at a time, with slower schedules for polytherapy, and they pause or reverse tapering if clinical events occur.[266,268]

EEG biomarkers are frequently used to refine risks of seizure recurrence. Postoperative interictal epileptiform discharges on scalp EEG are associated with higher seizure recurrence risk, and absence of IEDs for ≥6 months may support earlier withdrawal in carefully selected, low-risk children.[265,269] ioECoG biomarkers such as HFO occurrence[33] or spectral entropy (Chapter 3) may help predict postoperative outcome. These and other biomarkers could be used in models to predict seizure freedom after ASM withdrawal.

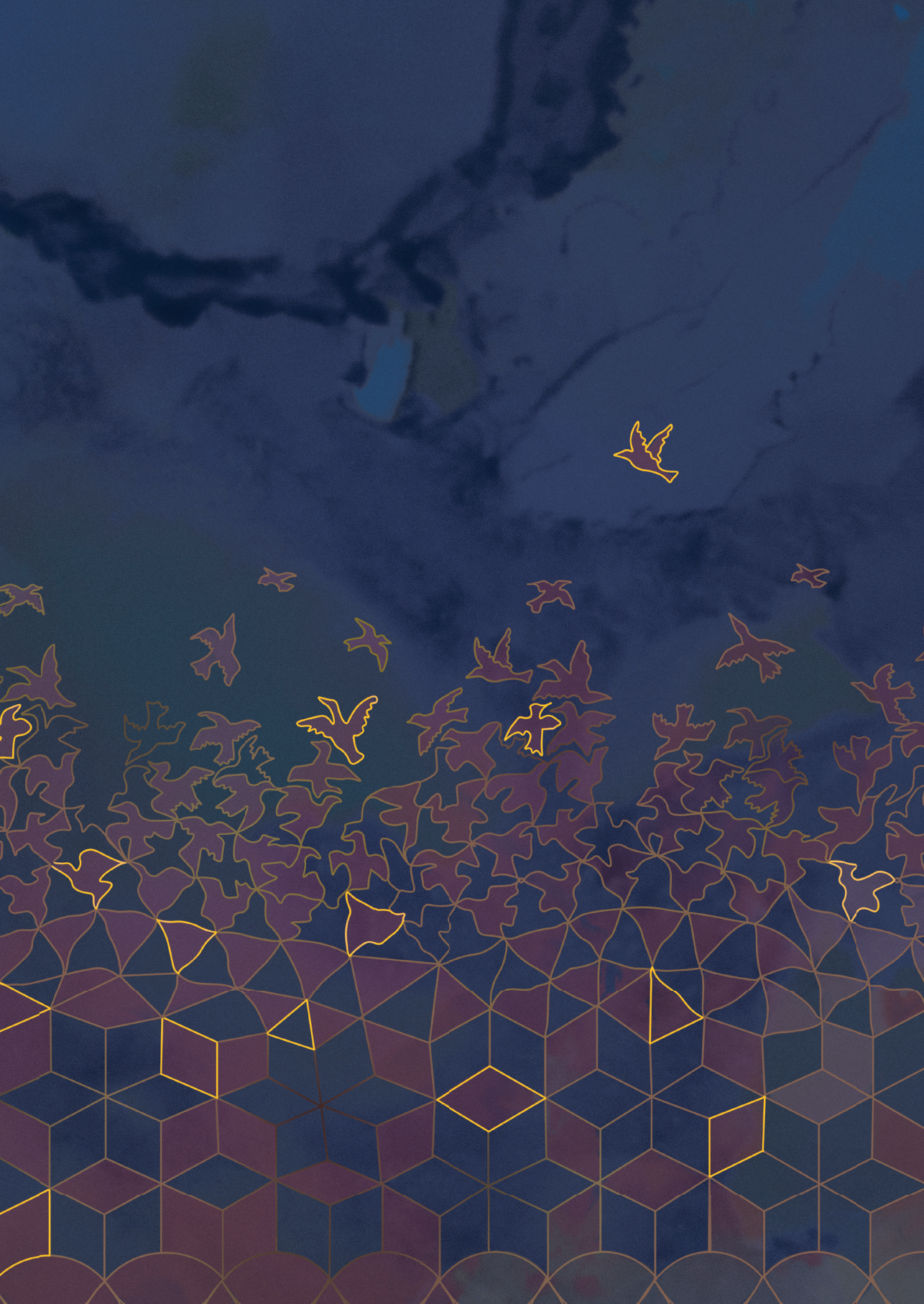
Ultimately, the purpose of epilepsy surgery extends beyond seizure freedom itself. Successful surgery can profoundly alter the trajectory of a patient's life. It enables independence, participation in work and education, and a huge relief from the social and psychological burden of uncontrolled seizures. Achieving seizure freedom reduces ASM use and thereby its side effects, it lowers healthcare utilization, and it improves cost-effectiveness compared to long-term medical management.[270,271] Also, quality of life consistently improves after successful resective surgery, with the strongest gains seen in cognitive, emotional, and social domains.[272] For many patients, this translates into a restored sense of self control and freedom: the ability to live without the constant anticipation of seizures, to make plans for the future, and to regain trust in one's own body. These are the ultimate goals that drive our scientific and clinical efforts: not only to stop seizures, but to return patients their independence.

Future perspectives

The studies presented in this thesis highlight that ioECoG is an underutilized tool with substantial potential beyond traditional visual assessment. With advanced analysis, ioECoG can contribute to more precise localization, better outcome prediction, and more informed surgical decisions.
Future directions include:

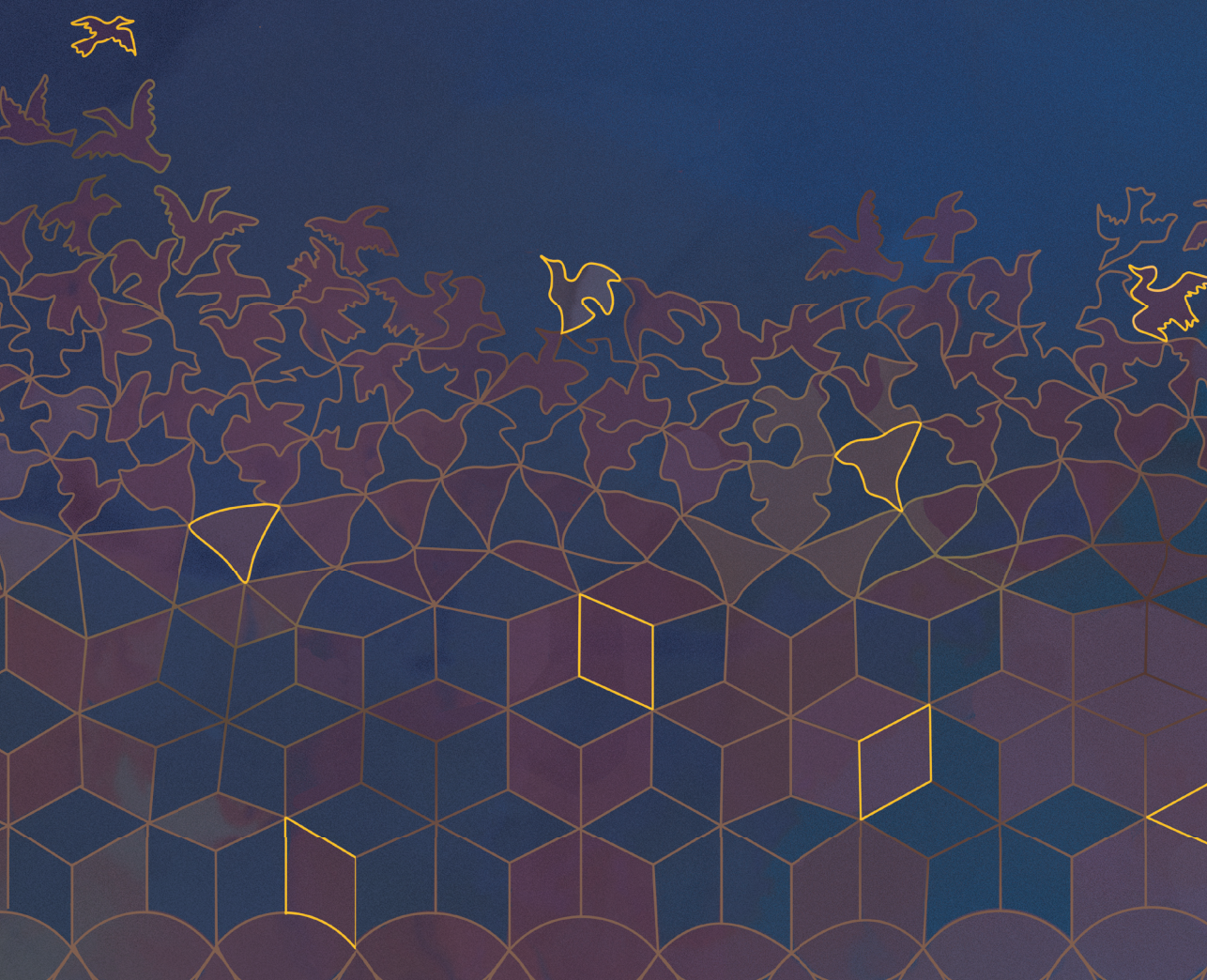
- Real-time automated analysis: Algorithms that detect spikes, HFOs, and spectral entropy in real time could provide immediate feedback during surgery. Integration into surgical navigation systems will allow clinical implementation.
- High-density electrodes: Wider adoption of HD-ioECoG could improve spatial resolution, particularly in lesions with subtle boundaries. Development of new grids, including flexible grids, will help the wider adoption.
- Multimodal integration: Combining ioECoG with advanced imaging (structural, metabolic, and functional) could create comprehensive surgical maps. AI could synthesize these data into individualized predictions.
- Clinical standardization: Establishing standardized acquisition, filtering, and analysis protocols is essential to enable multicenter trials and guideline development.
- Less invasive surgery: thermo-coagulation on stereo EEG electrodes and laser ablation have the possibility to interrupt epileptogenic networks caused by small lesions or lesions in brain locations that are hard to reach by resective surgery.
- Sustainability and accessibility: By reducing the need for invasive monitoring and lifelong medication, optimized ioECoG-guided surgery can lower costs and broaden access to surgical treatment worldwide.

Ultimately, the goal is not merely technical progress but concrete improvements in patient care: more seizure-free patients, fewer side effects, and better quality of life. For patients, especially children, this means a future less constrained by seizures and medication, and more open to normal development and participation in daily life.



Appendices

References
Nederlandse samenvatting | Dutch summary
Dankwoord | Acknowledgements
List of publications
About the author



References

1. Falco-Walter J. Epilepsy-Definition, Classification, Pathophysiology, and Epidemiology. Semin Neurol 2020; 40(6): 617-23.
2. Aronica E, Mühlebner A. Neuropathology of epilepsy. Handb Clin Neurol 2017; 145: 193-216.
3. Galan FN, Beier AD, Sheth RD. Advances in Epilepsy Surgery. Pediatr Neurol 2021; 122: 89-97.
4. Rugg-Gunn F, Miserocchi A, McEvoy A. Epilepsy surgery. Pract Neurol 2020; 20(1): 4-14.
5. Spencer S, Huh L. Outcomes of epilepsy surgery in adults and children. Lancet Neurol 2008; 7(6): 525-37.
6. Jehi L. The Epileptogenic Zone: Concept and Definition. Epilepsy Curr 2018; 18(1): 12-6.
7. Zijlmans M, Zweiphenning W, van Klink N. Changing concepts in presurgical assessment for epilepsy surgery. Nat Rev Neurol 2019; 15(10): 594-606.
8. Engel J, Jr. Surgical Treatment of the Epilepsies, 2nd edition; 1993.
9. Lapalme-Remis S, Nguyen DK. Neuroimaging of Epilepsy. Continuum (Minneap Minn) 2022; 28(2): 306-38.
10. Goel K, Pek V, Shlobin NA, et al. Clinical utility of intraoperative electrocorticography for epilepsy surgery: A systematic review and meta-analysis. Epilepsia 2023; 64(2): 253-65.
11. Jacobs J, LeVan P, Chander R, Hall J, Dubeau F, Gotman J. Interictal high-frequency oscillations (80-500 Hz) are an indicator of seizure onset areas independent of spikes in the human epileptic brain. Epilepsia 2008; 49(11): 1893-907.
12. Zijlmans M, Jiruska P, Zelmann R, Leijten FS, Jefferys JG, Gotman J. High-frequency oscillations as a new biomarker in epilepsy. Ann Neurol 2012; 71(2): 169-78.
13. Boran E, Ramantani G, Krayenbühl N, et al. High-density ECoG improves the detection of high frequency oscillations that predict seizure outcome. Clin Neurophysiol 2019; 130(10): 1882-8.
14. Zweiphenning WJEM, van 't Klooster MA, van Klink NEC, et al. Intraoperative electrocorticography using high-frequency oscillations or spikes to tailor epilepsy surgery in the Netherlands (the HFO trial): a randomised, single-blind, adaptive non-inferiority trial. Lancet Neurol 2022; 21(11): 982-93.
15. Demuru M, Kalitzin S, Zweiphenning W, et al. The value of intraoperative electrographic biomarkers for tailoring during epilepsy surgery: from group-level to patient-level analysis. Sci Rep 2020; 10(1): 14654.
16. Kannathal N, Choo ML, Acharya UR, Sadasivan PK. Entropies for detection of epilepsy in EEG. Comput Methods Programs Biomed 2005; 80(3): 187-94.
17. Bruhn J, Röpcke H, Hoeft A. Approximate entropy as an electroencephalographic measure of anesthetic drug effect during desflurane anesthesia. Anesthesiology 2000; 92(3): 715-26.
18. Azami H, Moguilner S, Penagos H, et al. EEG Entropy in REM Sleep as a Physiologic Biomarker in Early Clinical Stages of Alzheimer's Disease. J Alzheimers Dis 2023; 91(4): 1557-72.
19. Tjepkema-Cloostermans MC, de Carvalho RCV, van Putten M. Deep learning for detection of focal epileptiform discharges from scalp EEG recordings. Clin Neurophysiol 2018; 129(10): 2191-6.
20. da Silva Lourenço C, Tjepkema-Cloostermans MC, van Putten M. Efficient use of clinical EEG data for deep learning in epilepsy. Clin Neurophysiol 2021; 132(6): 1234-40.
21. Zhang Y, Lu Q, Monsoor T, et al. Refining epileptogenic high-frequency oscillations using deep learning: a reverse engineering approach. Brain Commun 2022; 4(1): fcab267.
22. Powell GE, Percival IC. A spectral entropy method for distinguishing regular and irregular motion of Hamiltonian systems. Journal of Physics A: Mathematical and General 1979; 12(11): 2053.
23. Inouye T, Shinosaki K, Sakamoto H, et al. Quantification of EEG irregularity by use of the entropy of the power spectrum. Electroencephalography and Clinical Neurophysiology 1991; 79(3): 204-10.
24. de Vries BM, Zwezerijnen GJC, Burchell GL, van Velden FHP, Menke-van der Houven van Oordt CW, Boellaard R. Explainable artificial intelligence (XAI) in radiology and nuclear medicine: a literature review. Front Med (Lausanne) 2023; 10: 1180773.
25. Rashed-Al-Mahfuz M, Moni MA, Uddin S, Alyami SA, Summers MA, Eapen V. A Deep Convolutional Neural Network Method to Detect Seizures and Characteristic Frequencies Using Epileptic Electroencephalogram (EEG) Data. IEEE J Transl Eng Health Med 2021; 9: 2000112.
26. Hoogteijling S, Zijlmans M. Deep learning for epileptogenic zone delineation from the invasive EEG: challenges and lookouts. Brain Commun 2022; 4(1): fcab307.
27. Wang Z, Guo J, van 't Klooster M, Hoogteijling S, Jacobs J, Zijlmans M. Prognostic Value of Complete Resection of the High-Frequency Oscillation Area in Intracranial EEG: A Systematic Review and Meta-Analysis. Neurology 2024; 102(9): e209216.
28. Gerstl JVE, Kiseleva A, Imbach L, Sarnthein J, Fedele T. High frequency oscillations in relation to interictal spikes in predicting postsurgical seizure freedom. Sci Rep 2023; 13(1): 21313.
29. Kanner AM, Bicchi MM. Antiseizure Medications for Adults With Epilepsy: A Review. Jama

2022; 327(13): 1269-81.
30. Lesko R, Benova B, Jezdik P, et al. The clinical utility of intraoperative electrocorticography in pediatric epilepsy surgical strategy and planning. J Neurosurg Pediatr 2020; 26(5): 533-42.
31. Tran TA, Spencer SS, Javidan M, Pacia S, Marks D, Spencer DD. Significance of spikes recorded on intraoperative electrocorticography in patients with brain tumor and epilepsy. Epilepsia 1997; 38(10): 1132-9.
32. Roessler K, Heynold E, Buchfelder M, Stefan H, Hamer HM. Current value of intraoperative electrocorticography (iopECoG). Epilepsy Behav 2019; 91: 20-4.
33. van 't Klooster MA, van Klink NE, Leijten FS, et al. Residual fast ripples in the intraoperative corticogram predict epilepsy surgery outcome. Neurology 2015; 85(2): 120-8.
34. van 't Klooster MA, van Klink NEC, Zweiphenning W, et al. Tailoring epilepsy surgery with fast ripples in the intraoperative electrocorticogram. Ann Neurol 2017; 81(5): 664-76.
35. Jahromi S, Matarrese MAG, Tamilia E, et al. Mapping Propagation of Interictal Spikes, Ripples, and Fast Ripples in Intracranial EEG of Children with Refractory Epilepsy. Annu Int Conf IEEE Eng Med Biol Soc 2021; 2021: 194-7.
36. Bruder JC, Schmelzeisen C, Lachner-Piza D, Reinacher P, Schulze-Bonhage A, Jacobs J. Physiological Ripples Associated With Sleep Spindles Can Be Identified in Patients With Refractory Epilepsy Beyond Mesio-Temporal Structures. Front Neurol 2021; 12: 612293.
37. van Klink N, Frauscher B, Zijlmans M, Gotman J. Relationships between interictal epileptic spikes and ripples in surface EEG. Clin Neurophysiol 2016; 127(1): 143-9.
38. Ferrier CH, Aronica E, Leijten FS, et al. Electrocorticographic discharge patterns in glioneuronal tumors and focal cortical dysplasia. Epilepsia 2006; 47(9): 1477-86.
39. Kerber K, LeVan P, Dümpelmann M, et al. High frequency oscillations mirror disease activity in patients with focal cortical dysplasia. Epilepsia 2013; 54(8): 1428-36.
40. Straumann S, Schaft E, Noordmans HJ, et al. The spatial relationship between the MRI lesion and intraoperative electrocorticography in focal epilepsy surgery. Brain Commun 2022; 4(6)
41. Baud MO, Perneger T, Rácz A, et al. European trends in epilepsy surgery. Neurology 2018; 91(2): e96-e106.
42. Demuru M, van Blooijs D, Zweiphenning W, Hermes D, Leijten F, Zijlmans M. A Practical Workflow for Organizing Clinical Intraoperative and Long-term iEEG Data in BIDS. Neuroinformatics 2022; 20(3): 727-36.
43. Blümcke I, Thom M, Aronica E, et al. The clinicopathologic spectrum of focal cortical dysplasias: a consensus classification proposed by an ad hoc Task Force of the ILAE Diagnostic Methods Commission. Epilepsia 2011; 52(1): 158-74.
44. Zijlmans M, Huiskamp GM, Cremer OL, Ferrier CH, van Huffelen AC, Leijten FS. Epileptic high-frequency oscillations in intraoperative electrocorticography: the effect of propofol. Epilepsia 2012; 53(10): 1799-809.
45. Maccabeo A, van 't Klooster MA, Schaft E, et al. Spikes and High Frequency Oscillations in Lateral Neocortical Temporal Lobe Epilepsy: Can They Predict the Success Chance of Hippocampus-Sparing Resections? Front Neurol 2022; 13: 797075.
46. Gaspard N, Alkawadri R, Farooque P, Goncharova, II, Zaveri HP. Automatic detection of prominent interictal spikes in intracranial EEG: validation of an algorithm and relationsip to the seizure onset zone. Clin Neurophysiol 2014; 125(6): 1095-103.
47. Fedele T, van 't Klooster M, Burnos S, et al. Automatic detection of high frequency oscillations during epilepsy surgery predicts seizure outcome. Clin Neurophysiol 2016; 127(9): 3066-74.
48. Benjamini Y, Hochberg Y. Controlling the False Discovery Rate: A Practical and Powerful Approach to Multiple Testing. J R Stat Soc, B: Stat Methodol 1995; 57(1): 289-300.
49. Hussain SA, Mathern GW, Hung P, Weng J, Sankar R, Wu JY. Intraoperative fast ripples independently predict postsurgical epilepsy outcome: Comparison with other electrocorticographic phenomena. Epilepsy Research 2017; 135: 79-86.
50. Shi W, Shaw D, Walsh KG, et al. Spike ripples localize the epileptogenic zone best: an international intracranial study. Brain 2024.
51. Engel J, Jr., Bragin A, Staba R, Mody I. High-frequency oscillations: what is normal and what is not? Epilepsia 2009; 50(4): 598-604.
52. Mölle M, Yeshenko O, Marshall L, Sara SJ, Born J. Hippocampal sharp wave-ripples linked to slow oscillations in rat slow-wave sleep. J Neurophysiol 2006; 96(1): 62-70.
53. Weiss SA, Orosz I, Salamon N, et al. Ripples on spikes show increased phase-amplitude coupling in mesial temporal lobe epilepsy seizure-onset zones. Epilepsia 2016; 57(11): 1916-30.
54. Weiss SA, Fried I, Engel J, et al. Fast ripples reflect increased excitability that primes epileptiform spikes. medRxiv 2023.
55. Alkawadri R, Gaspard N, Goncharova, II, et al. The spatial and signal characteristics of physiologic high frequency oscillations. Epilepsia 2014; 55(12): 1986-95.
56. Abdijadid S, Mathern GW, Levine MS, Cepeda C. Basic mechanisms of epileptogenesis in pediatric cortical dysplasia. CNS neuroscience & therapeutics 2015; 21(2): 92-103.
57. Weiss SA, Staba RJ, Sharan A, et al. Accuracy of high-frequency oscillations recorded intraoperatively for classification of epileptogenic regions. Sci Rep 2021; 11(1): 21388.

58. Bagshaw AP, Jacobs J, LeVan P, Dubeau F, Gotman J. Effect of sleep stage on interictal high-frequency oscillations recorded from depth macroelectrodes in patients with focal epilepsy. Epilepsia 2009; 50(4): 617-28.
59. Téllez-Zenteno JF, Ronquillo LH, Moien-Afshari F, Wiebe S. Surgical outcomes in lesional and non-lesional epilepsy: A systematic review and meta-analysis. Epilepsy Research 2010; 89(2): 310-8.
60. Cimbalnik J, Klimes P, Sladky V, et al. Multi-feature localization of epileptic foci from interictal, intracranial EEG. Clin Neurophysiol 2019; 130(10): 1945-53.
61. Sklenarova B, Zatloukalova E, Cimbalnik J, et al. Interictal High-Frequency Oscillations, Spikes, and Connectivity Profiles: a Fingerprint of Epileptogenic Brain Pathologies. Epilepsia 2023.
62. Conrad EC, Tomlinson SB, Wong JN, et al. Spatial distribution of interictal spikes fluctuates over time and localizes seizure onset. Brain 2020; 143(2): 554-69.
63. Greiner HM, Horn PS, Tenney JR, et al. Preresection intraoperative electrocorticography (ECoG) abnormalities predict seizure-onset zone and outcome in pediatric epilepsy surgery. Epilepsia 2016; 57(4): 582-9.
64. Guo J, Wang Z, van 't Klooster MA, et al. Seizure Outcome After Intraoperative Electrocorticography-Tailored Epilepsy Surgery: A Systematic Review and Meta-Analysis. Neurology 2024; 102(11): e209430.
65. Stefan H, Hopfengärtner R, Kreiselmeyer G, et al. Interictal triple ECoG characteristics of temporal lobe epilepsies: An intraoperative ECoG analysis correlated with surgical outcome. Clin Neurophysiol 2008; 119(3): 642-52.
66. Sugano H, Shimizu H, Sunaga S. Efficacy of intraoperative electrocorticography for assessing seizure outcomes in intractable epilepsy patients with temporal-lobe-mass lesions. Seizure 2007; 16(2): 120-7.
67. El Tahry R, Ferrao Santos S, de Tourtchaninoff M, et al. Post-resection electrocorticography has no added value in epilepsy surgery. Acta Neurol Belg 2016; 116(3): 279-85.
68. Southwell DG, Garcia PA, Berger MS, Barbaro NM, Chang EF. Long-term seizure control outcomes after resection of gangliogliomas. Neurosurgery 2012; 70(6): 1406-13; discussion 13-4.
69. Yu HY, Hsu SPC, Lin CF, et al. Prognostic significance of postoperative spikes varied in different surgical procedures for mesial temporal sclerosis. Seizure 2017; 52: 71-5.
70. Ortega GJ, Menendez de la Prida L, Sola RG, Pastor J. Synchronization clusters of interictal activity in the lateral temporal cortex of epileptic patients: intraoperative electrocorticographic analysis. Epilepsia 2008; 49(2): 269-80.
71. Taylor PN, Papasavvas CA, Owen TW, et al. Normative brain mapping of interictal intracranial EEG to localize epileptogenic tissue. Brain 2022; 145(3): 939-49.
72. Lundberg SM, Erion G, Chen H, et al. From Local Explanations to Global Understanding with Explainable AI for Trees. Nat Mach Intell 2020; 2(1): 56-67.
73. Mercaldo ND, Lau KF, Zhou XH. Confidence intervals for predictive values with an emphasis to case-control studies. Stat Med 2007; 26(10): 2170-83.
74. Sun X, Xu W. Fast Implementation of DeLong's Algorithm for Comparing the Areas Under Correlated Receiver Operating Characteristic Curves. IEEE Signal Processing Letters 2014; 21(11): 1389-93.
75. Dietterich TG. Approximate Statistical Tests for Comparing Supervised Classification Learning Algorithms. Neural Comput 1998; 10(7): 1895-923.
76. Akter MS, Islam MR, Iimura Y, et al. Multiband entropy-based feature-extraction method for automatic identification of epileptic focus based on high-frequency components in interictal iEEG. Scientific Reports 2020; 10(1): 7044.
77. Elahian B, Yeasin M, Mudigoudar B, Wheless JW, Babajani-Feremi A. Identifying seizure onset zone from electrocorticographic recordings: A machine learning approach based on phase locking value. Seizure 2017; 51: 35-42.
78. Grinenko O, Li J, Mosher JC, et al. A fingerprint of the epileptogenic zone in human epilepsies. Brain 2018; 141(1): 117-31.
79. Lima CA, Coelho AL. Kernel machines for epilepsy diagnosis via EEG signal classification: a comparative study. Artif Intell Med 2011; 53(2): 83-95.
80. Varatharajah Y, Berry B, Cimbalnik J, et al. Integrating artificial intelligence with real-time intracranial EEG monitoring to automate interictal identification of seizure onset zones in focal epilepsy. J Neural Eng 2018; 15(4): 046035.
81. Abou Jaoude M, Jing J, Sun H, et al. Detection of mesial temporal lobe epileptiform discharges on intracranial electrodes using deep learning. Clin Neurophysiol 2020; 131(1): 133-41.
82. Daoud H, Bayoumi M. Deep Learning Approach for Epileptic Focus Localization. IEEE Trans Biomed Circuits Syst 2020; 14(2): 209-20.
83. San-Segundo R, Gil-Martín M, D'Haro-Enríquez LF, Pardo JM. Classification of epileptic EEG recordings using signal transforms and convolutional neural networks. Comput Biol Med 2019; 109: 148-58.

84. Wang X, Trabatti C, Weeke L, et al. Early qualitative and quantitative amplitude-integrated electroencephalogram and raw electroencephalogram for predicting long-term neurodevelopmental outcomes in extremely preterm infants in the Netherlands: a 10-year cohort study. Lancet Digit Health 2023; 5(12): e895-e904.
85. Abela E, Pawley AD, Tangwiriyasakul C, et al. Slower alpha rhythm associates with poorer seizure control in epilepsy. Ann Clin Transl Neurol 2019; 6(2): 333-43.
86. de Jongh A, de Munck JC, Baayen JC, Jonkman EJ, Heethaar RM, van Dijk BW. The localization of spontaneous brain activity: first results in patients with cerebral tumors. Clin Neurophysiol 2001; 112(2): 378-85.
87. Douw L, van Dellen E, de Groot M, et al. Epilepsy is related to theta band brain connectivity and network topology in brain tumor patients. BMC Neurosci 2010; 11: 103.
88. Martire DJ, Wong S, Mikhail M, et al. Thalamocortical dysrhythmia in intraoperative recordings of focal epilepsy. J Neurophysiol 2019; 121(6): 2020-7.
89. van Klink NEC, Zweiphenning W, Ferrier CH, et al. Can we use intraoperative high-frequency oscillations to guide tumor-related epilepsy surgery? Epilepsia 2021; 62(4): 997-1004.
90. Stovall T, Hunt B, Glynn S, Stacey WC, Gliske SV. Interictal high frequency background activity as a biomarker of epileptogenic tissue. Brain Commun 2021; 3(3): fcab188.
91. Claus S, Leijten F, Kallansee P, et al. An electro-encephalogram beta gap after induction with diazepam: a localization method in epileptogenic lesions. Clin Neurophysiol 2009; 120(7): 1235-44.
92. Kim JJ, Gharpure A, Teng J, et al. Shared structural mechanisms of general anaesthetics and benzodiazepines. Nature 2020; 585(7824): 303-8.
93. Alamoudi OA, Ilyas A, Pati S, Iasemidis L. Interictal localization of the epileptogenic zone: Utilizing the observed resonance behavior in the spectral band of surrounding inhibition. Front Neurosci 2022; 16: 993678.
94. Cohen-Gadol AA, Wilhelmi BG, Collignon F, et al. Long-term outcome of epilepsy surgery among 399 patients with nonlesional seizure foci including mesial temporal lobe sclerosis. J Neurosurg 2006; 104(4): 513-24.
95. Karimi D, Dou H, Warfield SK, Gholipour A. Deep learning with noisy labels: Exploring techniques and remedies in medical image analysis. Med Image Anal 2020; 65: 101759.
96. Kreuzer M, Kochs EF, Schneider G, Jordan D. Non-stationarity of EEG during wakefulness and anaesthesia: advantages of EEG permutation entropy monitoring. J Clin Monit Comput 2014; 28(6): 573-80.
97. Rampil IJ. A primer for EEG signal processing in anesthesia. Anesthesiology 1998; 89(4): 980-1002.
98. Ibarz JM, Foffani G, Cid E, Inostroza M, De La Prida LM. Emergent dynamics of fast ripples in the epileptic hippocampus. Journal of Neuroscience 2010; 30(48): 16249-61.
99. Sato Y, Wong SM, Iimura Y, Ochi A, Doesburg SM, Otsubo H. Spatiotemporal changes in regularity of gamma oscillations contribute to focal ictogenesis. Sci Rep 2017; 7(1): 9362.
100. Sato Y, Ochi A, Mizutani T, Otsubo H. Low entropy of interictal gamma oscillations is a biomarker of the seizure onset zone in focal cortical dysplasia type II. Epilepsy Behav 2019; 96: 155-9.
101. Jiruska P, Alvarado-Rojas C, Schevon CA, et al. Update on the mechanisms and roles of high-frequency oscillations in seizures and epileptic disorders. Epilepsia 2017; 58(8): 1330-9.
102. Foffani G, Uzcategui YG, Gal B, Menendez de la Prida L. Reduced spike-timing reliability correlates with the emergence of fast ripples in the rat epileptic hippocampus. Neuron 2007; 55(6): 930-41.
103. Mooij AH, Frauscher B, Amiri M, Otte WM, Gotman J. Differentiating epileptic from non-epileptic high frequency intracerebral EEG signals with measures of wavelet entropy. Clin Neurophysiol 2016; 127(12): 3529-36.
104. Daida A, Zhang Y, Kanai S, Staba R, Roychowdhury V, Nariai H. AI-based localization of the epileptogenic zone using intracranial EEG. Epilepsia Open 2025.
105. Hoogteijling S, Schaft EV, Dirks EHM, et al. Machine learning for (non-)epileptic tissue detection from the intraoperative electrocorticogram. Clin Neurophysiol 2024; 167: 14-25.
106. Vieira JC, Guedes LA, Santos MR, Sanchez-Gendriz I. Using Explainable Artificial Intelligence to Obtain Efficient Seizure-Detection Models Based on Electroencephalography Signals. Sensors (Basel) 2023; 23(24).
107. Sun D, van 't Klooster MA, Ringeling EM, et al. Pausing propofol during neurosurgery to record intraoperative electrocorticography is feasible;10 years of clinical experience. Clin Neurophysiol 2024; 167: 84-91.
108. Schaft EV, Sun D, van 't Klooster MA, et al. Spatial and temporal properties of intraoperatively recorded spikes and high frequency oscillations in focal cortical dysplasia. Clin Neurophysiol 2024; 162: 210-8.
109. Flood MW, Grimm B. EntropyHub: An open-source toolkit for entropic time series analysis. PLoS One 2021; 16(11): e0259448.
110. Poldrack RA, Huckins G, Varoquaux G. Establishment of best practices for evidence for prediction: a review. JAMA psychiatry 2020; 77(5): 534-40.

111. Wang X, de Groot ER, Tataranno ML, et al. Machine Learning-Derived Active Sleep as an Early Predictor of White Matter Development in Preterm Infants. J Neurosci 2024; 44(5).
112. Jonckheere AR. A distribution-free k-sample test against ordered alternatives. Biometrika 1954; 41(1/2): 133-45.
113. Travnicek V, Klimes P, Cimbalnik J, et al. Relative entropy is an easy-to-use invasive electroencephalographic biomarker of the epileptogenic zone. Epilepsia 2023; 64(4): 962-72.
114. Jefferys JG, Menendez de la Prida L, Wendling F, et al. Mechanisms of physiological and epileptic HFO generation. Prog Neurobiol 2012; 98(3): 250-64.
115. Greiner HM, Horn PS, Tenney JR, et al. Should spikes on post-resection ECoG guide pediatric epilepsy surgery? Epilepsy Res 2016; 122: 73-8.
116. Dauwels J, Eskandar E, Cash S. Localization of seizure onset area from intracranial non-seizure EEG by exploiting locally enhanced synchrony. Annu Int Conf IEEE Eng Med Biol Soc 2009; 2009: 2180-3.
117. Jeong W, Jin SH, Kim M, Kim JS, Chung CK. Abnormal functional brain network in epilepsy patients with focal cortical dysplasia. Epilepsy Res 2014; 108(9): 1618-26.
118. Zweiphenning WJEM, Keijzer HM, van Diessen E, et al. Increased gamma and decreased fast ripple connections of epileptic tissue: A high-frequency directed network approach. Epilepsia 2019; 60(9): 1908-20.
119. Richman JS, Moorman JR. Physiological time-series analysis using approximate entropy and sample entropy. Am J Physiol Heart Circ Physiol 2000; 278(6): H2039-49.
120. Tonini C, Beghi E, Berg AT, et al. Predictors of epilepsy surgery outcome: a meta-analysis. Epilepsy Res 2004; 62(1): 75-87.
121. Choi SA, Kim KJ. The Surgical and Cognitive Outcomes of Focal Cortical Dysplasia. J Korean Neurosurg Soc 2019; 62(3): 321-7.
122. Rowland NC, Englot DJ, Cage TA, Sughrue ME, Barbaro NM, Chang EF. A meta-analysis of predictors of seizure freedom in the surgical management of focal cortical dysplasia. J Neurosurg 2012; 116(5): 1035-41.
123. Najm I, Lal D, Alonso Vanegas M, et al. The ILAE consensus classification of focal cortical dysplasia: An update proposed by an ad hoc task force of the ILAE diagnostic methods commission. Epilepsia 2022; 63(8): 1899-919.
124. Schwartz TH, Bazil CW, Forgione M, Bruce JN, Goodman RR. Do reactive post-resection "injury" spikes exist? Epilepsia 2000; 41(11): 1463-8.
125. Hosain S, Burton L, Fraser R, Labar D. Focal suppression-burst on electrocorticography after temporal lobectomy. Neurology 1995; 45(12): 2276-8.
126. Xu C, Yu T, Zhang X, et al. Focal burst suppression on intraoperative electrocorticography does not affect the surgical outcome in patients with temporal lobe epilepsy. Clin Neurol Neurosurg 2020; 193: 105785.
127. Fois C, Kovac S, Khalil A, et al. Predictors for being offered epilepsy surgery: 5-year experience of a tertiary referral centre. J Neurol Neurosurg Psychiatry 2016; 87(2): 209-11.
128. Zweiphenning W, Klooster MAV, van Klink NEC, et al. Intraoperative electrocorticography using high-frequency oscillations or spikes to tailor epilepsy surgery in the Netherlands (the HFO trial): a randomised, single-blind, adaptive non-inferiority trial. Lancet Neurol 2022; 21(11): 982-93.
129. Alarcon G, Garcia Seoane JJ, Binnie CD, et al. Origin and propagation of interictal discharges in the acute electrocorticogram. Implications for pathophysiology and surgical treatment of temporal lobe epilepsy. Brain 1997; 120 (Pt 12): 2259-82.
130. Kural MA, Tankisi H, Duez L, et al. Optimized set of criteria for defining interictal epileptiform EEG discharges. Clin Neurophysiol 2020; 131(9): 2250-4.
131. Kural MA, Duez L, Sejer Hansen V, et al. Criteria for defining interictal epileptiform discharges in EEG: A clinical validation study. Neurology 2020; 94(20): e2139-e47.
132. van Klink NEC, Van't Klooster MA, Zelmann R, et al. High frequency oscillations in intraoperative electrocorticography before and after epilepsy surgery. Clin Neurophysiol 2014; 125(11): 2212-9.
133. Mari F, Zelmann R, Andrade-Valenca L, Dubeau F, Gotman J. Continuous high-frequency activity in mesial temporal lobe structures. Epilepsia 2012; 53(5): 797-806.
134. Zelmann R, Mari F, Jacobs J, Zijlmans M, Dubeau F, Gotman J. A comparison between detectors of high frequency oscillations. Clin Neurophysiol 2012; 123(1): 106-16.
135. Burnos S, Frauscher B, Zelmann R, Haegelen C, Sarnthein J, Gotman J. The morphology of high frequency oscillations (HFO) does not improve delineating the epileptogenic zone. Clin Neurophysiol 2016; 127(4): 2140-8.
136. Duce B, Rego C, Milosavljevic J, Hukins C. The AASM recommended and acceptable EEG montages are comparable for the staging of sleep and scoring of EEG arousals. J Clin Sleep Med 2014; 10(7): 803-9.
137. Foldvary N, Caruso AC, Mascha E, et al. Identifying montages that best detect electrographic seizure activity during polysomnography. Sleep 2000; 23(2): 221-9.
138. Acharya JN, Acharya VJ. Overview of EEG Montages and Principles of Localization. J Clin Neurophysiol 2019; 36(5): 325-9.

139. Pickard AA, Skidmore CT. Montages for Invasive Monitoring. J Clin Neurophysiol 2019; 36(5): 337-44.
140. Weiss SA, Berry B, Chervoneva I, et al. Visually validated semi-automatic high-frequency oscillation detection aides the delineation of epileptogenic regions during intraoperative electrocorticography. Clin Neurophysiol 2018; 129(10): 2089-98.
141. Ferrari-Marinho T, Perucca P, Mok K, et al. Pathologic substrates of focal epilepsy influence the generation of high-frequency oscillations. Epilepsia 2015; 56(4): 592-8.
142. Acharya JN, Hani AJ, Thirumala PD, Tsuchida TN. American Clinical Neurophysiology Society Guideline 3: A Proposal for Standard Montages to Be Used in Clinical EEG. J Clin Neurophysiol 2016; 33(4): 312-6.
143. Michelmann S, Treder MS, Griffiths B, et al. Data-driven re-referencing of intracranial EEG based on independent component analysis (ICA). J Neurosci Methods 2018; 307: 125-37.
144. Caune V, Le Cam S, Ranta R, Maillard L, Louis-Dorr V. Dipolar source localization from intracerebral SEEG recordings. Annu Int Conf IEEE Eng Med Biol Soc 2013; 2013: 41-4.
145. Melani F, Zelmann R, Mari F, Gotman J. Continuous High Frequency Activity: a peculiar SEEG pattern related to specific brain regions. Clin Neurophysiol 2013; 124(8): 1507-16.
146. Schaft EV, Sun D, van 't Klooster MA, et al. Spatial and temporal properties of intraoperatively recorded spikes and high frequency oscillations in focal cortical dysplasia. Clin Neurophysiol 2024; 162: 210-8.
147. Dewey ME. Coefficients of agreement. Br J Psychiatry 1983; 143: 487-9.
148. Landis JR, Koch GG. An application of hierarchical kappa-type statistics in the assessment of majority agreement among multiple observers. Biometrics 1977; 33(2): 363-74.
149. Zaveri HP, Duckrow RB, Spencer SS. On the use of bipolar montages for time-series analysis of intracranial electroencephalograms. Clin Neurophysiol 2006; 117(9): 2102-8.
150. Toth M, Papp KS, Gede N, et al. Surgical outcomes related to invasive EEG monitoring with subdural grids or depth electrodes in adults: A systematic review and meta-analysis. Seizure 2019; 70: 12-9.
151. Lamberink HJ, Otte WM, Blümcke I, Braun KPJ. Seizure outcome and use of antiepileptic drugs after epilepsy surgery according to histopathological diagnosis: a retrospective multicentre cohort study. Lancet Neurol 2020; 19(9): 748-57.
152. Zentner J. The Current Place of Epilepsy Surgery. 2020: 379-91.
153. Tripathi M, Garg A, Gaikwad S, et al. intraoperative electrocorticography in lesional epilepsy. Epilepsy Res 2010; 89(1): 133-41.
154. Höller Y, Kutil R, Klaffenböck L, et al. High-frequency oscillations in epilepsy and surgical outcome. A meta-analysis. Front Hum Neurosci 2015; 9: 574.
155. Rosenow F, Lüders H. Presurgical evaluation of epilepsy. Brain 2001; 124(Pt 9): 1683-700.
156. Lemieux L, Daunizeau J, Walker MC. Concepts of connectivity and human epileptic activity. Front Syst Neurosci 2011; 5: 12.
157. Kramer MA, Cash SS. Epilepsy as a disorder of cortical network organization. Neuroscientist 2012; 18(4): 360-72.
158. Tomlinson SB, Bermudez C, Conley C, Brown MW, Porter BE, Marsh ED. Spatiotemporal Mapping of Interictal Spike Propagation: A Novel Methodology Applied to Pediatric Intracranial EEG Recordings. Front Neurol 2016; 7: 229.
159. Spencer SS. Neural networks in human epilepsy: evidence of and implications for treatment. Epilepsia 2002; 43(3): 219-27.
160. Korzeniewska A, Cervenka MC, Jouny CC, et al. Ictal propagation of high frequency activity is recapitulated in interictal recordings: effective connectivity of epileptogenic networks recorded with intracranial EEG. Neuroimage 2014; 101: 96-113.
161. van Diessen E, Diederen SJ, Braun KP, Jansen FE, Stam CJ. Functional and structural brain networks in epilepsy: what have we learned? Epilepsia 2013; 54(11): 1855-65.
162. Ghaffari-Rafi A, Leon-Rojas J. Investigatory pathway and principles of patient selection for epilepsy surgery candidates: a systematic review. BMC Neurol 2020; 20(1): 100.
163. Duncan JS, Winston GP, Koepp MJ, Ourselin S. Brain imaging in the assessment for epilepsy surgery. Lancet Neurol 2016; 15(4): 420-33.
164. Boonyapisit K, Najm I, Klem G, et al. Epileptogenicity of focal malformations due to abnormal cortical development: direct electrocorticographic-histopathologic correlations. Epilepsia 2003; 44(1): 69-76.
165. Jacobs J, Levan P, Châtillon CE, Olivier A, Dubeau F, Gotman J. High frequency oscillations in intracranial EEGs mark epileptogenicity rather than lesion type. Brain 2009; 132(Pt 4): 1022-37.
166. Vakani R, Nair DR. Electrocorticography and functional mapping. Handb Clin Neurol 2019; 160: 313-27.
167. Fernández IS, Loddenkemper T. Electrocorticography for seizure foci mapping in epilepsy surgery. J Clin Neurophysiol 2013; 30(6): 554-70.
168. Yang T, Hakimian S, Schwartz TH. Intraoperative ElectroCorticoGraphy (ECog): indications, techniques, and utility in epilepsy surgery. Epileptic Disord 2014; 16(3): 271-9.
169. Sabolek HR, Swiercz WB, Lillis KP, et al. A candidate mechanism underlying the variance of

interictal spike propagation. J Neurosci 2012; 32(9): 3009-21.
170. Badier JM, Chauvel P. Spatio-temporal characteristics of paroxysmal interictal events in human temporal lobe epilepsy. J Physiol Paris 1995; 89(4-6): 255-64.
171. Lai Y, van Drongelen W, Hecox K, Frim D, Kohrman M, He B. Cortical activation mapping of epileptiform activity derived from interictal ECoG spikes. Epilepsia 2007; 48(2): 305-14.
172. Frauscher B, Bartolomei F, Kobayashi K, et al. High-frequency oscillations: The state of clinical research. Epilepsia 2017; 58(8): 1316-29.
173. Chen Z, Maturana MI, Burkitt AN, Cook MJ, Grayden DB. High-Frequency Oscillations in Epilepsy: What Have We Learned and What Needs to be Addressed. Neurology 2021; 96(9): 439-48.
174. Kerber K, Dümpelmann M, Schelter B, et al. Differentiation of specific ripple patterns helps to identify epileptogenic areas for surgical procedures. Clin Neurophysiol 2014; 125(7): 1339-45.
175. Tamilia E, Park EH, Percivati S, et al. Surgical resection of ripple onset predicts outcome in pediatric epilepsy. Ann Neurol 2018; 84(3): 331-46.
176. Jacobs J, Zijlmans M, Zelmann R, et al. High-frequency electroencephalographic oscillations correlate with outcome of epilepsy surgery. Ann Neurol 2010; 67(2): 209-20.
177. Jacobs J, Wu JY, Perucca P, et al. Removing high-frequency oscillations: A prospective multicenter study on seizure outcome. Neurology 2018; 91(11): e1040-e52.
178. van 't Klooster MA, Leijten FS, Huiskamp G, et al. High frequency oscillations in the intraoperative ECoG to guide epilepsy surgery ("The HFO Trial"): study protocol for a randomized controlled trial. Trials 2015; 16: 422.
179. Wieser HG, Blume WT, Fish D, et al. ILAE Commission Report. Proposal for a new classification of outcome with respect to epileptic seizures following epilepsy surgery. Epilepsia 2001; 42(2): 282-6.
180. Fedele T, Ramantani G, Burnos S, et al. Prediction of seizure outcome improved by fast ripples detected in low-noise intraoperative corticogram. Clin Neurophysiol 2017; 128(7): 1220-6.
181. Fedele T, Ramantani G, Sarnthein J. High frequency oscillations as markers of epileptogenic tissue - End of the party? Clin Neurophysiol 2019; 130(5): 624-6.
182. Yushkevich PA, Piven J, Hazlett HC, et al. User-guided 3D active contour segmentation of anatomical structures: significantly improved efficiency and reliability. Neuroimage 2006; 31(3): 1116-28.
183. Ségonne F, Dale AM, Busa E, et al. A hybrid approach to the skull stripping problem in MRI. Neuroimage 2004; 22(3): 1060-75.
184. Noordmans HJ, van Blooijs D, Siero JCW, Zwanenburg JJM, Klaessens J, Ramsey NF. Detailed view on slow sinusoidal, hemodynamic oscillations on the human brain cortex by Fourier transforming oxy/deoxy hyperspectral images. Hum Brain Mapp 2018; 39(9): 3558-73.
185. Legland D. Geodesic distances and geodesic diameters within 2D / 3D images. MATLAB Central File Exchange. 2017. https://www.mathworks.com/matlabcentral/fileexchange/36724-geodesic-distances-and-geodesic-diameters-within-2d-3d-images (accessed September, 29 2021).
186. Lakens D. Calculating and reporting effect sizes to facilitate cumulative science: a practical primer for t-tests and ANOVAs. Front Psychol 2013; 4: 863.
187. Cohen J. Statistical Power Analysis for the Behavioral Sciences (2nd Ed.). Hillsdale, NJ: Lawrence Erlbaum Associates; 1988.
188. Hayes AF. Introduction to Mediation, Moderation, and Conditional Process Analysis: A Regression-Based Approach (2nd Ed.): Guilford Press; 2017.
189. Asano E, Juhász C, Shah A, et al. Origin and propagation of epileptic spasms delineated on electrocorticography. Epilepsia 2005; 46(7): 1086-97.
190. Diehl B, Tkach J, Piao Z, et al. Diffusion tensor imaging in patients with focal epilepsy due to cortical dysplasia in the temporo-occipital region: electro-clinico-pathological correlations. Epilepsy Res 2010; 90(3): 178-87.
191. Najm IM, Tilelli CQ, Oghlakian R. Pathophysiological mechanisms of focal cortical dysplasia: a critical review of human tissue studies and animal models. Epilepsia 2007; 48 Suppl 2: 21-32.
192. Chassoux F, Devaux B, Landré E, et al. Stereoelectroencephalography in focal cortical dysplasia: a 3D approach to delineating the dysplastic cortex. Brain 2000; 123 (Pt 8): 1733-51.
193. Krsek P, Maton B, Jayakar P, et al. Incomplete resection of focal cortical dysplasia is the main predictor of poor postsurgical outcome. Neurology 2009; 72(3): 217-23.
194. Palmini A, Gambardella A, Andermann F, et al. Intrinsic epileptogenicity of human dysplastic cortex as suggested by corticography and surgical results. Ann Neurol 1995; 37(4): 476-87.
195. Otsubo H, Iida K, Oishi M, et al. Neurophysiologic findings of neuronal migration disorders: intrinsic epileptogenicity of focal cortical dysplasia on electroencephalography, electrocorticography, and magnetoencephalography. J Child Neurol 2005; 20(4): 357-63.
196. Pallud J, Le Van Quyen M, Bielle F, et al. Cortical GABAergic excitation contributes to epileptic

activities around human glioma. Sci Transl Med 2014; 6(244): 244ra89.
197. Campbell SL, Buckingham SC, Sontheimer H. Human glioma cells induce hyperexcitability in cortical networks. Epilepsia 2012; 53(8): 1360-70.
198. Shamji MF, Fric-Shamji EC, Benoit BG. Brain tumors and epilepsy: pathophysiology of peritumoral changes. Neurosurg Rev 2009; 32(3): 275-84; discussion 84-6.
199. Tandon N, Esquenazi Y. Resection strategies in tumoral epilepsy: is a lesionectomy enough? Epilepsia 2013; 54 Suppl 9: 72-8.
200. Cepeda C, Levinson S, Nariai H, et al. Pathological high frequency oscillations associate with increased GABA synaptic activity in pediatric epilepsy surgery patients. Neurobiol Dis 2020; 134: 104618.
201. Chen J, Chen X, Huang C, et al. Predictors of seizure recurrence in patients with surgery for focal cortical dysplasia: pairwise and network meta-analysis and trial sequential analysis. Childs Nerv Syst 2019; 35(5): 753-67.
202. Palmini A, Gambardella A, Andermann F, et al. Operative strategies for patients with cortical dysplastic lesions and intractable epilepsy. Epilepsia 1994; 35 Suppl 6: S57-71.
203. Van Gompel JJ, Rubio J, Cascino GD, Worrell GA, Meyer FB. Electrocorticography-guided resection of temporal cavernoma: is electrocorticography warranted and does it alter the surgical approach? J Neurosurg 2009; 110(6): 1179-85.
204. Gelinas JN, Battison AW, Smith S, Connolly MB, Steinbok P. Electrocorticography and seizure outcomes in children with lesional epilepsy. Childs Nerv Syst 2011; 27(3): 381-90.
205. Giulioni M, Rubboli G, Marucci G, et al. Seizure outcome of epilepsy surgery in focal epilepsies associated with temporomesial glioneuronal tumors: lesionectomy compared with tailored resection. J Neurosurg 2009; 111(6): 1275-82.
206. Wray CD, McDaniel SS, Saneto RP, Novotny EJ, Jr., Ojemann JG. Is postresective intraoperative electrocorticography predictive of seizure outcomes in children? J Neurosurg Pediatr 2012; 9(5): 546-51.
207. Frauscher B, von Ellenrieder N, Zelmann R, et al. High-Frequency Oscillations in the Normal Human Brain. Ann Neurol 2018; 84(3): 374-85.
208. Thompson B. Effect sizes, confidence intervals, and confidence intervals for effect sizes. Psychology in the Schools 2007; 44(5): 423-32.
209. Ryvlin P, Cross JH, Rheims S. Epilepsy surgery in children and adults. Lancet Neurol 2014; 13(11): 1114-26.
210. Lüders H, Awad I, Burgess R, Wyllie E, Van Ness P. Subdural electrodes in the presurgical evaluation for surgery of epilepsy. Epilepsy Res Suppl 1992; 5: 147-56.
211. Kuruvilla A, Flink R. Intraoperative electrocorticography in epilepsy surgery: useful or not? Seizure 2003; 12(8): 577-84.
212. Paulk AC, Salami P, Zelmann R, Cash SS. Electrode Development for Epilepsy Diagnosis and Treatment. Neurosurg Clin N Am 2024; 35(1): 135-49.
213. Shamas M, Yeh HJ, Fried I, Engel J, Jr., Staba RJ. High-rate leading spikes in propagating spike sequences predict seizure outcome in surgical patients with temporal lobe epilepsy. Brain Commun 2023; 5(6): fcad289.
214. Matarrese MAG, Loppini A, Fabbri L, et al. Spike propagation mapping reveals effective connectivity and predicts surgical outcome in epilepsy. Brain 2023; 146(9): 3898-912.
215. Alarcon G, Guy CN, Binnie CD, Walker SR, Elwes RD, Polkey CE. Intracerebral propagation of interictal activity in partial epilepsy: implications for source localisation. J Neurol Neurosurg Psychiatry 1994; 57(4): 435-49.
216. Hufnagel A, Dümpelmann M, Zentner J, Schijns O, Elger CE. Clinical relevance of quantified intracranial interictal spike activity in presurgical evaluation of epilepsy. Epilepsia 2000; 41(4): 467-78.
217. Zweiphenning WJEM, van Diessen E, Aarnoutse EJ, et al. The resolution revolution: Comparing spikes and high frequency oscillations in high-density and standard intraoperative electrocorticography of the same patient. Clin Neurophysiol 2020; 131(5): 1040-3.
218. Sun J, Barth K, Qiao S, et al. Intraoperative microseizure detection using a high-density micro-electrocorticography electrode array. Brain Commun 2022; 4(3): fcac122.
219. Fisher RS, Cross JH, French JA, et al. Operational classification of seizure types by the International League Against Epilepsy: Position Paper of the ILAE Commission for Classification and Terminology. Epilepsia 2017; 58(4): 522-30.
220. von Ellenrieder N, Beltrachini L, Perucca P, Gotman J. Size of cortical generators of epileptic interictal events and visibility on scalp EEG. Neuroimage 2014; 94: 47-54.
221. Bragin A, Mody I, Wilson CL, Engel J, Jr. Local generation of fast ripples in epileptic brain. J Neurosci 2002; 22(5): 2012-21.
222. Robertson FC, Ullrich NJ, Manley PE, Al-Sayegh H, Ma C, Goumnerova LC. The Impact of Intraoperative Electrocorticography on Seizure Outcome After Resection of Pediatric Brain Tumors: A Cohort Study. Neurosurgery 2019; 85(3): 375-83.
223. Englot DJ, Han SJ, Lawton MT, Chang EF. Predictors of seizure freedom in the surgical treatment of supratentorial cavernous malformations. J Neurosurg 2011; 115(6): 1169-74.
224. Sarnthein J, Neidert MC. A profile on the WISE cortical strip for intraoperative

neurophysiological monitoring. Expert Rev Med Devices 2024; 21(5): 373-9.
225. Dimakopoulos V, Neidert MC, Sarnthein J. Low impedance electrodes improve detection of high frequency oscillations in the intracranial EEG. Clin Neurophysiol 2023; 153: 133-40.
226. Sarnthein J, Seidel K, Neidert MC, et al. Evaluation of a new cortical strip electrode for intraoperative somatosensory monitoring during perirolandic brain surgery. Clin Neurophysiol 2022; 142: 44-51.
227. Zelmann R, Zijlmans M, Jacobs J, Chatillon CE, Gotman J. Improving the identification of High Frequency Oscillations. Clin Neurophysiol 2009; 120(8): 1457-64.
228. Petito GT, Housekeeper J, Buroker J, et al. Diurnal rhythms of spontaneous intracranial high-frequency oscillations. Seizure 2022; 102: 105-12.
229. Baumgartner C, Koren JP, Britto-Arias M, Zoche L, Pirker S. Presurgical epilepsy evaluation and epilepsy surgery. F1000Res 2019; 8.
230. Rathore C, Radhakrishnan K. Concept of epilepsy surgery and presurgical evaluation. Epileptic Disord 2015; 17(1): 19-31; quiz
231. Fitzgerald Z, Morita-Sherman M, Hogue O, et al. Improving the prediction of epilepsy surgery outcomes using basic scalp EEG findings. Epilepsia 2021; 62(10): 2439-50.
232. Jehi L, Yardi R, Chagin K, et al. Development and validation of nomograms to provide individualised predictions of seizure outcomes after epilepsy surgery: a retrospective analysis. Lancet Neurol 2015; 14(3): 283-90.
233. Sanders MW, Van der Wolf I, Jansen FE, et al. Outcome of Epilepsy Surgery in MRI-Negative Patients Without Histopathologic Abnormalities in the Resected Tissue. Neurology 2024; 102(4): e208007.
234. Sheikh S, Jehi L. Predictive models of epilepsy outcomes. Curr Opin Neurol 2024; 37(2): 115-20.
235. Tveit J, Aurlien H, Plis S, et al. Automated Interpretation of Clinical Electroencephalograms Using Artificial Intelligence. JAMA Neurol 2023; 80(8): 805-12.
236. Morita-Sherman M, Li M, Joseph B, et al. Incorporation of quantitative MRI in a model to predict temporal lobe epilepsy surgery outcome. Brain Commun 2021; 3(3): fcab164.
237. Gerard IJ, Kersten-Oertel M, Hall JA, Sirhan D, Collins DL. Brain Shift in Neuronavigation of Brain Tumors: An Updated Review of intraoperative Ultrasound Applications. Front Oncol 2020; 10: 618837.
238. Bayer S, Maier A, Ostermeier M, Fahrig R. Intraoperative Imaging Modalities and Compensation for Brain Shift in Tumor Resection Surgery. Int J Biomed Imaging 2017; 2017: 6028645.
239. West TR, Mazurek MH, Perez NA, et al. Navigated Intraoperative Ultrasound Offers Effective and Efficient Real-Time Analysis of Intracranial Tumor Resection and Brain Shift. Oper Neurosurg 2025; 28(2): 148-58.
240. Shimamoto T, Sano Y, Yoshimitsu K, Masamune K, Muragaki Y. Precise Brain-shift Prediction by New Combination of W-Net Deep Learning for Neurosurgical Navigation. Neurol Med Chir (Tokyo) 2023; 63(7): 295-303.
241. Li C, Evans LT, Hong J, et al. Fully automated image updating for brain shift compensation after dural opening. J Neurosurg 2025: 1-11.
242. Skrinjar O, Nabavi A, Duncan J. Model-driven brain shift compensation. Med Image Anal 2002; 6(4): 361-73.
243. Zhuang DX, Liu YX, Wu JS, et al. A sparse intraoperative data-driven biomechanical model to compensate for brain shift during neuronavigation. AJNR Am J Neuroradiol 2011; 32(2): 395-402.
244. Haegelen C, Perucca P, Châtillon CE, et al. High-frequency oscillations, extent of surgical resection, and surgical outcome in drug-resistant focal epilepsy. Epilepsia 2013; 54(5): 848-57.
245. Liu Y, Wang Z, Jiao Y, et al. Flexible, high-density, laminated ECoG electrode array for high spatiotemporal resolution foci diagnostic localization of refractory epilepsy. Bio-Design and Manufacturing 2024; 7(4): 388-98.
246. Chiang CH, Wang C, Barth K, et al. Flexible, high-resolution thin-film electrodes for human and animal neural research. J Neural Eng 2021; 18(4).
247. Chinedu-Eneh EO, Chiang S, Andrews JP, et al. Influences of electrode density on intracranial seizure localisation: a single-blinded randomised crossover study. EBioMedicine 2025; 113: 105606.
248. Cai Z, Sohrabpour A, Jiang H, et al. Noninvasive high-frequency oscillations riding spikes delineates epileptogenic sources. Proc Natl Acad Sci U S A 2021; 118(17).
249. Jahromi S, Matarrese MAG, Fabbri L, et al. Overlap of spike and ripple propagation onset predicts surgical outcome in epilepsy. Ann Clin Transl Neurol 2024; 11(10): 2530-47.
250. Fabbri L, Matarrese MAG, Jahromi S, et al. Spikes on ripples are better interictal biomarkers of epilepsy than spikes or ripples. Brain Commun 2025; 7(1): fcaf056.
251. Nevalainen P, von Ellenrieder N, Klimeš P, Dubeau F, Frauscher B, Gotman J. Association of fast ripples on intracranial EEG and outcomes after epilepsy surgery. Neurology 2020; 95(16): e2235-e45.

252. Sun D, Schaft EV, van Stempvoort BM, et al. Intraoperative mapping of epileptogenic foci and tumor infiltration in neuro-oncology patients with epilepsy. Neurooncol Adv 2024; 6(1): vdae125.
253. Slegers RJ, Blumcke I. Low-grade developmental and epilepsy associated brain tumors: a critical update 2020. Acta Neuropathol Commun 2020; 8(1): 27.
254. Staba RJ, Wilson CL, Bragin A, Fried I, Engel J, Jr. Quantitative analysis of high-frequency oscillations (80-500 Hz) recorded in human epileptic hippocampus and entorhinal cortex. J Neurophysiol 2002; 88(4): 1743-52.
255. Liu S, Quach MM, Curry DJ, Ummat M, Seto E, Ince NF. High-frequency oscillations detected in ECoG recordings correlate with cavernous malformation and seizure-free outcome in a child with focal epilepsy: A case report. Epilepsia Open 2017; 2(2): 267-72.
256. Bénar CG, Chauvière L, Bartolomei F, Wendling F. Pitfalls of high-pass filtering for detecting epileptic oscillations: a technical note on "false" ripples. Clin Neurophysiol 2010; 121(3): 301-10.
257. Gliske SV, Irwin ZT, Chestek C, Stacey WC. Effect of sampling rate and filter settings on High Frequency Oscillation detections. Clin Neurophysiol 2016; 127(9): 3042-50.
258. Orihara A, Hara K, Hara S, et al. Effects of sevoflurane anesthesia on intraoperative high-frequency oscillations in patients with temporal lobe epilepsy. Seizure 2020; 82: 44-9.
259. Barkmeier DT, Shah AK, Flanagan D, et al. High inter-reviewer variability of spike detection on intracranial EEG addressed by an automated multi-channel algorithm. Clin Neurophysiol 2012; 123(6): 1088-95.
260. Nariai H, Wu JY, Bernardo D, Fallah A, Sankar R, Hussain SA. Interrater reliability in visual identification of interictal high-frequency oscillations on electrocorticography and scalp EEG. Epilepsia Open 2018; 3(Suppl Suppl 2): 127-32.
261. Sharifshazileh M, Burelo K, Sarnthein J, Indiveri G. An electronic neuromorphic system for real-time detection of high frequency oscillations (HFO) in intracranial EEG. Nature Communications 2021; 12(1): 3095.
262. Costa F, Schaft EV, Huiskamp G, et al. Robust compression and detection of epileptiform patterns in ECoG using a real-time spiking neural network hardware framework. Nat Commun 2024; 15(1): 3255.
263. de Tisi J, Bell GS, Peacock JL, et al. The long-term outcome of adult epilepsy surgery, patterns of seizure remission, and relapse: a cohort study. Lancet 2011; 378(9800): 1388-95.
264. Ferreira-Atuesta C, de Tisi J, McEvoy AW, et al. Predictive models for starting antiseizure medication withdrawal following epilepsy surgery in adults. Brain 2023; 146(6): 2389-98.
265. Wu Y, Zhang Z, Liang P, et al. Early antiseizure medication withdrawal and risk of seizure recurrence in children after epilepsy surgery: A retrospective study. Epilepsy Behav 2024; 150: 109556.
266. Terman SW, Slinger G, Rheaume CE, et al. Antiseizure Medication Withdrawal Practice Patterns: A Survey Among Members of the American Academy of Neurology and EpiCARE. Neurol Clin Pract 2023; 13(1): e200109.
267. Terman SW, van Griethuysen R, Rheaume CE, et al. Antiseizure medication withdrawal risk estimation and recommendations: A survey of American Academy of Neurology and EpiCARE members. Epilepsia Open 2023; 8(2): 386-98.
268. Gloss D, Pargeon K, Pack A, et al. Antiseizure Medication Withdrawal in Seizure-Free Patients: Practice Advisory Update Summary: Report of the AAN Guideline Subcommittee. Neurology 2021; 97(23): 1072-81.
269. Choi SA, Kim SY, Kim WJ, et al. Antiepileptic Drug Withdrawal after Surgery in Children with Focal Cortical Dysplasia: Seizure Recurrence and Its Predictors. J Clin Neurol 2019; 15(1): 84-9.
270. Ngan Kee N, Foster E, Marquina C, et al. Systematic Review of Cost-Effectiveness Analysis for Surgical and Neurostimulation Treatments for Drug-Resistant Epilepsy in Adults. Neurology 2023; 100(18): e1866-e77.
271. Maas L, Kellenaers J, van Mastrigt G, et al. Societal costs and quality of life analysis in patients undergoing resective epilepsy surgery: A one-year follow-up. Epilepsy Behav Rep 2023; 24: 100635.
272. Kellenaers JTF, Rijkers K, van Mastrigt G, et al. Resective Epilepsy Surgery, QUality of life and Economic evaluation (RESQUE): the change in quality of life after resective epilepsy surgery-protocol for a multicentre, prospective cohort study. BMJ Open 2023; 13(7): e064263.

Nederlandse samenvatting

Wereldwijd hebben ongeveer 50 miljoen mensen epilepsie. Bij epilepsie ontstaat er een verstoring van de elektrische activiteit in de hersenen, wat kan leiden tot aanvallen. Voor een deel van de mensen met epilepsie werken medicijnen onvoldoende. Voor hen kan epilepsiechirurgie een mogelijke genezende behandeling zijn. Het doel van epilepsiechirurgie is het bereiken van levenslange aanvalsvrijheid. Op basis van gepubliceerde gegevens ligt het percentage patiënten dat aanvalsvrij wordt na een operatie tussen de 36 en 76%, wat laat zien dat er ruimte is voor verbetering.

Bij epilepsiechirurgie is het essentieel om de epileptogene zone volledig te verwijderen: het hersengebied dat verantwoordelijk is voor het ontstaan van de aanvallen. Het nauwkeurig lokaliseren van deze zone is lastig en gebeurt voorafgaand aan de operatie met verschillende onderzoeken, zoals een EEG, MRI en soms aanvullende geavanceerde beeldvorming. Op basis van deze onderzoeken wordt een operatieplan gemaakt. Tijdens de operatie kan dit plan worden gecontroleerd en zo nodig aangepast met behulp van intraoperatieve electrocorticografie (ioECoG), waarbij hersenactiviteit direct van het hersenoppervlak wordt gemeten. Deze signalen worden tijdens de operatie direct beoordeeld. Hierbij wordt traditioneel vooral gekeken naar twee typen afwijkende signalen, zogenaamde biomarkers: interictale pieken en hoog frequente oscillaties (HFOs). Interictale pieken zijn korte, plotselinge ontladingen van zenuwcellen die wijzen op een verhoogde prikkelbaarheid van het hersenweefsel. HFOs zijn zeer snelle ritmische ontladingen in hoge frequenties (boven de 80Hz). Hierbij wordt onderscheid gemaakt tussen ripples (80-250Hz) en fast ripples (250-500Hz). Over het gebruik en de klinische betekenis van pieken en HFOs bestaat nog veel discussie. Deze discussie gaat zowel over welke biomarker geschikt is voor welke patiënt, als over hoe signalen het best gemeten en geïnterpreteerd kunnen worden.

Dit proefschrift onderzoekt het potentieel van ioECoG verder dan alleen de traditionele visuele beoordeling en heeft als doel bij te dragen aan een nauwkeurigere, efficiëntere en meer geautomatiseerde afbakening van de epileptogene zone. Daarbij wordt gefocust op twee complementaire thema's: geavanceerde signaalanalyse van ioECoG en de interpretatie van ioECoG, inclusief de klinische implementatie van hoge resolutie grids.

In **Hoofdstuk 2** bestudeerden we hoe interictale pieken en HFOs zich in de tijd tot elkaar verhouden en wanneer zij gelijktijdig voorkomen. Door uitsluitend patiënten te bestuderen die aanvalsvrij zijn na de operatie, kan het verwijderde weefsel worden beschouwd als het weefsel dat verantwoordelijk was voor het ontstaan van de aanvallen. In dit onderzoek vonden we dat vooral gelijktijdig voorkomende interictale pieken en ripples vaker aanwezig zijn in het verwijderde, epileptische weefsel. Daarnaast bleken ook subtiele tijdskenmerken van deze signalen, zoals het moment waarop zij optreden, informatie te geven over welk hersenweefsel epileptisch is.

In **Hoofdstuk 3** en **Hoofdstuk 4** onderzochten we of specifieke signaalkarakteristieken van het ioECoG kunnen helpen bij het herkennen van epileptisch weefsel. In **Hoofdstuk 3** onderzochten we of de variatie in complexiteit van het ioECoG, berekend als spectrale entropie, samenhangt met het resultaat van epilepsiechirurgie. We vonden dat deze maat zowel informatie

bevat om epileptisch weefsel te onderscheiden van gezond weefsel, als informatie over de kans op aanvalsvrijheid na de operatie. In **Hoofdstuk 4** is met behulp van kunstmatige intelligentie onderzocht welke frequentiecomponenten van het ioECoG bijdragen aan het onderscheiden van epileptisch en niet-epileptisch weefsel. Hierbij vonden we dat bepaalde veranderingen in het achtergrondsignaal, die niet direct met het blote oog zichtbaar zijn, toch informatief kunnen zijn. Waar we in **Hoofdstuk 2** en **Hoofdstuk 4** gebruik maakten van ioECoG wat gemeten was voorafgaand aan het verwijderen van het epileptisch weefsel en enkel van patiënten die aanvalsvrij zijn, gebruiken we in **Hoofdstuk 3** zowel het ioECoG gemeten voorafgaand aan als na het verwijderen van het epileptisch weefsel. Deze patiëntenpopulatie bevat zowel aanvalsvrije patiënten als patiënten die na de operatie nog aanvallen hebben.

In **Hoofdstuk 5** bekeken we of de manier waarop ioECoG-signalen worden weergegeven invloed heeft op het herkennen van interictale pieken en HFOS. We vergeleken verschillende weergaven van hetzelfde ioECoG-signaal en keken hoe goed de verschillende biomarkers zichtbaar waren. Hierbij vonden we dat de keuze van montage een grote invloed heeft op wat wel en niet wordt gezien, en dat sommige montages geschikter zijn dan andere voor het herkennen van specifieke biomarkers. Dit benadrukt dat de interpretatie van ioECoG niet alleen afhangt van het signaal zelf, maar ook van hoe het wordt gepresenteerd.

In **Hoofdstuk 6** bestudeerden we de relatie tussen de locatie van de afwijking op MRI beelden met de locatie van ioECoG-biomarkers. Hierbij vonden we dat deze relatie verschilt per onderliggende hersenaandoening. Dit benadrukt het belang van een gepersonaliseerde interpretatie van ioECoG. In **Hoofdstuk 7** beschrijven we de klinische implementatie van hoge resolutie grids om ioECoG metingen te doen. Deze grids bevatten vier keer zoveel elektroden als de traditionele grids (lage resolutie). Door gebruik te maken van deze grids worden er meer biomarkers gemeten, in het bijzonder de fast ripples, en kunnen spreidingspatronen van interictale pieken gedetailleerd in kaart worden gebracht.

De resultaten van dit proefschrift laten zien dat ioECoG waardevolle informatie kan bieden tijdens epilepsiechirurgie, maar dat geen enkele biomarker of methode op zichzelf voldoende is om epileptisch weefsel eenduidig te identificeren. Zowel interictale pieken, HFOs als meer subtiele signaalkarakteristieken verschillen in betekenis tussen patiënten en onderliggende hersenaandoeningen. Daarnaast wordt de interpretatie van ioECoG beïnvloed door technische keuzes, zoals de manier van meten en weergeven, en door praktische factoren in de operatiekamer. Door geavanceerde signaalanalyse te combineren met klinische expertise en door nieuwe meetmethoden, zoals hoge resolutie grids, zorgvuldig te implementeren, kan ioECoG zich ontwikkelen tot een meer objectief en reproduceerbaar hulpmiddel. Deze ontwikkelingen bieden perspectief op een verdere verbetering van epilepsiechirurgie, met als uiteindelijk doel een grotere kans op aanvalsvrijheid.

Dankwoord

Daar is ie dan: het laatste, maar waarschijnlijk meest gelezen, hoofdstuk van dit proefschrift. Een proefschrift schrijven doe je (gelukkig) niet alleen. Ik wil iedereen bedanken die, op wat voor manier dan ook, heeft bijgedragen aan het tot stand komen van dit proefschrift.

Ten eerste wil ik alle patiënten bedanken die meewerken aan wetenschappelijk onderzoek en toestemming hebben gegeven om hun gegevens te gebruiken.

Beste prof. dr. Zijlmans, lieve **Maeike**, dank voor je eindeloze enthousiasme voor bestaande en nieuwe onderzoeksideeën. Jij bent een enorme inspiratiebron als het gaat om zowel het bedenken van nieuwe projecten, het uitwerken van ideeën en omzetten naar concrete plannen, het altijd blijven zoeken naar de Schaft-biomarker en het opzetten van het hele EpiLab inclusief alle samenwerkingen daaromheen. Dank dat ik me bij jullie mocht aansluiten en onderdeel mocht zijn van de groei van een kleine club naar het lab zoals het er nu staat. Ook wil ik je bedanken voor het altijd steunen en dat je achter me bleef staan bij de uitbreiding van mijn klinische werkzaamheden en de logistieke uitdagingen die daarbij kwamen kijken.

Beste prof. dr. Ramsey, lieve **Nick**, jij stond iets verder van mijn onderzoeken af, maar dat betekende niet dat ik niet altijd bij je terecht kon. Jouw deur stond altijd open. In onze meetings kwamen jouw helicopterview en kritische blik altijd tot uiting. Ik bewonder je vermogen om te zien hoe een artikel beter leesbaar kan worden, jouw feedback op mijn conceptversies was altijd zeer constructief. Dankjewel voor het af en toe op de rem trappen en mij in te laten zien dat een artikel al ruim voldoende is.

Beste dr. van 't Klooster, lieve **Maryse**, dank voor je steun en begeleiding in de afgelopen jaren. Jij hebt mij vanaf het begin uitgedaagd om kritisch te blijven, de moeilijke dingen niet uit de weg te gaan en mijn eigen keuzes te maken. Dat ging niet altijd meteen goed, maar jij bleef mij steunen en helpen tot het wel lukte. Door jouw inzet en open deur heb ik mij kunnen ontwikkelen tot een zelfstandig onderzoeker en weet ik wat het allerbelangrijkste is: *always check your data*! In de loop van de jaren zijn we steeds meer collega's geworden in plaats van leerling en begeleider en de gesprekken en discussies die we nu kunnen hebben, vind ik enorm waardevol.

Ik wil de leden van de beoordelingscommissie, prof. dr. **Dennis Klomp**, prof. dr. **Pierre Robe**, prof. dr. **Kees Braun**, prof. dr. **Arjan Hillebrand** en dr. **Else Tolner**, bedanken voor het kritisch lezen en beoordelen van mijn proefschrift.

I would like to thank all **co-authors** for their collaboration on all the various projects and for their inspiring new ideas. Ook wil ik alle **studenten**, die ik heb mogen begeleiden, bedanken voor hun inspiratie en inzet.

Lieve **collega's van de KNF**, zonder jullie hulp was dit proefschrift er niet geweest. Velen van jullie hebben geholpen door het uitvoeren en zorgvuldig vastleggen van corticografie metingen, het meedenken en opzetten van nieuwe ideeën, maar ook voor heel veel gezelligheid. Ik heb me altijd thuis gevoeld bij jullie. **Sandra** en **Nizare**, geen KNF-afdeling zonder jullie keiharde werk en inzet. Ik bewonder hoe

jullie je samen bewegen in het ingewikkelde politieke veld en tegelijkertijd je altijd hard maken voor 'jullie' mensen. **Sandra**, ik heb genoten van onze OKs samen, de gezelligheid, de verbouw/nieuwbouw-struggles, en het delen van de verhalen van thuis. **Nizare**, we hebben veel te veel tijd besteed aan het correct invoeren of (keer op keer) aanpassen van mijn uren, maar dit zorgde wel voor een bijzondere band. Jij stond altijd voor me klaar en hebt je altijd hard gemaakt voor mijn plek in Utrecht, dankjewel daarvoor! **Frans**, jij hebt een enorm grote kennis van de neurologie en ik heb je altijd bewonderd hoe je dit in alle rust aan iedereen kan overbrengen. Dank voor je vertrouwen in mij in de kliniek en de gezelligheid op de OK (met af en toe een lege batterij van je fototoestel ;)). **Cyrille**, jij weet muziek, koken en de neurologie met elkaar te verbinden alsof het de normaalste zaak van de wereld is. Ik heb genoten van al onze gesprekken over eten, jouw kookvideo's en de proeverijen van de probeersels! **Ella**, wij konden bij elkaar de mooiste mode-trends (blauwe OK pakken) showen. Dank voor je warmte en gezelligheid! **Nicole**, jij bent een TGer in hart en nieren en de drijvende kracht achter innovatie op de KNF. **Geertjan**, jouw technische kennis gaat veel verder dan EEG. Jouw visie geeft altijd een interessant perspectief hoe je ook naar data kan kijken. **Nicole** en **Geertjan**, bij jullie kon ik altijd terecht voor een goede discussie over metingen, artefacten en resultaten. Dank voor al jullie kennis en gezelligheid! **Tineke**, **Meryem**, **Bert**, **Barbara**, **Raquelle** en alle andere KNF laboranten, zonder jullie zouden er geen corticografie metingen zitten in de database. Dank ook voor de hulp bij het opzetten en uitdenken en uitvoeren van de high-density studie en natuurlijk de gezelligheid! **Janine** en **Miranda**, jullie lopen hard voor elke patiënt. Ik wil jullie bedanken voor het informeren en includeren van al deze patiënten voor de RESPect database.

Graag wil ik de neurochirurgen, **Peter**, **Pieter** en **Friso**, bedanken voor alle hulp bij het onderzoek, jullie geduld bij nieuwe of extra metingen, maar ook zeker voor alle gezelligheid op de OK.

Veel dank aan de **BCI-onderzoeksgroep**. We konden altijd bij elkaar terecht voor het delen van kennis, het uitwisselen van materialen en handjes op de OK.

Lieve **EpiLab collega's**, ik had nooit kunnen bedenken dat we nu met zo'n grote groep zouden zijn. Dat is alleen mogelijk door de inzet en het enthousiasme van ieder van jullie. Allereerst the founders of the RESPect database, **Matteo**, **Dorien** en **Willemiek**, jullie hadden een visie op onderzoek en hebben deze helemaal uitgewerkt. Daar profiteert iedereen binnen EpiLab nu van. Wat jullie in gang hebben gezet, zorgt voor een enorm waardevolle database, waardoor iedereen met een enorme boost aan zijn of haar project kan beginnen. **Matteo**, your influence as computer scientist is still present. Instead of logical names for annotations, we still use xxx; and yyy; to annotate artefacts ;). Dorien, jouw goed georganiseerde manier van scripten heeft mij geïnspireerd en jouw stijl herken je nu ook terug in mijn scripts. Jij bent een geboren onderzoeker en ik hoop dat er een moment komt waarop je dit weer kan laten zien. **Willemiek**, jouw werk aan HFO detectors, connectiviteitsmaten en functionele netwerken is indrukwekkend. Dank voor het sparren over ideeën, methodes en resultaten. Ik ben benieuwd of onze systematic review er ooit nog eens komt! **Lotte**, jouw gezelligheid was vanzelfsprekend als ik in het WKZ was. Dank voor de vele borrels en de goede gesprekken. Ik bewonder je doorzettingsvermogen: ook als het niet lukt via plan A of B, ga jij gewoon door met C. En nu zit je helemaal op je plek in de opleiding tot neuroloog, echt heel tof om te zien! **Sem**, je kwam binnen als M2'er, en door corona hebben we elkaar in

die tijd nooit fysiek gezien. Bij jouw start als M3 voelde ik meteen een klik, en die is nooit meer weggegaan. Ik heb je zien groeien van een broekie-student naar een ervaren onderzoeker, iets wat ik met veel plezier heb mogen volgen. Inmiddels zijn we vrienden geworden en kunnen we overal over praten. Ik ga onze koffietjes missen! **Susanne** en **Irene**, de stimulatie-koninginnen van het EpiLab! Dank voor jullie gezelligheid en warmte, het was altijd fijn om bij jullie binnen te stappen. Jullie zijn niet alleen ontzettend kundig, maar ook ondernemend, altijd in voor nieuwe ideeën en plannen.
亲爱的 **Ziyi 和 JiaoJiao**，感谢你们在那些无穷无尽的 spike 和 HFO 标注工作中的巨大投入。你们似乎从未感到疲倦，永远斗志激昂。随着时间的推移，你们掌握了令人印象深刻的技术能力，并真正成长为优秀的研究人员。除此之外，你们也让我们对中国文化和美食有了美好的了解（我不会忘记月饼！）。 **而从我**们的角度来说，我们也把你们**"培养"成了真正的中荷混合体** （Chinese-Dutchies）。**我真心希望未来我**们还能再次相遇。祝愿你们在美国，或世界上任何地方的发展道路上一切顺利，前程似锦。
Lieve **allemaal**, gelukkig hebben we de reünietjes nog!

Lieve **Tessa**, soms hadden we veel contact en dan weer een hele tijd niet, maar als we elkaar spraken was het altijd gezellig en inspirerend. Ik denk met veel plezier terug aan de brainstormsessie bij jou thuis en de fijne gesprekken die we daar hebben gehad. Wij gaan nog wel eens samenwerken in de toekomst!

Lieve **nieuwe collega's in het LUMC**, dank voor het warme bad waar ik in terecht ben gekomen. Ik kijk uit naar onze verdere samenwerking in de toekomst!

Lief bestuur, **Tom**, **Inge**, **Max**, **Patrick** en **Fokke**, door het jaar heen zien we elkaar niet veel, maar ons jaarlijkse weekend weg is altijd geslaagd! Het is mooi om te zien hoe wij ons als groep hebben ontwikkeld en hoe een ieder zijn of haar eigen pad heeft gevolgd. Op naar de volgende 15 jaar!

Lieve **Judith**, **Machteld**, **Mathijs**, we hebben elkaar leren kennen in Enschede, maar ik ben heel blij dat onze vriendschap er nog steeds is! **Judith**, van samenwonen in een huis naar nu allebei mama, bijzonder om die fases samen mee te maken. Ondanks dat we niet bij elkaar om de hoek wonen, sta jij altijd voor mij klaar. Of het nu is om met de kids af te spreken of samen een biertje drinken in de kroeg, met jou is het altijd goed. **Machteld**, ik ben heel blij dat we elkaar weer hebben gevonden. Onze gesprekken zijn altijd waardevol en ik kan echt overal met je over praten. **Mathijs**, op heel veel manieren hebben we korte linkjes met elkaar, heel leuk! Van vrienden vanuit Enschede, meekijken met elkaar op werk, tot samenwerken aan NVvTG projecten. Maar ook privé weten we elkaar altijd weer te vinden, in goede maar zeker ook in mindere tijden.

Lieve vrienden van Vic, die voor mij ook heel belangrijk zijn geworden. **Danny** en **Jelma**, **Rutger** en **Vivian**, **Niels** en **Hannah**, **Stijn** en **Julia**, er zijn een hoop overeenkomsten in onze vriendschappen: lekker eten, goede gesprekken, veel spelletjes, weekendjes weg en bovenal een heleboel gezelligheid! Dankjewel dat jullie altijd voor ons klaar staan.

Lieve **Willemijn**, **Lisanne** en **Marian**, al vriendinnetjes vanaf de middelbare school en nu hebben we alle vier kids en wonen we ook nog steeds dicht bij elkaar. Jullie zijn lief, grappig, eigenwijs en we kunnen heerlijk lange gesprekken met elkaar hebben. Ik vind het fijn dat ik altijd op jullie kan rekenen. **Willemijn**, bij biologie bij meneer Moerman klikte het meteen. Jij en ik waren 'meant to be'.

We zijn enorm verschillend, wat er grappig genoeg voor zorgt dat we weer heel goed bij elkaar passen. Ik vind het knap hoe jij echt je eigen pad hebt gekozen en kijk eens waar je nu staat: mama van drie prachtige kids en een goedlopend eigen bedrijf, jij bent echt een powervrouw! **Lisanne**, jij laat je echt nergens door tegenhouden en blijft altijd doorgaan, zeker voor alle lieve mensen om je heen, ook al is dat niet altijd even makkelijk. Jouw FOMO helpt je hier niet altijd bij. ;) Bij jou kon ik mijn PhD-struggles kwijt en ik vind het knap hoe jij bepaalde keuzes durft te maken die goed zijn voor jou. **Marian**, we zien elkaar niet altijd veel, maar de momenten samen zijn heel fijn. Jij hebt altijd gelijk door hoe ik me voel en hier kan ik op een hele fijne manier met je over praten. **Lieverds**, ik kijk uit naar wat we nog allemaal gaan beleven, samen met én samen zonder kids.

Lieve **Dongqing** en **Sarah**, mijn PhD-buddies vanaf het begin. Ik vind het heel bijzonder en waardevol hoe wij in de afgelopen jaren zulke goede vriendinnen zijn geworden. Jullie stonden altijd voor mij klaar en trokken me erdoorheen als het even niet zo lekker liep met de PhD. Jullie moedigen mij aan om me verder te ontwikkelen en om grenzen te verleggen. Jullie zijn de besten om een verhelderende blik te laten schijnen op moeilijke situaties. Ik vind het een eer dat jullie als paranimfen naast mij staan vandaag, want niet alleen op werk, maar ook als vriendinnen betekenen jullie veel voor mij. Ik geniet van onze etentjes samen en alle andere dingen die we samen ondernemen.

Lieve **Madeleine**, **Frans**, **Roland**, **Wonneke** en **Max**, ik vind het bijzonder dat jullie niet meer als schoonfamilie voelen, maar echt als familie. Jullie hebben mij in jullie hart gesloten en ik jullie in die van mij. Ik mag mezelf zijn bij jullie en geniet van de momenten samen.

Lieve **papa**, **mama** en **Jacco**, 't gezinnetje, dankzij jullie heb ik de keuzes kunnen maken die ik heb gemaakt. Jullie lieten mij vrij in welke kant ik op wilde gaan en steunden me in de beslissingen die ik nam (ook al twijfelden jullie soms aan sommige van deze beslissingen ;)). Lieve **papa**, jij was niet van het opscheppen over je kinderen, maar soms maakte je er toch even gebruik van dat Jacco en ik het zo goed deden. Ik weet dat je supertrots zou zijn dat ik hier vandaag sta en ik vind het heel jammer dat je dit niet mee mag maken. Ik mis je. Lieve **mama**, ik hoor heel regelmatig hoeveel wij op elkaar lijken en dat maakt me trots: zo'n krachtige, lieve vrouw die alles doet voor iedereen van wie ze houdt, daar wil ik graag op lijken! Van jouw doorzettingsvermogen kunnen velen nog wat leren. Ik ben blij dat je **Hans** hebt gevonden en geniet ervan om jullie samen te zien. Lieve **Jaccie**, wij zijn pas later echt naar elkaar toegetrokken en nu kunnen we echt op elkaar aan. We komen graag bij elkaar over de vloer en kunnen goede gesprekken voeren over de lastige dingen in het leven. In **Stella** heb je een super leuke, lieve en gezellige meid gevonden en ik kijk uit naar wat de toekomst jullie brengt!

En dan de allerbelangrijkste: **Vic** en **Frey**. Bij jullie ben ik thuis. Lieve **Vic**, jij bent mijn maatje in alles en staat altijd achter me. Ik geniet van alle avonturen die we samen beleven en opzoeken, van gewoon samen op de bank, samen koken of lekker uit eten tot wilde avonturen op reis, tot het bouwen van een heel huis en nu een gigantische renovatie van ons nieuwe huis. Lieve **Frey**, jij bent de liefste boef die ik ken en ik geniet er enorm van om jouw mama te zijn. Lieve **mannen**, ik kijk uit naar wat we nog allemaal samen mogen beleven. Ik hou van jullie.

List of publications

This thesis

Spatial and temporal properties of intraoperatively recorded spikes and high frequency oscillations in focal cortical dysplasia
E.V. Schaft, D. Sun, M.A. van 't Klooster, D. van Blooijs, P.L. Smits, W.J.E.M. Zweiphenning, P.H. Gosselaar, C.H. Ferrier, M. Zijlmans
Clinical neurophysiology, Volume 162, June 2024

Explainable artificial intelligence unveils (non-) epileptiform spectral powers in intraoperative electrocorticography
S. Hoogteijling, **E.V. Schaft**, E.H.M. Dirks, S. Straumann, M. Demuru, P. van Eijsden, T.A. Gebbink, W.M. Otte, G.J.M. Huiskamp, M.A. van 't Klooster, M. Zijlmans,
Clinical neurophysiology, Volume 167, November 2024

Spectral entropy variability of intraoperative electrocorticography predicts outcome after epilepsy surgery in patients with focal cortical dysplasia
E.V. Schaft, S. Hoogteijling, D. Sun, C.H. Ferrier, P. van Eijsden, W.M. Otte, G. Anguelova, N.F. Ramsey, M.A. van 't Klooster, M. Zijlmans
Accepted in Epilepsia, January 2026

The optimal montage to mark epileptiform discharges and high frequency oscillations in intraoperative electrocorticography
Z. Wang*, J. Guo*, **E.V. Schaft**, S. Hoogteijling, C.H. Ferrier, G.H. Visser, D. Sun, F.W.A. Hoefnagels, T. Inada, S.M.A. van der Salm, G.J.M. Huiskamp, N.E.C. van Klink, M.A. van 't Klooster, M. Zijlmans
Clinical Neurophysiology Practice, Volume 10, July 2025

The spatial relationship between the MRI lesion and intraoperative electrocorticography in focal epilepsy surgery
S. Straumann, **E.V. Schaft**, H.J. Noordmans, J.W. Dankbaar, W.M. Otte, J. van Steenis, P.L. Smits, W.J.E.M. Zweiphenning, P. van Eijsden, T.A. Gebbink, L. Mariani, M.A. van 't Klooster, M. Zijlmans
Brain Communications, Volume 4, Issue 6, November 2022

Implementing intraoperative high-density electrocorticography during epilepsy surgery
E.V. Schaft*, D. Sun*, S. Hoogteijling, Z. Wang, F.S.S. Leijten, P. van Eijsden, N.F. Ramsey, P.A.J.T. Robe, M.A. van 't Klooster, M. Zijlmans
Epilepsia, Volume 66, Issue 5, February 2025

** These authors contributed equally*

Other

Value of machine learning in predicting TAVI outcomes
R. R. Lopes, M. S. van Mourik, **E.V. Schaft**, L. A. Ramos, J. Baan, J. Vendrik, B.A.J.M. de Mol, M.M. Vis. H.A. Marquering
Netherlands Heart Journal, Volume 27, May 2019

Spikes and High Frequency Oscillations in Lateral Neocortical Temporal Lobe Epilepsy: Can They Predict the Success Chance of Hippocampus-Sparing Resections?
A. Maccabeo, M.A. van 't Klooster, **E.V. Schaft**, M. Demuru, W.J.E.M. Zweiphenning, P.H. Gosselaar, T. Gebbink, W.M. Otte, M. Zijlmans
Frontiers in Neurology, Volume 13, August 2022

Signaalkarakteristieken in mensen met een focale corticale dysplasie
E.V. Schaft, M.A. van 't Klooster, M. Zijlmans
Epilepsie, periodiek voor professionals, September 2022

Robust compression and detection of epileptiform patterns in ECoG using a real-time spiking neural network hardware framework
F. Costa, **E.V. Schaft**, G.J.M. Huiskamp, E.J. Aarnoutse, M.A. van't Klooster, N. Krayenbühl, G. Ramantani, M. Zijlmans, G. Indiveri, J. Sarnthein
Nature Communications, Volume 15, April 2024

Intraoperative mapping of epileptogenic foci and tumor infiltration in neuro-oncology patients with epilepsy
D. Sun, **E.V. Schaft**, B.M. van Stempvoort, T.A. Gebbink, M.A. van 't Klooster, P. van Eijsden, S.M.A. van der Salm, J.W. Dankbaar, M. Zijlmans, P.A.J.T. Robe
Neuro-Oncology Advances, Volume 6, Issue 1, July 2024

Op de millimeter: ontwikkelingen in intraoperatieve ECoG bij epilepsiechirurgie
S. Hoogteijling, **E.V. Schaft**, D. Sun, C. Gelpke, M.A. van 't Klooster, M. Zijlmans
Epilepsie, periodiek voor professionals, December 2025

Multi-montage visualization of interictal epileptic events in high-density intraoperative electrocorticography
J. Guo, Z. Wang, N.E.C. van Klink, **E.V. Schaft**, D. Sun, S.M.A. van der Salm, M.A. van 't Klooster, M. Zijlmans
Clinical Neurophysiology Practice, Volume 11, December 2025

Advancing intraoperative brain mapping: First-in-human evaluation of flexible high-density electrocorticography grids for epilepsy surgery
S. Hoogteijling, C. Gelpke, **E.V. Schaft**, Z. Wang, T. Souhoka, P. van Eijsden, A. Diop, K. Janikowska, W.M. Otte, N.E.C. van Klink, M.A. van 't Klooster, M. Zijlmans
Neuroimage, Volume 330, April 2026

Changes In Cortical And Hippocampal θ–γ Phase Amplitude Coupling Under Anti-Seizure Medication Tapering In People With Refractory Epilepsy
E.V. Schaft*, G. Krivoshein*, P. van Eijsden, A.M.J.M. van den Maagdenberg, M. Zijlmans, M.A. van 't Klooster, E.A. Tolner
In preparation

Normative brain mapping with intraoperative electrocorticography for epileptogenic abnormality detection under propofol
S. Hoogteijling, C. Kozma, W.D. Maathuis, Z. Wang, **E.V. Schaft**, J. Guo, P. van Eijsden, W.M. Otte, N.E.C. van Klink, Y. Wang, M. Zijlmans, P.N. Taylor
In preparation

Scalp EEG features and outcome in children with epileptic encephalopathy with spike-and-wave activation in sleep
L. Noorlag, M.M.L. van Arnhem, B. van den Munckhof, S.R. Gefferie, **E.V. Schaft**, N.E.C. van Klink, M. Koroglu, H.C. van Teeseling, B.K. Bölsterli, K.P.J. Braun, F.E. Jansen, M. Zijlmans
In preparation

About the author

Eline was born in Leiderdorp, The Netherlands, on August 11th 1992. In 2010, she completed her secondary education at the Stedelijk Gymnasium Leiden. At the end of secondary school, her mathematics teacher encouraged her to pursue a degree in Mathematics. She deliberately chose not to follow this advice, as she was convinced that such a path would ultimately lead to a career in teaching: something she did not envision for herself at the time. Instead, she enrolled in the Technical Medicine program at the University of Twente in Enschede.

During her first year, she discovered that she missed the mathematical challenges. She therefore took additional mathematics courses alongside the Technical Medicine program. After obtaining her Bachelor's degree, she decided to formally combine both interest by pursuing two Master's degrees simultaneously: Technical Medicine and Applied Mathematics. She graduated from both programs on December 11th, 2019.

In January 2020 she started as a PhD student at the Clinical Neurophysiology Department in the University Medical Center Utrecht under the supervision of prof. dr. Maeike Zijlmans, prof. dr. Nick Ramsey and dr. Maryse van 't Klooster. Her research focused on signal analysis on intraoperative electrocorticography and she started the 'High-Density' study. Alongside her PhD, she worked clinically as a Technical Physician.

She currently works as a Senior Advisor Medical Technology at the Leiden University Medical Center. Alongside her work, she is, ironically, a teacher within the Master's Technical Medicine program at the Delft University of Technology, which she enjoys very much. She lives in Leiden with Victor and their son Frey.



UMC Utrecht

Universiteit Utrecht

ISBN 978-94-6534-297-9